ISTANBUL TECHNICAL UNIVERSITY ★ EURASIA INSTITUTE OF EARTH SCIENCES

QUANTIFICATION OF THE IMPACT OF UNCERTAINTY IN EMISSIONS ON AIR QUALITY MODEL ESTIMATES

Ph.D. THESIS

Ümmügülsüm ALYÜZ ÖZDEMİR

Department of Climate and Marine Sciences

Earth System Science Programme

JANUARY 2020

ISTANBUL TECHNICAL UNIVERSITY ★ EURASIA INSTITUTE OF EARTH SCIENCES

QUANTIFICATION OF THE IMPACT OF UNCERTAINTY IN EMISSIONS ON AIR QUALITY MODEL ESTIMATES

Ph.D. THESIS

Ümmügülsüm ALYÜZ ÖZDEMİR
(601122007)

Department of Climate and Marine Sciences

Earth System Science Programme

Thesis Advisor: Prof. Dr. Alper ÜNAL
Thesis Co-Advisor: Prof. Dr. Göksel DEMİR

JANUARY 2020

İSTANBUL TEKNİK ÜNİVERSİTESİ ★ AVRASYA YER BİLİMLERİ ENSTİTÜSÜ

EMİSYONLARDAKİ BELİRSİZLİĞİN HAVA KALİTESİ MODEL TAHMİNLERİNE ETKİSİNİN HESAPLANMASI

DOKTORA TEZİ

Ümmügülsüm ALYÜZ ÖZDEMİR
(601122007)

İklim ve Deniz Bilimleri Anabilim Dalı

Yer Sistem Bilimi Programı

Tez Danışmanı: Prof. Dr. Alper ÜNAL
Eş Danışman: Prof. Dr. Göksel DEMİR

JANUARY 2020

Ümmügülsüm ALYÜZ ÖZDEMİR, a Ph.D. student of ITU Eurasia Institute of Earth Sciences student ID 601122007, successfully defended the dissertation entitled "Quantification of the Impact of Uncertainty in Emissions on Air Quality Model Estimates", which she prepared after fulfilling the requirements specified in the associated legislations, before the jury whose signatures are below.

Thesis Advisor :   **Prof. Dr. Alper ÜNAL**   ....
Istanbul Technical University

Co-advisor :   **Prof. Dr. Göksel DEMİR**   ....
Health Sciences University

Jury Members :   **Prof. Dr. Tayfun KINDAP**   ....
Istanbul Technical University

Prof. Dr. Lokman Hakan TECER   ....
Namık Kemal University

Prof. Dr. Mete TAYANÇ   ....
Marmara University

Prof. Dr. Hüseyin Kurtuluş ÖZCAN   ....
Istanbul University

Assoc. Prof. Dr. Bülent Oktay AKKOYUNLU......................
Marmara University

Date of Submission : 20 December 2019
Date of Defense   : 16 January 2020

To my father,

FOREWORD

It was not easy to go through the PhD process in which many things changed in my life in a very short period of time. I would like to thank my husband Selkan ÖZDEMİR, my sister Emine Nur ALYÜZ, my mother Nesibe Kadife ŞENADLI, Hüsnü YAZGAN, my dear friend Dr. Özlem BAYDAROĞLU, my aunt Fatma BAYRACI and my husband's family for making their most to make my life easier.

Although I tried to do my best for planning, it was not easy to balance my time between PhD studies, intensive teaching activities and my family. I wrote this thesis on my annual leave, in Summer breaks and early in the mornings. Although I tried to make my best for organizing my time with him, by having a tired mother, my son Çınar ÖZDEMİR sacrificed much for this study without knowing it. I am also grateful to my husband Selkan ÖZDEMİR who skillfully balanced us. I hope those days are close when young academicians use their high motivation to produce real science in an appropriate environment.

I dedicate this study to my father, Bekir ALYÜZ, who believed me in all circumstances and always proud of me. I hope you are in the heaven.

January 2020   Ümmügülsüm ALYÜZ

TABLE OF CONTENTS

ABBREVIATIONS

1.A.1.A-10101-3.10 : Brown coal or lignite firing large wet and dry bottom boilers
1.A.1.A-10101-3.16 : Brown coal firing large fluid bed boilers
1.A.1.A-10102-3.10 : Brown coal or lignite firing medium size wet and dry bottom boilers
1.A.1.A-10102-3.12 : Natural gas firing dry bottom boilers
1.A.1.A-10104-3.17 : Gaseous fuels firing gas turbines
AIC : Akaike's Information Criterion
AirBase : European Air Quality Database
AP-42 : Air Pollution Emission Factor Database of EPA
AQM : Air Quality Model
AQMEII : Air Quality Modelling Evaluation International Initiative
AQMEII-3 : Air Quality Modelling Evaluation International Initiative Phase 3
Avg. : Average
BC : Black carbon
BIC : Bayesian Information Criteron
CAMx : Comprehensive Air Quality Model with Extensions
CB05 : Carbon Bond Chemical Mechanism version 5
CB05-TUCL : Carbon Bond Chemical Mechanism version 5 with updated toluene and chlorine chemistry
CB4 : Carbon Bond Chemical Mechanism version 4
CBM-IV : Carbon Bond Chemical Mechanism version 4
CCLM : The Consortium for Small-scale Modelling (COSMO) and Climate Limited-Area Modelling
Cd : Cadmium
CEIP : Centre on Emission Inventories and Projections
CH$_4$: Methane
CHIMERE : Multi-scale chemistry-transport model for atmospheric composition analysis and forecast
CI : Confidence Interval
CITEAIR : Common Information to European Air project
CLRTAP : Convention on Long-range Transboundary Air Pollution
CMAQ : Community Multiscale Air Quality Model
CO : Carbon Monoxide
CO$_2$: Carbon Dioxide
CTM : Chemical Transport Model
Cv : Coefficient of Variation
DDM-3D : Decoupled direct method in three dimensions
DE1 : Helmholtz-Zentrum Geesthacht from Germany in AQMEII-3 activity
DEHM : Danish Eulerian Hemisphere Model

DG ENV	:	European Commission Directorate-General for Environment
DK1	:	Aarhus University from Denmark in AQMEII-3 project
EC	:	European Commission
ECMWF	:	European Centre for Medium Range Weather Forecasts
EDGAR	:	Emissions Database for Global Atmospheric Research
EEA	:	European Environment Agency
EF	:	Emission Factor
EFs	:	Emission Factors
EMEP	:	European Monitoring and Evaluation Programme
EMR	:	Emission Measurement Report
EMRs	:	Emission Measurement Reports
ENSEMBLE	:	Web-based model evaluation platform of European JRC
EPA	:	Environmental Protection Agency of United States
ERA-interim	:	ECMWF re-analysis data
ES1	:	University of Murcia from Spain in AQMEII-3 project
EU	:	European Union
EUROS	:	European Operational Smog model
FI1	:	Finish Meteorological Institute in AQMEII-3 project
FRES1	:	INERIS and CIEMAT institutes jointly in AQMEII-3 project
GRIB	:	Gridded binary data
HFCs	:	Hydrofluorocarbons
Hg	:	Mercury
hPa	:	hectopascals
HTAP	:	Hemispheric Transport of Air Pollution
IoA	:	Index of Aggreement
IPCC	:	Intergovernmental Panel on Climate Change
IT1	:	Ricerca Sistema Energetico from Italy in AQMEII-3 project
IT2	:	University of L'Aquila from Italy in AQMEII-3 project
ITU	:	Istanbul Technical University
IUPAC	:	International Union of Pure and Applied Chemistry
JRC	:	European Joint Research Centre
KAMAG	:	Public Research Group of Turkey
Lat	:	Latitude
Lon	:	Longitude
LOTOS	:	Long Term Ozone Simulation
LRTAP	:	Long Range Transboundary Air Pollution
MACC	:	Monitoring Atmospheric Composition and Climate
MACC-II	:	Monitoring Atmospheric Composition and Climate Phase II
MEGAN	:	The Model of Emissions of Gases and Aerosols from Nature
N$_2$O	:	Nitrous oxide
NASA	:	National Aeronautics and Space Administration
NFR	:	Nomenclature for Reporting
NH$_3$	:	Ammonia
NL1	:	TNO group from Netherlands in AQMEII-3 project
NMVOC	:	Non-Methane Volatile Organic Carbon
NO$_2$	:	Nitrogen dioxide

NOAA/ESRL: National Oceanic & Atmospheric Administration / Earth System Research Laboratory

NO_x	: Nitrogen oxides
O_3	: Ozone
OC	: Organic carbon
Pb	: Lead
PBL	: Planetary Boundary Layer
PFCs	: Perfluorocarbons
PM	: Particulate Matter
PM_{10}	: Particulate Matter 10 micrometres or less in diameter
$PM_{2.5}$	: Particulate Matter 2.5 micrometres or less in diameter
PMcoarse	: Particulate Matter with a diameter between 2.5-10 micrometres
POP	: Persistent Organic Pollutant
SCC	: Source Classification Code of EPA AP42 Emission Factor Database
SF_6	: Sulphur hexafluoride
SI	: International System of Units
SIA	: Secondary inorganic aerosol
SNAP	: Standardized Nomenclature for Air Pollutants
SNAP/NFR	: Emission factor coding system of EMEP guidebook
SO_2	: Sulphur dioxide
SOA	: Secondary organic aerosol
SO_x	: Sulphur oxides
TF HTAP	: The Task Force on Hemispheric Transport of Air Pollution
TNO	: Netherlands Organisation for Applied Scientific Research
TR	: Turkey
TR1	: Istanbul Technical University in AQMEII-3 project
TurkStat	: Turkish Statistical Institute
U.K.	: United Kingdom
U.S.	: United States from England in AQMEII-3 project
UK1	: Kings College from England in AQMEII-3 project
UK2	: Ricardo Energy & Environment (Ricardo E&E)
UK3	: University of Hertfordshire from England in AQMEII-3 project
UNECE	: United Nations Economic Commission for Europe
UNFCCC	: United Nations Framework Convention on Climate Change
UTC	: Coordinated Universal Time
VBS	: Volatility basis set
WMO	: World Meteorological Organisation
WRF	: Weather Research and Forecasting Model
WRF-Chem	: Weather Research and Forecasting Model coupled with Chemistry
WS	: Wind speed

SYMBOLS

$\vec{F}_t$	: Turbulent flux of the pollutants
$ì_g$	: Geometric mean
$ó_g$	: Geometric standard deviation
$\widehat{\theta}^*$	: Estimated parameters from Bootstrap simulation
$\widehat{a}$	: Shape parameter of Gamma distribution
C_{kX}	: Coefficient of kurtosis
C_{sX}	: Fisher-Pearson coefficient of skewness
D_n	: Kolmogorov Smirnov Statistic
E'	: Centred difference (errors)
$\widehat{F}$	: Fitted distribution to a dataset
$\widehat{K}$	: Diffusivity tensor
$S_n(x)$	: Empirical cumulative distribution function
U_p	: Importance of uncertainty from emission sources
x_k	: Total emission inventory of the specific emission source category
$\overline{x}$	: Sample mean
$\overline{y}$	: Emission mean of the all subset sources of specific category
$\widehat{\beta}$	: Scale parameter of Gamma distribution
δx_{high}	: Upper bound of the 95% confidence interval of x
δx_{low}	: Lower bound of the 95% confidence interval of x
δy_{high}	: Upper bound of the 95% confidence interval of y
δy_{low}	: Lower bound of the 95% confidence interval of y
δz_{high}	: Upper bound of the 95% confidence interval of z
δz_{low}	: Lower bound of the 95% confidence interval of z
η	: Abatement efficiency
α	: Significance level
$\mu g/m^3$	: Micrograms per cubic meters
%	: Percent
A	: Activity data
B	: Number of bootstrap samples (generated by Monte Carlo method)
c	: Shape parameter of Weibull distribution
C	: Pollutant concentration average over time interval
Cv	: Coefficient of variation
E	: Total emission of a plant including all stacks
exp	: Exponential
F	: Underlying distribution of a dataset
$f(x)$	: Probability density function of a distribution
g/GJ	: Grams per gigajoule

GJ	:	Gigajoule
h	:	Hour
J$_\xi$	:	Vertical Jacobian of the terrain-influenced coordinate ξ
K	:	Diagonal components of the eddy diffusivity tensor in the generalised coordinates
k	:	Skale parameter of Weibull distribution
kcal	:	Kilocalories
kcal/kg	:	Kilocalories per kilogram
kcal/m^3	:	Kilocalories per cubic meters
kg/h	:	Kilograms per hour
kg/m^3	:	Kilograms pere cubic meters
kg/year	:	Kilograms per year
K$_H$	:	Horizontal turbulent exchange coefficients
K$_z$	:	Vertical turbulent exchange coefficients
Lmax	:	The maximized value of the log-Likelihood for the estimated model
m	:	Map scale factor or model
m/s	:	Meters per second
m^2/sec	:	Meters square per second
m^3	:	Cubic meters
m^3/h	:	Meters cube per hour
mg/m^3	:	Miligrams per cubic meters
MW	:	Megawatts
n or N	:	Number of the data points in the dataset
Nm^3/h	:	Normal meters cube per hour
o	:	Observations
^{o}C	:	Degrees celcius
ppm	:	Parts per million
Q	:	Source term
q$_i$	:	Species mass mixing ratio
r	:	Pearson's correlation coefficient
R	:	Removal term
r^2	:	Coefficient of determination
s^2	:	Unbiased sample variance
t	:	Time
U	:	Random sample from the $U(0,1)$ distribution
V	:	Vertical and horizontal wind components in the generalised coordinates
v	:	Vertical velocity
x	:	Final sum of the two values which are y and z
x*	:	Independent bootstrap sample
$\Gamma(\alpha)$	:	Gamma function
θ	:	Paaremeter of interest
ρ	:	Density of the air
σ	:	Standard deviation
φ_i	:	Trace species concentration

LIST OF TABLES

LIST OF FIGURES

QUANTIFICATION OF THE IMPACT OF UNCERTAINTY IN EMISSIONS ON AIR QUALITY MODEL ESTIMATES

SUMMARY

The Air Quality Model, especially Chemical Transport Model, prediction represents mean concentration over the entire grid volume. Predictions of CTMs may differ from observations due to four reasons; 1) inherent or stochastic variability in the observations, 2) errors in model physics and chemistry assumptions, 3) errors due to uncertainties in model input variables, and 4) numerical errors. Here, variability is a description of the range of spread of the values, and it is often expressed by statistical metrics such as variance and standard deviation. Therefore, inherent uncertainty can be considered as variability. Uncertainty refers to lack of knowledge regarding the true value of a quantity. Uncertainty can be reduced or eliminated with more or better data, where variability cannot be reduced. Among the four reasons of uncertainty, provided above, inputs are regarded to have the largest levels of uncertainty.

The aim of this study is to evaluate and quantify the contribution of uncertainties in input dataset to AQM estimates. For this purpose, it is necessary to define the problem that poor performance of the model is caused mostly by unfit data. In literature, models perform poor in the Eastern European countries. However, a more detailed study is needed to say that this poor performance is mostly due to model inputs. Because, as it is known, the poor performance of the models may also have other reasons. In the first part of this study, inter-model variability is defined quantitatively by participating in an international project. In the second part of the study, contribution of uncertainties to this problem is quantified by being part of a national project. In the second part, a sample of the solution is presented which includes development of country specific emission factors and compiling a probabilistic emission inventory.

As a part of an international project (AQMEII-3), 12 modelling groups were cooperated from different countries of Europe and conducted 18 model runs on Europe domain (covers 34 Europe countries) for 2010 by using 7 different AQMs, 3 meteorology models and 2 emission inventories. This study, for the first time in Turkey, contributed to AQMEII-3 which is organized by the joint leading of U.S. EPA and European JRC. One of the most important benefits of this project is that the model results of all groups can be reached through a common platform. In this dissertation, performance metrics were calculated and mapped for each of 1431 stations of Europe, and for each model for evaluation of model performances. Taylor diagrams were also used for seasonal evaluation.

Up to now, there are several air quality modelling studies for Turkey, however they are developed for a specific city or region of Turkey for a timescale starting from days to a few months, or by using just one type of AQM. Thanks to its wide coverage domain (Europe continent) and multi-model contributions from AQMEII-3 project, this study looks to the problem from a large perspective in order to define the problem and recommends a solution by representing a sample of the solution. Thus, an inventory study was conducted to overcome this problem by adopting a deep statistical

approach which is not encountered in Turkish inventory studies yet. To this end, country specific EFs are calculated for the energy production industry of Turkey, an inventory has been created for the energy production industry of the Marmara Region. Monte Carlo and Bootstrap approaches are used for uncertainty calculations at these stages.

According to results of modelling part of this dissertation, correlations between models and PM_{10} observations are 8% less in Eastern European countries when compared to Western European countries. BIAS of Eastern European countries is 2.5-fold of Western European countries, when all countries are considered. RMSE of Eastern countries is 90% more than Western countries average, where MAE is 99% and MNE is 25% more. From these results it is clear that, model predictions are significantly beyond the observations in Eastern European countries.

Turkey, which is located in the Eastern Europe, has one of the worst results calculated by all models. All models predict PM_{10} concentrations with an average of -40 μg/m^3 BIAS in stations of Turkey, where it is the worst value within 34 countries of Europe considered in this study. Moreover, models predict close to each other but quite far from the observations in 80% of the stations. MAE is over 20 μg/m^3 in 80% of all stations in Turkey. Remaining 20% of the stations encounters 18 over 101, mostly in Istanbul and some other big cities. In fact, when the results of the models are examined, it is seen that models generally make better predictions in big cities compared to the small cities. This may be due to the fact that inventory compilers have more information on emission sources in large cities.

In seasonal evaluation, it is seen that emissions in Winter cannot be well predicted, but in Summer it is relatively better predicted. This difference can be caused by inadequate representation of increased emissions (in the model inputs) in Winter months from residential heating and traffic emissions when compared to other months. In this case, it would not be unreasonable to suspect that the inputs to the models significantly affect predictions.

Model inputs are considered as a reason for poor model predictions in this study. However, problems caused by the model itself or erroneous measurements, or combination of all, may also cause this. In this study, problems due to the model itself are out of consideration since 6 different AQMs were used by 13 modelling groups where same models were also considered by different groups. The fact that all models give close CDFs in Western Europe despite they have different modelling configurations, where they are not close to observations in Eastern Europe countries even in same models, shows that problems in the models are not dominant in prediction errors. Since the number of observation stations included in the scope of this study is very high, measurement errors are not considered to be predominant in poor model estimates. Also, systematic errors are not thought to occur at all stations at the same time.

The quality of an emission inventory that will be used in air quality modelling is associated with its low-level uncertainty and adequate coverage of the sources. Emission inventories approach to the ultimate result as in-situ measurements and full activity data are available. In this study, in-situ measurements were conducted within the scope of the national KAMAG project in order to generate country-specific EFs, and an emission inventory was prepared in the light of the most consistent information possible. Besides, official emission measurement reports (EMRs), whose reliability is controversial as they were prepared by the companies under authorization of the

emission emitting plants, were also used for comparison with in-situ EFs. Country-specific dust, CO, SO_2, NO, NO_2 and NO_x EFs are calculated in this part of the study for each of coal combusting large wet/dry bottom boilers, coal combusting large size fluid bed boilers, coal combusting large wet and dry bottom boilers, natural gas combusting medium size boilers and gaseous fuels combusting gas turbines.

EFs are typically assumed to be representative of an average emission rate from a population of pollutant sources in a specific category. However, there may be uncertainty in the average emissions from population because of three reasons: random sampling error, measurement errors, or when the sample population is not representative for EF development. First two factors typically lead to imprecision in the estimate of the population average. The third factor may lead to possible biases or systematic errors in the estimated average. In order to avoid errors, it is important to understand and account for the uncertainty in the inventory. In the relevant part of this study, a probabilistic emission inventory is developed by considering statistical analysis of variability and uncertainty.

The development of a consistent procedure for the uncertainty evaluation is still a challenge for the scientific community. In this study a deep uncertainty analysis technique is applied in EF development, which is including Monte Carlo method and Bootstrap simulation. The uncertainty analysis described in this study can be used as a basis for developing probabilistic emission inventories. When the probability range of emissions to be given as input to air quality is known, it is possible to determine the probability of the model result. Thus, for example, the probability of achieving an air quality management goal can also be calculated.

In statistics, sampling error is a type of error caused by investigating a small part of the population rather than examining the whole population. It is calculated by the difference of a sample statistic used to estimate a population parameter and the actual but unknown value of the parameter. Since uncertainty is expressed as lack of knowledge regarding to true value of a quantity, random sampling error can be represented by a sampling distribution. In order to calculate uncertainty of EFs, a distribution is fitted ($\hat{F}$) to the EF dataset (x) where actual underlying distribution (F) is unknown. The goodness-of-fit is evaluated by some techniques. Then Monte Carlo method is applied in order to generate random datasets from assigned distribution, $\hat{F}$. In Bootstrap simulation part of the study, each of the alternative probability models generated by Monte Carlo approach (Bootstrap replicates) are simulated to develop a reasonably stable characterization of the percentiles of the distribution. Then parameters, $\hat{\theta}^*$, are estimated. In this study, uncertainty in the estimate of θ is reflected by dispersion of $\hat{\theta}^*$, which also gives random sampling error. A confidence interval for a statistic is a measure of the lack of knowledge regarding the true value of the statistic. The $\hat{\theta}^*$ data is sorted then, in order to calculate confidence interval for the fitted cumulative distribution function. Consequently, the results are compared to the original dataset by generating probability bands. Then results are compared to EMEP and EPA EFs.

At the end, dust EFs obtained from in-situ measurements are significantly lower than the literature for coal combusting plants. The reason of these large differences between in-situ measurements and literature EFs may be due to wide usage of dust abatement technologies in Turkish energy production plants. CO and SO_2 EFs are significantly larger than EMR, EMEP and EPA EFs in large coal combusting plants and in plants combusting gaseous fuels with gas turbines. But in all EFs, uncertainty is low when

compared to EMEP EFs. Country specific NO_x EFs are generally larger than all other studies and range of confidence interval is narrow when compared to them. This situation indicates low uncertainty in in-situ EFs. Since each stack measurement may differentiate from the real value due to variations in operating conditions, the overall uncertainty of the emission factors can also be referred as "uncertainty due to variability".

After calculating country specific EFs, next step is preparing an emission inventory for power plants of Marmara region and comparing it with the existing emission inventories. The most common emission inventories currently used by CTMs are the TNO-MACC and EDGAR-HTAP emission inventories. These two inventories are mainly used in AQMEII-3 models. EDGAR-HTAP emission inventory contains much more plants (34 plants) than TNO-MACC (19 plants) but is still far from the actual number of power plants (57 plants) that considered in this study for Marmara region of Turkey. Furthermore EDGAR-HTAP emission inventory has more plants than TNO-MACC in all regions of Turkey. From this point of view, it is clear that EDGAR-HTAP emission inventory is more inclusive than TNO-MACC emission inventory in Turkey in terms of number of plants. Also, it is more inclusive in Eastern Anatolian regions of Turkey where TNO-MACC emission inventory has almost no plants for public electricity and heat production sector. There are missing plants in EDGAR-HTAP and TNO-MACC emission inventories where there some unidentified plants in those emission inventories.

As a result of emission inventory calculations, NO_x emissions calculated in this study is 93,000 ton/year with lower CI as 69,000 ton/year and upper CI as 114,000 ton/year. When same emission inventory is calculated with EMEP EFs 60,000 ton/year with lower CI as 33,000 and upper CI as 90,000 ton/year. The inventory compiled by this study beyond the upper CI of EMEP and it is considerably larger than TNO (24,000 ton/year) and EDGAR-HTAP (42,000 ton/year).

SO_2 emissions are calculated as 152,379 tonne/year in this study. Same activity data is used in calculation of EMEP emission inventory and resulted 170,596 tonne/year, because in-situ SO_2 EF was smaller than EMEP EF for coal combustion plants. It is 69,000 ton/year in TNO and 125,00 ton/year in EDGAR-HTAP emission inventory. 4 large lignite combustion plants, which are not included in the TNO inventory, have resulted in 73,500 tons less SO_2 emissions in TNO emission inventory when compared to this study. 1000 tonnes of SO_2 emissions is also not included in the TNO inventory due to about 40 missing natural gas incineration plants.

Uncertainty range of NO_x emission inventory of this study is between 26 (lower bound of CI) to 23% (upper bound of CI). When same emission inventory is compiled with EMEP EFs, overall uncertainty range is 45 (lower) to 48% (upper). As it is clear, country specific EFs decrease uncertainty when compared to usage of EFs from literature. This situation is dominant in NO_x emission inventory than SO_2 and CO emission inventories, because number of natural gas combusting power plants are large (48 over 57 plants in Marmara region). TNO and EDGAR HTAP emission inventories are out of the uncertainty range of this study which proves their inadequacy for representing emissions of power plants in Marmara region.

Generally, the data on energy facilities is among the most easily accessed by inventory compilers. Such large differences in emissions from power plants reinforce doubts about the reliability of the entire TNO-MACC and EDGAR-HTAP emission inventories. In this case, it is quantifically proved that poor emission inventories are

primarily responsible for the poor air quality predictions in Turkey, and most probably in all Eastern European countries.

No matter how many and high-quality measurements are conducted, no matter how good models are used, it is not possible for air quality models to predict accurate results without a good emission inventory. Therefore, consistent, low uncertainty and comprehensive emission inventories should be compiled for the Eastern European countries, including Turkey. Development country specific EFs is the preliminary step of emission inventory development. Access to activity data used in these studies should be facilitated in order to make room for calculation of the representative EFs easily.

EMİSYONLARDAKİ BELİRSİZLİĞİN HAVA KALİTESİ MODEL TAHMİNLERİNE ETKİSİNİN HESAPLANMASI

ÖZET

Hava kalitesi modelleri tarafından yapılan tahminler, özellikle kimyasal taşınım modellerinde, tüm grid hacmindeki ortalama kirletici değerini verir. Kimyasal taşınım modellerinin tahminleri ölçümlerden farklı olabilir. Bunun dört nedeni vardır; 1) ölçümlerdeki doğal veya stokastik değişkenlik, 2) modelin fizik veya kimyasal hesaplamaları aşamasında yapılan bazı varsayımlardan kaynaklı hatalar, 3) modele girdi olarak verilen değişkenlerdeki belirsizliklerden kaynaklı hatalar, 4) sayısal hatalar. Burada bahsi geçen "değişkenlik" terimi, verilerin birbirinden ne kadar farklılaştığını ifade etmek için kullanılır ve genellikle varyans ve standart sapma gibi istatistiksel metrikler yardımı ile açıklanır. Bu nedenle ilk maddede belirtilen doğal veya stokastik nedenlerden kaynaklı hatalar "değişkenlik" başlığı altında düşünülebilir. "Belirsizlik" terimi ise bir şeyin gerçek değeri ile ilgili bilgimizin eksikliğini ifade eder. Daha iyi veya daha çok veri kullanılması durumunda belirsizlik azaltılabilirken, değişkenliğin azaltılması mümkün değildir. Yukarıda bahsi geçen belirsizliğin dört nedeni arasında, modele girdi olarak verilen değişkenlerdeki belirsizlik, genellikle diğer nedenlere kıyasla en büyük etkiyi gösterendir.

Bu çalışmanın amacı, verilerdeki hatalardan kaynaklı belirsizliğin hava kalitesi model tahminlerine etkisinin değerlendirilmesi ve hesaplanmasıdır. Bu kapsamla modellerin kötü performans vermesinin nedeninin yetersiz veriden kaynaklandığının kanıtlanması gerekmektedir. Literatürde modellerin özellikle Doğu Avrupa ülkelerinde kötü sonuç verdiği bilinmektedir. Bu problemi, geniş kapsamlı bir hava kalitesi modelinin sonuçlarını incelediğimizde görebiliriz. Fakat modellerin bu kötü performanslarının nedeni olarak, modellere verilen girdilerin büyük oranda sorumlu olduklarını söyleyeceksek daha detaylı bir çalışmaya ihtiyacımız olur. Çünkü, bilindiği gibi, modellerin kötü tahmin etmesinde verilerin dışında başka nedenler de bulunmaktadır. Bu çalışmanın ilk kısmında, modeller arası değişkenliği görmek için uluslararası bir proje olan AQMEII projesine katılarak, bir çoklu-model yaklaşımı kullanılmış, böylelikle bu problemin nicel olarak tanımlanması sağlanmıştır. Çalışmanın ikinci kısmında ise envanterlerin Türkiye'deki belirsizliğinin bu probleme katkısını anlayabilmek için ulusal bir proje kapsamında yapılan ölçümler kullanılarak Türkiye'ye özgü emisyon faktörleri türetilmiş, olasılıksal bir emisyon envanteri geliştirilmiş ve belirsizlik analizleri yapılarak literatürle kıyaslanmıştır.

AQMEII-3 isminde uluslararası projenin bir parçası olarak, Avrupa'nın farklı ülkelerinden 12 modelleme grubu ile iş birliği yapılmış, tüm Avrupa kıtasını kapsayan (toplam 34 ülke) 18 ayrı model çalışması yapılmıştır. 2010 yılı baz alınarak yapılan bu çalışmada, 7 farklı hava kalitesi modeli, 3 farklı meteoroloji modeli ve 2 ayrı emisyon envanteri kullanılmıştır. Amerika Çevre Ajansı (EPA) ve Avrupa Ortak Araştırma Merkezi (European JRC) liderliğinde düzenlenen AQMEII-3 projesine bu çalışma kapsamında ilk defa Türkiye'den katılım sağlanmıştır. Bu projenin en önemli yararlarından biri, tüm grupların model sonuçlarının ortak bir platform yardımıyla

ulaşılabilir olmasıdır. Bu tez kapsamında model performanslarının değerlendirilmesi aşamasında, Avrupa kıtasında bulunan 1431 tane hava kalitesi ölçüm istasyonu için performans metrikleri hesaplanmış, sonra da harita üzerinde gösterilmiştir. Model performanslarının mevsimsel değerlendirmeleri için ise Taylor diyagramlarından faydalanılmıştır.

Şu ana kadar, Türkiye için çeşitli hava kalitesi modelleme çalışmaları yapılmıştır. Fakat bu çalışmaların genellikle bir şehir veya bir bölge için, birkaç gün ile birkaç ay arasında bir zaman ölçeği için veya genellikle tek bir hava kalitesi modeli kullanarak yapıldığı görülmüştür. AQMEII-3 projesinin geniş bir alanı kapsaması (Avrupa kıtası) ve pek çok farklı modelin katkısı nedeniyle, bu çalışmada sorunu tanımlamak için geniş bir bakış açısıyla bakılabilmiş ve bir örnek yardımıyla bir çözüm önerisinde bulunulmuştur. Bu çözüm önerisinde, detaylı bir istatistiksel yaklaşım benimsenerek Türkiye'de henüz yapılmamış titizlikte bir envanter çalışması yapılmıştır. Bu amaçla Türkiye'deki enerji üretim tesisleri için ülkeye özgü emisyon faktörleri hesaplanmış, Marmara Bölgesindeki enerji tesisleri için bir envanter oluşturulmuştur. Bu aşamalarda belirsizlik hesapları için Monte Carlo ve Bootsrap yaklaşımları benimsenmiştir.

Bu tezin modelleme kısmının sonuçlarına göre, Doğu Avrupa ülkelerinde modellerin PM_{10} ölçümleri ile korelasyonu Batı Avrupa ülkelerine kıyasla %8 daha azdır. Doğu Avrupa ülkelerindeki ortalama hata (BIAS), Batı Avrupa ülkelerinin 2.5 katıdır. Doğu Avrupa ülkelerinde hataların ortalama kare kökü (RMSE) Batı Avrupa ülkelerinden %90 daha fazla iken, mutlak hataların ortalaması (MAE) %99, normalize hataların ortalaması (MNE) ise %25 fazladır. Bu sonuçlardan da görüldüğü üzere, Doğu Avrupa ülkeleri için modeller tarafından yapılan tahminler, ölçümlerden oldukça farklıdır.

Bir Doğu Avrupa ülkesi olan Türkiye, tüm modeller tarafından hesaplanan en kötü sonuçlardan birine sahiptir. Türkiye'deki istasyonlarda tüm modeller -40 µg/m³ ortalama hata (BIAS) ile tahmin yapmaktadır ve bu değer bu çalışma kapsamında dikkate alınan 34 Avrupa ülkesi içindeki en kötü değerdir. Üstelik, Türkiye'deki istasyonların %80'inde modeller ölçümlerden bu kadar farklı tahmin ederken, birbirlerine de o derecede yakın tahminler yapmaktadır. İstasyonların %80'inde mutlak hataların ortalaması (MAE) 20 µg/m³'ün üzerindedir. Kalan %20'lik kısım, Türkiye'deki 101 tane istasyonun 18 tanesine tekabül etmektedir ve bu istasyonların çoğunun İstanbul'da, bir kısmının da Türkiye'nin başka büyük şehirlerinde olduğu görülmüştür. Zaten model sonuçları incelendiğinde, modellerin küçük şehirlere kıyasla büyük şehirlerde daha iyi tahmin yaptığı görülmüştür. Bunun nedeni, envanter hazırlanması aşamasında büyük şehirlerdeki emisyon kaynaklarına ait verilere daha kolay ulaşılması olabilir.

Modellerin mevsimlere göre performansları incelendiğinde, emisyonların genellikle yaz aylarında kış aylarına göre daha iyi tahmin edildiği görülmüştür. Bu fark, kış aylarında artan ısınma ve trafik emisyonlarının model girdilerine yetersiz aksettirilmesi nedeniyle olabilir. Bu durumda, modele verilen girdilerin model tahminlerini oldukça etkilediğinden şüphelenmek mantıksız olmaz.

Bu çalışmada, model girdileri zayıf model tahminlerinin bir nedeni olarak kabul edilmektedir. Elbette, modelin kendisinden veya ölçümlerdeki hatalardan veya hepsinin birleşiminden kaynaklı problemler de buna neden olabilir. Bu çalışmada, 13 farklı grup tarafından çalıştırılan 6 farklı hava kalitesi modeli kullanıldığı, bazen aynı modelin farklı gruplar tarafından da çalıştırıldığı bilindiği için, modelin kendisinden kaynaklı hataların kapsam dışında olduğu düşünülmektedir. Birbirlerinden farklı

model konfigürasyonlarına sahip olmalarına rağmen tüm modellerin Batı Avrupa'da iyi tahmin yaparken, Doğu Avrupa'da ölçümlerden oldukça farklı olmaları, modellerden kaynaklı problemlerin kötü tahminlerde baskın olmadığını göstermektedir. Bu çalışmanın kapsamına dahil olan ölçüm istasyonu sayısı çok fazla olduğu için, ölçümlerden kaynaklı hataların da kötü model tahminlerinde baskın olduğu düşünülmemektedir. Ayrıca, ölçüm istasyonlarında olabilecek sistematik hataların da, aynı anda pek çok istasyonda olamayacağı düşünülmektedir.

Hava kalitesi modellemesinde kullanılan bir emisyon envanterinin kalitesi, belirsizliğinin düşük olması ve kapsadığı kaynakların yeterliliği ile ilişkilidir. Yerinde ölçümler ve tam aktivite verisi oldukça, emisyon envanterleri nihai değere yaklaşır. Bu çalışmada, ulusal bir proje olan KAMAG projesi kapsamında, ülkeye özgü emisyon faktörlerinin geliştirilmesi ve mümkün olan en tutarlı veri ile emisyon envanterinin hazırlanabilmesi amacıyla yerinde ölçümler yapılmıştır. Emisyon yayan tesislerin yetkilendirdiği firmalar tarafından hazırlandığı için güvenilirliği tartışmalı olan resmi emisyon ölçüm raporları da kıyaslama amacıyla kullanılmıştır. Çalışmanın bu kısmında ülkeye özgü CO, SO_2, NO, NO_2 ve NO_x emisyon faktörleri, ıslak/kuru tabanlı büyük kömür yakma kazanları, akışkan yataklı büyük kömür yakma kazanları, doğalgaz yakan orta ölçekli yakma kazanları ve gaz yakıt yakan gaz türbinlerinin her biri için ayrı ayrı hesaplanmıştır.

Emisyon faktörlerinin, kirletici kaynakları popülasyonundan oluşan emisyonların ortalamasını temsil ettiği varsayılır. Fakat rastgele örnekleme hatası, ölçüm hataları veya örnek olarak seçilen popülasyonun emisyon faktörü geliştirmek için temsil edici olmadığı durumlarda ortalama emisyonlarda belirsizlik artabilir. İlk iki neden, genellikle popülasyon ortalamasının tahmininde yanlışlığa yol açarken, üçüncü neden ortalama hatanın (BIAS) artmasına veya sistematik hataya neden olabilir. Bu hatalardan kaçınmak için, öncelikle envanterdeki belirsizliğin anlaşılması ve hesaplanması gerekmektedir. Bu çalışmanın son kısmında, değişkenlik ve belirsizliğin detaylı istatistiksel analizi yardımıyla olasılıksal bir emisyon envanteri geliştirilmiştir.

Belirsizliğin değerlendirilmesi için tutarlı bir prosedür geliştirilmesi, bilim insanları arasında hala geliştirilmekte olan bir konudur. Bu çalışmada uygulanan Monte Carlo analizi ile Bootstrap metotlarını birleştiren belirsizlik analizi yöntemi, olasılıksal emisyon envanterlerinin geliştirilmesinde kullanılabilir. Hava kalitesine girdi olarak verilecek emisyon miktarının hangi değerler arasında olacağı bilindiğinde, model sonucunun da olasılığı bilinebilir. Böylelikle örneğin hava kalitesi yönetimi kapsamında belirlenen bir hedef değere ulaşma olasılığı da bu şekilde hesaplanabilir.

İstatistikte örnekleme hatası, tüm popülasyonu incelemek yerine, popülasyonun küçük bir bölümünü temsil edici kabul ederek incelemenin neden olduğu bir hata türüdür. Örnekleme hatası, bir popülasyon parametresini tahmin etmek için kullanılan örnek bir istatistik ile bu parametrenin gerçek ancak bilinmeyen değerinin farkı alınarak hesaplanır. Belirsizlik, bir sayının gerçek değeri ile ilgili bilgi eksikliği olarak ifade edildiği için, rastgele örnekleme hatası bir örnekleme dağılımı ile ifade edilebilir. Gerçek dağılımı (F) bilinmeyen emisyon faktörlerinin bulunduğu bir veri setindeki belirsizliği hesaplamak için, bu veri setine literatürde özellikleri bilinen bir dağılım uydurulur ($\hat{F}$). Uydurulan bu yeni dağılımın elimizdeki veri setine ne kadar uygun olduğunu anlamak için bazı uygunluk testleri uygulanır. Daha sonra Monte Carlo metodu kullanılarak uydurulan bu dağılım üzerinden rastgele veri setleri (Bootstrap kopyası) üretilir, yani veri çoğaltılır. Çalışmanın Bootstrap simülasyonu kısmında ise, Monte Carlo yaklaşımı tarafından oluşturulan alternatif olasılık modellerinin her biri

(Bootstrap kopyası), dağılımın persentil değerleri istikrarlı bir şekilde stabil oluncaya kadar simüle edilir. Sonra parametreler ($\hat{\theta}^*$) tahmin edilir. Bu çalışmada, θ'nın tahmin edilmesindeki belirsizlik, rastgele örnekleme hatası da denilen $\hat{\theta}^*$'ın dağılımı ile ifade edilmiştir. Bir istatistik için güven aralığı, istatistiğin gerçek değeri ile ilgili bilgi eksikliğinin bir ölçüsüdür. Sonraki aşamada uydurulan kümülatif dağılım fonksiyonu için güven aralığını hesap etmek amacıyla $\hat{\theta}^*$ verisi sıralanır. Sonuç olarak, elde edilen sonuçların orijinal veri seti ile kıyaslanabilmesini kolaylaştırmak için olasılık bandı grafikleri oluşturulmuştur. Hesaplanan emisyon faktörleri EMEP ve EPA emisyon faktörleri ile kıyaslanmıştır.

Bu çalışmanın sonuçlarına göre, yakma tesisleri için hesaplanan ülkeye özgü toz emisyon faktörleri literatüre göre oldukça düşüktür. Bu çalışma kapsamında hesaplanan ülkeye özgü emisyon faktörleri ve literatür arasındaki bu büyük farklılığın nedeni, Türkiye'deki enerji üretim tesislerinde toz azaltım teknolojilerinin geniş kullanımı nedeniyle olabilir. Her ne kadar son yıllarda, baca gazları ile ilgili istisnai düzenlemeler olsa da, bu tezin baz aldığı 2010 ve 2012 yıllarında bu tesislerin çalışması için bu azaltım teknolojilerini sıkı bir şekilde uygulamaları beklenmekteydi.

CO ve SO_2 emisyon faktörleri, büyük kömür yakma tesislerinde ve gaz yakıtlı gaz türbini kullanan tesislerde emisyon izin raporlarından hesaplanan emisyon faktörlerinden, EMEP ve EPA emisyon faktörlerinden önemli ölçüde daha büyüktür. Fakat tüm emisyon faktörleri için hesaplanan belirsizlik, EMEP emisyon faktörlerinin belirsizliğinden oldukça düşüktür. Ülkeye özgü NO_x emisyon faktörü literatürdeki tüm çalışmalardan yüksek, belirsizlik aralığı ise hepsinden küçüktür. Sonuçta, ülkeye özgü hesaplanan emisyon faktörlerinin belirsizliğinin düşük olduğunu görüyoruz. Burada bahsi geçen belirsizlik için "değişenlikten kaynaklı belirsizlik" terimini de kullanabiliriz. Çünkü her ölçüm aslında aynı çıkması beklenen bir sonucun çeşitli nedenlerle değişikliğe uğraması sonucu değişmişti ve bu da nihai emisyon faktörünün belirsizliğini artırmıştır.

Ülkeye özgü emisyon faktörleri hesaplandıktan sonra, bir sonraki adım Marmara Bölgesindeki elektrik santralleri için bir emisyon envanteri hazırlamak ve mevcut emisyon envanterleri ile karşılaştırmaktır. Halen hava kalitesi modelleri tarafından en yaygın kullanılan emisyon envanterleri TNO-MACC ve EDGAR-HTAP emisyon envanterleridir. Bu iki emisyon envanteri AQMEII-3 projesinde de kullanılmıştır.

Bu çalışmada Türkiye'nin Marmara bölgesi için 57 tane enerji üretim tesisi belirlenmiştir, fakat EDGAR-HTAP emisyon envanterinde 34 tane, TNO-MACC emisyon envanteri de 19 tane enerji üretim tesisi bulunduğu görülmüştür. Zaten Türkiye'nin diğer bölgelerinde de aynı Marmara bölgesinde olduğu gibi, EDGAR-HTAP emisyon envanteri TNO-MACC emisyon envanterinden daha fazla sayıda tesis bulundurmaktadır. Sadece bu sayılara bakarak EDGAR-HTAP emisyon envanterinin Türkiye'deki tesisleri içermesi bakımından daha kapsayıcı olduğu ama yeterli olmadığı söylenebilir. Örneğin, Doğu Anadolu Bölgesi için TNO-MACC envanterinde hiç tesis yokken, EDGAR-HTAP envanterinde tesisler olduğunu görüyoruz. Sonuçta, bu çalışmadaki tesis sayısına bakıldığında her iki envanterde de önemli sayıda tesisin envantere eklenmediği görülüyor. Ayrıca bu envanterlerde bazı tanımlanamayan tesisler de mevcuttur.

Bu çalışma kapsamında hesaplanan emisyon envanteri sonuçlarına göre, Marmara Bölgesindeki enerji tesislerinden 93,000 ton/yıl NO_x emisyonu açığa çıkmaktadır. Güven aralığının alt sınırı 69,000 ton/yıl, üst sınırı da 114,000 ton/yıl olarak hesaplanmıştır. Aynı emisyon envanteri bu defa EMEP emisyon faktörleri kullanılarak

hesaplandığında NOx emisyonları 60,000 ton/yıl olarak bulunmuştur. Bunun güven aralığının alt sınırı 33,000 ton/yıl, üst sınırı da 90,000 ton/yıl olarak hesaplanmıştır. Görüldüğü üzere, bu çalışma kapsamında hesaplanan NO_x emisyon envanteri, EMEP ile hesaplananın üst güven aralığı sınırından bile fazladır. TNO-MACC envanterinde aynı tesisler için verilen 24,000 ton/yıl, EDGAR-HTAP tarafından verilen 42,000 ton/yıl NO_x emisyonundan ise belirgin şekilde fazladır. Bu çalışma kapsamında hesaplanan NO_x emisyon envanteri, TNO-MACC emisyon envanterinden %387 daha fazla, EDGAR-HTAP emisyon envanterinden ise %221 daha fazladır.

Marmara Bölgesindeki enerji tesislerinden 152,379 ton/yıl SO_2 emisyonu açığa çıkmaktadır. Aynı emisyon envanteri bu defa EMEP emisyon faktörleri kullanılarak hesaplandığında SO_2 emisyonları 170,596 ton/yıl olarak bulunmuştur. Bunun nedeni, kömür yakma tesisleri için bulunan ülkeye özgü SO_2 emisyon faktörünün, EMEP emisyon faktöründen küçük olmasıdır. TNO-MACC emisyon envanterinde SO_2 emisyonu 69,000 ton/yıl iken, EDGAR-HTAP emisyon envanterinde 125,000 ton/yıldır. TNO-MACC emisyon envanterinde 4 tane büyük linyit yakan tesisin olmadığı ve bu tesislerin TNO envanterinde bu çalışmaya göre yaklaşık 73,500 ton/yıl SO_2'nin daha az hesaplanmasına neden olduğu görülmüştür. TNO-MACC envanterinde eksik olan 1000 ton/yıl SO_2 emisyonu ise, TNO-MACC envanterinde olmayan 40 tane doğalgaz yakma tesisinden kaynaklanmaktadır. Sonuç olarak, bu çalışma kapsamında hesaplanan SO_2 emisyon envanteri, TNO-MACC emisyon envanterinden %220 daha fazla, EDGAR-HTAP emisyon envanterinden ise %121 daha fazladır.

Bu çalışmada hesaplanan NO_x emisyon envanterinin belirsizlik aralığı alt sınırı %26 iken, üst sınırı %23'e ulaşmaktadır. Aynı emisyon envanteri EMEP emisyon faktörleri ile hesaplandığında envanterin belirsizlik aralığı alt sınırı %45 iken, üst sınırı %48'e ulaşmaktadır. Görüldüğü gibi, ülkeye özgü emisyon faktörlerinin kullanımı, literatürdeki emisyon faktörlerinin kullanımına göre belirsizliği yaklaşık olarak yarı yarıya düşürmektedir. Bu fark NO_x emisyon envanterinde SO_2 ve CO emisyon envanterlerine göre daha baskındır, çünkü doğal gaz yakan enerji santrallerinin sayısı fazladır (Marmara bölgesindeki 57 tesisten 48'i).

Bu çalışma ile, TNO-MACC ve EDGAR HTAP emisyon envanterlerinin Marmara Bölgesindeki enerji tesislerine ait emisyonları yansıtmakta yetersiz kaldığı kanıtlanmıştır. Genellikle enerji tesislerine ait bilgiler, envanter derleyicileri tarafından en kolay ulaşılan bilgiler arasındadır. Bu tesislere ait emisyonlarda dahi böyle büyük farkların olması, TNO-MACC ve EDGAR-HTAP emisyon envanterlerinin tamamının güvenilirliği konusunda şüpheleri güçlendirmektedir. Zaten bu durumda hava kalitesi model sonuçlarının tüm Avrupa ülkeleri arasında neden Türkiye'de ve Doğu Avrupa ülkelerinde, en kötü sonuçları verdiği de hesaplamalar yapılarak açıklanmıştır.

Ne kadar çok hava kalitesi ölçüm noktası olursa olsun, ne kadar hatasız ölçüm yapılırsa yapılsın ve ne kadar iyi performanslı modeller kullanılırsa kullanılsın, hava kalitesi modellerinin iyi bir emisyon envanteri olmadan doğru sonuçları tahmin etmesinin mümkün olmadığı açıktır. Bu nedenle, Türkiye de dahil olmak üzere Doğu Avrupa ülkeleri için tutarlı, belirsizliği düşük ve kapsamlı emisyon envanterleri oluşturulmalıdır. Ülkeye özgü emisyon faktörlerinin geliştirilmesi, emisyon envanteri hesaplarının ön basamağıdır. Bu amaçla, yapılan ölçümlere ek olarak aktivite verilerine ulaşmak kolaylaştırılmalıdır.

1. INTRODUCTION

Air pollution is defined as the presence of substances including gases, particles, and biological molecules in the air in the levels that are detrimental to human health and the planet as a whole. SO_2, O_3, PM, NO_x, Pb and CO are called as criteria air pollutants, and these are the only air pollutants with national air quality standards (NAAQS) that define allowable concentrations of these substances in ambient air [1].

Air pollution problems started to come into consideration after industrial revolution which leaded to industrialization near cities and increasing population in those areas due to rural-urban migration. Demand for more energy and natural resources are increased with increasing industrialization and population. Thus, more power plants, industrial plants are needed to fulfil needs of new strongly urbanized cities. Furthermore, residential heating and number of vehicles increased. Entire of those are the anthropogenic sources of air pollution. Therefore, air pollution has started to be one of the most important problems in industrialized and urban areas.

Air pollution significantly impacts human health. Short term air pollution is associated with sudden increases in air pollution concentrations where it causes to short-term changes in health, which have typically been associated changes in mortality, hospital or emergency room admissions, incidence, duration or exacerbations of respiratory and other symptoms, and changes in lung function indices [2]. Long term air pollution is associated with continuous and high air pollution levels which cause long term exposure to pollutants. Mortality associated with air pollution is about 15 to 20 percent higher in cities with high levels of pollution compared to relatively cleaner cities [3]-[5].

Short term or long-term air pollution depends on many factors including discharging amount of the emitting source or local meteorological conditions. Generally short-term air pollution is affected from many different factors such as sudden industrial production increases, malfunction in stack gas control equipment, industrial accidents, and high traffic load in rush hours or meteorological conditions. Short term air

pollution can grow to long term air pollution when meteorological conditions (such as inversion or calm weather conditions) are feeding short term air pollution and there is a continuous high pollutant emitting sources. Furthermore, meteorological conditions are capable of making long term pollution for instance when there is continuous long-range transport of the pollution.

Ambient particulate matter (PM) pollution is one of the priority air pollution problems and causes a wide range of diseases that lead to a significant reduction in human life as it can be suspended over long time and travel over long distances in the atmosphere [6]. The size of particles has been directly linked to their potential for causing health problems. Inhalable coarse particles have 50% passing yield from a permeable matter has 10 micrometres (μm) or less aerodynamic diameter (PM_{10}), and it is most consistently been associated with short-term health effects in mortality [3]-[4]. In the literature there are many epidemiological studies which revealed the associations between exposure to PM_{10} and increasing risk of adverse effects on human health [6]-[8]. Inhalation and penetration of PM into the lungs and bloodstream can lead to respiratory, cardiovascular, immune, neural systems problems as well as lung cancer [5].

PM_{10} is emitted into the surrounding air by anthropogenic sources such as industrial combustion, power plants, quarrying, heavy traffic, house fire burning, or in natural ways as fine dust, volcanoes, salt spray and secondary particles formed in the air due to chemical reactions. Beyond emitting from a specific source, it can be transported from a more polluted area or can be formed from chemical reactions in the atmosphere (secondary pollutants), accumulated in an area with the help of the meteorological conditions, and finally causes visible air pollution. According to Karagulian F. et al. [9], the principal sources of airborne PM_{10} in Central and Eastern Europe are domestic fuel burning (45%), unspecified source of human origin which is mostly attributed to secondary particles formed from unspecified pollution sources of human origin (26%), industrial emissions including energy production (18%), traffic emissions (8%) and natural sources such as dust and sea salt emissions (3%). According to same study, for Turkey, percent contribution of the sources to urban ambient PM_{10} concentrations are summarized as 39% from unspecified source of human origin, 29 % is from industrial sources including energy production, 16% is from traffic emissions and remining 16% is from natural sources (dust and sea salt emissions). Percent contribution of industrial

sources (including energy production) in Turkey to airborne PM_{10} is highest when compared to percent contribution of industry in all other regions of the world [9].

According to European Environment Agency (EEA) the annual limit value (the 35-day acceptable limit is 50 μg /m^3) for PM_{10} (applying from 2005) was exceeded most often in Poland, Italy, Slovakia, the Balkan region, Turkey and also in several urban regions [5]. For instance in 2013, Budapest (Hungary) experienced high levels of air pollution 76 days beyond the 35-day acceptable limits (50 μg /m^3) of EU, where Rome (Italy) had 39 days, Berlin (Germany) had 31 days, Paris (France) had 14.5 days, Pernik (Bulgaria) had 180 days beyond that target level [10][11]. According to the data obtained from Ministry of Environment and Forestry of Turkey [12], in 2018, the 35-day acceptable limit value (50 μg /m^3) was exceeded 52 days beyond the 35-day limit value in Istanbul, 137 days in Bilecik, 234 days in Bursa, 69 days in Canakkale, 98 days in Edirne, 31 days is Kirklareli, 40 days in Kocaeli, 180 days in Sakarya, 47 days in Tekirdag and 11 days in Yalova. As in other some cities in Europe, cities of Turkey also experience high number of days with daily average PM_{10} concentrations beyond the limit value. All given cities are located in Marmara region of Turkey, which is the region of Turkey considered in the upcoming parts of this study.

According to the data obtained from World Health Organization (WHO) [13], there are 418 cities over 2965 cities in the world with an average annual PM_{10} concentration more than 50 μg/m^3, and 211 of them is from China, 47 is from Iran, 44 is from Turkey, 29 is from India and 22 is from Chile. When regions of the world considered, 66 cities are from Eastern Mediterranean region, 57 cities are from Europe, 35 cities are from South-East Asia, 221 cities are from Western Pacific countries (China, Philippines, Korea, Vietnam, Mongolia), 36 cities are from America region have more than 50 μg /m^3 annual average PM_{10} concentration. Annual average PM_{10} concentration is more than 50 μg /m^3 in 56 cities of Europe and 44 cities of these are from Turkey, in 2016.

As it is clear from these statistics derived from several international organizations, PM_{10} is a global problem. At the same time, although Europe cities experience episodic PM_{10} concentrations, Turkey suffers from long term high PM_{10} concentrations in more than half of its cities. For instance, as annual average PM_{10} concentrations, Igdir ranks 106th worst among 2965 cities in the world with an annual average PM_{10} concentration as 100 μg/m^3 in 2016, where Artvin, which has the best annual average PM_{10} concentration in Turkey as 16.8 μg /m^3 in 2016 and ranks 894th best city in the world.

However, SO_2, CO and NO_x should also be taken into account when talking about air quality. In order to deal with this problem, air quality management plans are developed in all Europe, also in Turkey.

Air quality management

Air quality management refers to the all activities applied by regulatory authorities for protecting human health and the environment from the harmful effects of air pollution by a dynamic process [14]. As it is given in Figure 1.1, air quality management process starts with establishment of the acceptable level of the goals for the pollutants in the air, then followed by determination emission reductions. Emission inventories, air monitoring and air quality models are used in the decision-making process of the goals. After development of emission reduction programs, they applied via regulations and other instruments. Results of the programs are evaluated periodically by means of observations and modelling studies for checking if air quality goals are being met. All these processes are contributed by scientific studies with essential understanding of how pollutants are emitted, transported and transformed in the air and their effects on human health and the environment.
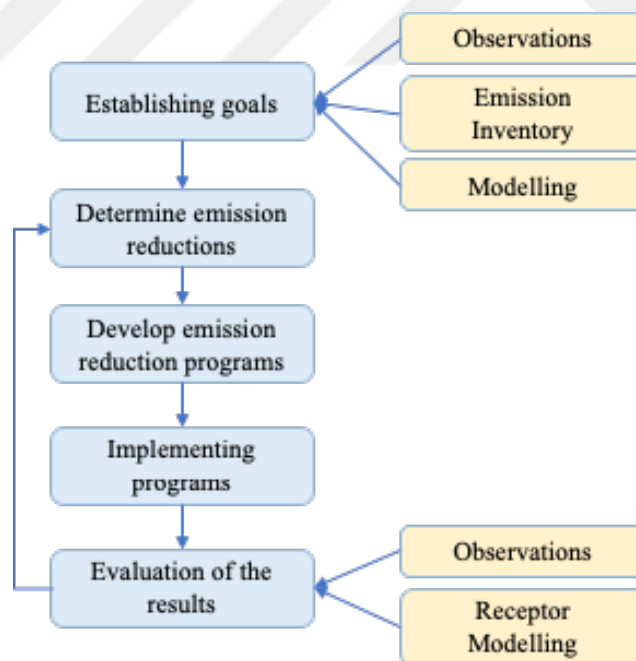
Figure 1.1 : Air quality management procedure.

Air quality monitoring

A critical component of air quality management is air quality measurements. The measurements are compared to emission standards which allow to set-up controlling

procedures when measurements are more. However, measurements give an idea of the point measured, where air quality management is considered in spatially wide locations in terms of cities, countries or regions. Number of measurement stations are vital in that point in order to ease spatial evaluation of air quality. However, setting up a dense measurement network is expensive; therefore, their spatial resolution is generally insufficient to qualify them as the real world. In Turkey there are 310 measurement station (1 station per 2527 km^2), which seems a high enough number, however it should be considered that urban environmental pollution can extremely change according to space. There are some receptor models which use statistics (such as Chemical Mass Balance - CMB - Model and Positive Matrix Factorization - PMF - Model) for concentrations in an area by using air quality measurements, however these models do not effective in large domains and generally used for source apportionment studies [15][16]. Although space measurements supply spatial coverage (not working well in cloudy areas), they also have some limitations due to its measurement technique which considers the number of particles in a column (Aerosol Optical Depth, AOD) which then makes hard distinguishing surface air quality data in the column, furthermore, temporal resolution of satellite measurements is limited [17]. Besides, air quality measurements have uncertainties due to calibration or measurement device problems. Hence, air pollution measurements give quantitative information about ambient concentration and deposition of pollutants, but they are limited in spatial and temporal coverage, therefore they are limited in identifying the causes of the air pollution problem. Air quality management requires spatial-temporally wide data, therefore there is a need for representing atmospheric composition and identify possible contribution of sources, then there is a need for air quality modelling.

Air quality modelling

Air quality modelling is a method which provides information on air quality on the basis of what we know of the emissions of chemical species, and of the atmospheric processes that lead to pollutant dispersion (meteorology), transport, chemical conversion and removal from the atmosphere by deposition [18] by representing physical and chemical processes in the atmosphere [19]. Air quality models (AQMs) are important because they integrate our understandings of the complex processes that affect the concentrations of pollutants in the atmosphere. The other important role of air quality model (AQM) is its help to design of emission control strategies that are

being developed to improve air quality [1] which has a direct impact on public health. Furthermore, by models, it is possible to quantify the contribution of an existing or planned emission source to air quality, or investigation the impact of alternative future emission scenarios on air quality, which is important for supporting air quality management. This makes air pollution models an invaluable tool in regulatory, research, and forensic applications [20]. Therefore, AQMs have been widely used in air quality management.

Large number of air quality models are developed in the literature and still research projects in this area are undertaken. Although there are several AQM classifications, in this part of study, the broad classification of Juda-Rezler K. [21] according to the basic model structure will be given here. Air quality models can be classified into two, which are nondeterministic and deterministic models. Nondeterministic models can be further divided into two groups which are statistical and physical models. The statistical model calculates concentration by statistical methods from meteorological and other parameters after the statistical relationship has been obtained empirically from measured concentrations. The physical model is one in which nature is simulated on a smaller scale in the laboratory, e.g., in a wind-tunnel. The statistical are very useful for short-term forecast of concentrations, and the physical models are of use if specific processes are being considered, e.g., influences of topography on the mean airflow. Deterministic models calculate the concentrations from an emission inventory and other independent, mostly meteorological, variables according to the solution of various equations which represent the relevant physical processes. In most cases, they use solutions of the turbulent diffusion equation derived in several ways and under different assumptions. The deterministic models are most suitable for long-term planning decisions. Deterministic models are divided into two categories which are closed form analytical models and numerical models. Closed form analytical models solve turbulent diffusion equation under a set of simplifying equations such as accepting steady state conditions and homogenous flow. Gaussian plume/puff models are closed form analytical models and due to these assumptions, they are simple, and can be applied for shorter distances ($\sim$10 km) and shorter travel times ($\sim$2 hours) with low computational cost. Numerical models are divided into two by First order-closure (K-Theory) models and Second order-closure models. First-order-closure (K-Theory) models use the gradient transfer theory (K-theory) [22], in order to solve turbulent

6

diffusion equation and those models are classified according to consideration about movement of air parcel and gridding system, which are Eularian grid, Lagrangian trajectory, hybrid Lagrangian-Eularian and Random-Walk (Monte-Carlo) trajectory systems. Numerical models are time-dependent; their structure allows space and time variations in the field of meteorological parameters, as well as the concentration field. Therefore, numerical models are capable of handling a much wider variety of air pollution problems than the analytical ones. In this study, we will focus on Eularian models, since the models included in this study are Eularian models. However, there is a need for clarifying Eularian models by comparing it with Lagrangian models.

According to Seinfeld and Pandis [19], in Lagrangian approach, an air parcel is considered and changes in the chemical composition of this air parcel is simulated as it is moved with the local wind in the atmosphere continuously. So, the model actually simulates concentrations at different locations at different times. In Lagrangian models, there is no mass exchange between the air parcel and its surroundings, with the exception of species emissions that are allowed to enter the parcel through its base. On the contrary of the first approach, Eulerian model simulates concentrations in each fixed location which is shown with an array of fixed computational cells in space. Species enter and leave each cell through its walls, and the model simulates the species concentrations at all locations (cells) as a function of time. The Eulerian description is the common way of treating heat and mass transfer phenomena. The two approaches yield different types of mathematical relationships for the species concentrations that can, ultimately, be related. Each approach has its own advantages and disadvantages. The main advantage of Lagrangian model is the simple numerical treatment of the transport term in the mass balance equation, however, the main disadvantage is neglecting exchange processes between the air parcels and wind shear which makes three dimensional Lagrangian models not very reliable [23]. In the Eularian models, numerical solution of the transport term becomes more difficult and often requires substantial computational resources to be accurate. However, the main advantage of the Eularian models is the well-defined three-dimensional formulation that is close to real-life and clearly needed for the complex air pollution problems [24]. Most commonly used Eularian, three-dimensional grid based, large scale AQMs in Europe are Community Multiscale Air Quality Model (CMAQ) [25], Weather Research and Forecasting Model coupled with Chemistry (WRF-Chem) [26], Comprehensive Air

Quality Model with Extensions (CAMx) [27], Multi-scale chemistry-transport model for atmospheric composition analysis and forecast (CHIMERE) [28], LOTOS (LOng Term Ozone Simulation)-EUROS (EURopean Operational Smog model), [29], and Danish Eulerian Hemisphere Model (DEHM) [30]. Entire of those models were used in this study.

As it was explained in this part of study, air quality modelling gives a complete picture of air quality in a zone in contrast to the limitations in the spatial coverage of air quality measurements, temporal coverage of space measurements. However, monitoring data are indispensable for inferring theories or parameters and calibrating or validating air quality simulations, because there are uncertainties in model estimates due to deficiencies in our knowledge of emissions and atmospheric processes. No matter how good the science is in an AQM, there will always be uncertainties due to data input errors and due to stochastic (turbulence) processes [31]-[34]. Hence, models don't predict exactly the real-values and this situation causes variability and uncertainties in model predictions. According to United States (U.S.) Environmental Protection Agency (EPA) [35], variability refers to the inherent heterogeneity or diversity of data in an assessment. It is a quantitative description of the range or spread of a set of values and is often expressed through statistical metrics such as variance, standard deviation, and interquartile ranges that reflect the variability of the data. Variability cannot be reduced, but it can be better characterized. Uncertainty refers to lack of knowledge regarding the true value of a fixed but unknown quantity [36]. Uncertainty can be reduced or eliminated with more or better data [35].

Uncertainties in AQM estimates

According to Fox D.G. [32] there are two types of uncertainties in AQM estimates, inherent uncertainty and reducible uncertainty. Inherent uncertainty results from the basic stochastic nature of the turbulent atmospheric motions that are responsible for transport and diffusion of released materials. Reducible uncertainty (error) results from improper or inadequate meteorological and air quality data inputs, and from inadequacies in the models. Therefore, the inherent uncertainty can be considered as variability [37]. Total model uncertainty is a sum of data errors, model errors and stochastic uncertainty. Data errors and model errors belongs to reducible uncertainty.

The AQM, especially Chemical Transport Model (CTM), prediction represents an ensemble mean over the entire grid volume. The CTM prediction differs from a point observation because of four primary considerations: 1) inherent or stochastic variability in the observations, 2) errors in model physics and chemistry assumptions, 3) errors due to uncertainties in model input variables, and 4) numerical errors [36]. Those differences cause uncertainties in model outputs. Among these sources, emissions are regarded to have the largest levels of uncertainty [38 - 42].

Errors due to uncertainties in model input variables is the one, that might influence the predictions in Eastern Europe due to uncertain inputs from Eastern Europe countries where quality of emission inventories are low, therefore this study focuses on quantifying the uncertainty AQM estimates due to emission inventories. A certain emission inventory is a path to a more certain air quality prediction. The development of a consistent procedure for the uncertainty evaluation is still a challenge for the scientific community.

Several studies were conducted for different aspects of uncertainty issues in AQMs. The first set of studies is related to integration of measurement uncertainty to model evaluation. Since calculation of measurement uncertainties have strict and complex guidelines [43], there were some attributes to calculate uncertainties of measurements by using output of the models. Thunis et al. [43] and Pernigotti D. et. al. [44] proposed performance criteria to evaluate AQMs for O_3, PM_{10} and NO_2 based on measurement uncertainty. Thunis et al. [45] proposal is based on the root mean square error between measured and modelled concentrations divided by the measurement uncertainty, the measurement uncertainty was assumed to remain constant regardless of the concentration level. Then Thunis et al. [43] improved former model by quantifying all possible sources of uncertainty for the particular case of O_3. Based on these uncertainty source quantifications, a simple relationship is proposed to formulate the measurement uncertainty which is then used to update the former approach and modes performance criteria proposed in Thunis et al. [43] with more accurate values. In the paper of Pernigotti D. et. al. [44], the same approach is applied for NO_2 and PM_{10}, but using different techniques for the uncertainty estimation.

The second set of studies is related with the evaluation of uncertainties originated from emission inventories which is close to the subject of this thesis. Napelenok S. L. et al. [46] presented a method and applied for evaluating an AQM's changes in pollutant

concentrations stemming from changes in emissions while explicitly accounting for the uncertainties in the base emission inventory. Specifically, the CMAQ model is evaluated for its ability to simulate the change in ozone (O_3) levels in response to significant reductions in NO_x emissions. The dynamic model evaluation (i.e., the evaluation of a model's ability to predict changes in pollutant levels given changes in emissions) differs from previous approaches by explicitly accounting for known uncertainties in the NOx emissions inventories. Uncertainty in three sectors of NOx emissions is considered – area sources, mobile sources, and point sources – and is propagated using sensitivity coefficients calculated by the decoupled direct method in three dimensions (DDM-3D). The change in O_3 levels between 2002 and 2005 is estimated based on differences in the empirical distributions of the modelled and observed data during the two years. Results indicate that the CMAQ model is able to reproduce the observed change in daily maximum 8-hr average O_3 levels at more than two-thirds of air quality monitoring locations when a relatively moderate amount of uncertainty (50%) is assumed in area and mobile emissions of NOx together with a low amount of uncertainty (3%) in the utility sector (elevated point sources) emissions. The impact of other sources of uncertainty in the model is also briefly explored.

Some other studies assessed uncertainty in local scale air quality modelling application by applying the procedures for some case studies. Sax T. and Isakov V. [47] established uncertainty analysis techniques to demonstrate a general method for assessing variability and uncertainty in Gaussian air pollutant dispersion modelling systems. To illustrate this method, they estimated variability and uncertainty in predicted hexavalent chromium concentrations generated by welding operations at a shipbuilding and repair facility in California. Using Monte Carlo statistical techniques, they propagated uncertainty across both ISCST3 and AERMOD, and estimated the contribution of variability and uncertainty from four model components: emissions, spatial and temporal allocation of emissions, model parameters, and meteorology.

A framework to estimate the uncertainty of AQMs due to the uncertainties in input parameters has been established by previous research work. Most of the research work has used Monte Carlo simulations with randomly sampled model inputs according to their probability distributions and then quantified the uncertainties of model outputs (e.g. pollutant concentrations and sensitivities) by using the ensemble outputs obtained from the Monte Carlo simulations [48]-[50]. However there are also analytical

methods for quantifying uncertainty as discussed in the studies of Hanna [36], Rao S.K. [37].

The quality of an emission inventory that will be used in air quality modelling is associated with its low-level uncertainty and adequate coverage of the sources. Due to transboundary structure of air pollution, there is a need for standardized delivery of the emissions in order to ease evaluating all countries emission inventories in one pot. In the literature there are several wide-coverage emission inventories which are reported by many countries and regions in different platforms. Each inventory has different uncertainty levels, which shows the quality of the inventories and they are presented in various formats. Although uncertainty of an emission inventory affects uncertainty of an AQM, it is calculated in a different way than uncertainty of AQM estimates.

In this part of the study, most commonly used and readily available emission inventories for air quality modelling are summarized. Although there are several emission inventories in the literature calculated by governments, non-governmental organizations, companies or scientists for some countries or for specific cities, only worldwide known and commonly used emission inventories are summarized here.

EMEP Emission inventory

The first international treaty to deal with air pollution is Convention on Long-range Transboundary Air Pollution (CLRTAP) was signed by in 1979 in order to reduce the amount of air pollutants destroying forests, causing fish loss in lakes and putting entire ecosystems at risks in the Northern Hemisphere, which is identified as 'acid rain' problem [51], by the organization of the United Nations Economic Commission for Europe (UNECE, founded in 1947). Over the years, the number of substances covered by the Convention and its protocols has been gradually extended, notably to ground-level ozone (O_3), POPs, heavy metals and PM. Due to the transboundary structure of air pollutants, the treaty was signed by 32 countries in 1979, now has 51 Parties [52]. The co-operative programme for monitoring and evaluation of the long-range transmission of air pollutants in Europe, unofficially European Monitoring and Evaluation Programme (EMEP), is a scientifically based and policy driven programme under the CLRTAP for international co-operation to solve transboundary air pollution problems. Centre on Emission Inventories and Projections (CEIP) is one of the five EMEP centres. Emission inventories are prepared annually by the parties (signatory countries) of CLRTAP for main pollutants (NO_x, NMVOCs, SO_x, NH_3, CO) and

particulate matter ($PM_{2.5}$, PM_{10}, PM_{coarse}), heavy metals (Pb, Cd, Hg) and POPS, (Benzo(a)pyrene, Benzo(b)fluoranthene, Benzo(k)fluoranthene, Indeno (1,2,3-cd) pyrene, Total polycyclic aromatic hydrocarbons, Dioxin and Furan, Hexachlorobenzene, Polychlorinated biphenyls) under the Convention and submitted to CEIP (available online from CEIP website [53]). Those emission inventories are prepared officially according to the EMEP technical guidelines [54]. Gridded emissions are also publicly available for AQM purposes.

Sectors covered in EMEP emission inventory are energy (combustion in energy, manufacturing industries, road and non-road sources), fugitive emissions from fuels, industrial processes and product use (mineral products, chemical industry, metal production, solvent and product use, other industry production including pulp and paper, food and averages industries, wood processing, production and consumption of persistent organic pollutants (POPs), and bulk products' consumption, storage transportation and handling processes), agriculture, waste (waste treatment operations, waste incineration, open burning etc.), natural and other sources.

IPCC Emission inventory

The United Nations Framework Convention on Climate Change (UNFCCC) collects emission inventories supplied by the signatory countries of the convention. Gridded emission inventories are prepared for specific years and emissions are spatially distributed over the region of interest in order to use in AQMs. The regions are divided into grids and emissions are distributed into those grids by using a mapping background with special algorithms.

According to Intergovernmental Panel on Climate Change (IPCC) emission inventory guidelines [55], the gases have global warming potentials, CO_2, CH_4, N_2O, Hydrofluorocarbons (HFCs), Perfluorocarbons (PFCs), Sulphur hexafluoride (SF_6) and halocarbons covered in Montreal protocol and some other listed halocarbons are included in IPCC emission inventory. Furthermore precursors, NO_x, NH_3, NMVOC and SO_2 are also reported in IPCC inventories. Greenhouse gas emission and removal estimates are divided into main sectors, which are groupings of related processes, sources and sinks: energy, industrial processes and product use, agriculture, forestry and other land use, waste and other (e.g., indirect emissions from nitrogen deposition from non-agriculture sources). Each sector comprises its own individual categories (e.g., transport sector comprises cars and motorcycles subsectors). Ultimately,

countries construct an inventory from the sub-category level because this is how IPCC methodologies are set out, and total emissions calculated by summation. A national total is calculated by summing up emissions and removals for each gas. IPCC emission inventory doesn't include all emissions required for air quality modelling purposes (such as particulates) however it is a valuable source for global climate change models.

EDGAR Emission inventory

Emissions Database for Global Atmospheric Research (EDGAR) emission inventory is being calculated since 1996 by contributions of several institutions. The latest emission dataset released as EDGAR v.4.3.1 was prepared in January 2016 [56]. EDGAR v.4. is a bottom-up emissions database based on European Joint Research Centre's (JRC) evaluation of internationally reported activity data (i.e. fuel use, land-use, quantity of industrial products, number of animals), and worldwide consistent assumptions on emission factors (EFs) associated with these activities for each technology and corrected for end-of-pipe abatement measures. The resulting sector-specific emission trends are publicly available as country totals or on a 0.1°x0.1° grid.

EDGAR-HTAP emission inventory

Hemispheric Transport of Air Pollution (HTAP), or The Task Force on Hemispheric Transport of Air Pollution (TF HTAP), is an international scientific cooperative was organized in 2005 under the auspices of the UNECE Long Range Transboundary Air Pollution (LRTAP) Convention (or CLRTAP) and reports to the Convention's EMEP Steering Body.

On request of the European Commission's (EC) the Directorate-General for Environment (DG ENV, responsible for EU policy on the environment in EC), JRC, together with a number of international organizations including U.S. EPA, compiled a harmonized global, gridded, air pollution emission dataset for 2000 to 2005 (to the extent possible) by using officially reported inventories at the national scale and complemented with science based inventories where nationally reported data were not available [57], for 10 aggregated sectors and on a global 0.1°×0.1 ° resolutions [58], for CH_4, CO, NO_x, NMVOC, NH_3, SO_2, $PM_{2.5}$, PM_{10}, organic carbon (OC), black carbon (BC). The sectors are for all substances defined as follows: international and domestic air, international shipping, power industry, manufacturing, mining, metal, cement, chemical, solvent industry, ground transport (including road, rail, pipeline,

inland waterways), heating/cooling of buildings and equipment/lighting of buildings and waste treatment. For NH_3 there is in addition sector, which is agriculture, but not agricultural waste burning.

Contributing international organizations are U.S. EPA, the EPA and Environment Canada (for Canada), EMEP and Netherlands Organisation for Applied Scientific Research (TNO) for Europe, and the Model Intercomparison Study for Asia (MICS-Asia III) for China, India and other Asian countries.

JRC's team in charge of the EDGAR named the resulting inventory, EDGAR-HTAP, which is a globally consistent inventory. A separate 0.5º×0.5º gridded dataset is available from the U.S. EPA [59], for the years 2002 and 2005, complementary to the data in EDGAR-HTAP, providing additional details in sectoral, spatial and temporal resolution than EDGAR-HTAP.

EDGAR-HTAP_V1 was prepared for 2000-2005 time period (but not recommended as consistent time series), for all world countries by covering emission sources including all human activities except Savannah burning, forest burning and diffusive sources such as pave and construction dust. The HTAP_V2 dataset consists of 0.1ºx0.1º grid maps for the years 2008 and 2010. The grid maps are complemented with EDGARv4.3 data for those regions where data are absent. The HTAP_v2.2 [60] air pollutant grid maps are considered to combine latest available regional information within a complete global data set. The disaggregation by sectors, high spatial and temporal resolution and detailed information on the data sources and references used will provide the user the required transparency. Because HTAP_v2.2 contains primarily official and/or widely used regional emission grid maps, it can be recommended as a global baseline emission inventory, which is regionally accepted as a reference and from which different scenarios assessing emission reduction policies at a global scale could start.

EDGAR-HTAP emission inventory is available from different platforms including EDGAR website [61], Edgar On Line Open Access (EOLO) system [62], Emissions of atmospheric Compounds and Compilation of Ancillary Data (ECCAD) Server [63] which is also Global Emission InitiAtive database (GEIA) and GEIA web site [64]. There was also Community Initiative for Emissions Research and Applications (CIERA) platform but now it is fully integrated with GEIA.

TNO - MACC emission inventory

Emission inventories are prepared by bottom-up approach and the use of official inventories often required when using regional chemical-transport modelling in policy studies. TNO inventory is a complete, consistent and spatially distributed inventory, which has used the official reported emissions as basis where possible [65]. Monitoring Atmospheric Composition and Climate (MACC) is a project of TNO and the standard MACC inventory covers Eastern Europe including Turkey and Russia; however, it does not cover North Africa. It is not publicly available, required information is available in ECCAD website [66].

TNO gridded emission inventory is prepared for CO, CH_4, NOx, NMVOC, SO_2, NH_3, $PM_{2.5}$, PM_{10} and CH_4 for the sectors non-industrial combustion, energy industry, industries, fossil fuel production and distribution, solvent and other product use, road transportation (exhaust gasoline, exhaust diesel, exhaust LPG and natural gas, gasoline evaporation, tyre, brake and road wear), non-road transportation, agriculture and waste.

MACC-II is emission inventory of TNO developed in second phase of MACC Project (TNO-MACCII), which is the most updated version of this gridded emissions are mainly taken from EMEP emission inventories, the gaps are filled with the data from GAINS model [67]. The GAINS model combines information on economic and energy development, emission control potentials and costs, atmospheric dispersion characteristics and environmental sensitivities towards air pollution [68] and by using these statistics built up a bottom-up inventory. Missing CO emissions were taken from EDGAR-HTAP emission inventory [60] and TREMOVE model [69] for disaggregate the energy use to detailed vehicle classes technologies for each country. Since this bottom-up inventory was originally only developed for the year 2005, emissions for the other years were estimated by scaling this inventory. Scaling factors for the different years were calculated from the EDGAR emission inventory v4.2 [70] which provides sector-specific annual emission estimates for CO for each country in the world. For the countries which did not report emissions such as Armenia, Azerbaijan and Georgia, EDGAR [70] data were used at SNAP (Selected Nomenclature for Air Pollution) level 1, which is energy industries sector, for all pollutants and all years. These were disaggregated to the same subcategories as the other countries by using

the relative contribution of each subsector to the SNAP level 1 sector for Turkey (for each pollutant and each year) as a blueprint.

Since both TNO-MACC and EDGAR-HTAP [60] emission inventories have been prepared for the European continent, they are approximately same over the common part of EU. Some discrepancies, e.g., in the emissions from ships, might exist among the two inventories [71]. Furthermore, they differ for regions outside European borders, such as North Africa. EDGAR-HTAP [60] emission inventory also covers Asia, Africa and Russia. Both inventories include emissions of Turkey.

Emissions of public electricity and heat production sector of Turkey

According to National Emission Inventory report (NIR) [72] and Informative Inventory Report (IIR) [73] of Turkey, public electricity and heat production sector is responsible from 65.1% of SO_2, 42.5% of CO_2 and 42.7% of NO_x emissions of Turkey. Given that public electricity and heat production sector makes high proportion of the national total. According to Turkish Statistical Institute (TurkStat), electricity is generated mainly from coal and natural gas in 2016 as it is given in Figure 1.2, which shows that fossil fuels are used as energy source in vast majority of the electricity generated in Turkey .
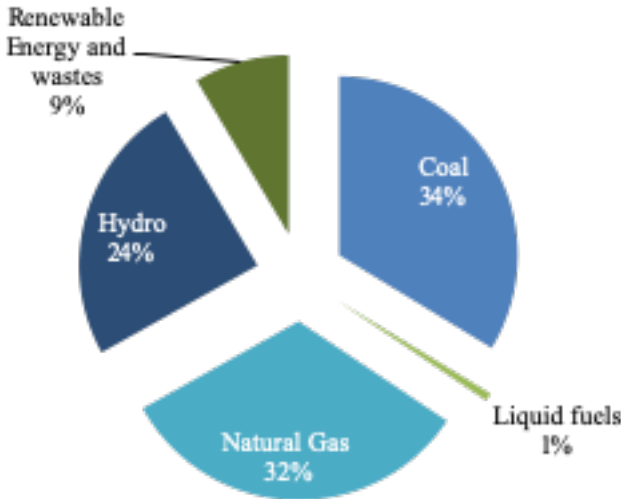
Figure 1.2 : Electricity generation shares by energy sources in Turkey in 2016.

Producing energy from fossil fuels involves the combustion of fuels like coal, gas, and oil, and fossil fuels combustion is one of the important sources of air pollution [19], which means that the contribution of public electricity and heat production sector's emissions to the anthropogenic emission inventory of Turkey is large. Therefore,

uncertainty in the emission inventory of public electricity and heat production sector contributes greatly to the uncertainty of the overall emissions inventory. For this reason, it is important to create a low-uncertainty emission inventory for this sector in terms of its contribution to the total value.

1.1 Purpose and Importance of the Thesis

Uncertainty refers to lack of knowledge regarding the true value of a quantity. It can be reduced or eliminated with more or better data, where variability cannot be reduced. Among the reasons of uncertainty, inputs are regarded to have the largest levels of uncertainty. The aim of this study is to evaluate and quantify the contribution of uncertainties in input dataset to AQM estimates, which belongs to data errors part of uncertainty. For this purpose, it is necessary to define the problem that poor performance of the model is caused mostly by unfit data.

In literature, models perform poor in the Eastern European countries. However, a more detailed study is needed to say that this poor performance is mostly due to model inputs, because, the poor performance of the models may also have other reasons. In the first part of this study, inter-model variability is defined quantitatively by participating in an international AQMEII-3 project. In the second part of the study, contribution of uncertainties to this problem is quantified by being part of a national project (KAMAG).

Thanks to the multi-national AQMEII-3 project that this study contributed, European continent has been studied by many models. 12 modelling groups were cooperated from different countries of Europe and conducted 18 model runs on Europe domain (covers 34 Europe countries) for 2010 by using 7 different AQMs, 3 meteorology models and 2 emission inventories in AQMEII-3 project. This study, for the first time in Turkey, contributed to AQMEII-3 which is organized by the joint leading of U.S. EPA and European JRC. In AQMEII-3, mostly, two separate versions of the emission inventory used in all models as one of the important inputs. In this case, if all models have poor performance in a region, it can be scientifically revealed that this is due to bad input data.

The subject of this thesis, which is uncertainty assessment of AQMs due to emission inventories which is an important input of AQMs, is under development in air quality

science. Quality of an emission inventory that will be used in air quality modelling is associated with its low-level uncertainty and adequate coverage of the sources. In the second part of this thesis, a sample inventory is developed in order to reveal contribution of data uncertainty to poor performance of the models. By calculating this reducible uncertainty in the model results, it is aimed that air quality models will perform better especially in Eastern European countries with better quality inputs.

Up to now, there are several air quality modelling studies for Turkey, however they are developed for a specific city or region of Turkey, for a timescale starting from days to a few months, by using just one type of AQM. Thanks to its wide coverage domain and multi-model contributions, this study looks to the problem from the large perspective in order to define the problem and recommends a solution by representing a sample of the solution. This will give a unique way for such an analysis which has not been conducted yet. This study applies a probabilistic variability and uncertainty estimation technique in order to quantify random errors and biases in EFs and emission inventories. Especially Monte Carlo and Bootstrap techniques are used first time in Turkey for such an analysis.

1.2 Objectives

In order achieve the purpose of this study, following steps were applied in order to quantify uncertainty due to input of AQMs;

1. A comparative quantitative assessment of AQM performances throughout Europe and Turkey withing the context of AQMEII-3 activity
   - Intra-seasonal and inter-model performance evaluation for countries in Europe for 2010,
   - Comparison of Eastern and Western Europe countries in terms of model performance metrics,
   - Inter-model comparison of the model predictions over Turkey (especially Marmara region) with European countries,
   - Discuss reasons of poor performing models over regions of Turkey by comparing other countries of Europe,
2. Estimation of country specific EFs
   - Developing country specific EFs from both in-situ measurements and emission measurement reports for public electricity and heat

production sector of Turkey by considering the plants in Marmara region.

- Quantify variability and uncertainty in those EFs by Monte Carlo and Bootstrap approaches.

- Comparing both EFs with EMEP and EPA EFs.

3. Development of a probabilistic emission inventory

- Development of a probabilistic emission inventory by using country specific EFs for public electricity and heat production sector of Turkey by considering the plants in Marmara region.

- Development of the same emission inventory with the EFs of EMEP and EPA.

- Comparison of sample emission inventory with EDGAR-HTAP and TNO-MACC emission inventories which are most commonly used emission inventories by air quality modelers.

- Quantifying contribution of newly developed emission inventories

- Discussing contribution emission inventories to uncertatinties to AQM predictions.

It is aimed to contribute to scientific community with the results of this thesis. The result can reveal the negative impact of uncertain emission inventories on AQM predictions. We hope that this study will encourage the air quality community to improve the quality of the emission inventories.

2. DATA AND METHODOLOGY

In this study, first of all an inter-model comparison study is conducted within the context of an international project. Then, performances of the models were evaluated for Europe, Turkey and Marmara region, which required to compile a sample probabilistic emission inventory for Marmara region of Turkey for public electricity and heat production sector by developing specific EFs and using the data obtained via a national project that this study also contributed.

2.1 Air Quality Modelling

This study benefits from a collaborative project of European JRC. The name of the project is Air Quality Modelling Evaluation International Initiative (AQMEII) which has volunteer contributors from the worldwide scientific community. AQMEII aims at promoting research on regional AQM evaluation across the European and North American atmospheric modelling communities, through the exchange of information on practices, the realization of inter-community activities and the identification of research priorities, keeping focus in policy needs [75]. This study contributed to Phase 3 of AQMEII project (from this point it will be called as AQMEII-3). The goals of the AQMEII-3 activity are to evaluate and compare global and regional modelling systems driven by consistent emissions over North America and Europe against a common set of measurements and to perform model evaluation analyses on global models coordinated with the analyses of regional models being performed under the AQMEII. Although AQMEII-3 was conducted for both North America and Europe domains, our group contributed European part of the study. Names and model configurations of the AQMEII-3 project contributors are given in Table 2.1 for European part of the study.

In AQMEII-3, there were 12 modelling groups (from 9 countries in Europe), including our group, contributing AQMEII-3 project's European domain simulations, which resulted 18 model runs. This study has a chance to use results of entire of those models via web-based ENSEMBLE [76] platform of JRC for evaluating atmospheric chemistry transport and dispersion models. Platform is open for AQMEII-3 project

contributors and closed for public use. The remining data provided in Figure 2.1 are explained in Chapter 2.1.3 .

Table 2.1 : Main modelling properties of modelling groups in AQMEII-3 project.

Group ID	Institute	Country	Meteorology Model	Air Quality Model	Emission Inventory	System ID
FI1	Finnish Meteorological Institute	Finland	Direct interpolation from ECMWF	SILAM v5.4 [78]	TNO MACC [66]	ECMWF-SILAM_M
FI1	Finnish Meteorological Institute	Finland	Direct interpolation from ECMWF	SILAM v5.4 [78]	EDGAR HTAP v2.2 [60]	ECMWF-SILAM_H
NL1	TNO	Netherlands	Direct interpolation from ECMWF	LOTOS-EUROS v1.0.1 [79]	TNO MACC [66]	LOTOS-EUROS
FRES1	INERIS and CIEMAT	France and Spain	Direct interpolation from ECMWF IFS	CHIMERE (v2013) [28]	EDGAR HTAP v2.2 [60] / TNO MACC [66]	ECMWF-CHIMERE
IT2	University of L'Aquila	Italy	WRF	WRF-Chem v3.6	TNO MACC [66]	WRF–WRF-Chem1
ES1	University of Murcia	Spain	WRF	WRF-Chem	TNO MACC [66]	WRF–WRF-Chem2
IT1	Ricerca Sistema Energetico	Italy	WRF	CAMx v6.10 [80]	TNO MACC [66]	WRF-CAMx
DK1	Aarhus University	Denmark	WRF	DEHM [81]	EDGAR HTAP v2.2 [60]	WRF-DEHM
TR1	Istanbul Technical University	Turkey	WRF	CMAQ v4.7.1 [25]	TNO MACC [66] / EDGAR HTAP v2.2 [60]	WRF-CMAQ1
UK2	Ricardo Energy & Environment (Ricardo E&E)	England	WRF v3.5.1	CMAQ v5.0.2 [25 82]	TNO MACC [66]	WRF-CMAQ2
UK3	University of Hertfordshire	England	WRF v3.4.1	CMAQ v5.0.2 [25 82]	TNO MACC [66]	WRF-CMAQ3
UK1	Kings College	England	WRF	CMAQ v5.0.2 [25 82]	TNO MACC [66]/ EDGAR HTAP v2.2 [60]	WRF-CMAQ4
DE1	Helmholtz-Zentrum Geesthacht	Germany	COSMO-CLM (CCLM) v4.8 [77]	CMAQ v5.0.1 [25 82]	EDGAR HTAP v2.2 [60]	CCLM-CMAQ

2.1.1 Domain

The domain that is used in model runs is as follows; North American Common Analysis Domain (130°W <-> 59.5°W, 23.5°N <-> 58.5°N) and European Common Analysis Domain (30°W <-> 60°E, 25°N <-> 70°N). Our group is running only European domain with 30 km resolution. The domain is given in Figure 2.1.

Figure 2.1 : Domain of the study.

The red one shows simulation grid and blue is the output grid of the models with Lambert conformal projection. After running models in red domain, the emissions data is prepared according to blue grid, and uploaded to the ENSEMBLE system of JRC. Although the simulation grid is the red one, contributors asked to prepare their data in blue grid, because of a need for a standardized gridding system in model comparisons. Parts of the output grid are outside of the simulation grid was filled with NaN values.

2.1.2 Data

AQMs require meteorology, emissions and boundary conditions data as an input for calculation of the emissions [18]. Furthermore, emission inventory development requires a wide range of the data about emission sources. Input data types and sources are explained in this part of study.

2.1.2.1 Meteorological data

AQM requires meteorological inputs which are produced by meteorology models. Also, meteorology models require meteorological data in order to produce meteorological outputs (detailed description of the meteorological modelling

approaches used in this study is in Section 2.1.3.1). In this part of study, input data of meteorological models used in AQMEI-3 project is described.

Our group used WRF meteorology model as indicated in Table 2.1. Input data of WRF model, which is ERA-Interim, was obtained from European Centre for Medium Range Weather Forecasts (ECMWF) for 2010 for our domain. ECMWF Re-analysis (ERA-Interim) is a reanalysis data of the global atmosphere covering the data-rich period since 1979 (originally, ERA-Interim ran from 1989, but the 10-year extension for 1979-1988 was produced in 2011) and continuing in real time [83]. Reanalysis data is produced by both of observations and models in order to develop a comprehensive record of how weather and climate are changing over time [83].

The ERA-Interim data assimilation and forecast suite produces four analyses per day, at 00, 06, 12 and 18 UTC (coordinated universal time); two 10-day forecasts per day, initialized from analyses at 00 and 12 UTC. The data is downloaded monthly in the gridded binary data (GRIB) format. GRIB is a format of World Meteorological Organization (WMO) for gridded data. GRIB is used by the operational meteorological centres for storage and the exchange of gridded fields.

The data includes, but not limited to temperature and dewpoint temperature at 2 meters, U and V wind components at 10 meters, albedo, boundary layer height and dissipation, radiation and available energy types, precipitation, snowfall, surface stresses, evaporation, surface roughness, cloud cover, ice-skin-soil temperatures according to layers, moisture flux, sensible heat flux, runoff, sea-ice area fraction, sea surface temperature, snowfall, snowmelt, sunshine duration, latent heat flux, solar radiation, thermal radiation, surface pressure, total column cloud ice water and liquid water, total column ozone, water and water vapor, vertical integrals of fluxes, energy and masses, ozone and volumetric soil water layers [84].

National Centres for Environmental Prediction (NCEP) Final (FNL) analyses data [85], on 1-degree by 1-degree grids prepared for every six hours, were used as an input to WRF model by our group. The analyses are available on the surface, at 26 mandatory (and other pressure) levels from 1000 millibars to 10 millibars, in the surface boundary layer and at some sigma layers, the tropopause and a few others. Parameters include surface pressure, sea level pressure, geopotential height, temperature, sea surface temperature, soil values, ice cover, relative humidity, u- and

v- winds, vertical motion, vorticity and ozone. The NCEP Global Forecast System (GFS) [86] is a global spectral data assimilation and forecast model system giving 6 hourly atmospheric variables at 26 levels with a resolution of 0.25 degree. NCEP GFS data was used by UK1 and UK2. ECMWF data was used by remaining groups.

According to Table 2.1, FRES1 group run AQM with meteorology provided ECMWF Integrated Forecasting System (IFS). In ECMWF IFS, atmospheric composition (greenhouse gases, aerosols, and chemical species) is modelled by the horizontal resolution of ~40 km and the data available in 3-hour intervals [87]. Other groups extracted meteorological inputs of AQM from the ECMWF operational archives as of our group.

2.1.2.2 Chemical boundary conditions

In AQMEII-3 project all groups used same chemical boundary conditions. CO, CH_4, SO_2, NO_x, NMVOC, organic matter, black carbon, sulphate and dust emissions at the boundaries of the domain were supplied by the Composition-Integrated Forecast System (C-IFS) model of ECMWF as it was explained by Flemming et. al. [88].

2.1.2.3 Emission inventory of the models

In this part of study, emission inventories which were used by modelling groups of AQMEII-3 project were explained for anthropogenic, biogenic, lightning and volcanic emissions. Furthermore, conversion methodology of annual and country-based emission inventories to hourly and gridded AQM inputs is summarized. Participating groups are expected to calculate emissions from biogenic and natural sources (e.g. sea salt, windblown dust) directly in their own model since these emissions are dependent on the simulated meteorology.

Anthropogenic emissions

There are two wide coverage emission inventories which are commonly used by air quality modelling groups, which are TNO-MACC and EDGAR-HTAP emission inventories. In AQMEII-3, mainly these two emission inventories were used either independently or in combination with the other one.

According to Table 2.1, EDGAR - HTAPv2.2 emission inventory [60] was used primarily by FI1, DK1 and DE1 groups. FRES1 primarily used EDGAR-HTAP emission inventory and then used TNO-MACC emission inventory in order to fill

gaps. On the contrary of this, TR1 (our group) and UK1 used TNO-MACC emission inventory primarily, then used EDGAR-HTAP emission inventory in order to fill gaps. Other groups used TNO-MACC emission inventory solely as anthropogenic emission input of AQMs.

TNO-MACC and EDGAR-HTAP emission inventories cover common part of EU, however EDGAR-HTAP emission inventory also covers regions outside EU borders. There are also differences within two inventories, for instance in the ship emissions. Detailed information on these two emission inventories were given in Section 1. Also, energy part of these two emission inventories are discussed detailly in the emission inventory part of this study.

Anthropogenic emissions used by AQMEII-3 groups are presented quarterly in Figure 2.2 for all domain by Box and Whisker plots, in order to show overall patterns of emissions for each modelling group by visualising the range and other characteristics of emissions for such a large group in a simple figure. In Figure 2.2, PM_{10} emissions of AQMEII-3 groups are accumulated per km^2 for quarter one (Q1) of 2010. Q1 comprises January, February and March of year 2010. Only six groups supplied emission data, therefore box plots of other groups are not existing in Figure 2.2.

According to Figure 2.2, the average of grid-based emissions ranges from 15 kg/km^2 (UK3) to 800 kg/km^2 (NL1) for all domain. The average of the emissions used in our model (TR1) is 120 kg/km^2. The average emission of all models is 360 kg/km^2. The maximum emissions are between 8,000 kg/km^2 (UK3) and 50,000 kg/km^2 (FI1_MACC). The average of maximum emissions is 26,000 kg/km^2. The emissions used by our group (TR1) are maximum 30,000 kg/km^2 in a grid.

FI1 group conducted two model runs, one is with EDGAR-HTAP emission inventory which is shown as "FI1_HTAP_bas", and the other one is with TNO-MACC emission inventory which is shown as "FI1_HTAP_bas2" in Figure 2.2. The box plot of FI1_HTAP_bas and FI1_HTAP_bas2 have close mean, max values and upper percentiles and only lower percentiles differ, which indirectly shows that EDGAR-HTAP and TNO-MACC emission inventories are almost close to each other in Europe domain.
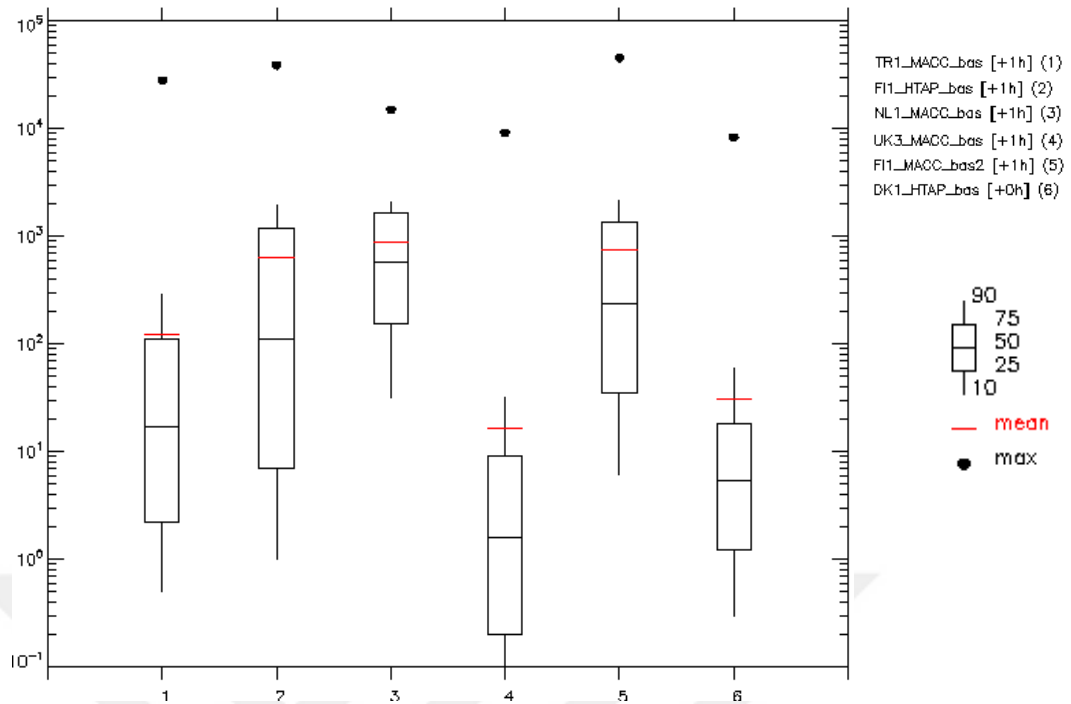
Figure 2.2 : Quarterly integrated Box and Whisker plots of PM$_{10}$ emissions used by AQMEII groups for Q1.

In Figure 2.2, our group (TR1_MACC_bas) is shown in the first left box. TNO-MACC emission inventory was primarily used by our group and EDGAR-HTAP emission inventory was used in order to fill gaps. Since our group's box plot, median and mean is lower than second (FI1_HTAP_bas), third (NL1_MACC_bas) and fifth (FI1_MACC_bas2) groups, our emission range is lower than those groups. However, our group's emissions range is higher than fourth (UK3_MACC_bas) group.

Box plot of third group (NL1_MACC_bas) is comparatively tighter than other groups, and its mean and median is generally higher than other groups. Therefore, third group generally used high emissions when compared to other groups. Furthermore, mean emissions of second (FI1_HTAP_bas) and fifth (FI1_MACC_bas2) groups have almost same with third group for each quarter however they don't have such high range of emissions as in third group since their inter-quartile ranges (middle 50% of the emissions) are too large comparatively.

The differences between box plots of groups that use the same emission inventory, (as in between FI1_HTAP_bas and DK1_HTAP_bas) is due to different approaches adopted by each AQMEII-3 group for spatial and temporal distribution of the anthropogenic emissions.

When other quarters investigated, compared median, mean and maximum values in box plots showed that, fourth group (UK3_MACC_bas) often has lowest range of emissions when compared to other groups. Other quarters plots are not given in here.

Distribution of emissions in TR1 model (our group) is given in Figure 2.3. This plot was created via ENSEMBLE system [76].

According to Figure 2.3, PM_{10} emissions are about 10 to 100 kg/km^2 in Central and Eastern Europe and also big cities make hotspots in the remaining countries in Q3 (comprises Summer months which are July, August and September). For instance, hotspots are located in Teheran, Isfahan, cities around Basra Bay, and in the marine passenger and freight transport route between the ports in Egypt, Tunisia and Spain. In Turkey, hotspots are mostly located in big cities of Western part. It is about 0.01 to 1 kg/km^2 in Scandinavian countries and in the Northern parts of Russia (above Moscow).
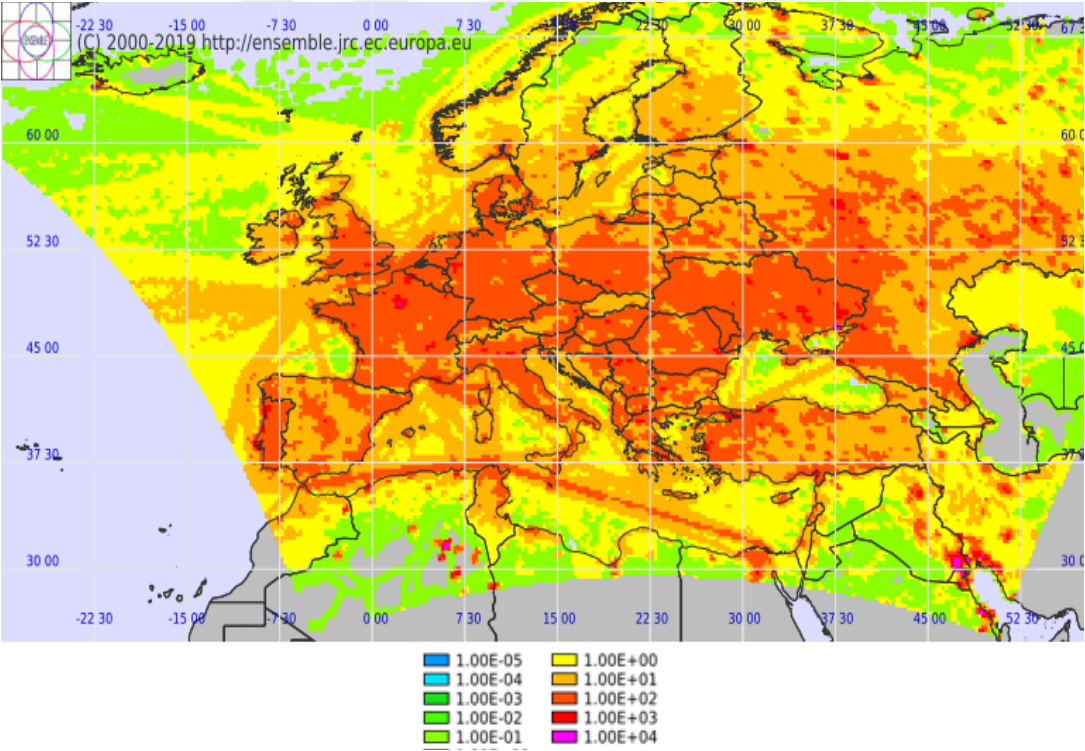
Figure 2.3 : Quarterly accumulated PM_{10} emissions in kg/km^2 used by TR1 (our group) for Q3 of 2010 [76].

Biogenic emissions

Since several meteorological models were used by modelling groups and biogenic emissions are dependent on meteorological conditions, they were specifically calculated by each group of AQMEII-3 for the year 2010.

TR1 (our group), FRES1, IT1, DK1, UK2 and UK3 calculated biogenic emissions through the Model of Emissions of Gases and Aerosols from Nature (MEGAN) model [89] where UK1, DE1 calculated biogenic emissions using the BEIS (Biogenic Emission Inventory System version 3) by implementing in SMOKE v2.6 [90] or by implementing directly into CMAQ. FI1 calculated biogenic emissions as in Poupkou et al. [91], and NL1 used the approach described in Beltman et al. [92].

Lightning and volcanic emissions

Lightning and volcanic emissions were not included in emission inventories since there were no robust methods that can be applied by all groups for calculation of lightning and volcanic emissions.

Wildfire and mineral dust emissions

Wildfire emissions are calculated with IS4FIRES Model and mineral dust emissions are calculated with WRF-Chem (available from the previous phase of AQMEII-3 project).

Emission processing

Typically, AQMs require spatially disaggregated hourly input values, however emission inventories are prepared as annual totals for countries (or regions). In order to convert annual and regional basis emission inventories as AQM inputs, emission processors use proxy variables and surrogate fields. Thus, annual total can be disaggregated spatially and allocated temporally. The overall model accuracy heavily depends on the degree of similarity between the disaggregation of total emission and the true spatial and temporal distribution [93]. Poor temporal representation of emissions generally influences diurnal cycle or short-term distribution of the predicted emissions [93]. The emissions being compiled on a country-wise basis, are affected by gaps and inconsistency across borders, which require further processing and manipulation [94]. Since EU emission inventories are prepared on country basis, distribution of the emissions spatially and temporally gains importance.

TNO-MACC and EDGAR-HTAP emission inventories were spatially distributed by two modelling groups (FRES1 and FI1) and made available for the use of other groups in case of need. TNO-MACC emission inventory was spatially redistributed by FRES1 group by considering national inventories (with higher spatial resolution) over France and the U.K. For the other countries, it was redistributed by considering point source locations, land use, and population. Population was not used as a parameter for spatially distributing the EDGAR-HTAP emissions [71].

In our group, a new code was generated by considering Sparse Matrix Operator Kernel Emissions (SMOKE) processing system [95]. Temporal and vertical distributions of the emissions were treated with the EURODELTA [96] factors for individual source sectors to calculate the hourly data by the modelers (see also Pouliot et al. [97]). Height profiles are taken from EURODELTA (EMEP), however they are prescribed as emission density profiles so that the emission at each height is the same, also with different vertical structures.

2.1.2.4 Observational data

In AQMEII-3, surface air quality monitoring network of EU were taken from the two databases, which are EMEP [98] and European Air Quality Database (AirBase) [99]. In this thesis, entire of those stations were considered for evaluation of the models. Map of stations throughout Europe is given in Figure 2.4. According to Figure 2.4, frequency of observation stations is high in Germany, Poland, Czech Republic, Holland, Belgium and North Italy where it is medium in South Italy, Spain, Portugal, Turkey, France, Greece and England, and low in Denmark, Norway, Finland and Balkan countries.

In this study, analyses were conducted on country basis, region basis and station basis. Eastern and Western Europe countries grouped in the analysis. The Eastern and Western countries lists of United Nations Statistics Division [100] and United States Department of Energy [101] were considered for identifying countries as Eastern or Western, and current situation of the countries in EU delegation were discarded when generating the lists. Additionally, gross domestic product (GDP) per capita [102] and geographical location of the countries were considered. Countries which didn't supply PM_{10} measurements to EMEP and Airbase [99] databases were not considered in the classification; therefore, Eastern and Western countries lists are unique to this study.
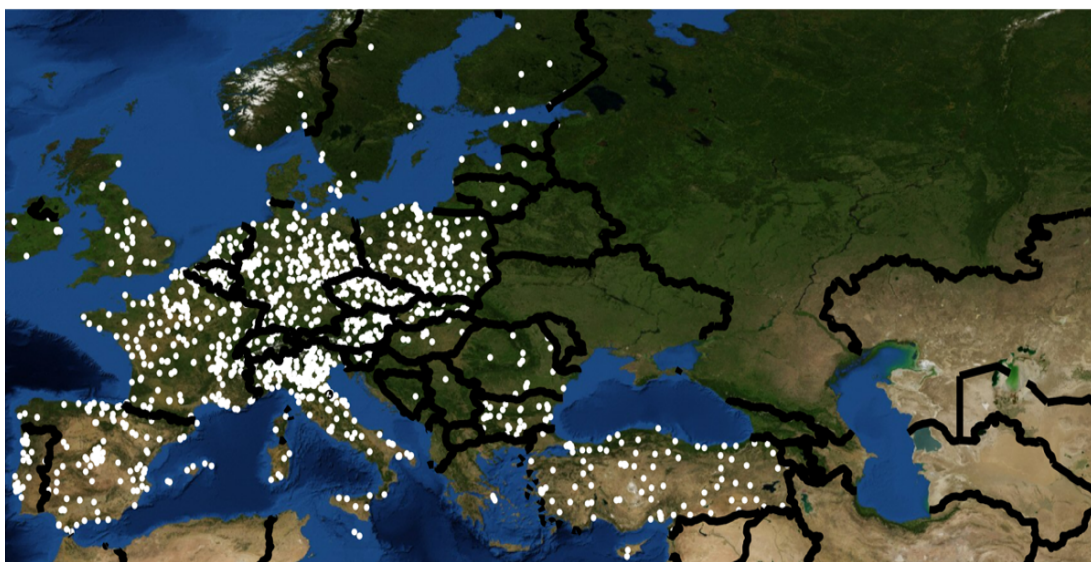
Figure 2.4 : PM_{10} observation stations in Europe.

The data taken into account in the classification of the countries as Eastern and Western are given in Table 2.2 for Western European countries and in Table 2.3 for Eastern European countries. Consequently, Sweden, Luxembourg, Finland, Ireland, Italy, England, Switzerland, Germany, Netherlands, Norway, Belgium, Iceland, France, Austria, Portugal, Denmark and Spain (totally 17 countries) were accepted as Western Europe countries. Latvia, Romania, Serbia, Turkey, Bosnia and Herzegovina, Bulgaria, Poland, South Cyprus, Moldova, Malta, Slovakia, Greece, Czech Republic, Estonia, Lithuanian, Hungary, Slovenia (totally 17 countries) were accepted as Eastern Europe countries.

Although Portugal does not have as high GDP per capita as the western countries, it was included in the Western countries list because of its geographical location. The average GDP per capita of Western European countries (\$56,793) is almost 3.5 times that of Eastern European countries (\$16,826).

Number of PM_{10} stations, population per station, serving area per station was calculated for each country in Table 2.2 for Western Europe countries and in Table 2.3 for Eastern Europe countries. In Table 2.2, 17 countries were listed as Western Europe countries, which have totally 984 PM_{10} observation stations, where it is 448 for Eastern Europe countries as indicated in Table 2.3. In order to ease comparing number of stations per country, population and area of the countries are also indicated in the tables and two indices were calculated. First one is number of people per station and second one is number of stations per 1000 km^2. Calculated indices should be evaluated

together. For instance, number of people per station (1 station per 2.663.000 people) in England is one of the worst among other countries however station number per 1000 km^2 (5.2 stations per 1000 km^2) is one of the good among other countries. This inconsistency is due to dense population living in a small area in England.

Table 2.2 : General information about Western European countries.

	Number of PM$_{10}$ stations	Area (1000 km^2) [102]	Population [102]	Population (*1000) per station	Serving area (1000 km^2) per station	GDP per capita ($) (2018) [102]
Austria	74	83.8	8,793,370	119	1.1	51,513
Belgium	38	30.6	11,350,000	299	0.8	46,556
Denmark	2	42.9	5,749,000	2,875	21.5	60,596
England	25	130.4	66,573,504	2,663	5.2	42,491
Finland	8	338.4	5,520,535	690	42.3	49,960
France	231	643.8	67,186,638	291	2.8	41,464
Germany	199	357.3	80,457,737	404	1.8	48,196
Iceland	2	103	357,050	179	51.5	73,191
Ireland	9	84.4	4,739,383	527	9.4	77,450
Italy	188	301.4	59,963,169	319	1.6	34,318
Luxembourg	3	2.5	602,005	201	0.9	114,340
Netherlands	28	42.5	17,283,008	617	1.5	52,978
Norway	9	385.2	5,353,363	595	42.8	81,807
Portugal	26	92.2	10,291,196	396	3.5	23,146
Spain	111	506	46,733,038	421	4.6	30,524
Sweden	9	450.3	10,041,160	1,116	50.0	54,112
Switzerland	22	41.2	8,544,034	388	1.9	82,839
	Sum: 984	**Sum:** 3,636	**Sum:** 409,538,190	**Avg.:** 711	**Avg.:** 14	**Avg.:** $56,793

Scandinavian countries (Sweden, Norway and Denmark), Finland and Iceland has the lowest number of stations based on population and area, which can be due to not inclusion of all stations to EMEP [98] and AirBase systems [99]. By ignoring North Europe countries due to this reason, Western Europe countries are listed in an order of their representative number of stations considered with both per km^2 and population as follows; Austria, Luxembourg, Belgium, Italy, Germany, Switzerland, France, Netherlands, Portugal, Spain, Ireland and England.

Eastern European countries are listed in order of their representative number of stations per km^2 and population as follows; Malta, Czech Republic, Estonia, Slovenia, Slovakia, Poland, Bulgaria, South Cyprus, Hungary, Turkey, Lithuanian, Latvia, Romania, Greece, Moldova, Bosnia and Herzegovina and Serbia, respectively.

Turkey is 9th in Eastern countries in terms of number of stations per area and population. Distribution of PM_{10} observation stations in Turkey are given in Figure 2.5.

Table 2.3 : General information about Eastern European countries.

	Number of PM_{10} stations	Area (km^2) [102]	Population [102]	Population (*1000) per station	Serving area (1000 km^2) per station	GDP per capita ($) (2018) [102]
Bosnia	1	51,197	3,849,891	3,850	51	5,951
Bulgaria	32	110,994	7,036,848	220	3.5	9,273
Czech Rep.	95	78,865	10,625,250	112	0.8	22,973
Estonia	4	45,227	1,303,798	326	11.3	22,928
Greece	4	131,957	11,124,603	2,781	33	20,324
Hungary	14	93,030	9,778,371	698	6.6	15,939
Latvia	4	64,589	1,934,000	484	16	18,089
Lithuanian	5	65,300	2,785,000	557	13	19,090
Malta	2	316	475,701	238	0.2	30,075
Moldova	1	33,846	3,547,539	3,548	34	3,189
Poland	136	312,679	37,977,000	279	2.3	15,424
Romania	13	238,397	19,524,000	1,502	18.3	12,301
Serbia	1	88,361	7,001,444	7,001	88	7,234
Slovakia	22	49,035	5,443,120	247	2.2	19,547
Slovenia	11	20,273	2,066,880	188	1.8	26,234
Cyprus	2	9,251	864,236	432	4.6	28,159
Turkey	101	783,562	82,004,000	812	7.8	9,311
	Sum: 448	**Sum:** 2,176,879	**Sum:** 207,341,681	**Average:** 1369	**Average:** 17	**Average:** $16,826

Generally, there are at least one station in 81 cities of Turkey in 2010, except Bitlis, Muş, Şırnak and Van. There is more than one station in big cities, such in Istanbul (11 stations), Izmir (8 stations), Ankara (6 stations), Kocaeli (3 stations), Canakkale (2 stations), Konya (2 stations) and Trabzon (2 stations).

Figure 2.5 : PM$_{10}$ Observation stations in Turkey (above), Marmara Region (bottom left) and Istanbul (bottom right).

Distribution of stations according to 7 regions of Turkey are given in Table 2.4, and regions (with cities inside following parenthesis) are Mediterranean Region (Adana, Antalya, Burdur, Hatay, Isparta, Kahramanmaraş, Mersin, Osmaniye), Eastern Anatolia Region (Ağrı, Ardahan, Bingöl, Bitlis, Elazığ, Erzincan, Erzurum, Hakkari, Iğdır, Kars, Malatya, Muş, Tunceli, Van), Aegean Region (Afyonkarahisar, Aydın, Denizli, İzmir, Kütahya, Manisa, Muğla, Uşak), South Eastern Anatolia Region (Adıyaman, Batman, Diyarbakır, Gaziantep, Mardin, Siirt, Şanlıurfa, Şırnak, Kilis), Central Anatolia Region (Aksaray, Ankara, Çankırı, Eskişehir, Karaman, Kayseri, Kırıkkale, Kırşehir, Konya, Nevşehir, Niğde, Sivas, Yozgat), Marmara Region (Balıkesir, Bilecik, Bursa, Çanakkale, Edirne, İstanbul, Kırklareli, Kocaeli, Sakarya, Tekirdağ, Yalova) and Black sea Region (Amasya, Artvin, Bartın, Bayburt, Bolu,

34

Çorum, Düzce, Giresun, Gümüşhane, Karabük, Kastamonu, Ordu, Rize, Samsun, Sinop, Tokat, Trabzon, Zonguldak).

Table 2.4 : General information about regions of Turkey.

Region	Number of cities	Number of PM$_{10}$ Stations in 2010	Population
Mediterranean Region	8	11	10,461,409
Eastern Anatolia Region	14	14	6,058,499
Aegean Region	8	17	10,514,200
South Eastern Anatolia Region	9	9	8,847,980
Central Anatolia Region	13	23	13,114,013
Marmara Region	11	22	25,034,570
Black Sea Region	18	20	7,973,211
SUM	**81**	**116**	**82,003,882**

Maximum number of stations are in Black Sea region (20 stations), Central Anatolia region (23 stations) and Marmara region (22 stations) where least number of stations is in South Eastern Anatolia region (9 stations). Actually, number of stations are more than those values, however inactive stations (in 2010) were not considered in this table. Some of the stations were eliminated after making quality control procedures which were summarized below. Consequently, number of stations used in this study is 101.

Quality control

In this study, observational data was subject to quality control procedures for identifying potentially erroneous measurements. Adopted methodology is summarized as follows;

- Station based hourly observations considered in air quality checks.

- PM$_{10}$ concentrations less than 0 μg/m^3 and more than 600 μg/m^3 marked as erroneous, flagged and further checked. Assigned as 'NA', if suspicious.

- The current hour's value compared with the previous hour's value. If one is ten times of the other, flagged and further checked. Assigned as 'NA', if suspicious.

- Repetitive hourly concentrations (two digits after point) of three consecutive times were assigned as suspicious and assigned as 'NA'.

- If 50% of the data is not validated by abovementioned quality control procedures, the station was disregarded totally.

2.1.3 Modelling Methodology

As a framework for simulating the interactions of multiple complex atmospheric processes, an air quality modelling system consists typically of a meteorological information, emissions rates from sources of emissions that affect air quality and an AQM [103]. Modelling configuration of each AQMEII-3 group is described in general in this part of study, and our group's modelling methodology is summarized in detail in Figure 2.6. As indicated in Table 2.1, our group (TR1) used CMAQ v.4.7.1 and Weather Research and Forecasting (WRF) Model v.3.5. Abbreviations related with other groups and their models are indicated in Table 2.1, and will be used throughout the thesis as it is given in the table.

2.1.3.1 Meteorology model

The meteorological model calculates the three-dimensional fields of wind, temperature, relative humidity, pressure, and in some cases, turbulent eddy diffusivity, clouds and precipitation as a function of time [103]. According to Table 2.1, CCLM model was used by DE1, and WRF model was used by eight groups (IT1, IT2, ES1, DK1, UK1, UK2, UK3 and our group, TR1). FI1, FI2, NL1 and FRES1 used the meteorological inputs extracted by the ECMWF operational archive.

The COnsortium for Small-scale MOdeling (COSMO) and Climate Limited-Area Modelling (CLM), COSMO-CLM, will be called as CCLM from this point, is the regional climate model and operational non-hydrostatic mesoscale weather forecast model developed initially by the German Weather Service (DWD) [104] and then by the European Consortium which is COSMO [77]. COSMO CLM is employed at spatial resolution between 1 and 50 km, can able to run long-term simulations, therefore called as climate model.

WRF Model, which is also used in this study in order to prepare meteorological files for CMAQ run, is a mesoscale numerical weather prediction model. It is designed for simulation of the atmospheric processes by using real data (observations, analyses) or idealized conditions. The model is used for a wide range of meteorological applications across scales from tens of meters to thousands of kilometres [105]. WRF

model is used by 8 groups (including our group, TR1) of 12 in AQMEII-3. Table 2.5 summarizes the configuration of the WRF runs, detailing difference and commonalities. The detailed description of the data which was used as the input for each meteorology model was described in Chapter 2.1.2.1. In this part of the study, the approaches considered in meteorology model configurations are summarized.

There are several planetary boundary layer (PBL) schemes in meteorology models which can be local, nonlocal or hybrid. Mellor–Yamada Nakanishi–Niino (MYNN) PBL scheme [106] and Mellor–Yamada–Janjic (MYJ) PBL scheme [107] are local schemes, the Yonsei University (YSU) PBL scheme [108] is a nonlocal scheme, and the Asymmetric Convective Model with nonlocal upward mixing and downward mixing (ACM2) [109] can be regarded as a hybrid scheme in that it incorporates local and nonlocal closures for potential temperature and velocity, resulting in more accurate vertical mixing [71]. Without going into the detail on each parameterization, it can be said that the differences among the PBL formulations (detailed review provided by Cohen et al. [110]) have a profound impact on the discussion of the errors in air quality estimations. For instance, local and nonlocal closure of the PBL equations differ when indicating the depth over PBL variables which influence the air quality predictions at a given point [71, 110]. According to Banks and Baldasano [111], generally WRF model underpredicts PBL height with YSU, ACM2, MYJ and Bougeault-Lacarrère (Boulac) schemes. PBL height and air quality predictions of O_3 and NO_2 was best represented by a non-local scheme, such as ACM2. However, PM_{10} predictions were have lowest correlations between the CMAQ model and observations in all PBL schemes, which can be due to poor simulations of the PBL height from the WRF model and other sources of uncertainty from emission inventory. As summarized in Table 2.5, UK1, UK2 and UK3 used ACM2 PBL scheme; ES1, IT1 and TR1 used YSU PBL scheme; IT2 used MYNN PBL scheme and DK1 used MYJ PBL scheme.

Surface layer height (first layer height) is defined as the region at the bottom 10% of the boundary layer where turbulent fluxes and stress vary by less than 10% of their magnitude [112]. Anthropogenic sources are mainly located on the surface layer of the Earth, and human health related air quality management is generally associated with the inhalable part of the atmosphere. Therefore, vertical resolution of the meteorology model and the starting point of the first layer is important in air quality modelling. First layer height and number of vertical layers should be selected when configuring WRF

model, which are important in calculation of PBL height which in turn may affect the concentration of the pollutants [113]. There are around 10 PBL schemes [113] in WRF. Some PBL parameterizations are designed to be strongly coupled with surface layer properties. In this context, the externally determined lowest model level height can influence the behaviour of a PBL scheme, which in turn affects the performance of prediction skill for atmospheric states. MYJ, MYNN and YSU PBL schemes of WRF can work with low vertical and horizontal resolutions [113]. According to Shin H. H. et al. [114], the YSU scheme is the most sensitive to first layer height, the ACM2 is the second, and the MYJ scheme is the least sensitive. Our group, TR1, selected lowest surface layer height (10m) among other groups, and used YSU scheme which is the most sensitive scheme to the first layer height.

Selection of land surface model strongly affect the prediction of temperature and humidity, since they are used to compute the surface heat and moisture fluxes. Land surface models used by AQMEII-3 modellers are NOAH [115], RUC [116] and 5-layer thermal diffusion model [126]. The NOAH land surface model [115]-[117], which is mostly preferred by AQMEII-3 modellers, predicts soil moisture and temperature in 4 layers. The layer thickness is 10, 30, 60 and 100 cm from top to bottom [118]. The Rapid Update Cycle (RUC) land surface model includes multilevel soil model with 6 default levels and the number of levels can be increased [118]. The 5-layer thermal diffusion LSM (TD LSM) is based on the 5-layer soil temperature with the thicknesses 1, 2, 4, 8 and 16 cm [118]. Several comparative studies show that the results of meteorological models are sensitive to the choice of the land surface model. In the study of Mooney et al. [119], NOAH surface scheme yields more accurate surface temperature results compared to RUC. Our group, TR1, used NOAH land surface model as most of the AQMEII-3 groups.

The surface layer schemes calculate friction velocities and exchange coefficients that enable the calculation of surface heat and moisture fluxes by the land-surface models. These fluxes provide a lower boundary condition for the vertical transport done in the PBL Schemes. MM5 similarity theory [120] was used by IT2; Pleim-Xiu [121] and Rapid Update Cycle (RUC) [122] schemes were used by UK1, UK2 and UK3 groups. Remining groups, including our group, were used ETA similarity theory.

The representation of clouds in WRF model includes major uncertainties in predictions of short- and long-term weather. Cloud microphysics parameterization is required in

meteorological models because a sophisticated, explicit prediction of the evolution of cloud microstructure is either impossible or impractical even with the most advanced computing resources [123]. Precipitation amount and intensity are calculated, and the growth and development of water droplets in warm and cold rain processes are simulated by cloud microphysics schemes. Furthermore, energy, momentum, and moisture are redistributed among model grid points and interact closely with radiation processes and the atmospheric boundary layer [123]. Single-moment 3-class microphysics scheme of WRF (WSM3) [124] was used by our group, single-moment 5-class microphysics scheme of WRF (WSM5) [125] was used by DK1, single-moment 6-class microphysics scheme of WRF (WSM6) was used by UK1 and UK2 [125], Lin scheme was used by [126] ES1, and Morrison scheme [127] was used by IT1 and UK3.

Cumulus convection transfers sensible and latent heat from the Earth's surface into the lower troposphere [128]. Cumulus parameterization schemes strongly influence the dynamics and precipitation variability [129]. Several cumulus convection schemes are used in WRF model in order to express the interaction between the larger scale flow and complicated physics and dynamics of the convective clouds in simple parameterized terms. Grell-Freitas [130] cumulus convection scheme was used by IT1 and IT2, and remaining groups used Kain-Fritsch2 [131] scheme.

Radiative fluxes are assessed in WRF by using various radiation options. IT1, IT2, ES1, UK3 groups used Rapid Radiative Transfer Method for Global for solar and infrared radiation (RRTMG) for both shortwave (SW) and longwave (LW) radiation.

TR1, UK1, UK2 groups used Dudhia's method [137] as SW radiation option and Rapid Radiative Transfer Method for infrared radiation (RRTM) [138] as LW radiation option. CAM scheme [136] was used by DK1 for SW and LW radiation.

Data assimilation (nudging) technique is used for producing high resolution four dimensional meteorological datasets (such as horizontal winds, temperature and water vapor) between normal analysis times, for air quality models. The second reason of using nudging is creating smooth start up forecast time zero by dynamic initialization for pre-forecast period. The third reason for using nudging is preparation of boundary conditions through forecast by nudging them with an outer domain that covers the domain of interest.

Table 2.5 : Configuration of the WRF model by participating modelling groups.

	Operated by	Meteorology Input Data Provider	Number of vertical layers	1st layer height	PBL model	Surface layer	Land Surface Model	Cloud Microphysics	Cumulus convection	SW /LW radiation	Data assimilation technique
IT2	University of L'Aquila	ECMWF	33	10 m	MYNN [106]	MM5 Similarity [120]	NOAH [115][117]	Morrison [127]	Grell-Freitas [130]	RRTMG [135]	Grid analysis nudging above PBL
ES1	University of Murcia	ECMWF	33	21 m	YSU [108]	ETA Similarity [132][133]	NOAH [115][117]	Lin [126]	Kain-Fritsch2 [131]	RRTMG [135]	Grid analysis nudging above PBL
IT1	Ricerca Sistema Energetico	ECMWF	33	25 m	YSU [108]	ETA Similarity [132][133]	NOAH [115][117]	Morrison [127]	Grell-Freitas [130]	RRTMG [135]	Grid analysis nudging also within PBL
DK1	University of Aarhus	ECMWF	29	20 m	MYJ [107]	ETA Similarity [132][133]	NOAH [115][117]	WSM5 [125]	Kain-Fritsch2 [131]	CAM [136]	Grid analysis nudging above PBL
TR1	Istanbul Technical University	NCEP FNL	30	10 m	YSU [108]	ETA Similarity [132][133]	NOAH [115][117]	WSM3 [124]	Kain-Fritsch2 [131]	Dudhia [137]/ RRTM [138]	Grid analysis nudging also within PBL
UK1	Kings College	NCEP GFS	23	14 m	ACM2 [109]	Pleim-Xiu [121] RUC [122]	RUC [116]	WSM6 [125]	Kain-Fritsch2 [131]	Dudhia [137]/ RRTM [138]	Grid analysis nudging also within PBL
UK2	Ricardo E&E	NCEP GFS	23	15 m	ACM2 [109]	Pleim-Xiu [121] RUC [122]	RUC [116]	WSM6 [125]	Kain-Fritsch2 [131]	Dudhia [137]/ RRTM [138]	Grid analysis nudging above PBL
UK3	University of Hertfordshire	ECMWF	36	25 m	ACM2 [109]	Pleim-Xiu [121] RUC [122]	5-layer thermal diffusion [134]	Morrison [127]	Kain-Fritsch2 [131]	RRTMG [135]	Grid analysis nudging above PBL

Applying nudging to boundary conditions and outer domain makes benefit of providing smoother boundary conditions to domain of interest. The popular nudging methods used for dynamical downscaling include grid nudging and spectral nudging. For grid nudging, each grid-point is nudged towards a value that is time-interpolated from analyses. In spectral nudging each grid point is nudged using a weighted average of differences from observations within a radius of influence and time window [139]. Grid nudging technique was used by all AQMEII-3 groups which used WRF as meteorology model. According to Mai X. et al. [140], nudging above the PBL obviously improved the simulation of meteorological elements at the upper layers, but was not ideal for simulations near the surface and at lower layers in some areas. Therefore, nudging also within PBL gains importance in air quality modelling. In AQMEII-3, IT1, TR1 and UK1 applied grid analysis nudging above and within PBL. Remaining WRF users applied nudging only above PBL.

2.1.3.2 Air quality model

There are various mathematical models that can be used to simulate meteorology and air quality at the mesoscale domain. Although mathematical models differ in their treatment of meteorology or air quality (e.g. in considering feedback mechanisms), all three-dimensional models are based on a similar framework and consist of the same major components.

Seven different AQMs were used by modelling groups of AQMEII-3 project, which are SILAM (v5.4), LOTOS-EUROS (v.1.0.1), CHIMERE (v2013), WRF-Chem (v3.6) CAMx (v6.10), DEHM and CMAQ (v.4.7.1 and v.5.0.2). According to Table 2.1, five groups operated the CMAQ model, which are TR1, UK1, UK2, UK3 and DE1. SILAM model was operated by FI1 group, LOTOS-EUROS operated by NL1 group, CHIMERE model was operated FRES1 group, WRF-Chem was operated by ES1 and IT2 groups, CAMx was operated by IT1 and DEHM model was operated by DK1 group.

SILAM (System for Integrated modeLling of Atmospheric coMposition) was developed in the leadership of Finnish Meteorological Institute as an open-code model which works from global to beta-meso scale (~1km resolution) [141].

LOTOS-EUROS, was developed for TNO and Dutch National Institute, is an open-source CTM that calculates the formation and dispersion of O_3, NO_2, NH_3, organic and

elemental carbon, mineral dust, sea spray, secondary aerosols and heavy metals across Europe. The default model resolution is approximately 25 x 25 km[2,] but it is possible to zoom in on urban and industrial areas [29].

CHIMERE multi-scale model was designed primarily for air quality estimates in Europe [142] to produce daily forecasts of ozone, aerosols and other pollutants and make long-term simulations (entire seasons or years) for emission control scenarios. CHIMERE runs over a range of spatial scale from the regional scale (several thousand kilometres) to the urban scale (100-200 km) with resolutions from 1-2 Km to 100 km developed by the cooperation of École Polytechnique Institute Le Laboratoire de Météorologie Dynamique, The French National Institute for Industrial Environment and Risks (INERIS) of French Ministry of the Environment and mixed universities atmospheric research laboratory (LISA) in France [143].

WRF-Chem is the WRF model coupled with Chemistry. The model simulates the emission, transport, mixing, and chemical transformation of trace gases and aerosols simultaneously with the meteorology. The model is used for investigation of regional-scale air quality, field program analysis, and cloud-scale interactions between clouds and chemistry and developed in the leadership of National Oceanic & Atmospheric Administration / Earth System Research Laboratory (NOAA/ESRL) scientists of U.S. Department of Commerce [26].

CAMx is a multi-scale photochemical grid model for gas and particulate air pollution by comprising a "one-atmosphere" treatment of tropospheric air pollution over spatial scales ranging from neighbourhoods to continents developed by ENVIRON division of RAMBOLL company of Denmark [27].

DEHM for regional sources is developed by Aarhus University is a three-dimensional, offline, large-scale, Eulerian, atmospheric chemistry transport model developed for studying long-range transport of air pollution in the Northern Hemisphere [30 81].

CMAQ model is an active open-source development project of the U.S. EPA that consists of a suite of programs for conducting AQM simulations. CMAQ is a three-dimensional Eulerian atmospheric chemistry and transport modelling system that simulates O_3, PM, toxic airborne pollutants, visibility, and acidic and nutrient pollutant species throughout the troposphere. Designed as a "one-atmosphere" model, CMAQ can address the complex couplings among several air quality issues simultaneously

across spatial scales ranging from local to hemispheric [144]. The one-atmosphere perspective emphasizes that the influence of interactions at different dynamic scales and among multi-pollutants cannot be ignored, therefore multi-pollutant interactions should be considered simultaneously and there should be consistent algorithmic linkage between meteorological and chemical transport models.

The CMAQ model is based upon the underlying concept of preserving mass through a series of contiguous three-dimensional grid cells covering a fixed model grid (i.e., x-y-z array that is fixed in space and covers a particular domain, i.e., the geographic area of interest) [144]. Therefore, CMAQ belongs to the Eulerian class of mathematical models which calculates mass balance for each grid cell by solving the transport equation for boundaries of each cell and solving chemical transformations within each cell during a given time period [144]. The CMAQ modelling system is capable of processing diverse information from complicated emission mixtures and complex distributions of sources, to modelling the complexities of atmospheric processes that transport and transform these mixtures in a dynamic environment that operates over a large range of time scales, from minutes to days and weeks [145].

CMAQ is a deterministic numerical model which uses first order-closure (K-theory or the gradient transfer theory) technique in order to solve basic turbulent diffusion equation's unknown term, which is turbulent flux of the pollutants, $\vec{F}_t$.

Basically, CMAQ model (and also all numerical models) is based on mass conservation principle. The basic turbulent diffusion equation can be derived from the mass conservation principle, which has the following form:

$$\frac{\partial C}{\partial t} = -\vec{U}\nabla C - \nabla \vec{F}_t + Q + R \qquad (2.1)$$

where C is pollutant concentration average over time interval, t is time, $\vec{U}$ is the wind vector (U[u, v, w]) average over time interval in m/sec, $\vec{F}_t$ is turbulent flux of the pollutants ($\vec{F}_t[\overline{u'C'},\ \overline{v'C'},\ \overline{w'C'}]$, Q is the source term and R is the removal term with the unit of mass/volume.time, and $\nabla\ is\ \vec{\imath}\frac{\partial}{\partial_x} + \vec{\jmath}\frac{\partial}{\partial_y} + \vec{k}\frac{\partial}{\partial_z}$.

This equation can be solved only by means of numerical methods, as it is done in numerical models. However, under a set of simplifying assumptions, the analytical solutions of this equation can be obtained, and such a solution is used in Gaussian

plume/puff models [7]. This part is not the scope of this study, therefore is not explained more. The main problem of Equation 2.1 is the $\vec{F}_t$ term which is unknown. The first order-closure (K-Theory) models, which CMAQ model adopts, uses K-theory of Schmidt W. (1925) [22]. This theory is an approximation for the closure of the basic diffusion equation (equation 2.1) via parameterizing $\vec{F}_t$ by the product of an eddy diffusivity and the local spatial gradient of the quantity being transported. For the pollution concentration this approximation is;

$$\vec{F}_t = \overline{\vec{U}'C'} = -\hat{K}.\nabla C \tag{2.2}$$

Where $\hat{K}$ is diffusivity tensor and can generally be simplified by employing isotropic argument in most first-order-closure models used in planetary boundary layer applications. Finally, the off-diagonal components can be represented by a horizontal term K_H and by a vertical term K_Z, (K_H and K_Z are horizontal and vertical turbulent exchange coefficients in the unit of m²/sec), resulting following K-theory diffusion equation, called also advection-diffusion equation;

$$\frac{\partial C}{\partial t} = -\left\{ u\frac{\partial C}{\partial x} + v\frac{\partial C}{\partial y} + w\frac{\partial C}{\partial z} \right\} + \frac{\partial}{\partial z}K_H\frac{\partial C}{\partial x} + \frac{\partial}{\partial y}K_H\frac{\partial C}{\partial y} + \frac{\partial}{\partial z}K_H\frac{\partial C}{\partial z} + Q + R \tag{2.3}$$

For the Eularian grid system, equation 2.3 is allowed for space variations in the fields of meteorological parameters, and the governing atmospheric diffusion equation in generalized coordinates are given as follows where the turbulent flux terms are expressed using the eddy diffusion theory [146];

$$\underbrace{\frac{\partial(\overline{\varphi_i}\,J_\xi)}{\partial t}}_{(a)} + \underbrace{m^2\nabla_\xi\left(\frac{\overline{\varphi_i}\,\overline{V}\,J_\xi}{m^2}\right)}_{(b)} + \underbrace{\frac{\partial(\overline{\varphi_i}\,\overline{\hat{v}^3}\,J_\xi)}{\partial \hat{x}^3}}_{(c)}$$

$$\underbrace{-\,m^2\frac{\partial}{\partial x^{-1}}\left[\frac{\overline{\rho}\,J_\xi}{m^2}\left(K^{11}\frac{\sigma q_i}{\partial x^1}\right)\right] - m^2\frac{\partial}{\partial x^2}\left[\frac{\overline{\rho}\,J_\xi}{m^2}\left(K^{22}\frac{\sigma q_i}{\partial x^2}\right)\right]}_{(d)}$$

$$\underbrace{-\,\frac{\partial}{\partial x^3}\left[\rho\,J_\xi\left(K^{33}\frac{\sigma q_i}{\partial x^3}\right)\right]}_{(e)}$$

$$- m^2 \frac{\partial}{\partial x^{-1}} \left[\frac{\bar{\rho} J_\xi}{m^2} \left(K^{13} \frac{\sigma q_i}{\partial x^3} \right) \right] - m^2 \frac{\partial}{\partial x^2} \left[\frac{\bar{\rho} J_\xi}{m^2} \left(K^{23} \frac{\sigma q_i}{\partial x^3} \right) \right]$$

(f)

$$- \frac{\partial}{\partial x^3} \left[\bar{\rho} J_\xi \left(K^{31} \frac{\sigma q_i}{\partial x^1} + K^{32} \frac{\sigma q_i}{\partial x^2} \right) \right]$$

(g)

$$= J_\xi R_{\varphi i}(\bar{\varphi}_i, \dots, \bar{\varphi}_N) + J_\xi Q_{\varphi i}$$

(h) (i)

$$+ \left. \frac{\partial (\bar{\varphi}_i J_\xi)}{\partial t} \right|_{cld} + \left. \frac{\partial (\bar{\varphi}_i J_\xi)}{\partial t} \right|_{aero} + \left. \frac{\partial (\bar{\varphi}_i J_\xi)}{\partial t} \right|_{ping} \qquad (2.4)$$

(j) (k) (l)

(a) time rate of change of pollutant concentration;

(b) horizontal advection;

(c) vertical advection;

(d) diagonal term of horizontal eddy diffusion;

(e) diagonal term vertical eddy diffusion;

(f) off-diagonal horizontal diffusion;

(g) off-diagonal vertical diffusion;

(h) production or loss from chemical reactions;

(i) emissions;

(j) cloud mixing and aqueous-phase chemical production or loss;

(k) aerosol process;

(l) plume-in-grid process.

where φ_i is the trace species concentration in density units (e.g. kg/m^3), J_ξ is the vertical Jacobian of the terrain-influenced coordinate ξ, m is the map scale factor, v is the vertical velocity (=d ξ/dt), **V** stands for the vertical and horizontal wind components in the generalised coordinates, x length for grid, q_i (=φ_i/ ρ) is the species mass mixing ratio, ρ is the density of the air, K values are the diagonal components of the eddy diffusivity tensor in the generalised coordinates.

The dry deposition process can be included in the vertical diffusion process as a flux boundary condition at the bottom of the model layer and this governing equation can be rewritten for trace species [146].

Our group used CMAQ model which uses coupled mathematical representations of actual chemical and physical processes to simulate air quality. As indicated on the CMAQ modelling system operational procedure, which is given on the centre of Figure 2.6, CMAQ model requires emission input, meteorology input and boundary conditions. By using entire of those data, the model calculates concentrations of pollutants for each grid cell.

In our modelling procedure, gridded surface and pressure levels data was downloaded monthly from ECMWF by using a download code created by Python programming language.

Then this data was used as an input to WRF pre-processing system (WPS). Then outputs of WRF model is given to Meteorology Chemistry Interface Processor (MCIP) version 3.6 [147] which combines emissions with meteorology outputs, then converts to input of the CMAQ model. The MEGAN v2.1 [148] model was used to calculate the biogenic VOC emissions from vegetation, using surface temperature and radiation from MCIP output. Furthermore, boundary conditions data is taken from ECMWF and converted into the required data format as input to CMAQ v4.7.1 [25] was configured with the CB05 chemical mechanism and the AERO5 module [25] for the simulation of gas phase chemistry and aerosol and aqueous chemistry, respectively. Finally, emissions are produced with CMAQ model.

Windblown dust emissions

CMAQ model users (UK1, UK2 and UK3 groups) use inline windblown dust calculation of CMAQ model, which was a new feature of CMAQ version 5.0 and upper [25 82], and those groups use CMAQ versions 5.0.1 and upper. Our group, TR1, use CMAQ 4.7.1, so there was no inline dust module, therefore we used dust calculations previously calculated in AQMEII-2. FI1 and FI2, FRES1 groups included windblown dust only from the lateral boundary conditions. DE1 group didn't take into account dust emissions since CCLM model doesn't have dust module.
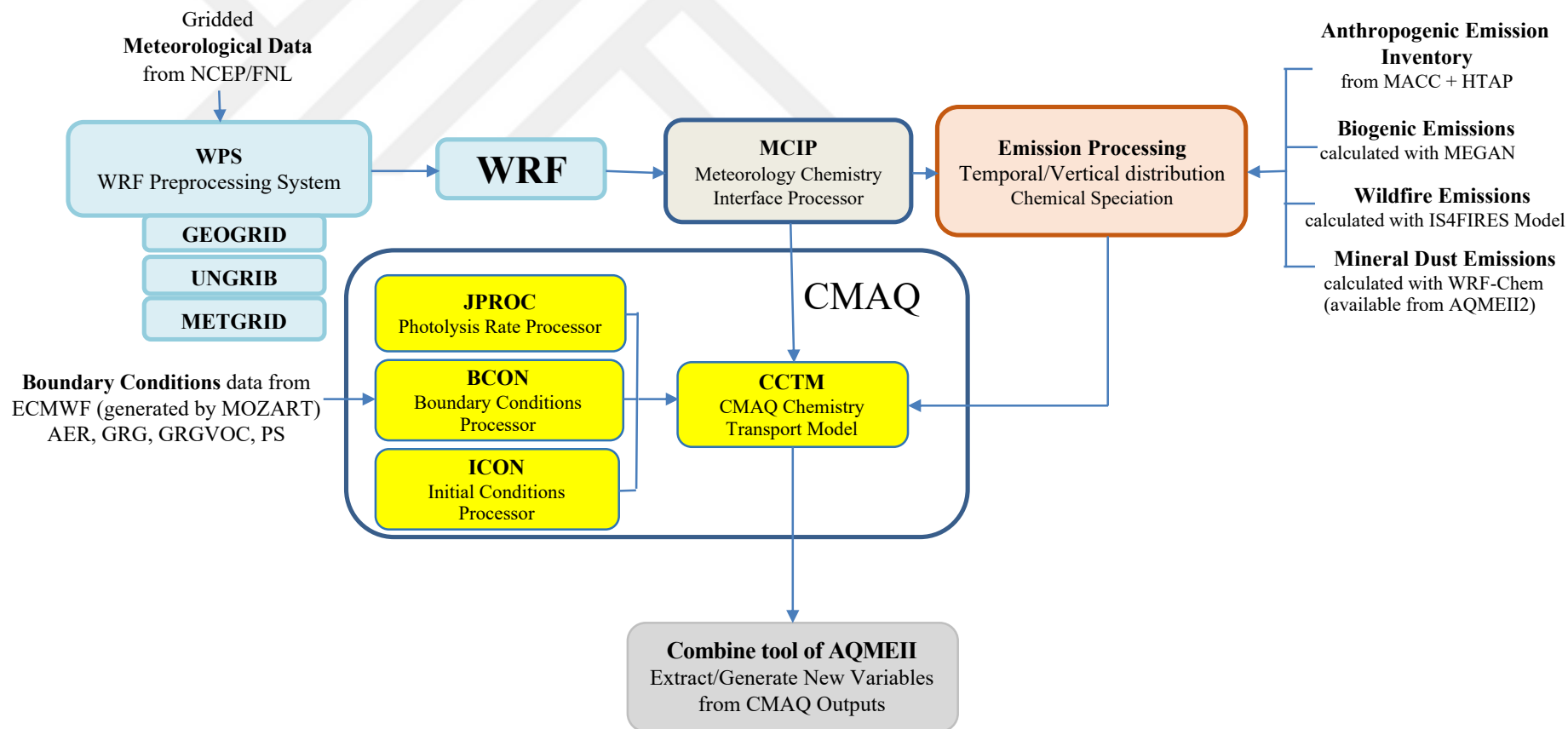
Figure 2.6 : CMAQ modelling flowchart applied in this study by our group (TR1).

Sea salt and wildland fire emissions

FI1 and FI2 groups included sea salt emissions as in Sofiev et.al. [149] (but not from the boundaries). FRES1 group calculated sea salt emissions inside the domain according to the study of Monahan E.C. [150].

IT1 group computed sea salt emissions using algorithms of de Leeuw et al. [151] and Gong S.L. [152]. UK1 group computed emissions according to Gantt et al. [153]. DE1 group calculated in-line sea salt emissions by CMAQ, including sulphate emissions based on an average sulphate content of 7.7 %. Background sea salt emissions were considered by none of the models. Sea salt at the boundaries, although provided by chemical boundary conditions, was not used due to unrealistically high values.

FI1 and FI2 wildland fire emissions are considered as in Soares et al. [154]. There is no data for other groups.

Gas phase chemistry reaction rates

An important component of AQMs is the gas-phase chemical mechanism, which describes reactions that take place in the atmosphere and interactions among chemicals [155]. In AQMEII-3 project, several gas phase mechanisms were used by the contributing groups, including Carbon Bond 4 (CB4 or CBM-IV), the 2005 version of CBM-IV (CB05), gas-phase chemical mechanism of CB05 with updated toluene and chlorine chemistry (CB05-TUCL).

CBM-IV [171] (revealed in 1989) has 96 reactions and 45 of them are inorganic reactions. There are 46 species and 30 of them are organic species in CB4. CB4 has several versions and the version in CMAQ has 14 species and 15 reactions more than the original CB4 [155]. CB05 is an updated version of CB4 in 2005 therefore called as CB05. In CB05, reaction rate constants were updated, additional inorganic reactions were included, and 10 organic species were added to better represent stable organic species and radicals in the atmosphere [169]. Hence, CB05 has 156 reactions and 63 of them are inorganic reactions. There are 59 species and 41 of them are organic species in CB05. Approximate run time of CB05 relative to CB4 is 1.14 in 12 km domain, where it is 1.23 in 36 km domain [155].

IT2 group's WRF-Chem model uses the RACM-ESRL gas-phase chemical mechanism [173] which is an updated version of the Regional Atmospheric Chemistry Mechanism (RACM) [178].

Table 2.6 : Air quality modelling system properties.

Operated by	Horizontal grid resolution	Vertical grid resolution	Deposition scheme	NOx emission share of NO and NO2	Gaseous Chemistry Model
Finnish Meteorological Institute **(FI1)**	0.25×0.25° Lat×Lon	12 uneven layers up to 13 km. First layer ~30m	Dry: Kouznetsov and Sofiev [156] Wet: Kouznetsov and Sofiev [157]	90/10	CBM-IV [171]
Netherlands Organization for Applied Scientific Research **(NL1-TNO)**	0.5×0.25° Lat×Lon	Surface layer (~25m depth), mixing layer, two reservoir layers up to 3.5 km.	Dry: Zhang et al. [158] for particles, Depac (Van Zanten et al.[159] for gases Wet: below-cloud scavenging	97/3	CBM-IV [171]
INERIS/CIEMAT **(FRES1)**	0.25×0.25° Lat×Lon	9 layers up to 500 hPa. First layer ~20m	Dry: resistance approach as Emberson [160 161] Wet: in-cloud and sub-cloud scavenging for gases and aerosols (Menut et al.[162])	95% NO 4.5% NO2 0.5% HONO	MELCHIOR2 [172]
University of L'Aquila **(IT2)**	270×225 cells, 23km	33 levels up to 50 hPa. 12 layers below 1 km. First layer ~12m	Dry: Wesely [163] Wet: Grell and Freitas [130]	95/5	RACM-ESRL [173]
Ricerca Sistema Energetico **(IT1)**	265×220 cells, 23km×23km	33 levels, from ~24m to 50 hPa	Dry: resistance model for gases (Zhang et al., 2003 [165]) and aerosols (Zhang et al. [158]) Wet: scavenging model for gases and aerosols (Seinfeld and Pandis [19])	95/5	CB05 [169]

49

Table 2.6 (continued) : Air quality modelling system properties.

Operated by	Horizontal grid resolution	Vertical grid resolution	Deposition scheme	NOx emission share of NO and NO2	Gaseous Chemistry Model
Ricerca Sistema Energetico **(IT1)**	265×220 cells, 23km×23km	33 levels, from ~24m to 50 hPa	Dry: resistance model for gases (Zhang et al., 2003 [165]) and aerosols (Zhang et al. [158]) Wet: scavenging model for gases and aerosols (Seinfeld and Pandis [19])	95/5	CB05 [169]
University of Aarhus **(DK1)**	16.7 km×16.7 km	29 layers up to 100 hPa	Wet and dry as in Simpson et al. [166]	90/10	Brandt et al. [81]
Istanbul Technical University **(TR1)**	184×156 cells, 30km×30km	24 layers up to 10 hPa	Wet and dry as in Foley et al. [25]	95/5	CB05 [169]
Kings College **(UK1)**	15km×15km	23 layers up to 100 hPa, 7 layers below 1 km. First layer ~14m	Dry: electrical resistance analogy model Wet: taken from the RADM (Chang et al., [167])	90/10	CB05 [169]
Ricardo E&E **(UK2)**	30km×30km	23 layers up to 100 hPa, 7 layers below 1 km. First layer ~15m	Dry: Pleim and Ran [168] Wet: Byun and Schere [82]	Road transport: 86/14; non-road: 95/5	CB05-TUCL [169 170]
Helmholtz- Zentrum Geesthacht **(DE1)**	24km×24km	30 vertical layers from ~40m to 50 hPa	Dry: Pleim and Ran [168] Wet: Byun and Schere [82]	90/10	CB05-TUCL [169 170]
University of Hertfordshire **(UK3)**	18km×18km	35 vertical layers from ~20m to ~16km	Dry: resistance analogy model (Wesely [163]). Wet: asymmetric convective model algorithm in CMAQ cloud module	90/10	CB05-TUCL [169 170]

In FI1 and FI2 groups, the gas phase chemistry was simulated with CBM-IV, with reaction rates updated according to the recommendations of International Union of Pure and Applied Chemistry (IUPAC) [175] and the National Aeronautics and Space Administration (NASA) Jet Propulsion Laboratory [176]. NL1 group's gas-phase chemistry is based on CBM-IV (modified reaction rates; see Sauter et al. [79]).

TR1 configured CMAQ v4.7.1 with the CB05 chemical mechanism and the AERO5 module [25] for the simulation of gas phase chemistry and aerosol and aqueous chemistry, respectively. IT1 using CAMx version 6.10 [177] with CB05 gas-phase chemistry [169]. UK3 used the gas-phase chemical mechanism with updated toluene and chlorine chemistry (CB05-TUCL) [169 170], and the aerosol chemical reaction was treated with AERO6 module. CB05-TUCL was also used by UK2 and DE1.

DK1 employed the technique of Brandt et al. [81], which includes 58 chemical species, 9 primary particles, and 122 chemical reactions.

Photolysis rates

In FI1, pressure and latitude dependent photolysis rates of the FinROSE model [179] are used and reduced proportionally to cloud cover below the clouds down to half the original value at full cloud cover. Photolysis rates of NL1 are based on clear-sky photolysis rate by Roeth's flux algorithm (function of solar zenith angle [180]) and multiplied by an attenuation factor in case of clouds. IT2 calculated the photolysis frequencies with the Fast-J scheme [181]. Dry deposition and photolysis schemes were modified to take into account the effects of the soil snow coverage [182].

Plume rise

The majority of models employed the prescribed vertical distribution by EMEP [183], while UK1 adopted the Briggs plume rise algorithm [184][185]. FI1, FI2, FRES1 and DE1 adopted the sector-dependent vertical emission profiles [186]. F1 and FI2 did not account for extra plume rise in addition to that prescribed by the emission profiles, since SILAM model doesn't take it into account. NL1 group did not take into account extra plume rise in addition to that prescribed by the emission profiles. A specific feature of the model that NL1 used (LOTOS) is that it only covers the lower 3.5 km of the atmosphere, with a static 25m surface layer, a dynamic mixing layer and two dynamic reservoir layers. This makes the model relatively fast in terms of computation

time but has implications for the vertical mixing of species for instances where the mixing layer rapidly changes in height.

Secondary aerosols

FI1 and FI2 computed the secondary inorganic aerosol (SIA) formation with the updated DMAT scheme [187] and secondary organic aerosol (SOA) formation with the volatility basis set (VBS) [188]. SIA formation on ISORROPIA II [189] was used by NL1. Modelled terpene emissions were reduced by 50% to limit their contribution to SOA formation, which was found to be too high. Version 3.6 of the WRF-Chem has been used by IT2, modified to include the new chemistry option implemented by Tuccella et al. [190] that includes a better representation of the secondary organic aerosol mass in the simulation of direct and indirect aerosol effects, calculated as in Ahmadov et al. [188]. Here only direct effects were included in the simulation, for computational expediency. DK1 calculated SOA by following the two-product approach assuming that hydrocarbons undergo oxidation through O_3, OH, and NO_3 and for only two semi-volatile gas products [191]. However, the module is simple because it does not include aging processes and further reactions in the gas and particulates.

2.1.3.3 Performance Evaluation Framework

In the literature there are a variety of performance metrics which are including but not limited to mean bias/error (MB/ME), mean normalized bias/error (MNB/MNE), fractional bias/error (FB/FE), root/normalized mean square error (RMSE/NMSE), normalized mean bias/error (NMB/NME), unpaired peak accuracy (UPA), index of agreement (IoA), Pearson's correlation coefficient (PCC) and the coefficient of determination (r^2). Their definitions, ranges and best values are given in Table 2.7.

Each metric has its own drawbacks and benefits which have been discussed in the literature up to day. The operational metrics (magnitude of the error, sign of the bias, associativity) provide an overall sense of model strengths and deficiencies, while apportioning the error to its constituent parts (bias, variance, and co- variance) can help assess the nature and quality of the error [71]. These metrics are used for summarizing AQMEII model performances.

In the literature Taylor Diagrams are also presented as a valuable tool for performance evaluation, which is a 2 dimensional plot showing three statistical quantities; the ratio of variances of both model and observed fields, the cantered RMSE and the PCC between the two fields for the model variable under consideration in one point [192]. It can summarize the agreement between the observations and the model predictions.

Table 2.7 : Definitions of performance metrics.

Abbreviation	Definition	Formula	Range	Best
MB (or BIAS)	Mean Bias	$\dfrac{1}{N}\sum (M_i - O_i)$	-	0
ME (or MAE)	Mean (Absolute) Error	$\dfrac{1}{N}\sum |M_i - O_i|$	≥ 0	0
MNB	Mean Normalized Bias	$100*\dfrac{1}{N}\sum \left(\dfrac{M_i - O_i}{O_i}\right)$	-100% to $+\infty$	
MNE	Mean Normalized Error	$100*\dfrac{1}{N}\sum \left|\dfrac{M_i - O_i}{O_i}\right|$	0 to $+\infty$	0
FB (or MFB)	(Mean) Fractional Bias	$100*\dfrac{2}{N}\sum \dfrac{(M_i - O_i)}{(M_i + O_i)}$		
FE (or MFE)	(Mean) Fractional Error	$100*\dfrac{2}{N}\sum \dfrac{|M_i - O_i|}{(M_i + O_i)}$	0-100%	0
NMB (or NBIAS)	Normalized (Mean) Bias	$100*\dfrac{\sum(M_i - O_i)}{\sum O_i}$	±100%	0
NME	Normalized Mean Error	$100*\dfrac{\sum|M_i - O_i|}{\sum O_i}$	0-100%	0
RMSE	Root Mean Squared Error	$\sqrt{\dfrac{\sum(M_i - O_i)^2}{N}}$		

Table 2.7 (continued) : Definitions of performance metrics.

Abbreviation	Definition	Formula	Range	Best
NMSE	Normalized Mean Square Error	$\dfrac{\sum s_i{}^2 (1-k_i)^2}{\sum s_i k_i}$ $(s_i = \frac{O}{\bar{O}} \text{ and } k_i = \frac{M}{O})$		0
UPA	Unpaired Peak Accuracy	$100 * \dfrac{(M_{peak} - O_{peak})}{O_{peak}}$	$\pm 100\%$	0
IoA	Index of Agreement	$1 - \dfrac{\sum (M_i - O_i)^2}{\sum(|M_i - \bar{O}| + |O_i - \bar{O}|)^2}$	0-1	1
PCC (or r)	Pearson Correlation Coefficient	$\dfrac{\sum (M_i - \bar{M})(O_i - \bar{O})}{(N-1)\sigma_M \sigma_O}$	$-1 \le r \le 1$	± 1
r^2	Coefficient of Determination	$\left(\dfrac{\sum ((M_i - \bar{M})(O_i - \bar{O}))}{\sqrt{\sum (M_i - \bar{M})^2 \ \sum (O_i - \bar{O})^2}} \right)^2$	0-1	1

Nonetheless all performance metrics were calculated for each station in this study. Since it is not possible to give all metrics for 1447 air quality stations in Europe, they are summarized on maps and given in Appendix 1. Furthermore, Taylor Diagrams will be used for comparisons of the AQMEII models.

In the literature Taylor Diagrams are presented as a valuable tool for performance evaluation. It is a 2 dimensional plot showing three statistical quantities; the ratio of variances of both model and observed fields, the centered RMSE and the PCC between the two fields for the model variable under consideration in one point [192]. Taylor diagrams can summarize the agreement between the observations and the model predictions.

The formulas used in the generation of Taylor diagram are given as follows;

$$E' = \sqrt{\frac{\sum[(M_i-\bar{M})-(O_i-\bar{O})]^2}{N}} \qquad (2.5)$$

$$\sigma_m = \sqrt{\frac{\sum(M_i-\bar{M})^2}{N}} \qquad (2.6)$$

$$\sigma_O = \sqrt{\frac{\sum(O_i - \bar{O})^2}{N}} \qquad (2.7)$$

$$r = \frac{\sum(M_i - \bar{M})(O_i - \bar{O})}{(N-1)\sigma_M \sigma_O} \qquad (2.8)$$

where E' is the centred difference (errors) of Root Mean Squares (centred RMSE) and best value is 0, σ is standard deviation, r is Pearson's correlation coefficient, M stands for model, O stands for observations, N is number of values where overbar indicates averaging.

Observed standard deviation is indicated with a black star on the x axis and follows the dashed black arc above. White curves originated from x axis (and meets with the same value on the y axis) indicate standard deviations. Standard deviation of the models can be read by following the white curve where the model number located. Standard deviation of the model should be close to standard deviation of the observations. In Taylor diagram, the closer model to the dashed black arc, the closest standard deviation to the observations. In the best case, it can be said that the variability in the measurements is captured by the model. Model performance is associated with its close standard deviation to standard deviation of the observations, but this assessment does not give an idea of model performance solely. Other statistical items of Taylor Diagram should be considered holistically.

The second statistical performance metric of Taylor diagram is Pearson's Correlation coefficient (PCC). Correlation is a measure of the relationship between model results and measurements. The higher the correlation, the better the model results are matched with the measurements. Correlation of the model should be high, best value is 1. In Taylor diagram, the model closes to the x axis more correlated with observations than the above model.

The third statistical performance metric in Taylor diagram is cantered RMSE which is shown with black arcs around standard deviation of observations which is showed with a black star in x axis. Best RMS difference value is 0.

Consequently, the position of each letter appearing on the plot enables visually assess how closely that model's simulated PM_{10} concentration pattern matches observations [192]. Best model should have close standard deviation with observations, strong correlation (r close to 1) and low cantered RMSE (best is zero). By combining all three

metrics, it is clear that best model will lie nearest the point marked "observed" on the x-axis.

2.2 Country-Specific EF Development

Currently national emission inventories of Turkey is calculated via EFs from guidebooks of global agencies such as EEA [54] and IPCC [55]. Those EFs were calculated by considering power plants in selected countries, which appertains for specific production practices. Furthermore, abatement technologies depend on current regulation of each country, then EFs are representative for those specific conditions. Thus, development and usage of country-specific EFs are strongly encouraged by global advisory agencies [54][55]and[193]. In this study, local EFs were calculated from measurements when possible. If there were no adequate data for calculation of the local EFs, most representative EFs were selected for calculation of the emission inventory.

2.2.1 Data used in country-specific EF development

EF calculation part of this study benefits from Public Research Support Group (KAMAG) project (project number is 111G037) of the Scientific and Technological Research Council of Turkey (TUBITAK) [194]. Point, line and area sources of Marmara region was considered in KAMAG project, but this study focuses on the industrial emissions part (point sources) of the project. In industrial part of the project, country-specific EFs were developed by in-situ measurements and official emission measurement reports (EMRs). 120 stack measurements were conducted in 8 plants (11 stacks) by KAMAG measurement team for only public electricity and heat production plants in Marmara region. Furthermore, official EMRs of 32 energy production plants with 113 stacks were considered in the calculation of EFs, which resulted 339 measurements. The reliability of official EMRs, which are prepared by the facility-company cooperation, is questioned by the administrative and academic community. Therefore, measurements conducted by the KAMAG project team were used in this study as much as possible, which includes at least two visits per plant turning with 8 recurrent measurements from each visit. In the absence or insufficient measurements, official EMRs were used. In such cases, the calculated EF has been revised by comparing with the international EFs and the final decision has been made

accordingly, by expert judgement. The specific data according to plants were hidden in the thesis due to confidential reasons required by the project regulations.

In-situ measurements include following parameters with 8 replicates at a time: facility name, city, date of sampling, stack name, measurement number, fuel type, fuel calorific value, flue gas flow (Nm^3/h), dry flue gas flow (Nm^3/h), gas temperature ($^\circ$C), gas velocity (m/s), moisture content (%), reference oxygen (%), dust (mg/m^3 and kg/h), CO (mg/m^3 and kg/h), NO (mg/m^3 and kg/h), NO_2 (mg/m^3 and kg/h), SO_2 (mg/m^3 and kg/h), CO_2 (mg/m^3 and kg/h), Benzene (mg/m^3 and kg/h), Toluene (mg/m^3 and kg/h), Ethyl Benzene (mg/m^3 and kg/h), Xylene (mg/m^3 and kg/h), Cd (mg/m^3 and kg/h), Cr (mg/m^3 and kg/h), Cu (mg/m^3 and kg/h), Ni (mg/m^3 and kg/h), Pb (mg/m^3 and kg/h). Total number of parameters is 43. In the meantime, a questionnaire form requested from the plant operators regarding to the general properties of the plant, firing practices, fuel and stack properties. A sample of the questionnaire form is given in Appendix A.

There are many data in the EMRs, but in the scope of this study, the following parameters were taken into account for the calculation of EFs and emission inventory; facility name, source name, city, date of sampling, measurement number, fuel type, thermal power of the plant (MW), fuel amount (m^3/h), fuel calorific value, flue gas flow (Nm^3/h), moisture content (%), gas velocity (m/s), dry flue gas flow (Nm^3/h, m^3/h), gas temperature ($^\circ$C), gas velocity (m/s), Oxygen (%), CO (mg/m^3 and kg/h), NO (ppm or mg/m^3 and kg/h), NO_2 (mg/m^3 and kg/h), NO_x (mg/m^3 and kg/h), SO_2 (mg/m^3 and kg/h), dust (mg/m^3 and kg/h) and soot count (on Bacharach scale). According to local regulations, Fluorine (mg/m^3 and kg/h) and Chlorine (mg/m^3 and kg/h) emissions are also measured in power plants with a capacity greater than 300 MW.

2.2.2 Methodology adopted in country-specific EF development

Before starting the EF calculations, each stack was examined in detail. Due to the CLTRAP treaty [51] signed by Turkey, emission inventory of Turkey is compiled annually according to EMEP guidebook [54] by Turkish Ministry of Environment and Urbanization [53]. For this reason, the coding system in EMEP was taken into consideration in order to group the emission sources in this study. Public electricity

and heat generation category is indicated by "1.A.1.a" as NFR (Nomenclature for Reporting) code in EMEP guidebook [54].

The tables in the EMEP guidebook [54] are classified as Tier 1 and Tier 2 according to the detailed status of the data held by the emission inventory developers. The tables with Tier 1 codes include generalized EFs by fuel types. Since our aim in this study is not to develop generalized EFs as in Tier 1 category of EMEP guidebook [54] but to develop country-specific EFs as detailed as possible, we consider Tier 2 codes at this stage. In Tier 2 tables, the SNAP (Standardized Nomenclature for Air Pollutants) code appears in addition to the NFR code. The SNAP codes depend on the type of fuel used, the installation technology and the capacity of the plant. Detailed investigation of the stack and also the connected production line of this stack is required in order to assign correct SNAP/NFR code. The subject of the production, the method of the production and detailed understanding of the manufacturing processes is vital for correct decision making. SNAP/NFR code assignment, requires not only deep understanding of the processes but also the understanding of European SNAP/NFR coding system.

There are 12 different EF tables under the title of Public Electricity and Heat generation title in EMEP (Tier 2), which are classified by fuel type, combustion technology and power. Since not all technology and fuel types in EMEP guidebook [54] are available in the Marmara Region of Turkey (the region considered in this study), EFs were only calculated for five SNAP/NFR categories of EMEP in this study. The list of SNAP/NFR codes used in this study is given in Table 2.8. In EMEP guidebook [54], 1.A.1.A-10101-3.10 and 1.A.1.A-10102-3.10 codes are represented in a single table with same EFs, however different EFs are calculated for each code in this study.

After assigning correct SNAP/NFR code for 124 stacks (11 stacks from in-situ measurements and 113 stacks from EMRs) by a thorough understanding of the manufacturing process, emissions are transferred into a database. Ultimately, this database includes 459 stack measurements (120 in-situ measurements and 359 measurements from EMRs) for all parameters listed below.

Table 2.8 : SNAP/NFR codes of EMEP guidebook [54] considered in this study.

NFR	SNAP	Table No	SNAP Definition	Fuel	Technology
1.A.1.A	10101	3_10	Public power - Combustion plants >= 300 MW (boilers)	Brown Coal/ Lignite	Wet and Dry Bottom Boilers
1.A.1.A	10102	3_10	Public power - Combustion plants >= 50 and < 300 MW (boilers)	Brown Coal/ Lignite	Wet and Dry Bottom Boilers
1.A.1.A	10101	3_16	Public power - Combustion plants >= 300 MW (boilers)	Brown Coal	Fluid Bed Boilers
1.A.1.A	10102	3_12	Public power - Combustion plants >= 50 and < 300 MW (boilers)	Natural Gas	Dry Bottom Boilers
1.A.1.A	10104	3_17	Public power - Gas turbines	Gaseous Fuels	Gas Turbines

In order to handle this large dataset an R code was written which used this dataset as an input. This code applies a quality control procedure for both in-situ measurements and the data from official emission reports, initially, which summarized below;

- If the difference between the eight consecutive in-situ measurements was more than twice, the data was examined more carefully.

- The second of the in-situ measurements (in-situ measurements were performed eight times in two separate visits) was flagged and further investigated, if there were more than twice the difference between measurements of first and second visits.

- The above steps were applied for all parameters measured, not just concentration data.

After applying quality control procedure, EF is calculated for each measurement by two different methods. The first is based on the mass flow rate (in the unit of kg/h) in the flue gas and the second is based on the concentration (in the unit of mg/m^3) data in the flue gas. With the help of the R code, one EF was calculated for each measurement and for each pollutant by both methods. The EFs calculated in the two methods should be identical. Based on this assumption, the quality control procedure was continued and in case the EF calculated by both methods were not identical, the data of the related measurement was examined. If there was an error, the measurement was deleted accordingly.

The EF calculation formula from the flue gas concentration is as follows;

$$Emission\ Factor\ \left(\frac{g\ emission}{GJ\ fuel}\right) = Concentration\ \left(\frac{mg\ emission}{m^3}\right)$$

$$* \frac{1\ g}{1000\ mg} * Dry\ flue\ gas\ flow\ \left(\frac{m^3}{h}\right) * \frac{1}{Fuel\ rate\ (\frac{kg}{year})}$$

$$* \frac{number\ of\ working\ days}{year} * \frac{number\ of\ working\ hour}{day}$$

$$* \frac{1}{fuel\ calorific\ value\left(\frac{kcal}{kg}\right)} * \frac{10^6\ kcal}{4.1868\ GJ} \tag{2.9}$$

where g is gram, mg is milligrams, kg is kilograms, GJ is gigajoules, m^3 is cubic meters, h is hour, and kcal is kilocalories. The amount of fuel was taken in the unit "kg/year" for solid fuels and in "m^3/year" for liquid and gaseous fuels. The calorific value of the fuel was taken in the unit of "kcal/kg" for solid fuels and in "kcal/m^3" for liquid and gaseous fuels. The information on annual number of working days, daily working hours and annual consumption of fuel for the associated stack was obtained via questionnaire forms (Appendix A) asked from site operators during in-situ measurements. If there is any missing information, firstly the facilities were called and asked. If the call is failed or information is unclear or absent, the information was accessed from emission permit report of the facility. If the information is still not available, the measurement was not used in the calculations.

The EF calculation formula from the mass flow is as follows;

$$Emission\ Factor\ \left(\frac{g\ emission}{GJ\ fuel}\right) = mass\ flow\ rate\ \left(\frac{kg\ emission}{h}\right) * \frac{1000g}{kg}$$

$$* \frac{1}{fuel\ rate\ \left(\frac{kg}{h}\right)} * \frac{1}{fuel\ caloriphic\ value\ \left(\frac{kcal}{kg}\right)} * \frac{10^6\ kcal}{4.1868\ GJ} \tag{2.10}$$

The amount of fuel was taken in the unit "kg/h" for solid fuels and in "m^3/h" for liquid and gaseous fuels. For each measurement, EF was calculated separately using both mass and volumetric concentrations as given in equations 1 and 2. Under normal circumstances, the calculation of both methods should give the same EF. By comparing the two results, it is possible to verify the calculations and data. When two

EFs are not identical, the calculation steps and data are reviewed, the EF calculated for that measurement is excluded if a satisfactory result is not reached.

In the next step, the stacks having the same SNAP/NFR code were grouped and their averages were calculated. EFs derived from in-situ measurements and EFs calculated from the EMRs were treated separately in this step. At the end of this step there were two EFs for each SNAP/NFR category. In addition to the averages, confidence intervals and some other statistical parameters were calculated for each EF, which will be used in the calculation of uncertainties during the development of emission inventory.

At this stage, EFs that fall into the same SNAP/NFR category were investigated from the literature. Since this study (as a part of KAMAG project [194]) is the first in Turkey for the development of country-specific EFs from in-situ measurements in Turkey, two international guidebooks were considered for comparing EFs, which are EMEP guidebook [54] and AP-42 [193] database of U.S. EPA. After comparing results with literature, EFs derived from in-situ measurements have been used primarily because of the drawbacks about the reliability of official EMRs as discussed in Section 2.2.1 .

Although all those SNAP/NFR codes were considered in this study, EFs were developed only for 1.A.1.A-10102-3.12 and 1.A.1.A-10104-3.17 since there are no plants included in KAMAG database [194] attributed to remaining SNAP/NFR codes or the data was not adequate for calculation of specific EFs.

2.2.3 Variability analysis method

Variability refers to the heterogeneity of the values in a dataset with respect to time, space or a population [195]. Since the measurements used in the EF calculations are made at different times and in different stacks or plants, there is often a high inter-measurement variability. Precision in the estimate of the statistics such as mean, standard deviation or parameters of a distribution fit to a data set describing inter-measurement variability influences uncertainty quantification based upon random sampling error [196]. In this part of the study, the method for quantification of variability between EFs is summarized.

The first step of the quantification of variability is visualizing the data in order to evaluate central tendency (may be called as the centre or location of the distribution) and dispersion of the data, and identifying the outliers in the data [196]. Plotting the

dataset as an empirical cumulative distribution function (CDF) is a specific technique in order to visualize and evaluate the dataset. In a CDF, cumulative probability of each value is calculated and plotted according to values. Since cumulative probability is the probability that the random variable has values less than or equal to a specific numerical value of the random variable, CDFs can provide a relationship between fractiles (percentage basis fraction of the values that are less than or equal to specific value of a random variable) and quantiles (the value of a random variable associated with a given fractile) [74]. In this step, the shape of the empirical distribution is visually inspected in order to fit the probability distribution model in the next step. The shape of the distribution is reflected by the quantities such as skewness (shows the asymmetry of a distribution) and kurtosis (shows the peakedness of a distribution). Dispersion of a distribution reflected by the 95% probability range of values, which is often of particular interest in air quality studies, indicates the range of the data values enclosed by the 0.025 and 0.975 fractiles (2.5 and 97.5 percentiles).

In addition to visual assessment of the data, the dispersion of a distribution is measured by the standard deviation or variance. Relative standard deviation (also known as the coefficient of variation, Cv), which is obtained by the ratio of standard deviation and mean, provides a normalized indication of the dispersion of data values. Large Cv indicates relatively large variability in the dataset [74].

$$\overline{X} = \text{mean} = \frac{\sum X_i}{N} \tag{2.11}$$

$$\sigma^2 = \text{variance} = \frac{\sum (X_i - \overline{X})^2}{N} \tag{2.12}$$

$$\sigma = \text{standard deviation} = \sqrt{\frac{\sum (X_i - \overline{X})^2}{N}} \tag{2.13}$$

$$Cv(\%) = \frac{\sigma}{\overline{X}} * 100 \tag{2.14}$$

Skewness and kurtosis are used to identify the shape of the distribution, where the skewness shows the asymmetry in a distribution and kurtosis shows the peakedness of a distribution. These statistics are also used as an aid when fitting a parametric probability distribution model to the data [197]. Although there are several different formulas for skewness and kurtosis, in this study following formulas are used;

$$C_{SX} = \frac{\frac{N}{(N-1)(N-2)}\left[\frac{\sum_{i=1}^{N}(X_i-\bar{X})^3}{N}\right]}{\sigma^3} \tag{2.15}$$

$$C_{kX} = \frac{\frac{N}{(N-1)(N-2)}\left[\frac{\sum_{i=1}^{N}(X_i-\bar{X})^4}{N}\right]}{\sigma^4} - 3 \tag{2.16}$$

where C_{SX} is Fisher-Pearson coefficient of skewness (in r fisher option with unbiased moment), where the left term of the upper part is used as an adjustment for sample size. For normal distribution and any symmetric data C_{SX} is close to zero, negative values for the skewness indicate left skewed data and positive values indicate data that are skewed right. By skewed right, we mean that the right tail is long relative to the left tail. C_{kX} is the coefficient of kurtosis where it is zero for standard normal distribution. s (in r excess option) [198]. AuvTool is used for quantification of variability and uncertainty [196].

2.2.4 Uncertainty quantification method

Analytical and numerical solutions are available for quantifying uncertainty in the mean or standard deviation. Analytical solutions can be used under one or more of the following conditions; underlying distribution of a dataset is normal, variance is low or the sample size is large enough (e.g. >30) [199]. Analytical methods based on normality may lead to significant errors in the estimation of confidence intervals when following conditions are not valid. Numerical methods are flexible in terms of underlying distribution for estimating confidence intervals. Bootstrap simulation is one of the widely used numerical methods in quantifying confidence intervals based on random sampling error from parametric distributions. In this study, numerical solution was considered in quantifying uncertainties in the generation of country specific EFs. General methodology adopted in generation of country specific EFs are summarized in Figure 2.7. The method is adopted from the study of Cullen and Frey (1999) [197].

The flue gas measurements used to calculate country-specific EFs (x = {x1, x2, ..., xn} where n is the number of the calculated EFs in Figure 2.7) in this thesis are discrete measurements. Therefore, the temporal variability of the data is uncertain. That is, it only contains the flue gas values gathered at the time of the measurement. Installation of continuous flue gas measurement systems in Turkey is compulsory for the plants

above a certain capacity. Even if there is continuous emission measurement data, then uncertainties may occur due to errors in the measuring instrument and changes due to operating conditions. Even if we try to converge to the real value as much as possible, for these reasons, the EFs we calculate using flue gas measurements do not represent absolute values but gives an idea. In such cases where it is not possible to accurately sample the entire population, a representative sample must be used [74]-[199]. When a sample group is used, it is possible to obtain an idea about the entire population, but it can never fully match the entire population. For this reason, there will always be some likelihood of random sampling error [74]. In this study, our sampling group is the set of EFs calculated from discrete flue gas measurements.

In statistics, sampling error is a type of error caused by investigating a small part of the population rather than examining the whole population. It is calculated by the difference of a sample statistic used to estimate a population parameter and the actual but unknown value of the parameter. Uncertainty is expressed as lack of knowledge regarding to true value of a quantity [196]. Uncertainty in a statistic attributable to random sampling error can be represented by a sampling distribution [197]. A confidence interval for a statistic is a measure of the lack of knowledge regarding the true value of the statistic [199].

In order to calculate uncertainty, a distribution is fitted ($\hat{F}$) to the EF dataset (x) where actual underlying distribution (F) is unknown, as given in Figure 2.7. Fitting distribution methodology is described in Section 2.2.4.1. The goodness-of-fit is evaluated by some techniques described in Section 2.2.4.2. The parameter of interest, θ, is a characteristic of the distribution of F, $\theta = f(F)$, such as the mean, variance, shape or scale parameter, or any fractile or quantile of the distribution F. An estimate of θ is the statistic θ , which is determined from the data set, $\theta = f(x)$.

Then Monte Carlo method is applied in order to generate random datasets from assigned distribution, $\hat{F}$ (described in detail in Section 2.2.4.4). This process is repeated up to generate a number of alternative probability distribution models from which the original dataset is a plausible random sample.

In Bootstrap simulation part of the study (described in detail in Section 2.2.4.5), each of the alternative probability models generated by Monte Carlo approach (Bootstrap replicates) are simulated to develop a reasonably stable characterization of the

percentiles of the distribution. In this step, a distribution is fitted to each of the bootstrap sample, then parameters, $\hat{\theta}^*$, are estimated. In this study, uncertainty in the estimate of θ is reflected by dispersion of $\hat{\theta}^*$, which also gives random sampling error.

The $\hat{\theta}^*$ data is sorted then in order to calculate confidence interval for the fitted cumulative distribution function. Consequently, the results are compared to the original dataset by generating probability bands.

2.2.4.1 Fitting a distribution

Selection of the probability distribution model for variability by fitting a distribution to each of the dataset is required in order to generate random samples that will be used in uncertainty analysis. Probability distribution models may be empirical (a discrete distribution that gives equal probability to each value in the dataset [200], therefore has CDF with a step function of original dataset), parametric (assumed by considering the parameters of the distribution of the dataset) or combinations of both.

One of the main shortcomings of empirical distribution models is that the resampled (sampled from the data calculated via empirical distribution function) datasets are limited to the minimum and maximum values within the dataset. When only small datasets are available, this can lead to biases in the representation of a given model output. Air quality measurements include data at a given time, which can be measured more or less in subsequent measurements.

The complex structure of the empirical distribution models is another shortcoming. In parametric distribution there are particular type of parametric functions and the calculation methodology of its parameters are well defined. Therefore, parametric probability distribution models are capable of describing data points (even the larger number of data points) in a compact manner based on a particular type of parametric distribution function and the values of its parameters, where it is complex in empirical probability distribution models [201]. Minimum and maximum values of the distribution are limited to minimum and maximum values of the data in conventional empirical distributions; however, it is possible to make predictions in the tails of the distribution beyond the range of observed data in parametric distribution models [196].

MONTE CARLO METHOD

STEP 4 - Generation of Random Variables from Distribution

Generated Dataset 1	Generated Dataset 2	Generated Dataset ..	Generated Dataset B
$\begin{bmatrix} x^{*1} \\ \dots \\ x^{*n} \end{bmatrix}$	$\begin{bmatrix} x^{*1} \\ \dots \\ x^{*n} \end{bmatrix}$	… … …	$\begin{bmatrix} x^{*1} \\ \dots \\ x^{*n} \end{bmatrix}$

$B =$ Number of bootstrap samples
(generated datasets by Monte Carlo method)

$x^* =$ Independent bootstrap sample

Original Emission Factor Dataset

$$\begin{bmatrix} x_1 \\ \dots \\ x_n \end{bmatrix}$$

n = sample size
F = unknown probability distribution
θ = parameter of the unknown distribution

θ = f(F)

DISTRIBUTION FITTING

STEP 1 - Fitting Distribution to the Original Dataset
Define population distribution
$\widehat{F}$ = The distribution assigned for estimating unknown F

STEP 2 - Estimation of the parameters
$\widehat{\theta} =$ A statistic estimated from θ

$$\widehat{\theta} = f(x)$$

STEP 3 - Evaluation of goodness of fit
Visual comparison by CDFs and Histograms
Goodness of fit tests /criteria

BOOTSTRAP METHOD

STEP 5 - Fitting a distribution for each of the bootstrap sample

STEP 6 - Estimation of the parameters for each bootstrap sample
Mean, Standard Deviation, 1st parameter and 2nd parameter is calculated for each B

$\widehat{\theta}^* =$ Bootstrap replicate of $\widehat{\theta}$ (independent estimate of θ)

$$\widehat{\theta}^* = f(x^*)$$

STEP 7- Sorting bootstrap samples
from small to large for each random variable (q)

STEP 8- Calculation of the Confidence Intervals
Calculation of the selected percentiles of for each random variable (q)
by "Percentile Method"
(Percentiles → Confidence intervals)

STEP 9 - Generating Probability Band
For evaluating adequacy of the fitted model

Figure 2.7 : Uncertainty and variability quantification methodology adopted in country-specific EF development.

Considering all this information, it was decided to take parametric probability distribution models into consideration when fitting a parametric distribution model to the generated EFs. Selection of the parametric distribution for variability requires combination of a deep knowledge about theoretical and empirical considerations.

All these statistics and visual inspection of the CDFs were combined with goodness-of-fit statistics and goodness-of-fit criteria for selecting best fitting parametric probability distribution model to our data. Furthermore, the processes that generate the data should be considered.

Parametric probability distribution models used in AuvTool include the normal, lognormal, Weibull, gamma, beta, uniform, symmetric triangle parametric distributions. Normal distribution is not appropriate for representing non-negative quantities because it has an infinite negative tail, however it can be used when Cv is less than 0.2 [202]. The lognormal, gamma and Weibull distributions are useful for representing non-negative and positively skewed data [196]. Although two-parameter beta distribution has flexibility to represent data with a variety of central tendency and skewness [196], it was not considered in this study since it is bounded by zero and one. The uniform and symmetric triangle distributions are most commonly used to represent expert judgments made in the absence of data [196]. These two distributions were considered when EFs of the same code are clustered around two or more extreme values.

2.2.4.2 Evaluating goodness-of-fit

CDFs and histograms were used in order to visually evaluate the fit of parametric distribution. In addition, goodness-of-fit statistic and goodness-of-fit criteria were used in order to select best fitting parametric distribution.

Goodness-of-fit statistics are not limited but including Kolmogorov-Smirnov statistic, Cramer-von Mises statistic, Anderson-Darling statistic. Also, goodness-of-fit criteria is not limited but including Akaike's Information Criterion and Bayesian Information Criterion. These statistics were calculated with "fitdistrplus" package [203] of R software.

Kolmogorov-Smirnov Statistic

Kolmogorov-Smirnov statistic is based on the maximum distance between CDF of the fitted parametric distribution and empirical CDF of the data. Then maximum distance is compared to a tabulated critical value for a significance level and rejected if the distance is larger than the critical value. For best fitting distributions, the maximum distance should be less than the critical value [197]. It can be applied to normal, lognormal, Weibull, gamma, beta, uniform, symmetric triangle parametric distributions with two limitations as being sensitive near the centre of the distribution than at the tails, and being valid only in continuous distributions

Kolmogorov-Smirnov statistic calculation steps are [197][199][204]-[207];

- Rank the original dataset in an ascending order where $X_k < X_{k+1}$ (k=1, 2, …, n) where X is the ordered dataset is X, n is the number of the data points in X, X_k is the data.

- Develop a stepwise cumulative density function as follows;

$$S_n(x) = \begin{cases} 0 & x < x_1 \\ k/n & x_k \leq x \leq x_{k+1} \\ 1 & x \geq x_n \end{cases} \qquad (2.17)$$

where $S_n(x)$ is the empirical cumulative distribution function.

- Calculate the D_n which is the maximum difference (distance) between $S_n(x)$ and the CDF of the fitted distribution, F(x), over the entire range of X.

$$D_n = \max |F(x) - S_n(x)| \qquad (2.18)$$

- Decide significance level (α) and find critical value from the tables generated for Kolmogorov-Smirnov statistic in the literature. Generally, 95% confidence interval (α=1-confidence interval = 1-0.95=0.05) is considered in EF estimates. Therefore, critical value table of the Kolmogorov-Smirnov statistic for α=0.05 significance level is given in Table 2.9. Linear interpolation can be used for the not listed n values [205].

Table 2.9 : Critical value of maximum distance (D_n) for 95% confidence interval [206][207] for Kolmogorov-Smirnov statistic.

n	Critical Value
5	0.337
8	0.285
10	0.258
12	0.242
15	0.220
16	0.213
18	0.200
20	0.190
25	0.180
30	0.161
>30	$1.886/\sqrt{n}$

- Kolmogorov-Smirnov statistic (Dn) should be less than critical value (given in Table 2.9) in order to pass goodness-of-fit test.

Akaike's Information Criterion

Akaike's Information Criterion (AIC) is a technique for evaluating the likelihood of a model to predict the future values [208]. In this thesis, AIC is used to evaluate the appropriateness of the fitted distribution to the data. Lowest value of the AIC indicates best fitted parametric distribution to our data. The AIC formula is as follows;

$$AIC = \left(\frac{2n}{n-k-1}\right)k - 2\ln[L_{max}] \qquad (2.19)$$

where n is the number of data values, k is the number of the parameters to be estimated (for instance number of the parameters is two for normal distribution, which are mean and standard deviation), L_{max} is the maximized value of the log-Likelihood for the estimated distribution (for instance it is the natural logarithm of the Likelihood after estimating the parameters of the fitted distribution by Method of Matching Moments).

Bayesian Information Criterion

Bayesian Information Criterion (BIC) is used for selecting best fitting model to a dataset. Lowest value of the BIC indicates best fitting parametric distribution to our data. BIC can be defined as;

$$BIC = \ln(n)\,k - 2\ln(\hat{L}) \qquad (2.20)$$

where n is the number of the data points, k is the number of free parameters to be estimated and $\hat{L}$ is the maximized value of the likelihood function of the model [209].

2.2.4.3 Estimating parameters of the distribution

Once a parametrical distribution has been selected, a key step is to estimating values of the parameters of a parametric probability distribution. There are two most typical statistical techniques used for estimating parameters of a distribution; the method of Maximum Likelihood Estimation (MLE) and the Method of Matching Moments (MoMM) [196]. The MLE method does not always yield minimum variance or unbiased estimates for small sample sizes, however, for larger sample sizes, the MLE method tends to better estimate statistically than other methods [210]. There are convenient solutions for MoMM parameter estimates for the normal, lognormal, gamma, and beta distributions [211], as well as for the uniform and symmetric triangle distributions. However, they are not easy to calculate [196]. In this study, MoMM method was used in order to estimate parameters of the fitted distribution. AuvTool was used for calculating of the parameters.

MoMM is based upon matching the moments or central moments of a parametric distribution (e.g., mean, variance) to the moments or central moments of the data set. The MoMM estimators for each of the parametric distributions are presented in this part of the thesis.

Normal Distribution

Parameters for the normal distribution are the arithmetic mean, ì, and the arithmetic variance, ó². The MoMM estimator of the mean is the sample mean, $\bar{X}$ where MoMM estimator of the variance is the unbiased sample variance, s² [202 212 and 196].

$$\hat{\mu} = \bar{X} = \frac{1}{n}\sum_{i=1}^{n} X_i \qquad (2.21)$$

$$\hat{\sigma}^2 = s^2 = \frac{1}{n-1}\sum_{i=1}^{n}(X_i - \bar{X})^2 \qquad (2.22)$$

Probability density function of normal distribution is written in the following form where x is between 0 and ∞;

70

$$f(x) = \frac{1}{\sqrt{2\pi\sigma^2}} e^{\frac{-(x-\mu)^2}{2\sigma^2}} \tag{2.23}$$

Lognormal Distribution

There are two types of parameters for the lognormal distribution [202 212 and 196] which are,

- geometric mean ($\grave{\iota}_g$) estimated by $\hat{\mu}_g$, and geometric standard deviation ($\acute{o}_g$) estimated by $\hat{\sigma}_g$ or

- The mean of the logarithm of X ($\grave{\iota}_{\ln(x)}$) estimated by $\hat{\mu}_{\ln(x)}$, and standard deviation of the logarithm of X estimated by $\hat{\sigma}_{(lnx)}$. In this study, these parameters are used since they are included in AuvTool.

$$\hat{\mu}_{\ln(x)} = \ln(\bar{X}) - \frac{1}{2}\hat{\sigma}^2{}_{\ln(x)} \tag{2.24}$$

$$\hat{\sigma}^2{}_{\ln(x)} = \sqrt{ln(\bar{X}^2 + s^2) - 2\ln(\bar{X})} \tag{2.25}$$

Probability density function of lognormal distribution is written in the following form where x is between 0 and ∞;

$$f(x) = \frac{1}{x\sqrt{2\pi\sigma_{\ln(x)}{}^2}} e^{\frac{-(\ln x - \mu_{lnx})^2}{2\sigma^2}} \tag{2.26}$$

Gamma Distribution

The parameters of the gamma distribution are the shape parameter $\hat{a}$ (estimate of $\acute{a}$) and $\hat{\beta}$ (estimate of $\hat{a}$), which are estimated through relationships with the sample mean ($\bar{x}$) and unbiased sample variance (s^2) [202 212 and 196].

$$\hat{a} = \frac{\bar{X}^2}{s^2} \tag{2.27}$$

$$\hat{\beta} = \frac{s^2}{\bar{X}} \tag{2.28}$$

Probability density function of gamma distribution is written in the following form where x is between 0 and ∞, $\Gamma(\alpha)$ is the gamma function and tabulated well in the literature for positive values of α ($\Gamma(\alpha) = \int_0^\infty x^{\alpha-1}e^{-x}$);

$$f(x) = \frac{\beta^{-\alpha}x^{\beta-1}e^{-x/\beta}}{\Gamma(\alpha)} \tag{2.29}$$

Weibull Distribution

There is no closed form solution for the MoMM estimator of the parameters of the Weibull distribution. Therefore, as an alternative, a parameter estimation method based upon regression analysis of a probability plot is used in AuvTool as described by Cullen and Frey [197]. In the probability plot method, if a data set is reasonably described by a Weibull distribution, then the following transformation may be used to plot the data;

$$ln\left\{ln\left[\frac{1}{\bar{F}(x_i)}\right]\right\} = c\ln(x_i) - c\ln(k) \tag{2.30}$$

$$\bar{F}(x_i) = 1 - F(x_i) \tag{2.31}$$

where c is the shape parameter and k is the scale parameter. $\bar{F}(x_i)$ is the complementary CDF of x. An empirical estimate of the CDF can be obtained using Hazen equation [213] which is a commonly used equation for finding plotting position of a data point by estimating cumulative probability of it;

$$F_x(x_i) = \Pr(X < x_i) = \frac{i-0.5}{n}, for\ i = 1, 2, ..., n\ and\ x_1 < x_2 < \cdots \tag{2.32}$$

Where i is the rank of the data point when the dataset is arranged in an ascending order, n is the number of the data points, $x_1 < x_2 < \cdots$ are the data points in the rank-ordered dataset, $\Pr(X < x_i)$ is the cumulative probability of obtaining a data point whose value is less than x_i. In AuvTool, the positions of the data points were estimated by Hazen's equation for all parametric distributions.

Probability density function of Weibull distribution is written in the following form where x is between 0 and ∞,

$$f(x) = \frac{c}{k}\left(\frac{x}{k}\right)^{c-1}\exp\left(-\left(\frac{x}{k}\right)^c\right) \tag{2.33}$$

Uniform Distribution

The parameters of the uniform distribution are the endpoints, a and b, which are estimated by $\hat{a}$ and $\hat{b}$. The parameter estimation formula using MoMM are as follows [202][196];

$$\hat{a} = \bar{X} - \sqrt{3}s \tag{2.34}$$

$$\hat{b} = \bar{X} + \sqrt{3}s \tag{2.35}$$

Probability density function of uniform distribution is written in the following form where x is between a and b,

$$f(x) = \frac{1}{b-a} \tag{2.36}$$

Symmetric Triangle Distribution

The parameters of the symmetric triangle distribution are a and b, which are estimated by $\hat{a}$ and $\hat{b}$. The parameter estimation formule using MoMM are as follows [202][196];

$$\hat{a} = \bar{X} \tag{2.37}$$

$$\hat{b} = \sqrt{6}s \tag{2.38}$$

Probability density function of symmetric triangle distribution is written in the following form where x is between a and b,

$$f(x) = \frac{b-|x-a|}{b^2} \tag{2.39}$$

2.2.4.4 Monte Carlo method

In this study, Bootstrap samples are generated by using random Monte Carlo simulation. The starting point of the Monte Carlo simulation is fitting a probability distribution for each model. Then random values are generated from the assigned probability distribution model by numerical methods based on the use of pseudo random number.

Pseudo random numbers are uniformly random numbers generated in a completely deterministic manner which are statistically uniform and independent, reproducible,

efficiently implementable as quickly and economically [214]. The number of the random values that are generated from the original dataset is based upon the beginning of the same sequence repetition, which is called as "period length" [199][214].

There are a variety of methods for generating pseudo random numbers. In Auvtool, that was used by this study, combined Multiple Recursive Generators (MRGs) is used [215], which combines two or more MRGs in order to produce pseudo random numbers.

$$Z_n = (X_n - Y_n) \bmod m_1 \tag{2.40}$$

where Z_n is a combined MRG with two underlying MRGs, X_n and Y_n.

$$X_n = (a_1 X_{n-1} + a_2 X_{n-2} + a_3 X_{n-3}) \bmod m_1 \tag{2.41a}$$

$$Y_n = (b_1 X_{n-1} + b_2 X_{n-2} + b_3 X_{n-3}) \bmod m_2 \tag{2.41b}$$

where $m_1 = 2^{31}-1 = 2147483647$, $m_2 = 2145483479$, $a_1 = 0$, $a_2 = 63308$ and $a_3 = -183326$, $b_1 = 86098$, $b_2 = 0$ and $b_3 = -539608$. Calculations of those coefficients are not discussed here and can be found in the study of L'Ecuyer (1996) [215].

Generation of pseudo random numbers differs according to fitted distribution type in AuvTool [204]. Calculation steps according to distribution types are summarized superficially from this point of study.

Box-Muller method, called as polar method [216], was used in this study with the application method of Law and Kelton (1991) [217], for generation of random variables form a normal distribution.

Lognormal samples are generated by using a special property of lognormal distribution. Namely, if $Y \sim N(\grave{\imath}_{lnx}, \sigma^2{}_{lnx})$, then $e^Y \sim LN(\grave{\imath}_{lnx}, \sigma^2{}_{lnx}$, where "~" denotes "is distributed as", N is normal distribution, LN is lognormal distribution, ì is mean and σ^2 is standard deviation. Therefore, lognormal random samples are generated by $X = e^Y$ algorithm where X is lognormal random sample.

For generation of Gamma random variables, acceptance-rejection algorithm [217] [204]and[199] is used.

Method of inversion using the inverse CDF [202] was used for generation of random samples (X) for Weibull and Uniform distributions.

In this method, CDF of the Weibull distribution can be written as;

$$F(x) = 1 - exp^{-(\frac{x}{k})^c}$$ (2.42)

where X is random variate, c is the shape parameter and k is the scale parameter of the Weibull distribution. Then;

$$X = F^{-1}(U) = k[-ln(1 - U)]^{1/c}$$ (2.43)

where U is a random sample from the U(0,1) distribution.

The method of inversion is applied as follows for generating uniform distributions with any arbitrary endpoint;

$$X = a + (b-a)U$$ (2.44)

where U is a random sample from the U(0,1) distribution, a and b are the endpoints (parameters in this case) of the uniform distribution .

The method of inversion is applied as follows for generating symmetric triangle distributions as follows;

$$X = (a - b) + b(2U)^{1/2} \text{ where } 0 \leq U \leq 0.5$$ (2.45a)

$$X = (a + b) - b(2-2U)^{1/2} \text{ where } 0.5 \leq U \leq 1$$ (2.45b)

U is a random sample from the U(0,1) distribution, a and b are the parameters of the symmetric triangle distribution.

2.2.4.5 Bootstrap simulation

Bootstrap simulation was originally developed by Efron [200] in 1979, for the purpose of estimating confidence intervals for statistics based on random sampling error [199]. Confidence interval is a range of values that is likely to contain an unknown population parameter. In this study, Bootstrap method is used to estimate confidence intervals for the fitted CDF for each country-specific EF. Bootstrap method can use the data generated by Monte Carlo method, directly [218].

Bootstrap simulation is a numerical method which can provide solutions where exact analytical solution is unavailable or inadequate. It can be applied even the original

dataset is not normally distributed or the sample size is small. These advantages of Bootstrap simulation over analytical methods makes it as a more versatile and robust method for estimating uncertainty in a statistic due to sampling error, especially for non-normal datasets [197].

The Bootstrap technique illustrated by Frey and Rhodes (1996) [219] is used in this study which is also basis for AuvTool. The method is summarized in Figure 2.7, and addresses the issue of quantifying the random sampling error that is introduced by estimating some statistic of interest from a limited number of randomly sampled data points. Basically, Bootstrap method starts after applying following steps;

- fitting a distribution ($\hat{F}$) to the EF dataset (x) where actual underlying distribution (F) is unknown, as described in section 2.2.4.1,

- determining statistic $\hat{\theta}$ from the data set with $\hat{\theta} = f(x)$, which is an estimate of θ (mean, variance, shape or scale parameter, or any fractile or quantile of the known distribution F, where θ = f(F)), as described in section 2.2.4.3,

- evaluating goodness-of-fit as described in section 2.2.4.2.

- generating random datasets (Bootstrap samples, $\hat{\theta}^*$), which are Bootstrap replicates of $\hat{\theta}$, by a random simulation method from assigned distribution, $\hat{F}$. In this study Monte Carlo method is used as described in section 2.2.4.4.

In Bootstrap simulation part of the study following steps are applied;

- fitting a distribution to each Bootstrap sample.

- estimation of the distribution parameters for each Bootstrap sample ($\hat{\theta}^*=f(x^*)$). In this study, uncertainty in the estimate of θ is reflected by dispersion of $\hat{\theta}^*$, which also gives random sampling error

- sorting the $\hat{\theta}^*$ data

- calculating confidence interval for the fitted cumulative distribution function by "Percentile Method"

- Comparison of the results to the original dataset by generating probability bands

There is no gold standard for selecting the best method for forming confidence intervals [199]. In Auvtool, percentile method is used since it is widely used in practice

and for its simplicity. The other benefit of using the percentile method to other methods is that it can be applied to any type of Bootstrapped distribution [220].

After ordering B Bootstrap replicates of $\hat{\theta}^*$ ($\hat{\theta}^{*1}, \hat{\theta}^{*2}, \ldots, \hat{\theta}^{*B}$), the upper and lower bounds of the expected confidence interval is estimated by using following formula;

$$\text{Lower bound of the confidence interval} = (100.\alpha)^{\text{th}} \text{ percentile}$$

$$= (B.\alpha)^{\text{th}} \text{ largest value of } \hat{\theta}^* \qquad (2.46)$$

$$\text{Upper bound of the confidence interval} = [100.(1-\alpha)]^{\text{th}} \text{ percentile}$$

$$= [B.(1-\alpha)]^{\text{th}} \text{ largest value of } \hat{\theta}^* \qquad (2.47)$$

$$\alpha = 1-CI/100 \qquad (2.48)$$

where α is the significance level (for 95% confidence interval, α is 1-95/100 = 0.05).

For instance, assume B=1000 and α=0.05 for 95% confidence interval. The lower and upper bounds of confidence interval for the values of a Bootstrap statistic in the ordered set are calculated as;

Lower bound of the confidence interval = 0.05 percentile = 50th largest value of the ordered $\hat{\theta}^*$

Upper bound of the confidence interval = 95 percentile = 950th largest value of the ordered $\hat{\theta}^*$

Bootstrap simulation can be used to help evaluate the goodness-of-fit of a distribution with respect to the original data by graphically comparing confidence intervals for CDF of the fitted distribution to the data. In this study probability band, or confidence band, is used in order to evaluate results of Bootstrap simulation. A probability band is composed of the fitted line plot that depict the upper and lower confidence bounds for all points within the range of data.

2.2.4.6 Uncertainty propagation

In this part of study, propagation of uncertainties in terms of addition is described, because it is necessary to sum the uncertainties in this study. If there is a need to find the uncertainty associated with sum of two individual uncertainties by assuming errors as random and uncorrelated, uncertainties can be calculated by taking square root of sum of squares (quadrature) [221];

$$x \ (\delta x_{low} \text{ and } \delta x_{high}) = y \ (\delta y_{low} \text{ and } \delta y_{high}) + z \ (\delta z_{low} \text{ and } \delta z_{high}) \tag{2.49a}$$

$$x = y + z \tag{2.49b}$$

$$\delta x_{low} = \frac{\sqrt{(\delta y_{low} * y)^2 + (\delta z_{low} * z)^2}}{y + z} \tag{2.49c}$$

$$\delta x_{high} = \frac{\sqrt{(\delta y_{high} * y)^2 + (\delta z_{high} * z)^2}}{y + z} \tag{2.49d}$$

where x is the final sum of the two values which are y and z in this case, δx_{low}, δy_{low} and δz_{low} are 95% lower confidence interval of x, y and z values, respectively. δx_{high}, δy_{high} and δz_{high} are 95% upper confidence interval of x, y and z values, respectively.

2.2.4.7 Percentage uncertainty

Following formula is used in order to express uncertainty as a percent.

$$\text{Percentage uncertainty (lower)} = 100 * (x - \delta x_{low \ or \ high}) \ / \ x \tag{2.50}$$

$$\text{Percentage uncertainty (upper)} = 100 * (\delta x_{low \ or \ high} - x) \ / \ x \tag{2.51}$$

where x is the final sum of the two values which are y and z in this case as described in equation 2.5.a and 2.5.b, $\delta x_{low \ or \ high}$ can be either δx_{low} or δx_{high}, and represents either 95% lower (δx_{low}) or upper (δx_{high}) confidence interval of x.

2.3 Probabilistic Emission Inventory

An emission inventory is compiled in this study, for public electricity and heat production sector of Marmara region. Emission inventory development and EF calculation methodology is summarized below.

2.3.1 Inventory data

Although emission calculation methodology seems a simple multiplication of activity data and EF for industrial plants as in equation 2, each item of the formula requires a deep data collection and analysis effort at the background. In developing countries, especially activity data collection for industrial sources is most time-consuming part for emission inventory developers. Due to its unstable nature of the activity data, inventory developers should have at least the simple descriptive information on the sources before commencement of the works in order to know where to search current data for updating and developing in-hand data.

Activity data sources are including but not limited to the sources we have used in KAMAG project [194] (up to the permission of Ministry of Environment and Urbanization), also open sources including web pages, annual reports of the companies, one to one negotiations with the company representatives, development reports of Ministry of Industry, official asking to Ministry by obeying Turkish law of information acquisition, data acquisition from Turkish Statistical Institute, personal communications with industrial zone representatives, academic studies and opinions of experts both from universities and sector. In urgent cases when there is no data despite all the efforts, then expert judgement was used as a final way for selection of activity data by considering the conditions in Turkey.

If official activity data is not available, then the data was tried to be collected unofficially from the open sources and personal communication. Stack measurements conducted in this study were used for two reasons. First reason is for comparing with official measurements in order to capture outstanding discrepancies between these two measurements conducted with two independent teams; second reason is for using these measurements directly in the calculation of EFs. Finally, EFs were selected from EMEP [54], IPCC [55] and EPA [193] if there is no adequate data for calculation of EFs.

Data combining, data screening and data evaluating were used during the data handling process. Data combining was applied when a data was available from several sources. Data screening was applied when a data doesn't have enough information in the calculations. Data evaluating was used in order to select representative EFs for comparing country specific EFs, and activity data.

2.3.2 Electricity generation plants included in this study

According to Union of Chambers and Commodity Exchanges of Turkey [222], 30.7% of electricity that is produced in Turkey is produced in cities of Marmara region by the total number of the electricity producers as 130. This number includes all small- and large-scale plants without distinction even though they produce electricity for internal use, not for public use. In this study, only public electricity and heat production plants considered which corresponds to middle and large-scale plants.

According to EMEP [54], the size of the plants considered under public electricity and heat production (NFR is 1.A.1.a) exceed 50 MWth. Smaller plants were considered as "small combustion" plants even if the produced energy is sold for public use. According to U.S. EPA [193], this value is accepted as 100 MMBtu/hr heat input, which corresponds to 30 MWth in International System of Units (SI), and smaller plants were considered under "small boilers" category (Source Classification Code, SCC is 1-01-006-01 for natural gas combustion plants). In this study, by taking average of two studies, 40 MWth value is accepted as a lower limit for selection of "public electricity and heat production plants". There are 57 public electricity and heat production plants in Marmara region. Marmara region of Turkey is shown in Figure 2.8, and the public electricity and heat generation plants that were considered in this study are indicated on the right-hand side figure.

However, some of the data was not adequate for calculations, and number of plants were not representative for Marmara region. Therefore, a detailed research was conducted in order to find the plants which are not included in the project database and finding missing information that is required for calculations. For this scope, scientific articles, technical reports, official state reports, annual reports of the plants, and open sources such as plant web sites were investigated, plants were asked directly by personal communication. Finally, the number of the public electricity and heat production plants reached to 57 in Marmara region.

Two of the plants produce electricity from domestic lignite with a total of 530 MW installed power. One of the plants is equipped with electrostatic precipitator and flue gas desulphurization as the abatement technologies. Pulverized and circulating fluidized bed boilers are used as combustion technologies. Caloriphic value of the coal is between 2160 and 2940 kcal/kg. Three of the 57 plants produce electricity from

imported coal with 2442 MW installed power, circulating fluidized bed boilers. The calorific value of the coal was accepted around 6000 kcal/kg. As it is clear from calorific values, imported coals energy content is about three times of domestic coals.

47 of 57 plants produce energy based on natural gas. Totally 14.5 Billion m^3 natural gas is consumed by those plants. Since natural gas is imported, calorific value of the natural gas is almost the same in all plants which is 8250 kcal/m^3. Mostly gas turbines are used as firing practice. Two plants use natural gas and liquid fuels alternately in their combustion system, and they have 1106 MW installed power. Calorific value of the fuel oil was accepted as 10247 kcal/kg.
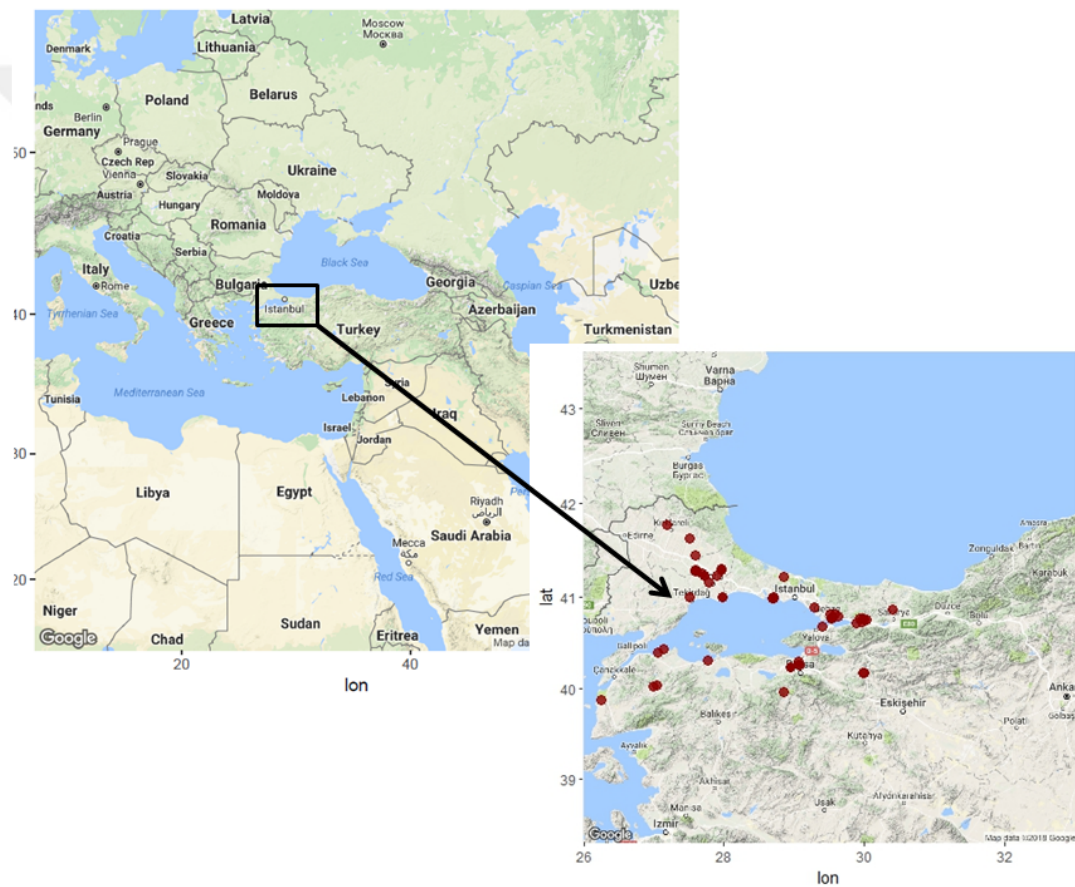
Figure 2.8 : Map of electricity generation plants in Marmara region of Turkey.

One of the 57 plants use waste biogas of landfill as the source of energy in their cogeneration units with an installed power of 34 MW. Calorific value of waste heat was accepted as 4450 kcal/m^3. One other plant use waste heat as the source of energy. The capacity of the plant is around 50 MW and the calorific value of the waste heat was accepted as 8108 kcal/m^3.

2.3.3 Emission calculation methodology

EF development is initial step of emission inventory development ahead of air quality modelling, setting and follow up air quality standards. EFs that are used in industrial emission inventories can either be selected from literature by considering pollutant type, abatement technology, production technology, fuel type or can be developed directly from in-situ measurements. This step is strongly affected from the data in hand. EFs are generally given on production method / pollutant / technology/ abatement technology basis in emission inventory guidebooks including EMEP/EEA Emission Inventory Guidebook [54]. Less data you have means less representative EF. Of course, there are generalized EFs for the plants which has no information other than production amount, but these EFs will not accurately represent current emissions of a particular facility when used in an inventory.

After calculation (or selection) of EFs and gathering the representative activity data emissions are calculated simply by equation 2.

$$E = \Sigma^n A_{1,n} \, EF'_{1,n} \, (1 - C_{1,n} \, \eta_{1,n}) \qquad (2.52)$$

where E is the total emission of a plant including all stacks; A is activity data that is related to each stack; EF' is uncontrolled EF for the related stack; C is control technology application rate in the stack depending on the operation conditions of the process; n is the number of stacks per plant; η is removal efficiency of the control technology as percentage.

2.3.4 Propagation of the uncertainty into sources

Correlation coefficient method was applied in order to quantify uncertainty contributions of emission sources [202][197].

$$U_p = \frac{\sum_{k=1}^{m}(x_k - \bar{x})(y_k - \bar{y})}{\sqrt{\sum_{k=1}^{m}(x_k - \bar{x})^2(y_k - \bar{y})^2}} \qquad (2.53)$$

where U_p is importance of uncertainty from emission sources, x_k is total emission inventory of the specific emission source category, $\bar{x}$ is the mean of the all sources of specific emission category, y_k is the subset source category for the emission inventory, $\bar{y}$ is the mean of the all subset sources of specific emission category. Large values of U_p indicates a stronger linear dependence between the subset source

category (y_k) and   total emission inventory (x_k), then subset source category is a key source of uncertainty in the total emission inventory.

3. RESULTS

The results obtained in this study are explained in three parts. The first part covers the results of the modelling study conducted within the scope of an international project. The second part includes country-specific emission factors and their uncertainty calculations calculated within the context of a national project. In third part, the results of the new inventory are presented and discussed by comparing other inventories.

3.1 Multi-Model Evaluation

PM_{10} concentrations for Europe domain were calculated by several groups within the context of AQMEII-3 activity. Turkey was included in this modelling domain. In this chapter, several regional scale air quality modelling systems were compared over the European continent, Turkey and Marmara region within the context of AQMEII-3 project.

3.1.1 Evaluation of meteorology model outputs

Some meteorology model outputs of the models are plotted in Figure 3.1 and Figure 3.2 for selected parameters. Vertical profiles of temperature mean bias for the selected stations are given in Figure 3.1 (selected by considering best and worst behaviours of models in surface). Figures were adopted from Stefano et. al [71] which is a study that was contributed by also this study. According to Figure 3.1, temperature mean bias profiles of the models ranges are less than 1K, for the best case as shown for a sample station (053) in Figure 3.1.

In Figure 3.1 and Figure 3.2, model names are given according to group IDs; where CMAQ1 is TR1, CMAQ3 is UK3, CCLM-CMAQ is DE1, CMAQ4 is UK1, SILAM is FI1 (meteorology is from ECMWF), WRF-Chem1 is IT2, DEHM is DK1. CMAQ1, CMAQ3, CMAQ4 and DEHM models use WRF as meteorology model.

The bias for temperature in all EU domain ranges between −3K (calculated by DE1 with CCLM model at station 308, Figure 3.1) and +2K (calculated by UK1 with WRF model at station 308 and calculated by FI1 with SILAM model at station 156) at the

surface, which shows the worst case for the models. Reasons for fluctuations of mean bias around zero might be due to the difference of station altitudes, the complexity of the terrains where stations are located, and the model itself.
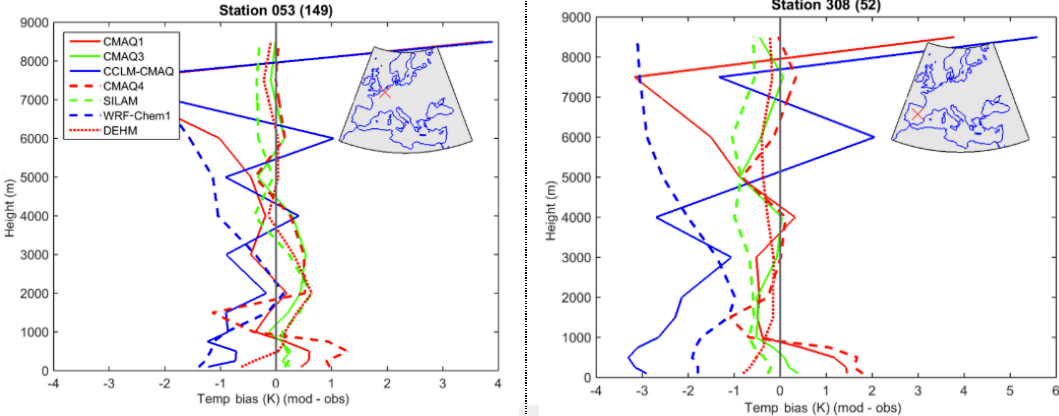
Figure 3.1 : Mean bias (model–observations) for the vertical profiles of temperature measured by ozonesondes launched from indicated locations on the upper right map of each panel.

Vertical mean bias profiles of wind speed (WS) for the selected stations are given in Figure 3.2 by considering best and worst behaviours of models in surface.
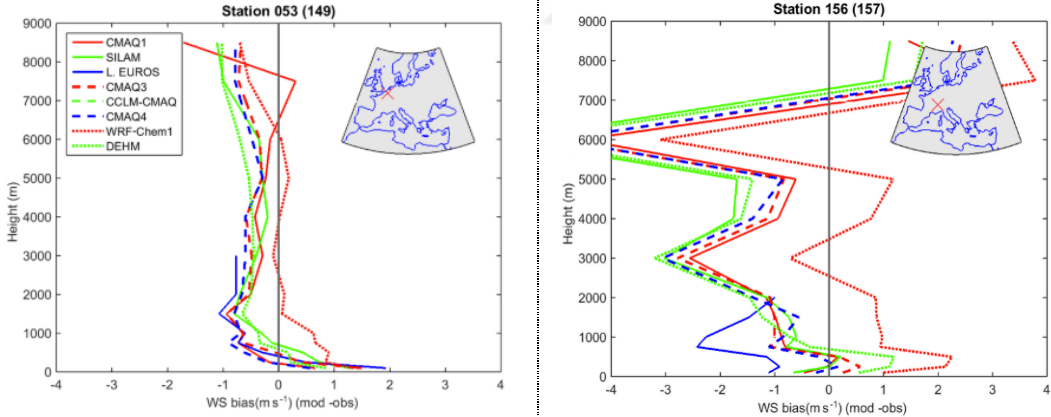
Figure 3.2 : Mean bias (model–observations) for the vertical profiles of wind speed measured by ozonesondes launched from indicated locations on the upper right map of each panel.

Since bias is positive in most of the models in PBL and decreases above ~1000 m; models show a tendency of overestimation of the WS in the PBL and of underestimation above ~1000 m although there are some exceptions for different models and/or launching stations. Since ES1 (WRF-Chem1) group adopted the nudging of meteorological fields only above the PBL and only during the first 12 hours of meteorological spin-up, while for the other WRF instances the nudging is active

during the entire run, generally WRF-Chem1 has the largest positive bias at all sites, with the bias staying positive well above the PBL at all stations in contrast with all other models. Furthermore, WS overestimation by WRF-Chem is a known concern (e.g., Jimenez and Dudhia [134]; Tuccella et al., [223], Mass and Ovens [224]) and it is likely to have a major impact on the dispersion of pollutants [71].

3.1.2 Model performance evaluation on Europe

Each model's base case simulations have been evaluated on a daily mean basis using available surface observations from Europe domain, including Turkey. Distribution of PM_{10} observation stations used in this study are given in Figure 2.4and detailed information according to stations are supplied in Chapter 2.1.2.4. Hourly values are first daily averaged then performance metric was calculated for each station for year 2010. As explained in Chapter 2.1.3.3, not only standard statistical performance metrics which are listed in Table 2.7 but also Taylor diagrams were produced for each station in Europe.

Map of showing MAE on station basis for PM_{10} concentrations were produced for each model in order to compare model performances over the entire domain. In Figure 3.3, MAE results are given on a map for only our model (TR1). MAE is expected as 0 for the best performing models and gives an idea about average absolute difference of the model from observations.

Colouring of the performance metrics at the stations was done by considering the values at all stations. Quartile 1 (Q1) and Quartile 3 (Q3) values, which are frequently encountered in air quality studies, were taken into consideration. In the Python code written for this mapping purpose, the respective performance metrics of all stations are sorted from small to large, 25% of the data (Q1) is green, and it is yellow between 25% (Q1) and 75% (Q3). If the station's performance metric is included in Q3, it is shown with red bubbles. The best value for all performance metrics given in the Figure 3.3 is zero. That is, the model results at Q1 stations, whose performance metric is shown in green, are close to the measurement results when compared to yellow and red. The size of the bubbles represents the size of the performance metric at the respective station.

Since the UPA metric may be less than zero, Q1, Q2 and Q3 values were calculated separately for positive and negative numbers. The downward-facing triangle indicates that the UPA value at this station is negative, and vice versa. It is clear from the colour

of the triangles how close the UPA is to the best value (how close the model results are to the measurements at that station). From the best UPA to the worst, the colours are listed as green, yellow, blue and red, respectively.

When looking at the map of the MAE performance metric in Figure 3.3, the green stations (where average absolute difference between model and observation is less than or equal to 9 $\mu g/m^3$) are mostly located in Western Europe (especially in England, Ireland, Holland, Belgium, France, Germany and Sweden). Red stations are located mainly in Eastern Europe (especially in Turkey, Bulgaria, Greece and Poland) and in two Western Europe countries which are Spain and North Italy. The largest red bubbles are in Turkey. This means that the model gives worst results in stations of Turkey. So, the MAE at these stations is quite high.
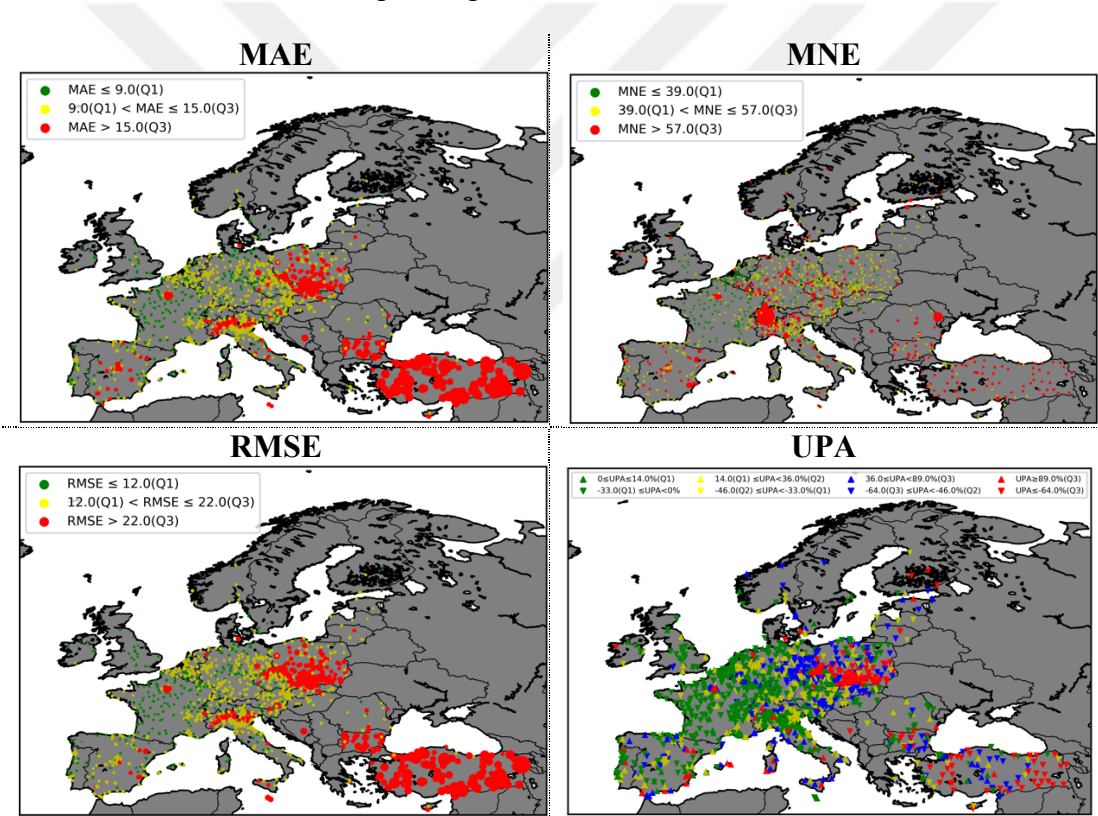
Figure 3.3 : Map of some performance metrics calculated by our group (TR1 model) for PM$_{10}$ in observation stations throughout Europe for 2010.

MNE is the normalized version of MAE by observed values, formula is given in Table 2.7. MNE best value is 0 and it is expressed as percentage in our study. Normally when model or observation is twice the other, MNE is 50%. MNE results are given on a map for only our model (TR1) in Figure 3.3. Green dots (showing MNE results less than 39% which is also Q1) are common in Western Europe (especially in England, Holland, Belgium, France and Germany). Red stations are located mainly in Eastern

Europe (especially in Turkey, Bulgaria, Greece Romania) and in two Western Europe countries which are Spain and North Italy. Since MNE at the station in Switzerland is so high, the red bubbles in Turkey seems small despite being the highest in Europe. As in MNE, the results of the model seem to be the worst in stations in Turkey.

RMSE, which is a non-normalized error metric, represents the sample standard deviation of the difference between modelled and observed values regardless of whether the modelled values are higher or lower than observations. Best value is 0 for RMSE. Figure 3.3 shows RMSE values for modelled and observed PM_{10} in stations throughout Europe. As in MAE and MNE maps, the green stations (where RMSE is less than or equal to 12 $\mu g/m^3$) are mostly located in Western Europe (especially in England, Ireland, Holland, France, Germany, Sweden and Finland). Red stations are located mainly in Eastern Europe (especially in Turkey, Poland, Bulgaria and Greece) and in North Italy. The largest red bubbles are in Turkey.

The UPA metric is intended to measure a model's ability to capture peak pollutant concentrations but does not pair the model estimates with observations in time or space and best value is 0. In Figure 3.3, UPA values were expressed as percentages. Since UPA is not an absolute metric, the dots were redesigned for inclusion of the negative values as explained in the legend of the figure. Values between -Q1 and zero were indicated with green rectangular, downward rectangular indicates model peak values less than observation peak values, and the upper ward green rectangular tells the opposite. This metric is valuable when the models capture of peak values were needed to be considered, because for the best models it is expected to have high values at the same time in model when observations were also high. If those peak values are close to each other than UPA value is close to zero. If peak values are not close, then model cannot be able to catch the correct peak value. In Figure 3.3, UPA values are close to zero in France, Germany, England, Spain and Portugal. In those countries there are also yellow rectangular which shows moderate UPA values (between Q1 and Q2). Red and blue rectangular show worst UPA results which are common in Poland, Czech Republic, Turkey and Bulgaria. Worst UPA means, model cannot capture peaks well.

From this point of view, when Figure 3.3 is investigated (for further investigation refer to Appendix A), performance metrics are generally give bad results in Eastern Europe countries (especially in Turkey), which means TR1 model (our group) cannot capture observations in Eastern Europe countries where model give pretty good results in

Western Europe. In this point, behaviour of other models reveals as question. In order to address this question same maps were generated for other groups, and sample model results is given in Figure 3.4 for MAE metric (remaining maps were given in Appendix A for all metrics).

When Figure 3.4 is examined, it is seen that, all models usually give quite different results from measurements in Eastern Europe, but again the worst results are in Turkey. Furthermore, all these models give close results to our model (TR1) as discussed with Figure 3.3.
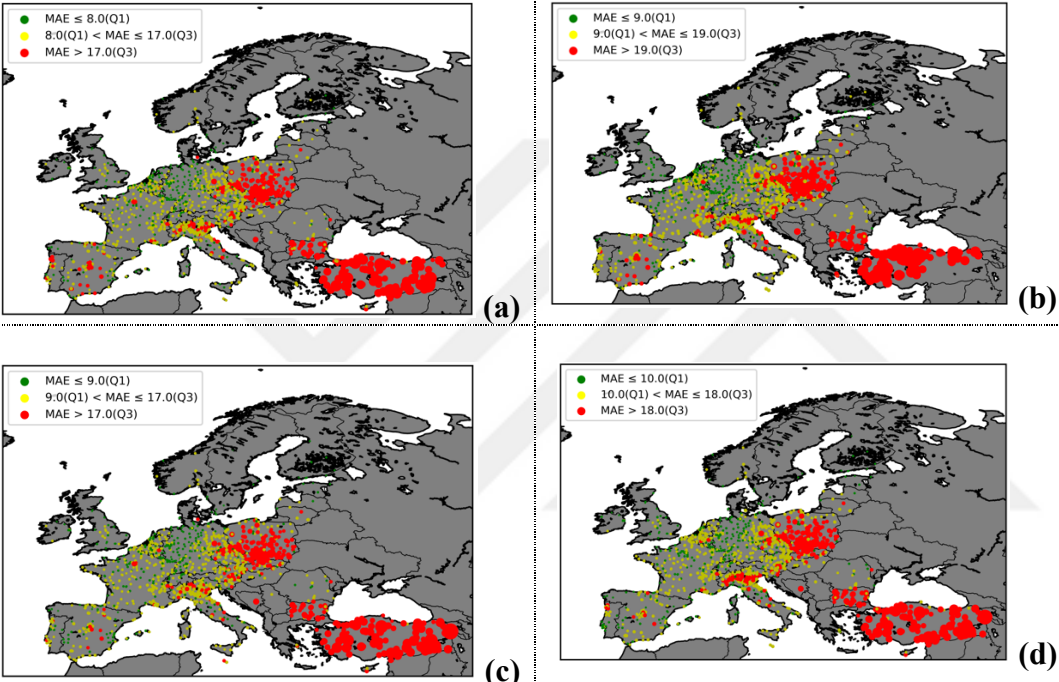
Figure 3.4 : Map of MAE results for PM$_{10}$ in observation stations throughout Europe for 2010 calculated by groups from: (a)England (UK1_MACC_bas). (b)Denmark (DK1_HTAP_bas). (c)Finland (FI1_MACC_bas). (d)Italy (IT2_MACC_bas).

In order to discuss behaviours of the models in each country, CDFs of MAEs in each station are plotted for each model and for each country, and given in Figure 3.5 for selected countries. Totally 27 countries were considered in the European part of AQMEII-3 project. Number of observation stations are less than 10 in some countries (e.g. Switzerland, Slovakia, Romania), therefore they were considered out of discussion in this part of the analysis. Number of stations for the considered countries are indicated at the bottom of each plot in Figure 3.5. Countries with narrow, medium

and large CDFs were selected for Figure 3.5.
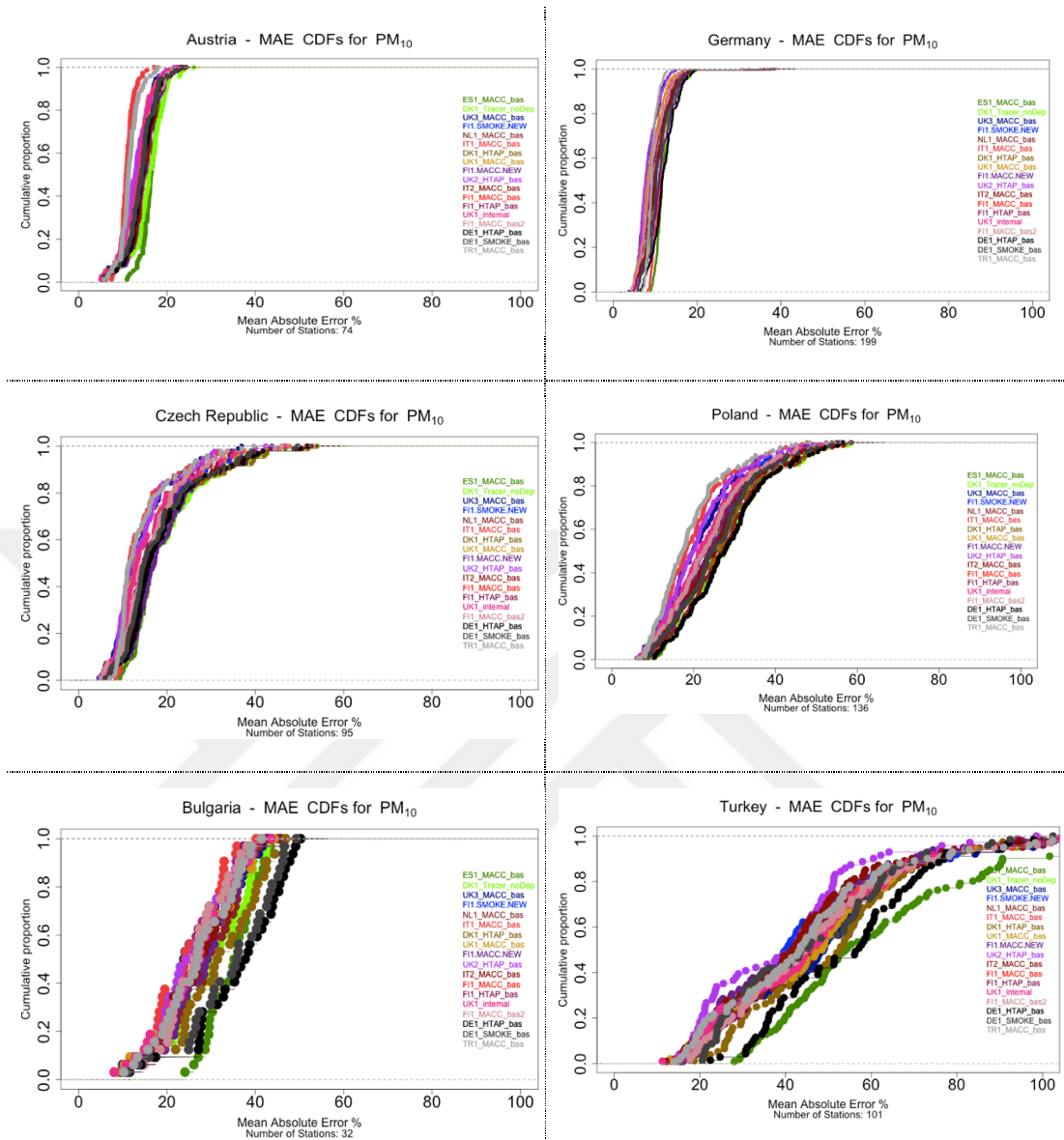
Figure 3.5 : CDFs for MAE results of PM_{10} in observation stations for some countries (countries are indicated on the title of each sub plot).

In the CDFs of stations in Austria, all models are following nearly close CDF paths, means that models generally found close predictions when compared to observations. MAE is less than 20 $\mu g/m^3$ in all model predictions, in all stations. The situation is same in Germany.

Looking at the CDFs of stations in the Czech Republic, all models have similar errors (MAE plots are close to each other). However, in 40% of the stations, the MAE is above 20 $\mu g/m^3$. In Poland, MAE is above 20 $\mu g/m^3$ in 70% of stations.

In Bulgaria, CDFs were shown as dots, since number of stations were not enough to create the CDF in a line view. However, it is clear that, MAE is more than 20 $\mu g/m^3$ in almost all stations in Bulgaria. In Turkey, the range of MAE CDFs are broadened, which is between 20 $\mu g/m^3$ and 100 $\mu g/m^3$. CDFs of all models in Turkey indicates high variability of the models.

Some of the performance metrics averaged for selected countries and given in Table 3.1. In Table 3.1, there are four Western Europe countries (Germany, France, Spain and Italy) representing good model performances, and three Eastern Europe countries representing worst model performances (Turkey, Poland and Bulgaria). Averages of all performance metrics for other countries are given in Appendix D. According to Table 3.1, RMSE is less than 20 in the selected West European countries (Germany, France, Spain and Italy), where it is between 35 and 62 in some of the Eastern Europe countries (Turkey, Poland and Bulgaria). Average of BIAS of Eastern European countries is 2.5-fold of Western European countries, when all countries are considered. Furthermore, MAE is between 10 and 15 $\mu g/m^3$ in Western European countries, where it is between 24 and 48 $\mu g/m^3$ in Eastern Europe countries. NBIAS is more than 50% in Eastern Europe countries where it is maximum 32% in Western Europe countries.

Table 3.1 : Country based performance metric averages for selected countrries.

	Turkey	Germany	France	Spain	Italy	Poland	Bulgaria
Number of stations	101	199	231	111	188	136	32
Mean ($\mu g/m^3$)	27	13	15	14	17	15	18
Median ($\mu g/m^3$)	22	11	13	10	14	13	14
Stand. Dev.	20	8	9	13	12	10	15
Variance	727	70	109	341	213	104	324
RMSE	62	15	16	18	20	35	41
BIAS ($\mu g/m^3$)	-40	-7	-9	-7	-9	-23	-25
MAE ($\mu g/m^3$)	48	10	12	13	15	24	29
NBIAS (%)	-50	-32	-36	-29	-31	-57	-53

Performance metrics are averaged on Eastern and Western Europe countries and percent difference of Eastern countries from Western countries are given in Table 3.2. Percent differences are given with "+" or "-" signs in Table 3.2. indicate given with shows the upper percent value of Eastern countries where downward arrow indicates opposite. For instance, MAE is 21 $\mu g/m^3$ for the stations of Eastern European countries where it is 16 $\mu g/m^3$ for the stations in Western European countries. Here, +99% (given

on the right column) says that MAE of Eastern countries are 99%larger than MAE of Western countries.

Table 3.2 : Eastern – Western Europe averaged performance metrics.

	Eastern Countries	Western Countries	Difference of Eastern Countries (%)
Number of Stations	444	988	-55
Stand. Dev. ($\mu g/m^3$)	13	9	+40
Variance ($\mu g/m^3$)	333	156	+113
RMSE	30	16	+90
BIAS ($\mu g/m^3$)	-15	-5	-177
MAE ($\mu g/m^3$)	21	11	-99
MNE (%)	91	73	+25
NBIAS (%)	-40	-21	-88
NME (%)	62	59	+5
MFB (%)	-54	-37	-46
MFE (%)	78	63	+23
NMSE	2.1	1.5	+41
PCC	0.38	0.41	-8
IOA	0.52	0.54	-3

According to Table 3.2, RMSE of Eastern countries is 90% more than Western countries average, where MAE is 99% and MNE is 25% more. BIAS average is -5 $\mu g/m^3$ in Western European countries where it is 15 $\mu g/m^3$ in Eastern European countries, which means that models predict approximately 15 $\mu g/m^3$ beyond the observations. Correlations between models and observations are 8% less in Eastern European countries when compared to Western European countries. When all metrics were investigated, it is clear from Table 3.2 that, Western European countries give better results when compared to Eastern European countries in terms of performance metrics.

3.1.3 Model performance evaluation for Turkey

As detailly discussed in Chapter 3.1.2 BIAS average of the models for stations in Western Europe countries is 2.5-fold of stations located in Western European countries. Turkey, which is located in the Eastern Europe, has one of the worst results calculated by all models. All models predict PM_{10} concentrations with an average of -40 $\mu g/m^3$ BIAS in stations of Turkey, where it is the worst value within 34 countries of Europe considered in this study. In this part of study, Turkey will be focused deeply

in order to discuss possible reasons behind those poor results of AQMs. Regarding to the local regulation of Turkey [225], which is also compatible with EU Regulation [226], daily PM_{10} concentration cannot exceed 50 μg/m^3 more than 35 times in a year and this rule will certainly be applied after 2019. Furthermore, air quality limit is 40 μg/m^3 PM_{10} for calendar year average. Over Istanbul annual mean concentration is more than 50 μg /m^3 in the recent years.

3.1.3.1 Regional evaluation of performances

In the first step of analysis, CDFs of PM_{10} predictions by models and CDFs of PM_{10} observations are generated on station basis. As in discussed in Chapter 3.1.2 models generally give good results in Western Europe countries. Although Turkey is located in the Eastern part of Europe, where models don't give predict well as Western Europe, models continue to predict better in some stations of Turkey. However, number of those stations are limited. CDFs of some of the stations whose PM_{10} estimates are consistent with the measurements are given in Figure 3.6 for four biggest cities of Turkey.
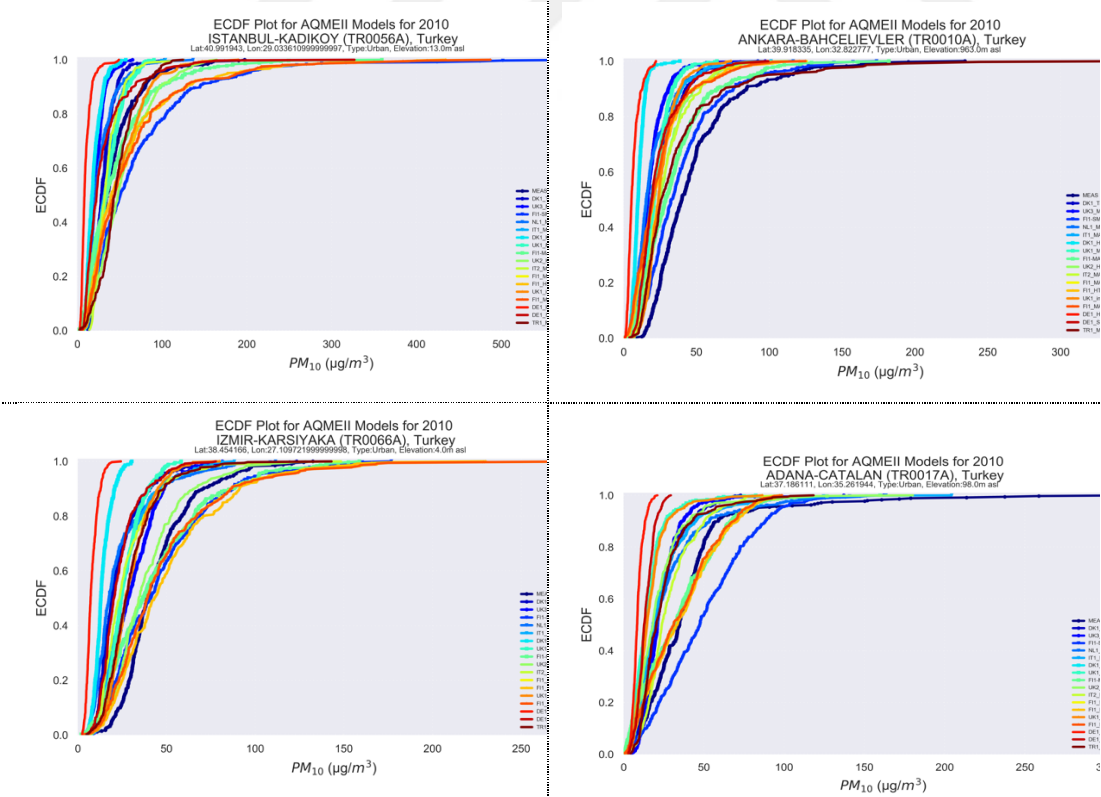
Figure 3.6 : Comparison of CDFs for selected stations from Turkey which are well predicted by all models.

Each CDF line represents an estimate of a different model. The navy-blue CDF line in Figure 3.6 shows the observations in said station. According to Figure 3.6, CDF lines of models are around observation line, some of them are very close to observation line. Although models vary among themselves, they generally predict PM_{10} concentrations close to observations in those stations. When CDFs of all stations in Turkey are examined, such good CDFs are encountered in 18 of 101 stations of Turkey (approximately 20%), especially in all stations of Istanbul (except Kartal station). 11 of 18 good results are located in Marmara region of Turkey, one is in Canakkale, one is in Yalova and remaining stations are all located in Istanbul. Four stations of Izmir (Alsancak, Cigli, Guzelyali and Karsiyaka) in Aegean Region also have good CDFs. Two stations of Adana (Catalan and Dogankent) from Mediterranean Region and Ankara Bahcelievler station from Central Anatolia Region have good CDFs.
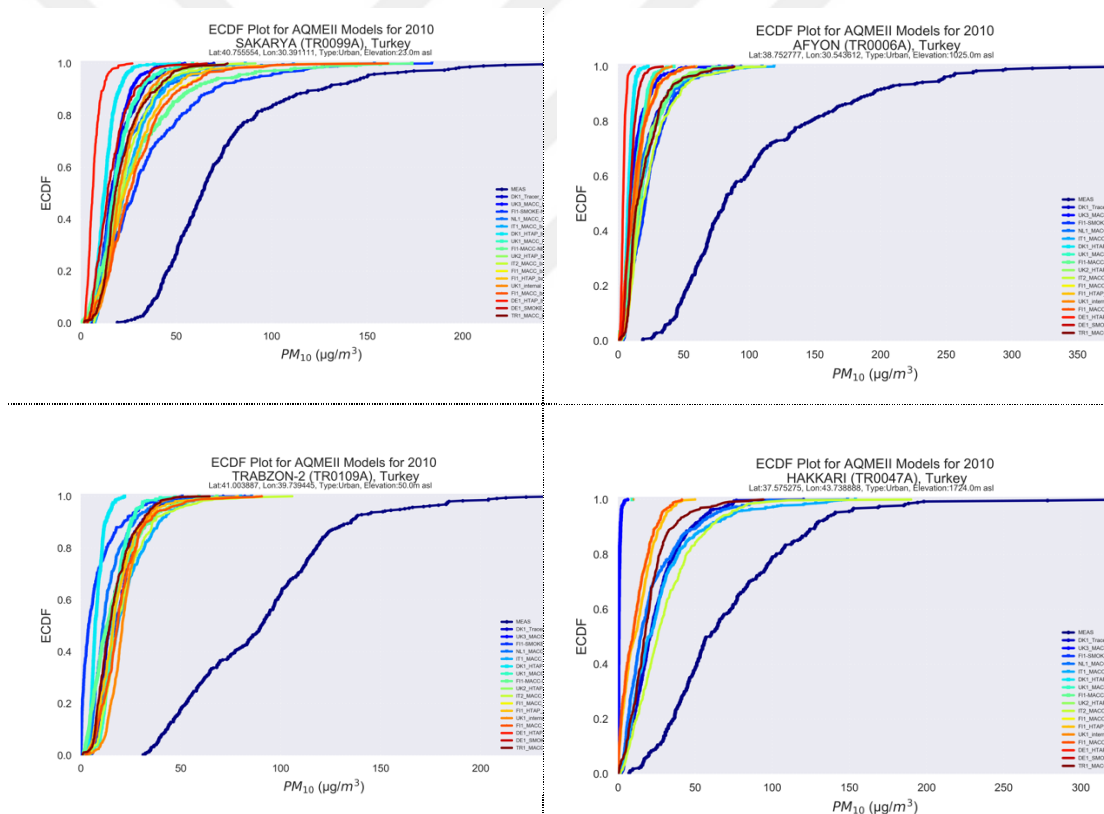
Figure 3.7 : Selected stations from Turkey which are predicted poor by all models.

Although PM_{10} is predicted well in some stations, there were no such good predictions in approximately 80% of the stations. CDFs of some of the selected stations, whose PM_{10} estimates are not consistent with the measurements, are given in Figure 3.6.

According to Figure 3.6, models predict close to each other but quite far from the observations. Generally, models predict better in big cities however model predictions in smaller cities are not good as big cities.

3.1.3.2 Performance of the models in Marmara Region

In Marmara region number of valid stations, after quality control procedures described in Chapter 2.1.2.4, is 18. Entire of those stations will be investigated in this part of study.

In Table 3.3, BIAS and MNE values of models were summarized for each city in Marmara region. The name of the model that predicts the indicated BIAS or MNE value above the parentheses is given inside parentheses in Table 3.3. As indicated in Table 2.7, best value is zero for each BIAS and MNE. In Table 3.3, best values of BIAS (with best performing models inside parenthesis) are given in a separated column, where best values of MNE (%) are given in 'Min' column of MNE. According to Table 3.3, in Marmara region, worst BIAS value is in Balikesir (68 $\mu g/m^3$) and calculated by DE1_HTAP model (Detailed information according to models were given in Table 2.1). Furthermore, when all worst BIAS values were investigated, DE1_HTAP model gives minimum BIAS in all cities. Which means that this model underestimates in all cities of Marmara region. Furthermore, absolute minimum BIAS is more than maximum BIAS in all cities, therefore it can be inferred that DE1_HTAP model is the worst performing model in Marmara region according to BIAS metric.

Maximum BIAS is negative in Balikesir, Edirne, Kocaeli and Sakarya, which means that predictions are generally more than observations, and all models underpredicted in those cities. ES1_MACC model predicts best in those 4 cities in terms of BIAS metric. Furthermore, best prediction of the models is in Istanbul Sariyer which is calculated by FI1_HTAP model with a BIAS of -0.1 $\mu g/m^3$. Our group (TR1_MACC) calculated best BIAS in four of the stations which are all located in Istanbul (Aksaray, Besiktas, Esenler and Kadikoy). Worst MNE results are calculated in Canakkale (calculated by ES1_MACC) which is 193%, second worst MNE is in Istanbul Aksaray which is 109% (calculated by UK1_Internal). Nevertheless UK1_MACC model calculated best MNE results in Marmara region which is 29% for each of Istanbul Alibeykoy and Uskudar. MNE results are generally lower in Istanbul when compared to other cities in Marmara region.

Table 3.3 : BIAS and MNE metric values (and models) for cities of Marmara region.

	BIAS				MNE (%)		
	Min	Max	Best	Average	Min	Max	Average
Balikesir	-68 (DE1_HTAP)	-19 (ES1_MACC)	-19 (ES1_MACC)	51	53 (FI1_SMOKE-NEW)	88 (DE1_HTAP)	66
Bilecik	-42 (DE1_HTAP)	11 (ES1_MACC)	11 (ES1_MACC)	-28	51 (IT1_MACC)	91 (ES1_MACC)	65
Canakkale	-25 (DE1_HTAP)	20 (ES1_MACC)	-2 (FI1-SMOKE-NEW)	-8	47 (DK1_HTAP)	193 (ES1_MACC)	76
Edirne	-58 (DE1_HTAP)	-25 (ES1_MACC)	-25 (ES1_MACC)	-46	62 (IT1_MACC)	89 (DE1_HTAP)	70
Istanbul Aksaray	-36 (DE1_HTAP)	30 (UK1_Internal)	0.7 (TR1_MACC)	-1	39 (UK3_MACC)	109 (UK1_Internal)	61
Istanbul Alibeykoy	-39 (DE1_HTAP)	21 (FI1-SMOKE-NEW)	-2 (FI1-MACC-NEW)	-6	29 (UK1_MACC)	75 (DE1_HTAP)	49
Istanbul Besiktas	-35 (DE1_HTAP)	27 (FI1-SMOKE-NEW)	2 (TR1_MACC)	-2	34 (IT2_MACC)	82 (FI1_SMOKE-NEW)	54
Istanbul Esenler	-40 (DE1_HTAP)	25 (UK1_Internal)	-1 (TR1_MACC)	-5	38 (IT2_MACC)	88 (UK1_Internal)	53
Istanbul Kadikoy	-32 (DE1_HTAP)	29 (FI1-SMOKE-NEW)	3 (TR1_MACC)	-1	41 (UK1_MACC)	118 (ES1_MACC)	65
Istanbul Kartal	-65 (DE1_HTAP)	8 (UK2_HTAP)	8 (UK2_HTAP)	-36	44 (TR1_MACC)	83 (DE1_HTAP)	58
Istanbul Sariyer	-35 (DE1_HTAP)	12 (UK1_Internal)	-0.1 (FI1_HTAP)	-6	37 (TR1_MACC)	82 (ES1_MACC)	50

Table 3.3 (continued) : BIAS and MNE metric values (and models) for cities of Marmara region.

	BIAS				MNE (%)		
	Min	Max	Best	Average	Min	Max	Average
Istanbul Umraniye	-34 (DE1_HTAP)	22 (FI1-SMOKE-NEW)	1 (UK2_HTAP)	-5	39 (UK1_MACC)	91 (ES1_MACC)	53
Istanbul Uskudar	-31 (DE1_HTAP)	30 (FI1-SMOKE-NEW)	-5.4 (UK1_MACC)	1	29 (UK1_MACC)	77 (ES1_MACC)	50
Istanbul Yenibosna	-51 (DE1_HTAP)	5 (FI1-SMOKE-NEW)	0.26 (FI1_MACC)	-19	37 (TR1_MACC)	80 (DE1_HTAP)	51
Kirklareli	-37 (DE1_HTAP)	2 (ES1_MACC)	2 (ES1_MACC)	-24	48 (IT1_MACC)	84 (DE1_HTAP)	61
Kocaeli	-56 (DE1_HTAP)	-12 (ES1_MACC)	-12 (ES1_MACC)	-37	49 (FI1_SMOKE-NEW)	85 (DE1_HTAP)	59
Sakarya	-66 (DE1_HTAP)	-22 (ES1_MACC)	-22 (ES1_MACC)	-49	55 (FI1_SMOKE-NEW)	89 (DE1_HTAP)	66
Yalova	-44 (DE1_HTAP)	32 (UK2_HTAP)	1 (ES1_MACC)	-12	44 (IT1_MACC)	98 (UK2_HTAP)	58

In Istanbul, BIAS is between -65 μg/m^3 (in Kartal) and 30 μg/m^3 (in both Aksaray and Uskudar). MNE is between 29% (Uskudar and Alibeykoy) and 109% (Aksaray). In London BIAS is between -10 μg/m^3 (calculated by DE1_HTAP for London Bloomsbury station) and 18 μg/m^3 (calculated by IT1_MACC model for London N. Kensington Partisol Station). In Paris BIAS is between -13 μg/m^3 (calculated by DE1_HTAP for Paris 18eme station station) and 39 μg/m^3 (calculated by TR1_MACC model for Paris 18eme station). In Berlin BIAS is between -16 μg/m^3 (calculated by DK1_Tracer_noDep for B.Schöneberg-Belziger Straße station) and 1.74 μg/m^3 (calculated by TR1_MACC model for B.Schöneberg-Belziger Straße station). In Istanbul although there are best estimating models, generally BIAS is larger than other metropoles of Europe.

In Istanbul, MNE is between 29% (for Alibeykoy and Uskudar calculated by UK1_MACC) and 118% (calculated by ES1_MACC model for Kadikoy), where MNE is 35 (UK2_HTAP for B.Schöneberg-Belziger Straße station) and 64% (ES1_MACC for B.Schöneberg-Belziger Straße station) in Berlin, between 9% (calculated by DK1_Tracer_noDep for PARIS 1er Les Halles station) and 40% (calculated by TR1_MACC model for Paris 18eme station) in Paris, and between 4% (calculated by UK1_MACC for London N. Kensington Partisol station) and 18% (calculated by IT1_MACC model for London N. Kensington Partisol Station) in London.

Although BIAS and MNE upper and lower ranges are large, models predict better in Istanbul when compared to other cities in Marmara Region of Turkey. However minimum MNE is 29% in Marmara region (for Uskudar and Alibeykoy) which is even a high value for PM_{10} concentration estimations.

3.1.3.3 Seasonal evaluation of model estimates

In order to compare model performances according to seasons of 2010, Taylor diagrams were generated. In Figure 3.8, Taylor diagram of Balikesir station is given for all seasons of 2010, where December, January and February are Winter months, March, April and May are Spring months, June, July and August are Summer months and September, October and November are Autumn months. In Taylor diagrams, a number was assigned to each modelling group and given in the legend of plot. Taylor diagram was generated for all stations of Marmara region. Diagrams of other stations in Marmara region are in Appendix E.

According to Figure 3.8, standard deviation of observations in Balikesir station is largest in Winter and Autumn (60 $\mu g/m^3$) and smallest in Summer (16 $\mu g/m^3$). It is 29 $\mu g/m^3$ in Spring. Although the standard deviation of measurements is high in Autumn and Winter, we see that standard deviation in Summer falls to almost a quarter of Winter. Finally, variability of observed emissions is highest in Winter and Autumn where it is lowest in Summer.

Seasonal change of standard deviations in other cities of Marmara region is given in Table 3.4. According to Table 3.4, as in Balikesir station, generally standard deviation is highest in Winter and Autumn in almost all stations, and lowest in Summer, which

shows that PM$_{10}$ observations vary widely in Winter and Autumn however close to each other in Summer.
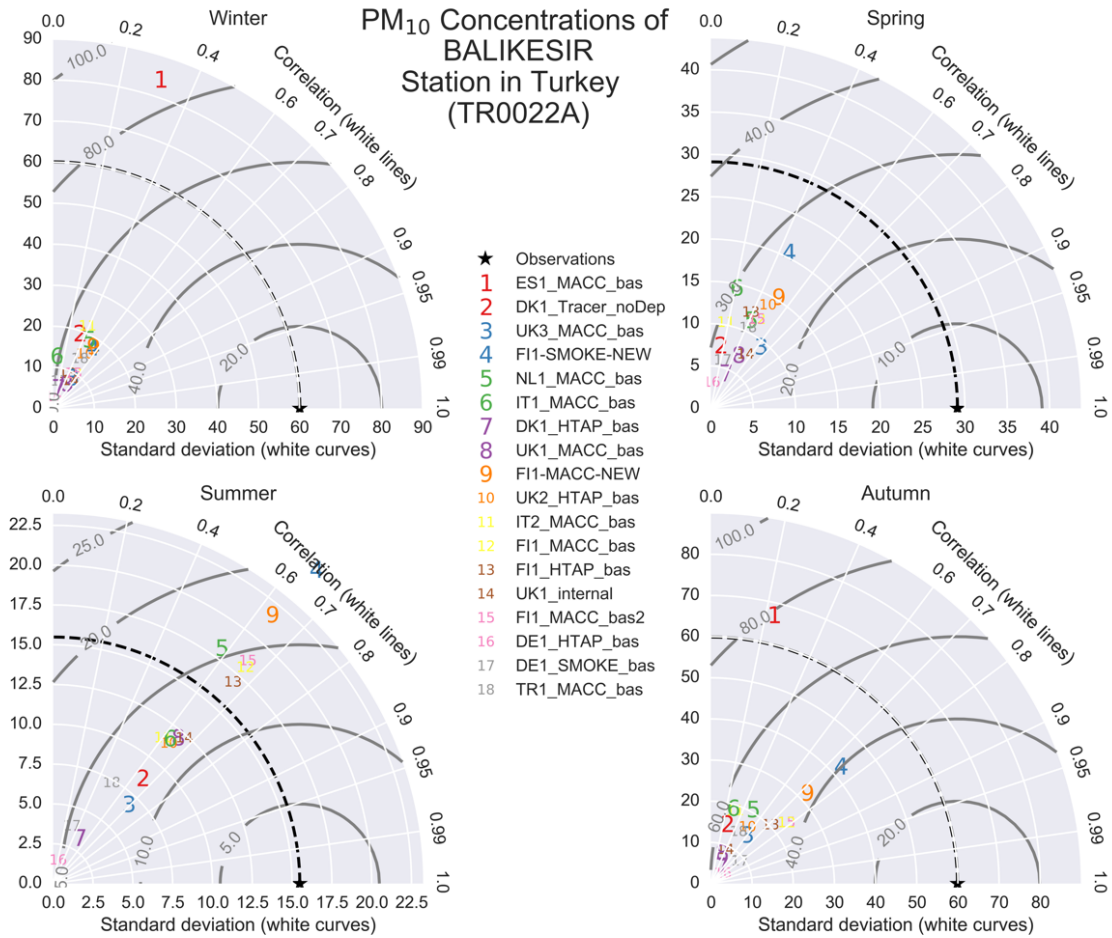
Figure 3.8 : Seasonal Taylor diagram displaying a statistical comparison with observations of eighteen model estimates of the PM$_{10}$ concentration for Balikesir station.

As described in Section 2.1.3.3, standard deviation of the models is expected to be close to the standard deviation of the observations. Thus, it is assumed that the variability in measurements is captured by the model. In Figure 3.8, standard deviation of the models are less than 25 µg/m^3 in Winter (except ES1_MACC model with a standard deviation more than 80 µg/m^3) where standard deviation of the observations is 60 µg/m^3. Furthermore, standard deviation of the models is less than 40 µg/m^3 in Autumn (except ES1_MACC model with a standard deviation of 68 µg/m^3) where standard deviation of the observations is 60 µg/m^3. In Summer many models' standard deviation is close to the standard deviation of observations as we don't see in Winter and Autumn.

Table 3.4 : Seasonal change of standard deviations ($\mu g/m^3$) of observations in the stations of Marmara Region. (Bold numbers show highest value, underlined values show minimum value per station and season).

City	Winter	Spring	Summer	Autumn
Balikesir	**60**	29	_16_	**60**
Bilecik	20	_15_	19	**21**
Canakkale	**38**	19	_7_	10
Edirne	39	25	_13_	**49**
Istanbul Aksaray	18	_17_	_17_	**25**
Istanbul Alibeykoy	**33**	19	_15_	29
Istanbul Besiktas	**23**	_15_	21	**23**
Istanbul Esenler	27	23	_15_	**30**
Istanbul Kadikoy	24	23	_22_	**42**
Istanbul Kartal	**54**	38	_24_	40
Istanbul Sariyer	26	_19_	**35**	28
Istanbul Umraniye	25	21	_14_	**38**
Istanbul Uskudar	21	16	_12_	**27**
Istanbul Yenibosna	**38**	37	_19_	36
Kirklareli	**35**	17	_11_	31
Kocaeli	**50**	29	_17_	35
Sakarya	41	23	_14_	**52**
Yalova	**31**	23	_14_	25
Average	**33**	**23**	**17**	**33**

In Figure 3.8, correlation of the models (according to the position of the models on the white line in Figure 3.8) with observations is mostly less than 0.6. Worst correlations of the models with observations are in Winter.

In Balikesir station, in Winter, correlation of the ES1_MACC model is about 0.3, which is also close to correlation of other models. Furthermore, centred RMSE of ES1_MACC model is more than 80 where it is less than 60 in other models. Consequently ES1_MACC model captures variability in the observations (as its standard deviation is closest to observations when compared to other models) and its predictions are 30% correlated with observations, however there is much difference between predicted and modelled PM_{10} concentrations in Winter.

Taylor diagrams of other stations in Marmara region are given in Appendix E. When the Taylor diagrams of other stations are examined, we see models cannot capture observations in Winter but performs well in Summer as in Balikesir station, except Istanbul stations. This difference can be caused by inadequate representation of

increased emissions (in the model inputs) from residential heating and traffic emissions during Winter months when compared to other months. In this case, it would not be unreasonable to suspect that the inputs to the models do not cover this difference. For this reason, model results may be able to capture variability in measurements more easily in Summer. The reason why model estimates do not differ much in the stations in Istanbul between summer and winter may be due to the fact that the emissions in Istanbul are given better to the model.

Model inputs to the model are considered as a reason for poor model predictions in this study. However, problems caused by the model itself or erroneous measurements, or combination of all, can also cause this. In this study, problems due to the model itself are out of consideration since 6 different AQMs were used by 13 modelling groups where same models were also considered by some groups. All models give close CDFs in Western Europe despite they have different modelling configurations, where they are not close to each other in Eastern Europe countries even in same models. (Detailed information for the models is available in Figure 2.1). Problems due to observations are not subject of this study, since number of stations more. Systematic errors are not thought to occur at all stations at the same time. Discussion of the models according to stations are available in Section 3.1.3.2.

3.2 Country-Specific EFs

Thanks to the KAMAG project [194] that this study benefited from, it was possible to calculate country-specific EFs from two data sources; in-situ measurements conducted within the context of the project and EMRs (emission measurement reports) prepared by the companies. In Section 2.2.1 detailed information on both data sources are given.

As discussed in Section 2.2.1 there are questions on trusting the data in EMR. Therefore, the data in the EMR should not be considered in the calculation of country specific EFs. However, EFs were calculated in this part of the study from both sources in order to compare the results and reveal the difference of these two emission data sources. Since the use of in-situ EFs is given priority in the thesis and in order to save space in the thesis text, goodness-of-fit statistics/criteria for EFs derived from EMRs are given in Attachment F.

Country-specific dust, CO, SO$_2$, NO, NO$_2$ and NO$_x$ EFs are calculated in this part of the study. Although NO and NO$_2$ EFs are calculated within the scope of this thesis, NO$_x$ EFs are also calculated under a separated section since they are commonly given in the literature.

SNAP/NFR codes of EMEP were considered as the codes of EFs calculated in this dissertation. Codes of EFs are given with the sequence of "NFR-SNAP-Table No" throughout the dissertation. For instance, for an EF with "1.A.1.a – 10101 – 3.10" code, "1.A.1.a" is NFR code, "10101" is SNAP code and "3.10" is the table number in EMEP guidebook [54]. Definitions of the codes considered in this study are given in Table 2.8, besides briefly summarized in the subsequent sections.

3.2.1 Coal combusting large wet/dry bottom boilers

Coal combusting large boilers are represented with "1.A.1.a–10101–3.10" code. In detail, the code represents brown coal or lignite combustion plants with a capacity greater than 300 MW, and with wet and dry bottom boilers as the combustion technology for production of public power.

In Marmara region there are no plants falling under this SNAP/NFR category. Although KAMAG project [194] covers the plants in Marmara region, a few in-situ measurements were conducted from outside of the region. Country-specific EFs are generated for this SNAP/NFR category from a plant outside of Marmara region, but not used in the emission inventory part of this study, since there is no plant falling under this SNAP/NFR category in Marmara Region.

Consequently, 16 in-situ measurements from one plant is used in the calculation of country-specific EF for this SNAP/NFR code. Furthermore 12 emission measurements from EMRs were also used for comparison of the results.

Dust

Summary statistics of dust EFs for "1.A.1.a–10101–3.10" SNAP/NFR category are given in Table 3.5 for EFs derived from both in-situ measurements and EMRs. Although variance and standard deviation of in-situ measurements and EMRs are close to each other, Cv is 151% for in-situ measurements where it is 45% for EMRs, which

indicates large variability for in-situ measurements. The large variability is heavily affected from outliers.

Table 3.5 : Summary statistics of dust EFs derived from both in-situ measurements and EMRs for "1.A.1.a–10101–3.10".

	In-situ Measurements	EMR
Number of data points	16	12
Minimum	0.19	0.34
Maximum	4.58	4.78
Median	0.29	2.78
Variance [1]	1.15	1.59
Standard Deviation [2]	1.07	1.26
Cv (%) [3]	151	45
Skewness [4]	3.32	-0.48
Kurtosis [5]	11.8	0.55

[1] According to equation 2.12
[2] According to equation 2.13
[3] According to equation 2.14
[4] According to equation 2.15
[5] According to equation 2.16

According to Figure 3.29, looking at the CDF of EFs derived from EMR, it is seen that 60% of EFs range from 2.5 to 3.3 g/GJ. In the CDF of EFs from in-situ measurements, 90% of EFs are less than 1.8 g/GJ, however, there is one EF which is more than 4 g/GJ, which can be treated as outlier. Variability contribution of one outlier value in the CDF of EFs from in-situ measurements, should be considered when evaluating large variability in the in-situ EFs. Consequently, we see that one outlier data has a large effect on final variability, although 90% of the data is below 1.8 g/GJ in in-situ EFs.

There is positive skewness in the EFs derived from in-situ measurements where it is negative in EMR EFs. When the histograms given in Figure 3.9 are compared, it is seen that the asymmetry in the histogram of EFs derived from in-situ measurements is higher than those derived from EMR. Therefore, the skewness value for in-situ measurements in Table 3.6 is higher than EMR's. Due to a large peak in the EMR histogram, the kurtosis value is expected to be higher than in-situ measurements, but lower in the Table 3.6. This is due to the presence of values close to this peak in the EMR EFs, as it is also clear in the CDF of EMR which is given in Figure 3.9. Consequently, EMR has less kurtosis and skewness value.
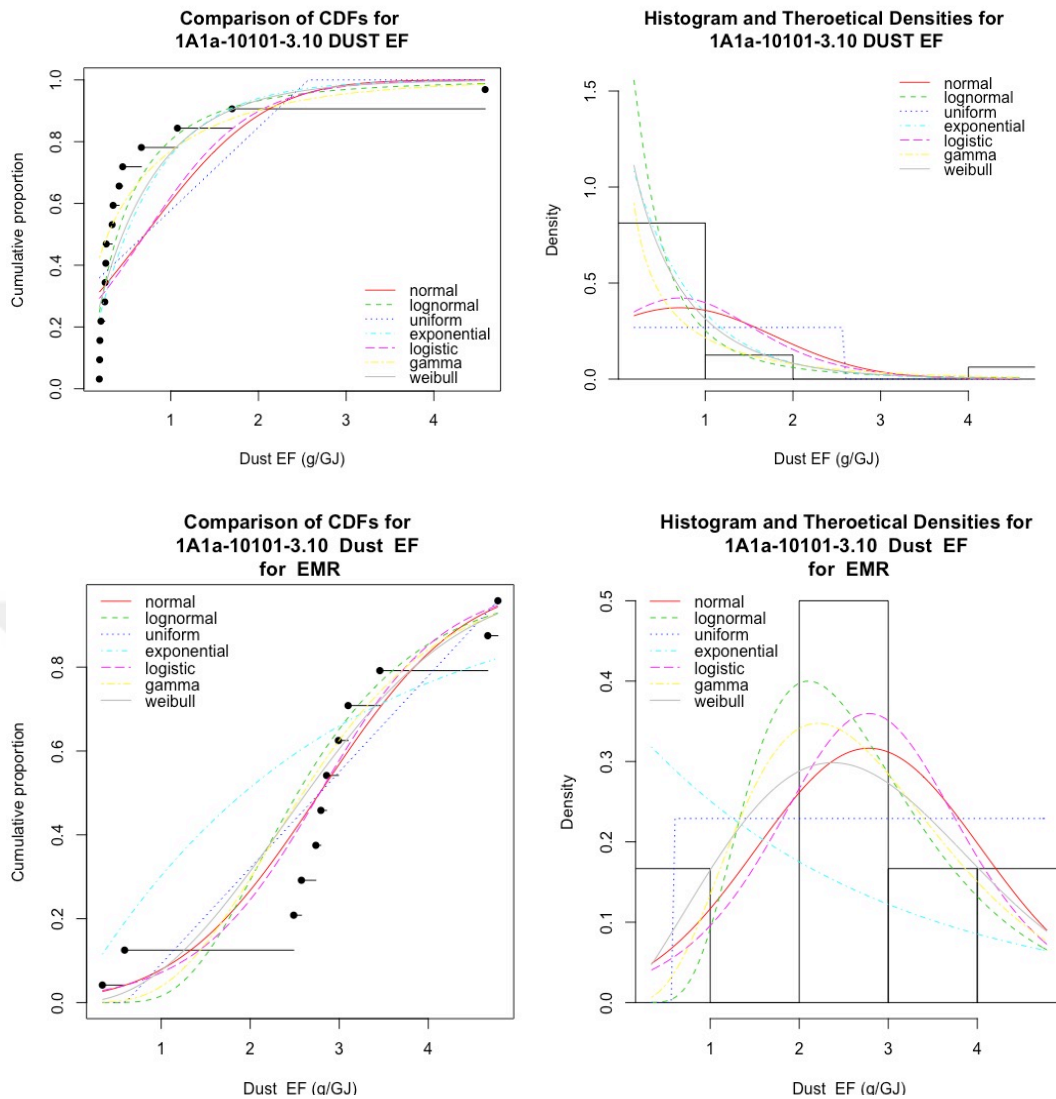
Figure 3.9 : Distribution fitting comparisons of dust EF on CDF and Histogram for both in-situ measurements and EMRs of "1.A.1.a – 10101 – 3.10".

According to Figure 3.9, looking at the CDF and histogram of EFs derived from in-situ measurements, lognormal and Weibull distributions are close to CDF and histogram of the in-situ EFs, visually. In addition to CDF and histograms given in Figure 3.9, goodness-of-fit statistics and goodness-of-fit criteria for dust EFs derived from in-situ measurements were also calculated and given in Table 3.6, in order to quantitatively support parametric probability distribution function fitting for our data, and making a base for expert opinion.

Table 3.6 : Goodness-of-fit statistics/criteria for dust EF derived from in-situ measurements of "1.A.1.a – 10101 – 3.10".

Type of distribution	Goodness-of-fit statistics			Goodness-of-fit criteria	
	Kolmogorov-Smirnov statistic	Cramer-von Mises	Anderson-Darling statistic	Akaike's Information Criterion	Bayesian Information Criterion
Normal	0.34	0.58	3.08	52	53
Lognormal	**0.25**	**0.19**	**1.11**	**18**	**20**
Uniform	0.36	0.63	-	-	-
Exponential	0.28	0.32	1.73	23	24
Logistic	0.36	0.58	2.92	47	48
Gamma	0.42	0.49	2.45	31	33
Weibull	0.26	0.29	1.58	25	26

* Bold values indicate lowest values.

Critical value of Kolmogorov-Smirnov statistic is 0.213, as it is given in Table 2.9. Kolmogorov-Smirnov statistic are more than critical value in all distribution types, however close to the critical value in lognormal distribution. Other goodness-of-fit statistics and criteria are also lowest for lognormal distribution. Therefore, best fitting distribution is selected as the lognormal distribution for dust EFs derived from in-situ measurements for "1.A.1.a–10101-3.10" SNAP/NFR category.

Goodness-of-fit statistics/criteria table for EFs derived from EMRs is given in Attachment F since the use of EFs derived from in-situ measurements is given priority in the thesis, and in order to save space in the thesis text. In EMR, normal and logistic distribution's Kolmogorov-Smirnov statistic is close to critical value. Logistic distribution is best for EMR data, however second-best fitting data, which is normal distribution, was accepted for EMR dataset since uncertainty calculations of logistic distribution was not available in AuvTool.

After assigning best fitting parametric distribution, Monte Carlo simulation is applied as in Section 2.2.4.4 and Bootstrap method is applied as in Section 2.2.4.5. Then, average EF and confidence intervals are calculated for both of in-situ EFs and EMR EFs, and results are given in Table 3.7.

It is seen that, the EFs derived from EMRs are higher than the EFs derived from in-situ measurements. However, the EFs calculated from both sources are significantly lower than the EMEP and EPA EFs.

Table 3.7 : Uncertainty analysis results for dust EF of "1.A.1.a–10101–3.10" and comparisons with other studies.

	In-situ measurements	EMR	EMEP [54]	EPA [193]
Fitted distribution type	Lognormal	Normal		
Mean	0.69 g/GJ	2.77 g/GJ	11.7 g/GJ	between
95% CI (Lower, Upper) as g/GJ	0.34–1.375	2.07–3.48	1.2 -117	63 [5] and
Uncertainty (Lower, Upper)	51-99%	25-26%	90-900%	13752 [6]
First parameter	-0.938 [1]	2.78 [3]		g/GJ
Second parameter	1.09 [2]	1.32 [4]		

[1] mean of ln(x) for lognormal parametric probability distribution function
[2] standard deviation of ln(x) for lognormal parametric probability distribution function
[3] mean for normal parametric probability distribution function
[4] standard deviation for normal parametric probability distribution function
[5] for filterable PM, controlled with baghouse filter
[6] for filterable PM, for uncontrolled conditions

Although the EF derived from EMR is within the EMEP confidence interval limits, it is considerably lower than the EPA EF. The EF generated from in-situ measurements is so low that it is almost half of the lower limit of the EMEP confidence interval. Country-specific EF, which is 0.69 g/GJ, is very low compared to EMEP [54] (11.7 g/GJ) and EPA [193] (minimum 63 g/GJ). The reason of this difference can be due to abatement technologies used in the plant and/or the seasonality effect. In the plant, electrostatic filter is used as dust abatement technology with more than 95% abatement efficiency. Also, emission measurements were conducted in May-June for both of in-situ EFs and EMR EFs. Therefore, it is not expected to be affected by seasonal capacity changes. Furthermore, in the surveys conducted to facility managers within the scope of the project, it was stated that there are no seasonal or monthly capacity changes. Consequently, using abatement technology reduces the dust EF. From this point, it is important to know in-site usage practices of these abatement technologies. In this point, the data supplied by continuous measurement systems is important.

One important indication that a distribution is properly fitted is that almost all points on the probability band are within 50% CI range [219]. Although EFs derived from in-situ measurements often remain within the 50% CI limits in Figure 3.10, it is seen that EFs derived from EMR are even beyond the 95% CI limits. In this case, it would be more appropriate to use EFs derived from in-situ measurements. Consequently, country specific dust EF is 0.69 g/GJ for "1.A.1.a–10101-3.10" SNAP/NFR category, with 95% lower CI as 0.34 g/GJ and upper CI as 1.375 g/GJ.
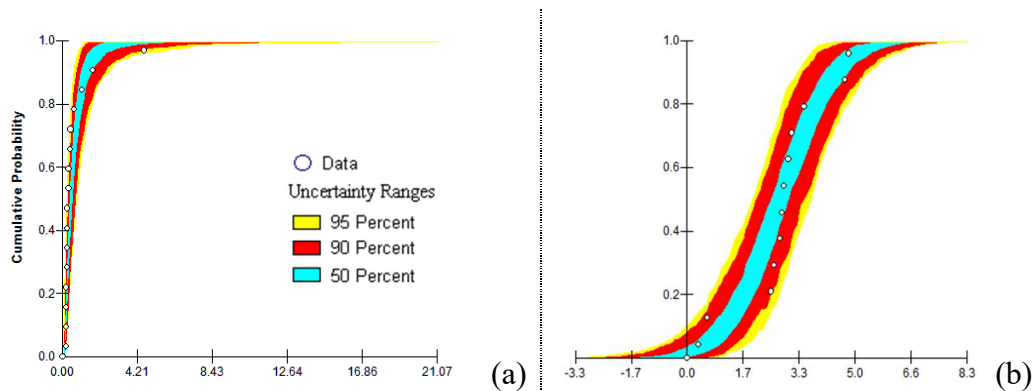
Figure 3.10 : Probability band of dust EFs for "1A1a-10101-3.10" as cumulative distribution of (a)lognormal distribution fitted to dust EFs derived from in-situ measurements (b)normal distribution fitted to dust EFs derived from EMRs.

CO

Summary statistics of CO EFs for "1.A.1.a–10101–3.10" SNAP/NFR category are given in Table 3.8 for EFs derived from both in-situ measurements and EMRs. When min, max and median of the EFs derived from in-situ measurements and those derived from EMR are compared in Table 3.8, it is clear that CO EFs obtained from in-situ measurements are in a greater range than that reported in the EMRs. So, it can be inferred that that there were lower CO concentrations in EMRs for "1.A.1.a–10101–3.10" SNAP/NFR category for this plant. Therefore, the variance and standard deviation of in-situ EFs are greater than those derived from EMRs.

Table 3.8 : Summary statistics for CO EFs derived from both in-situ measurements and EMRs for "1.A.1.a–10101–3.10".

	In-situ Measurements	EMR
Number of data points	16	12
Minimum	5.22	0.29
Maximum	45.06	4.49
Median	15.01	3.47
Variance [1]	140.7	3.27
Standard Deviation [2]	11.86	1.81
Cv (%) [3]	64	61
Skewness [4]	0.71	-0.74
Kurtosis [5]	-0.49	-1

[1] According to equation 2.12
[2] According to equation 2.13
[3] According to equation 2.14
[4] According to equation 2.15
[5] According to equation 2.16

In Figure 3.11, EFs are distributed homogeneously in the CDF of EFs derived from in-situ measurements, while EFs derived from EMR show a clustered distribution. When the EMR data was examined, it was seen that each clustered data represents the measurements taken from different stacks of the plant. In this case, we can assume that the variability in EMR EFs is more than in-situ EFs.
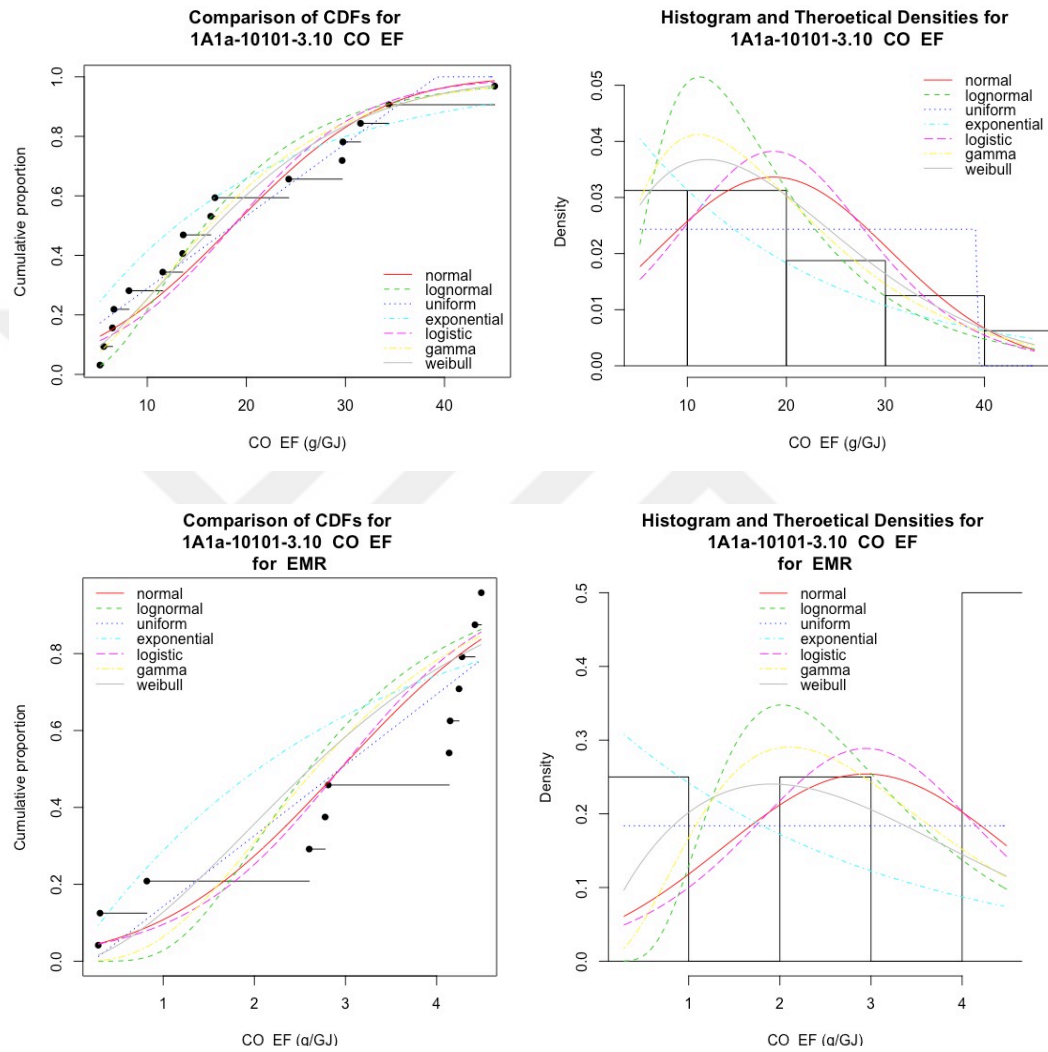
Figure 3.11 : Distribution fitting comparisons of CO EF on CDF and Histogram for both in-situ measurements and EMRs of "1.A.1.a – 10101 – 3.10".

However, variance and standard deviation of EMR EFs are less than in-situ EFs, because the range of EMR EFs is less than in-situ EFs. However, Cv value, which represents the variability in the EFs within each measurement source as a percentage, is quite close to each other in both cases. Although the EFs calculated from both sources are quite different from each other, the variability within in-situ EFs and EMR EFs is similar. EFs derived from both in-situ measurements and EMRs have low Kurtosis and Skewness values.

According to Figure 3.11, looking at the CDF and histogram of EFs derived from in-situ measurements, Weibull distribution is close to CDF and histogram of the in-situ EFs. Table 3.9 is created in order to quantitatively support this qualitative interpretation and includes goodness-of-fit statistics and goodness-of-fit criteria for CO EFs derived from in-situ measurements.

Table 3.9 : Goodness-of-fit statistics/criteria for CO EF derived from in-situ measurements of 1.A.1.a – 10101 – 3.10.

Type of distribution	Goodness-of-fit statistics			Goodness-of-fit criteria	
	Kolmogorov-Smirnov statistic	Cramer-von Mises	Anderson-Darling statistic	Akaike's Information Criterion	Bayesian Information Criterion
Normal	0.19	0.11	0.63	128.55	130.10
Lognormal	0.18	0.11	0.92	125.09	126.63
Uniform	0.17	0.08	-	-	-
Exponential	0.24	0.16	1.02	127.67	128.44
Logistic	0.19	0.14	0.79	129.82	131.37
Gamma	0.15	0.07	0.44	**124.09**	**125.64**
Weibull	**0.14**	**0.06**	**0.41**	124.40	125.95

* Bold values indicate lowest values.

Critical value of Kolmogorov-Smirnov statistic is 0.213, as it is given in Table 2.9. Kolmogorov-Smirnov statistic of entire of the distributions are less than critical value (0.213), except exponential distribution. Minimum Kolmogorov-Smirnov statistic is in Weibull distribution. Other goodness-of-fit statistics are also lowest for Weibull distribution. Goodness of fit criteria are not lowest in Weibull distribution, but they are very close to minimum. Since Weibull distribution seems best in in-situ EFs in Figure 3.11, and due to lowest goodness-of-fit statistics in Table 2.9, best fitting distribution is selected as the Weibull distribution for CO EFs derived from in-situ measurements. Since the variability and clustered data in the EMR EFs were high, the uniform distribution was considered for EFs derived from EMRs. Goodness-of-fit statistics/criteria for CO EF derived from EMRs are given Attachment F.

After assigning best fitting parametric distribution, Monte Carlo simulation is applied as in Section 2.2.4.4 and Bootstrap method is applied as in 2.2.4.5. Then average EF and confidence intervals are calculated for each of in-situ EFs and EMR EFs and given in Table 3.10. It is seen that the EFs derived from EMR are pretty lower than the EFs derived from in-situ measurements. There is no abatement technology for CO emissions in the plant.

Table 3.10 : Uncertainty analysis results for CO EF of "1.A.1.a – 10101 – 3.10" and comparisons with other studies.

	In-situ Measurements	EMR	EMEP [54]	EPA [193]
Fitted distribution type	Weibull	Uniform		
Mean (g/GJ)	18.87	2.9	8.7	between
95% CI (Lower, Upper) as g/GJ	13.47-25.33	2.01-3.78	6.72-60.5	13 [5] and
% Uncertainty (Lower, Upper)	29-34%	31-30%	23-595%	32 [6]
First parameter	20.97 [1]	0.1 [3]		g/GJ
Second parameter	1.65 [2]	5.8 [4]		

[1] scale parameter (k) for Weibull parametric probability distribution function
[2] shape parameter (c) for Weibull parametric probability distribution function
[3] minimum value (a) for Uniform parametric probability distribution function
[3] maximum value (b) for Uniform parametric probability distribution function
[5] for uncontrolled external combustion of lignite for electricity generation (SCC is 10100302 and 10100303)
[6] for uncontrolled external combustion of lignite for electricity generation (SCC is 10100301)

Consequently, country-specific CO EF is calculated as 18.87 g/GJ which is within the 95% confidence interval range of EMEP (6.72 and 60.5) [54] and compatible with EPA (between 13 and 32 g/GJ) [193]. Lower and upper confidence interval range of country-specific CO EF is small when compared to EMEP and EPA confidence interval ranges. Probability band of CO EFs are given in Figure 3.12.
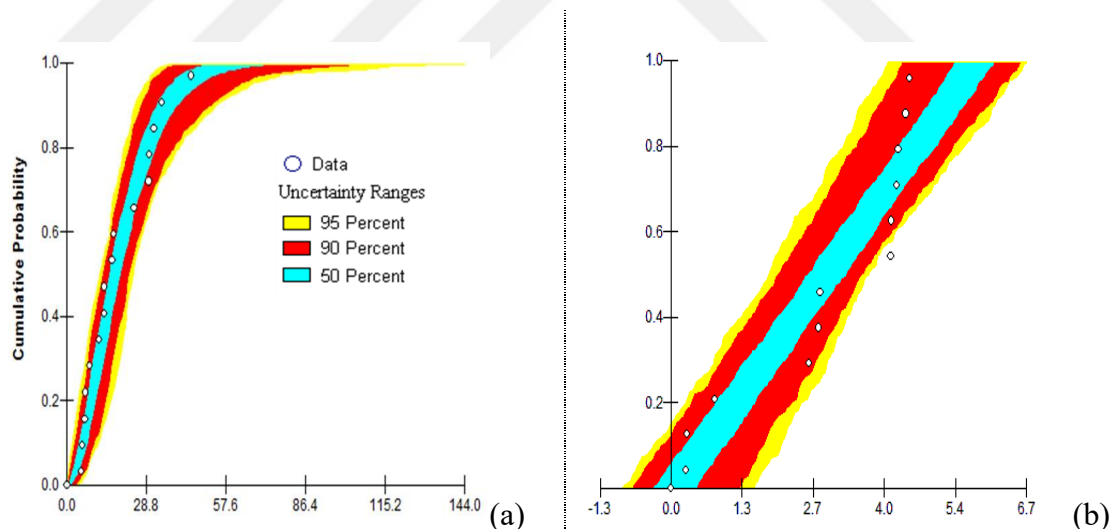
Figure 3.12 : Probability band of CO EFs for "1A1a-10101-3.10" as cumulative distribution of (a)lognormal distribution fitted to CO EFs derived from in-situ measurements. (b)normal distribution fitted to CO EFs derived from EMRs.

Although EFs derived from in-situ measurements often remain within the 50% CI limits, it is seen that EFs derived from EMR are even beyond the 95% CI limits. In this case, it would be more appropriate to use EFs derived from in-situ measurements.

SO₂

Summary statistics of SO₂ EFs for "1.A.1.a–10101–3.10" SNAP/NFR category are given in Table 3.11 for EFs derived from both in-situ measurements and EMRs. When min, max and median of the EFs derived from in-situ measurements and those derived from EMR are compared in Table 3.11, it is clear that SO₂ EFs obtained from in-situ measurements are three times more EFs calculated from EMRs. Therefore, the variance and standard deviation calculated from in-situ EFs are greater than those derived from EMRs. When the CDFs and histograms given in Figure 3.13 are compared, the EFs are distributed homogeneously in the CDF of in-situ EFs and EMR EFs. Cv value, which represents the variability in the EFs within each source as a percentage, may be considered low in itself, but more than EMR. Finally, variability of in-situ EFs is larger than EMR's. EFs derived from both in-situ measurements and EMRs have close Kurtosis and Skewness values.

Table 3.11 : Summary statistics for SO₂ EFs derived from both in-situ measurements and EMRs for "1.A.1.a–10101–3.10".

	In-situ Measurements	EMR
Number of data points	16	12
Minimum	112.71	42.2
Maximum	315.12	91
Median	247	69.7
Variance [1]	4310	2.7
Standard Deviation [2]	63.5	1.57
Coefficient of variation (%) [3]	28	2
Skewness [4]	-0.43	-0.46
Kurtosis [5]	-1.04	1.24

[1] According to equation 2.12
[2] According to equation 2.13
[3] According to equation 2.14
[4] According to equation 2.15
[5] According to equation 2.16

According to Figure 3.13, Weibull and Normal parametric distributions seem best fitting distributions for in-situ EFs, where Normal, Weibull and Logistic distributions are appropriate for EMR EFs. In addition to CDF and histograms given in Figure 3.13, goodness-of-fit statistics and goodness-of-fit criteria were also calculated in order to determine best fitting parametric probability distribution function for our data, and given in Table 3.12. Critical value of Kolmogorov-Smirnov statistic is 0.213, as it is given in Table 2.9. Kolmogorov-Smirnov statistic is less than critical value for the distributions other than lognormal and exponential distributions. Minimum

Kolmogorov-Smirnov and Cramer-von Mises statistics are in Uniform and Weibull distributions. However, Weibull distribution is selected as the best fitting distribution for in-situ EFs since it takes minimum values in the remaining goodness-of-fit statistics and criteria.
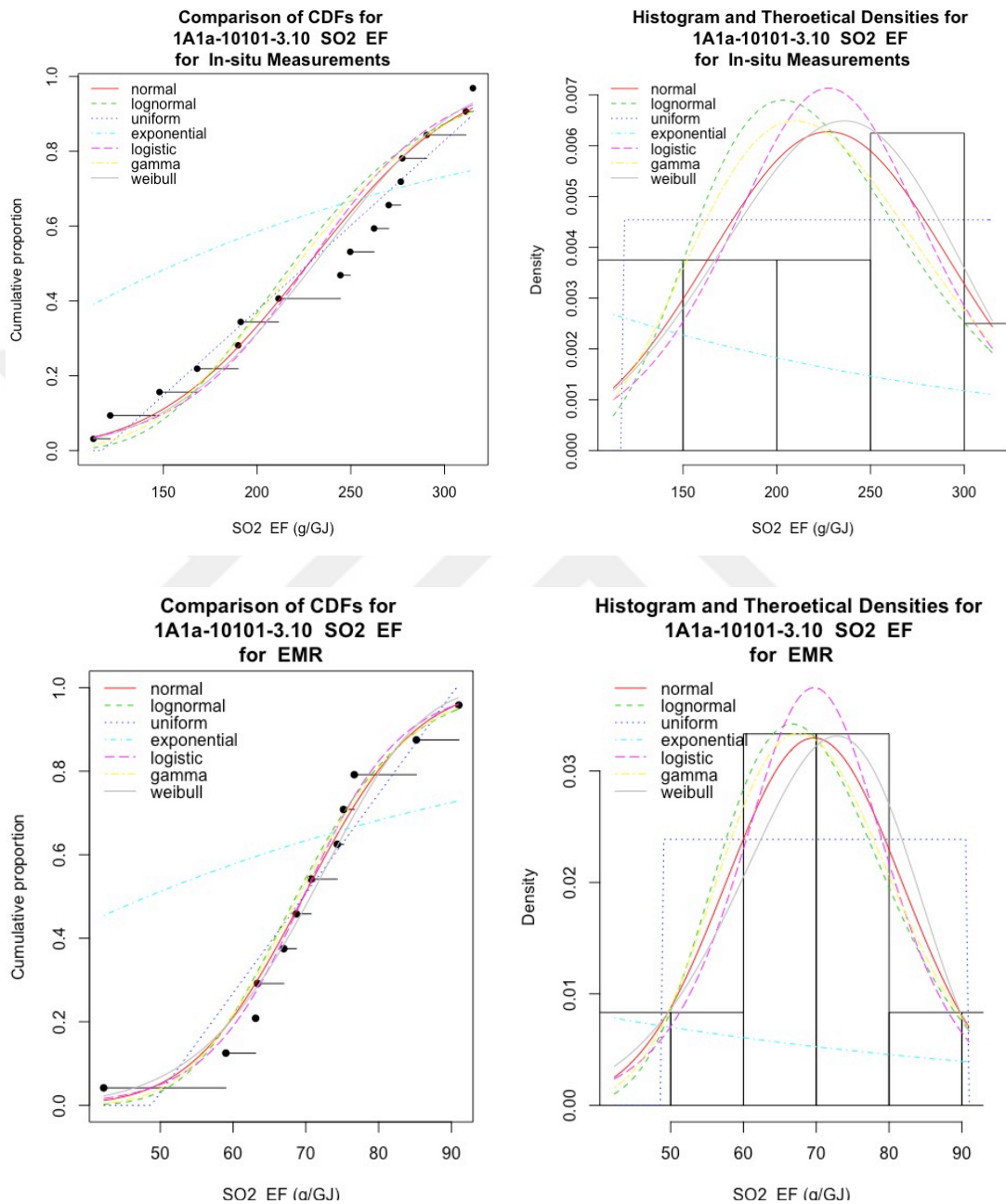

Figure 3.13 : Distribution fitting comparisons of SO_2 EF on CDF and Histogram for both in-situ measurements and EMRs of ""1.A.1.a–10101–3.10".

Weibull distribution is also considered as best fitting distribution for EFs derived from EMRs. Goodness-of-fit statistics of EMR EFs are given in Attachment F.

Table 3.12 : Goodness-of-fit statistics/criteria for SO_2 EF derived from in-situ measurements of 1.A.1.a – 10101 – 3.10.

Type of distribution	Goodness-of-fit statistics			Goodness-of-fit criteria	
	Kolmogorov-Smirnov statistic	Cramer-von Mises	Anderson-Darling statistic	Akaike's Information Criterion	Bayesian Information Criterion
Normal	0.17	0.07	0.44	182.27	183.82
Lognormal	0.22	0.13	0.91	185.54	187.09
Uniform	**0.14**	**0.05**	-	-	-
Exponential	0.39	0.76	3.77	207.68	208.45
Logistic	0.18	0.10	0.59	183.87	185.41
Gamma	0.20	0.11	0.68	183.84	185.38
Weibull	0.15	0.07	**0.43**	**181.39**	**182.93**

* Bold values indicate lowest values.

After assigning best fitting parametric distribution, Monte Carlo simulation is applied as in Section 2.2.4.4 and Bootstrap method is applied as in 2.2.4.5. Then average EF and confidence intervals are calculated for each of in-situ EFs and EMR EFs and given in Table 3.13. It is seen that the in-situ EFs are almost three times of EMR EFs.

Table 3.13 : Uncertainty analysis results for SO_2 EF of "1.A.1.a–10101–3.10" and comparisons with other studies.

	In-situ Measurements	EMR	EMEP [54]	EPA [193]
Fitted distribution type	Weibull	Weibull		
Mean (g/GJ)	229.2	70.1	1680	between
95% CI (Lower, Upper) as g/GJ	191.8-265	62.3-76.7	330-5000	190 [3]
% Uncertainty (Lower, Upper)	16.3-15.6%	11.1-9.4%	80.4-198%	and 569
First parameter	252.77 [1]	75.08 [1]		[4] g/GJ
Second parameter	3.7 [2]	6.08 [2]		

[1] scale parameter (k) for Weibull parametric probability distribution function
[2] shape parameter (c) for Weibull parametric probability distribution function
[3] for uncontrolled external combustion of lignite with atmospheric fluidized bed technology for electricity generation (SCC is 10100316 and 10100317)
[4] for uncontrolled external combustion of lignite with other technologies for electricity generation (SCC is 10100311, 10100312, 10100313 or 10100314)

Country specific SO_2 EF is calculated from in-situ measurements as 229.2 g/GJ which is even below the 95% lower limit of EMEP (330 g/GJ) [54], and less than EPA EF (569 g/GJ) [193]. In the plant, flue gas desulphurization is used as SO_2 abatement technology with more than 95% abatement efficiency. By considering abatement technology, country-specific EF (229.2 g/GJ) is compatible with EPA [193], which is

between 190 and 569 g/GJ for uncontrolled conditions (there is no EF for controlled conditions).

Since almost all points fall into the 50% CI range in probability band of in-situ measurements given in Figure 3.14a, Weibull distribution is appropriate for EFs derived from in-situ EFs. Although EF derived from EMR (70.1 g/GJ) appears to be well calculated as all points fall into 50% CI range in Figure 3.14b, it remains low compared to the literature.
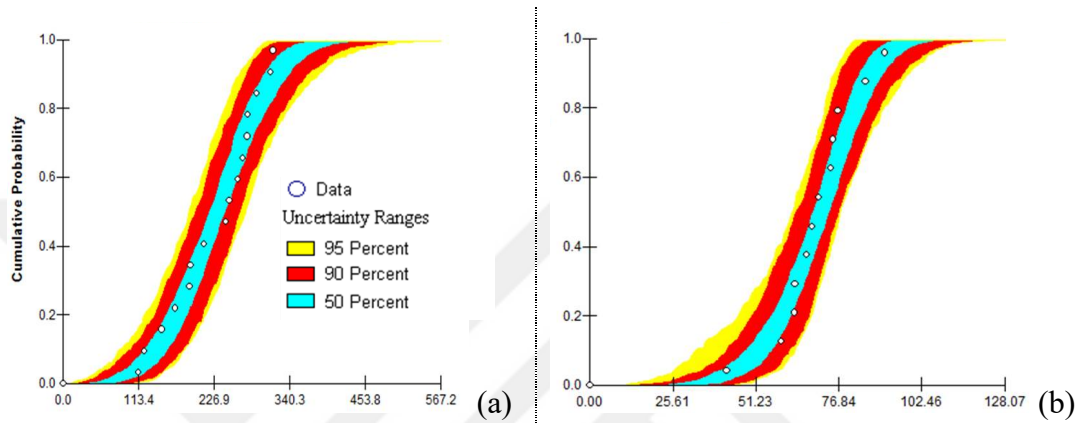

Figure 3.14 : Probability band of SO_2 EFs for "1A1a-10101-3.10" as cumulative distribution of Weibull distribution fitted to SO_2 EFs derived from (a) in-situ measurements (b) EMRs.

NO

Summary statistics of NO EFs for "1.A.1.a–10101–3.10" SNAP/NFR category are given in Table 3.14 for EFs derived from both in-situ measurements and EMRs. When min, max and median of the EFs derived from in-situ measurements and those derived from EMR are compared in Table 3.14, it is clear that NO EFs obtained from in-situ measurements are more than three times than calculated from EMRs. Therefore, the variance and standard deviation calculated from in-situ EFs are greater than those derived from EMRs. Furthermore, Cv value, which represents the variability in the EFs as a percentage, may be considered low in itself. Consequently, variability of EMR EFs is larger than in-situ EFs. One outlier value in the EMR EFs, which is 30.3 g/GJ, increases variability in the EMR EFs, as it is clear on the CDF of EFs derived from EMRs which is given in Figure 3.15. Low skewness in EFs derived from both in-situ measurements and EMRs in Table 3.14 indicate low asymmetry. Large Kurtosis in EFs derived from in-situ measurements indicate large peak in the distribution as it is also visualized in Figure 3.15.

Table 3.14 : Summary statistics of NO EFs derived from both in-situ measurements and EMRs for "1.A.1.a–10101–3.10".

	In-situ Measurements	EMR
Number of data points	16	12
Minimum	100.4	30.4
Maximum	151.9	64
Median	126.4	45.17
Variance [1]	242	83.5
Standard Deviation [2]	15.5	9.1
Cv (%) [3]	12	19
Skewness [4]	0.13	0.075
Kurtosis [5]	-1.06	-0.4

[1] According to equation 2.12
[2] According to equation 2.13
[3] According to equation 2.14
[4] According to equation 2.15
[5] According to equation 2.16

According to Figure 3.15, looking at the CDF and histogram of EFs derived from in-situ measurements, none of the distribution is well fitted due to high variability. In this case Uniform distribution may be considered. In addition to CDF and histograms given in Figure 3.15, goodness-of-fit statistics and goodness-of-fit criteria for in-situ EFs were also calculated and given in Table 3.15, in order to determine best fitting parametric probability distribution function for our data. Even in this table, the uniform distribution appears to be the best fitting distribution since it has the lowest values for entire of goodness-of-fit statistics and criteria.

Goodness-of-fit statistics and criteria of EFs derived from EMRs are given in Attachment F. Lognormal distribution is selected as best fitting parametric distribution for EMR EFs.

After assigning best fitting parametric distribution, Monte Carlo simulation is applied as in Section 2.2.4.4 and Bootstrap method is applied as in 2.2.4.5. Then average EF and confidence intervals are calculated for each of in-situ EFs and EMR EFs and given in Table 3.16. EFs derived from in-situ measurements are almost three times of EFs derived from EMRs in Table 3.16.
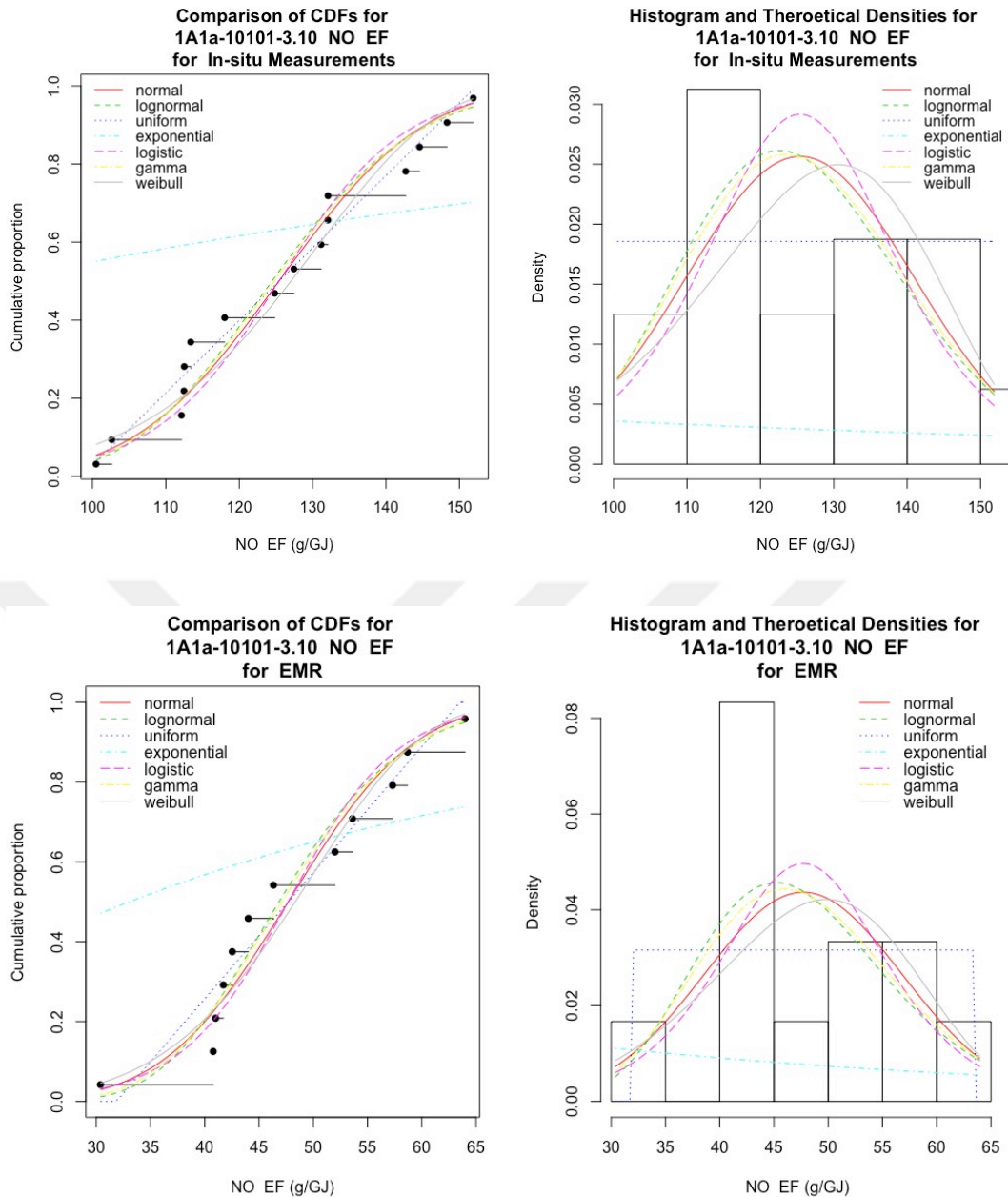
Figure 3.15 : Distribution fitting comparisons of NO EF on CDF and Histogram for both in-situ measurements and EMRs of 1.A.1.a – 10101 – 3.10.

Country-specific NO EF is calculated as 125.9 g/GJ, where it is 48 g/GJ for EF derived from EMR. There is no abatement technology in the plant. NO EFs are not supplied by EMEP [54], therefore there is no room for comparison. All of the NO_x emissions in this category are accepted as NO by EPA [193] and given as 385 g/GJ for uncontrolled conditions. In this case, the EF calculated from in-situ measurements is one third of the EPA EF.

Table 3.15 : Goodness-of-fit statistics/criteria for NO EF derived from in-situ measurements of "1.A.1.a–10101–3.10".

Type of distribution	Goodness-of-fit statistics			Goodness-of-fit criteria	
	Kolmogorov-Smirnov statistic	Cramer-von Mises	Anderson-Darling statistic	Akaike's Information Criterion	Bayesian Information Criterion
Normal	0.16	0.05	0.35	137.22	138.76
Lognormal	0.15	0.05	0.35	137.09	138.64
Uniform	**0.13**	**0.04**	**0.25**	**131.57**	**133.11**
Exponential	0.55	1.22	5.66	188.61	189.39
Logistic	0.18	0.07	0.48	138.77	140.32
Gamma	0.15	0.05	0.34	137.08	138.62
Weibull	0.15	0.06	0.39	137.95	139.50

* Bold values indicate lowest values.

Since almost all in-situ EFs fall into the 50% CI range, which is considered a criterion of goodness-of-fit [219], Uniform distribution is appropriate for EFs derived from in-situ EFs, as it is shown in the probability band in Figure 3.16. Also, Lognormal distribution fitted good in EFs derived from EMR, since they are mostly within the 50% CI range.

Table 3.16 : Uncertainty analysis results for NO EF of "1.A.1.a – 10101 – 3.10" and comparisons with other studies.

	In-situ Measurements	EMR	EPA [193]
Fitted distribution type	Uniform	Lognormal	
Mean (g/GJ)	125.9 g/GJ	48 g/GJ	
95% CI (Lower, Upper) as g/GJ	118.2-135.2	43.1-54.2	385 [5]
% Uncertainty (Lower, Upper)	6.1-7.4%	14.2-9.1%	g/GJ
First parameter	97.6 [1]	1.349 [3]	
Second parameter	153.2 [2]	0.0149 [4]	

[1] minimum value (a) for Uniform parametric probability distribution function
[2] maximum value (b) for Uniform parametric probability distribution function
[3] mean of lnx for Lognormal parametric probability distribution function
[4] standard deviation of lnx for Lognormal parametric probability distribution function
[5] for uncontrolled external combustion of lignite for electricity generation (SCC is 10100301)

Although EF derived from EMR (48 g/GJ) appears to be well calculated and appropriate as on the probability band given in Figure 3.16b, it remains low compared to the literature.
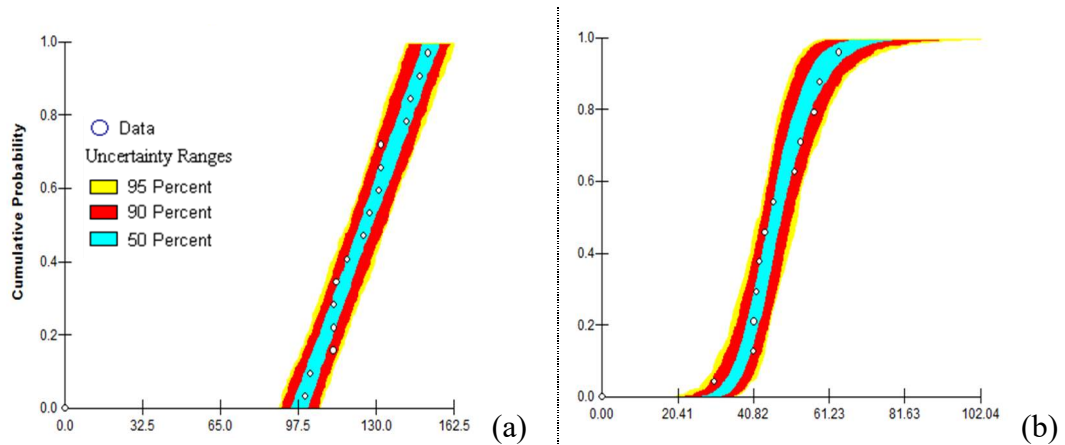
Figure 3.16 : Probability band of NO EFs for "1A1a-10101-3.10" as cumulative distribution of (a)lognormal distribution fitted to NO EFs derived from in-situ measurements (b)normal distribution fitted to NO EFs derived from EMRs.

NO$_2$

Summary statistics of NO$_2$ EFs for "1.A.1.a–10101–3.10" SNAP/NFR category are given in Table 3.17 for EFs derived from both in-situ measurements and EMRs. When min, max and median of the EFs derived from in-situ measurements and those derived from EMR are compared in Table 3.17, it is clear that NO$_2$ EFs obtained from in-situ measurements are approximately three times of EFs calculated from EMRs. Therefore, the variance and standard deviation of in-situ EFs are greater than those derived from EMRs. Furthermore, Cv of in-situ measurements are low when compared to EMRs. This low Cv (12%) shows that there is agreement between in-situ measurements, therefore variability is low.

Table 3.17 : Summary statistics of NO$_2$ EFs derived from both in-situ measurements and EMRs for "1.A.1.a–10101–3.10".

	In-situ Measurements	EMR
Number of data points	16	12
Minimum	161.84	49.1
Maximum	244.8	103.3
Median	204.4	45.17
Variance [1]	630.6	215.78
Standard Deviation [2]	25.93	14.7
Cv (%) [3]	12	19
Skewness [4]	0.11	0.075
Kurtosis [5]	-1.07	-0.4

[1] According to equation 2.12
[2] According to equation 2.13
[3] According to equation 2.14
[4] According to equation 2.15
[5] According to equation 2.16

The large variability is heavily affected from outliers. Comparison of CDFs and histograms with possible parametric distribution fitting options are given in Figure 3.17. According to Figure 3.17, looking at the CDF of EFs derived from EMR, there is one outlier value which is the lowest EF (49.2 g/GJ). This outlier value in the EMR EFs increases variability in the EMR EFs.
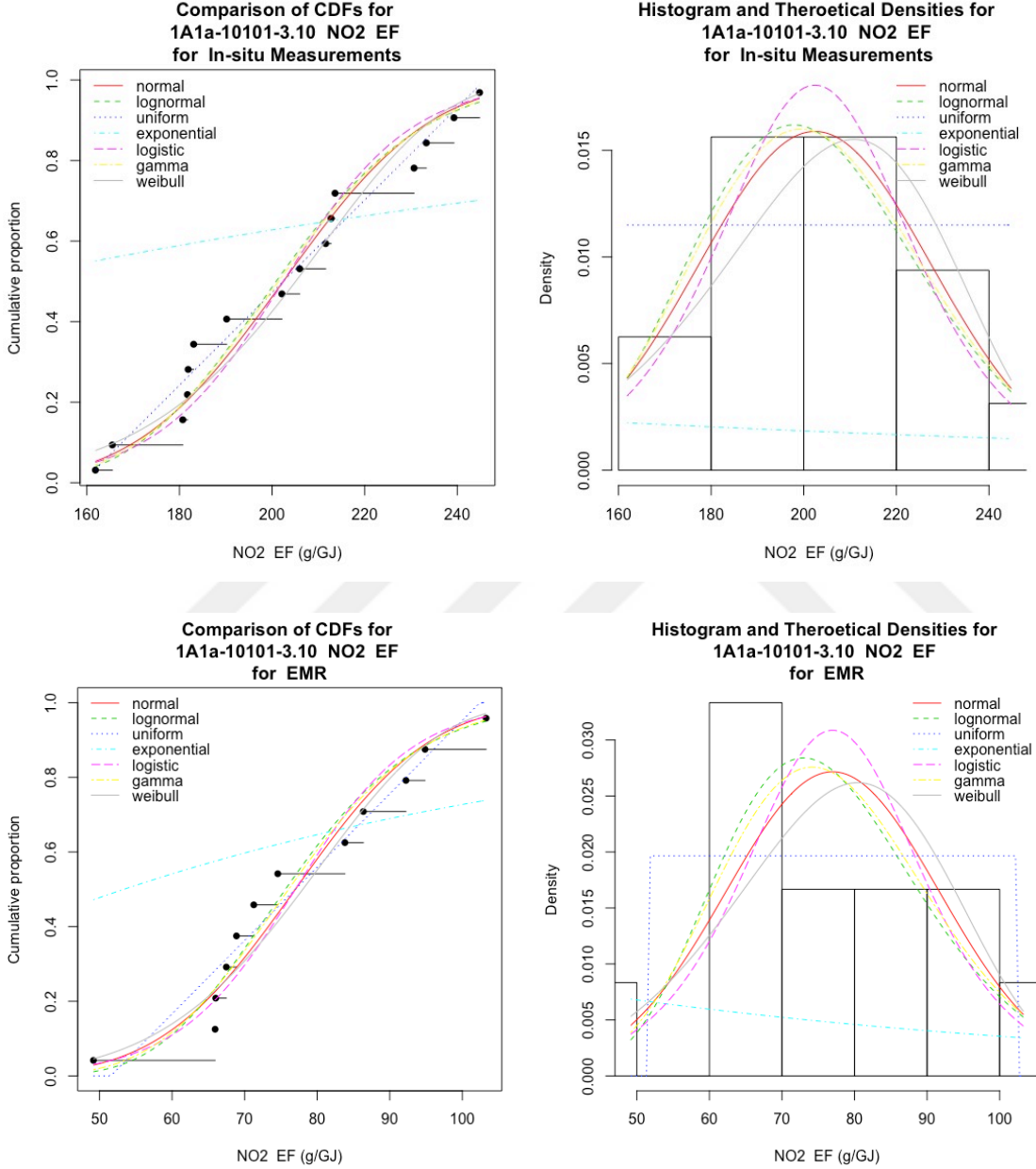

Figure 3.17 : Distribution fitting comparisons of NO_2 EF on CDF and Histogram for both in-situ measurements and EMRs of 1.A.1.a – 10101 – 3.10.

Low skewness in both in-situ and EMR EFs in Table 3.17 indicate low asymmetry. Large Kurtosis in EFs derived from in-situ measurements indicate large peak in the distribution as it is also visualized in Figure 3.17.

According to Figure 3.17, looking at the CDF and histogram of EFs derived from in-situ measurements, Normal and Gamma distribution seems close to CDF and histogram of the in-situ EFs. Table 3.18 is created in order to quantitatively support this qualitative interpretation and this table includes goodness-of-fit statistics and goodness-of-fit criteria for in-situ NO_2 EFs.

Critical value of Kolmogorov-Smirnov statistic is 0.213, as it is given in Table 2.9. Kolmogorov-Smirnov statistic of entire of the distributions are less than critical value (0.213), except exponential distribution. Minimum Kolmogorov-Smirnov statistic is in Uniform distribution. Other goodness-of-fit statistics are also lowest for Uniform distribution. Although Normal or Gamma distributions are found to be appropriate fitting distribution in visual examination, goodness-of-fit statistics/criteria indicate uniform distribution for in-situ EFs. Gamma distribution is selected as best fitting parametric distribution for EMR EFs, and goodness-of-fit statistics and criteria are given in Attachment F.

Table 3.18 : Goodness-of-fit statistics/criteria for NO_2 EF derived from in-situ measurements of 1.A.1.a – 10101 – 3.10.

Type of distribution	Goodness-of-fit statistics			Goodness-of-fit criteria	
	Kolmogorov-Smirnov statistic	Cramer-von Mises	Anderson-Darling statistic	Akaike's Information Criterion	Bayesian Information Criterion
Normal	0.155	0.054	0.349	152.55	154.10
Lognormal	0.149	0.054	0.347	152.46	154.01
Uniform	**0.125**	**0.036**	**0.234**	**146.91**	**148.45**
Exponential	0.550	1.218	5.659	203.93	204.71
Logistic	0.177	0.074	0.483	154.11	155.66
Gamma	0.150	0.053	0.339	152.44	153.98
Weibull	0.153	0.061	0.390	153.24	154.78

* Bold values indicate lowest values.

After assigning best fitting parametric distribution, Monte Carlo simulation is applied as in Section 2.2.4.4 and Bootstrap method is applied as in 2.2.4.5. Then average EF and confidence intervals are calculated for each of in-situ EFs and EMR EFs and given in Table 3.19. EFs derived from EMR are pretty lower than in-situ EFs.

Since almost all EFs of in-situ measurements fall into the 50% CI range, which is considered a criterion of goodness-of-fit [219], Uniform distribution is appropriate for EFs derived from in-situ EFs, as it is shown in the probability band in Figure 3.18.

Table 3.19 : Uncertainty analysis results for NO_2 EF of 1.A.1.a – 10101 – 3.10 and comparisons with other studies.

	In-situ Measurements	EMR
Fitted distribution type	Uniform	Gamma
Mean (g/GJ)	202.64	76.7
95% CI (Lower, Upper) as g/GJ	191.16-216.47	69.7-87.3
% Uncertainty (Lower, Upper)	5.7-6.8%	9.1-13.8%
First parameter	155.51 [1]	25.17 [3]
Second parameter	247.36 [2]	3.05 [4]

[1] minimum value (a) for Uniform parametric probability distribution function
[2] maximum value (b) for Uniform parametric probability distribution function
[3] scale parameter (α) for Gamma parametric probability distribution function
[4] shape parameter (β) for Gamma parametric probability distribution function

Also, it is seen in Figure 3.18 that the Gamma distribution fitted good to EFs derived from EMR, since they are mostly within the 50% CI range. Consequently, country specific NO_2 EF is 202.64 g/GJ for "1.A.1.a–1010-3.10" SNAP/NFR category, with 95% lower CI as 191.16 g/GJ and upper CI as 216.47 g/GJ.
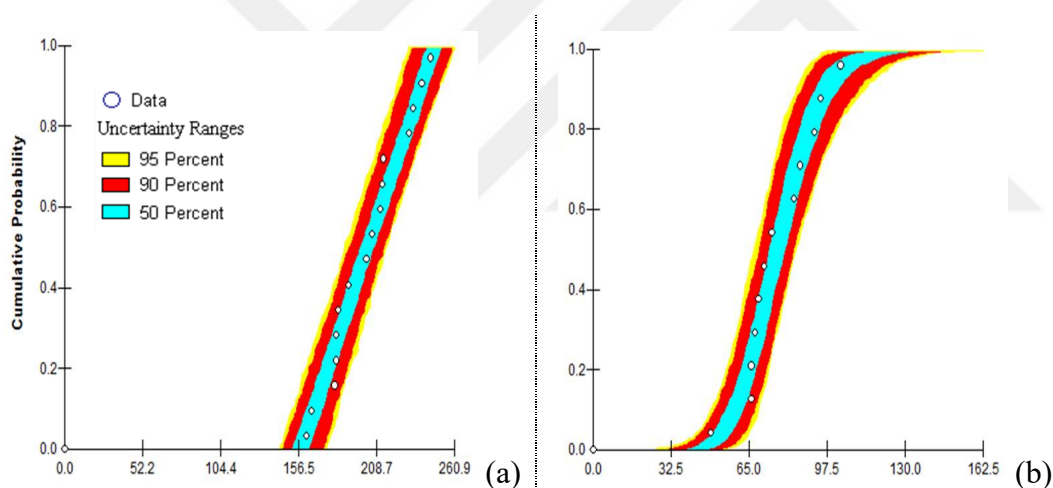

Figure 3.18 : Probability band of NO_2 EFs for "1A1a-10101-3.10" as cumulative distribution of (a)Uniform distribution fitted to NO_2 EFs derived from in-situ measurements (b)Gamma distribution fitted to NO_2 EFs derived from EMRs.

NO_x

NOx EF is calculated as the sum of NO and NO_2 emissions. However, since the uncertainty levels of NO and NO_2 EFs are different, the formulas given in equation 2.1a-2.1d were applied in order to calculate the total uncertainty of NO_x EF. NOx EF of "1.A.1.a–10101–3.10" SNAP/NFR category and comparisons with other studies are given in Table 3.20.

Table 3.20 : NO$_x$ EF of "1.A.1.a–10101–3.10" and comparisons with other studies.

	In-situ Measurements	EMR	EMEP [54]	EPA [193]
NOx EF (NO+NO$_2$) as g/GJ	328.54	124.7	247	between
95% CI (Lower, Upper) as g/GJ	314.72-345.21	116.2-137	143-571	70 [1] and
% Uncertainty (Lower, Upper)	5.1-4.2%	6.9-9.8%	42-131%	385 [2]
NO/NO$_2$ share	0.62	0.63		g/GJ

[1] for uncontrolled external combustion of lignite for electricity generation (SCC is 10100301)
[2] for uncontrolled external combustion of lignite for electricity generation (SCC is 10100302)

Country specific NO$_x$ EF is calculated as 328.54 g/GJ which is almost three times of in-situ EF. NO$_x$ EF is more than EMEP EF [54], which is 247 g/GJ, however it is within 95% CI of EMEP. Although NO$_x$ EF is close to upper value (385 g/GJ) of EPA EFs [193], it is also compatible with EPA EF. There is no NO$_x$ abatement technology in the plant.

The ratio of NO and NO$_2$ is 0.6 for both in-situ and EMR EFs for "1.A.1.a–10101–3.10" SNAP/NFR category.

3.2.2 Coal combusting large size fluid bed boilers

Coal combusting medium size boilers are represented with "1.A.1.a–10101–3.16" code. In detail, the code represents brown coal combustion plants with a capacity greater than 300 MW and with fluid bed boilers as the combustion technology for production of public power [54].

There are 2 plants falling under this SNAP/NFR category in Marmara region. In-situ measurements were conducted in one plant within the context of KAMAG project [194], and measurements from EMRs were available for both of two plants. Consequently, 16 in-situ measurements from one plant is used in the calculation of country-specific EF for this SNAP/NFR code. Furthermore 7 to 10 emission measurements from EMRs were also used for comparison.

Dust

Summary statistics of dust EFs for "1.A.1.a–10101–3.16" SNAP/NFR category are given in Table 3.21 for both of in-situ and EMR EFs. When min, max and median of the EFs derived from in-situ measurements and those derived from EMRs are compared in Table 3.21, it is clear that dust EFs obtained from EMRs are in a greater range than in-situ measurements.

Table 3.21 : Summary statistics of dust EFs derived from both in-situ measurements and EMRs for "1.A.1.a–10101–3.16".

	In-situ Measurements	EMR
Number of data points	16	7
Minimum	0.02	0.31
Maximum	1.01	3.27
Median	0.14	2.76
Variance [1]	0.08	0.98
Standard Deviation [2]	0.29	0.99
Cv (%) [3]	108	45
Skewness [4]	1.75	-1
Kurtosis [5]	2.58	0.12

[1] According to equation 2.12
[2] According to equation 2.13
[3] According to equation 2.14
[4] According to equation 2.15
[5] According to equation 2.16

Also, variance and standard deviation of in-situ EFs is lower than that of EMR EFs. In-situ EFs are generally less than 1 g/GJ, causing variance and standard deviation to be low while Cv of in-situ EFs was calculated quite much than EMR EFs. The small number of EFs from EMRs should also be considered when evaluating variability. Consequently, there is large variability in in-situ EFs, where variability is relatively low in EMR EFs. In Figure 3.19, comparison of CDFs and histograms with possible parametric distribution fitting options are given.

The large variability is heavily affected from outliers. According to Figure 3.19, looking at the CDF of EFs from in-situ measurements, more than 80% of EFs are less than 0.4 g/GJ, however, there are two EFs which are more than 0.9 g/GJ, which can be treated as outlier. Variability contribution of these outliers in the CDF of in-situ EFs should be considered when evaluating large variability. There is positive skewness in the EFs derived from in-situ measurements where it is negative in EF's of EMRs.

According to Figure 3.19, looking at the CDF and histogram of EFs derived from in-situ measurements, Gamma and Weibull distributions are close to CDF and histogram of the in-situ EFs. In addition to CDF and histograms given in Figure 3.19, goodness-of-fit statistics and goodness-of-fit criteria for dust EFs derived from in-situ measurements are also calculated and given in Table 3.22.
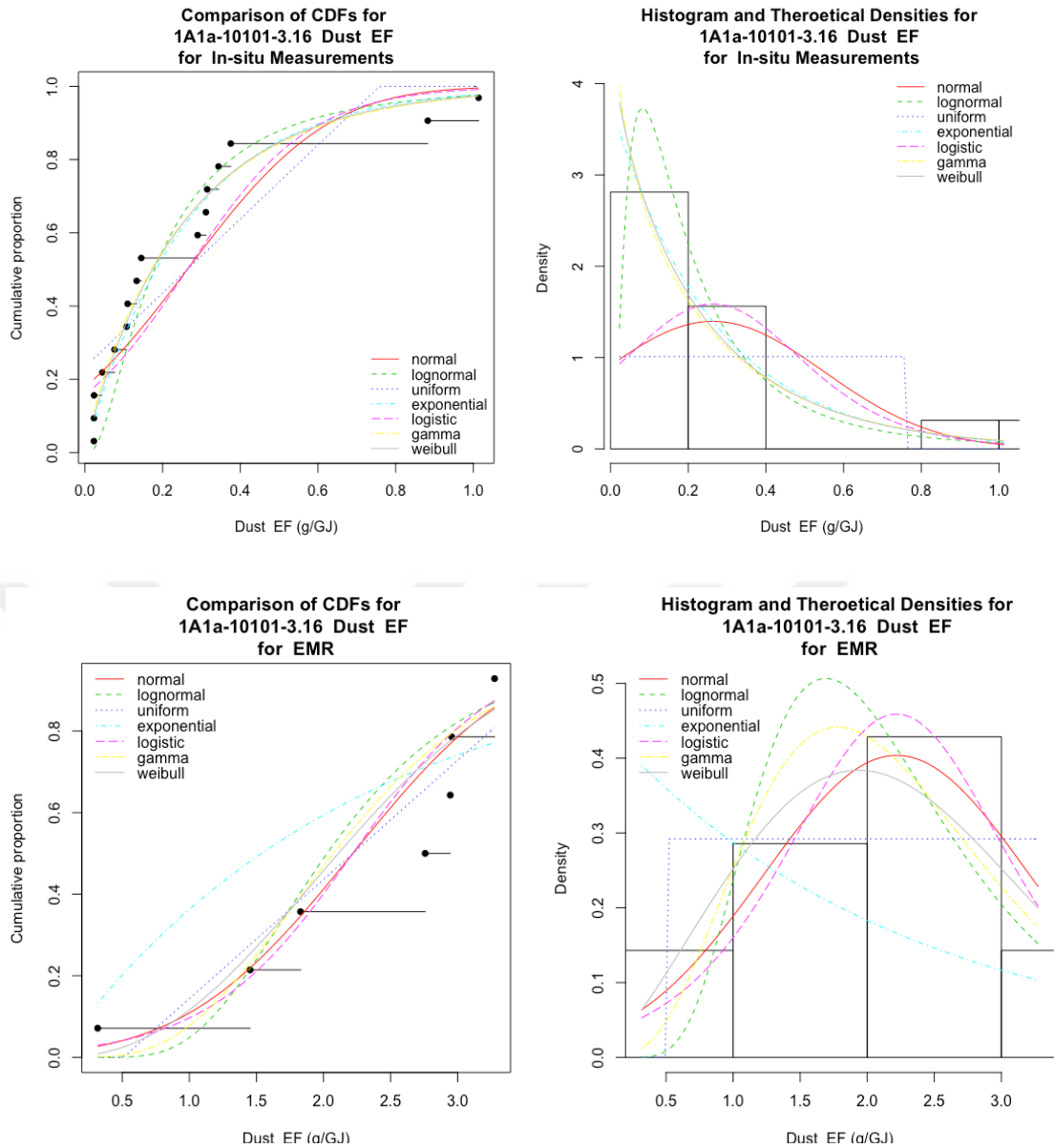
Figure 3.19 : Distribution fitting comparisons of dust EF on CDF and Histogram for both in-situ measurements and EMRs of "1.A.1.a– 10101–3.16".

Critical value of Kolmogorov-Smirnov statistic is 0.213, as it is given in Table 2.9. Lowest Kolmogorov-Smirnov statistic is in Gamma Distribution which is also lowest in Cramer-von Mises and Anderson-Darling statistics. Finally, best fitting distribution is selected as Gamma distribution for in-situ dust EFs for "1.A.1.a–1010-3.16" SNAP/NFR category.

Table 3.22 : Goodness-of-fit statistics/criteria for dust EF derived from in-situ measurements of 1.A.1.a – 10101 – 3.16.

Type of distribution	Goodness-of-fit statistics			Goodness-of-fit criteria	
	Kolmogorov-Smirnov statistic	Cramer-von Mises	Anderson-Darling statistic	Akaike's Information Criterion	Bayesian Information Criterion
Normal	0.223	0.226	1.440	9.314	10.859
Lognormal	0.192	0.141	1.646	-2.950	-1.405
Uniform	0.262	0.281	-	-	-
Exponential	0.139	0.060	0.438	-8.667	-7.895
Logistic	0.242	0.221	1.333	7.963	9.509
Gamma	**0.116**	**0.046**	**0.351**	-6.563	-5.018
Weibull	0.120	0.048	0.364	-6.760	-5.215

* Bold values indicate lowest values.

Since the number of data points is not sufficient, goodness-of-fit statistics/criteria are not calculated for EMR dust EFs of "1.A.1.a–10101–3.16". After assigning best fitting parametric distribution, Monte Carlo simulation is applied as in Section 2.2.4.4 and Bootstrap method is applied as in Section 2.2.4.5. Then, average EF and confidence intervals are calculated for in-situ EFs, and results are given in Table 3.23.

Table 3.23 : Uncertainty analysis results for dust EF of "1.A.1.a–10101–3.16" and comparisons with other studies.

	In-situ measurements	EMEP [54]	EPA [193]
Fitted distribution type	Gamma		between
Mean	0.26 g/GJ	10.2	17.3 [3]
95% CI (Lower, Upper) as g/GJ	0.14-0.41	3.4-30.6	and
% Uncertainty (Lower, Upper)	46-58	67-200	41.7[4]
First parameter	0.798 [1]		g/GJ
Second parameter	0.33 [2]		

[1] mean of ln(x) for lognormal parametric probability distribution function
[2] standard deviation of ln(x) for lognormal parametric probability distribution function
[3] for condensable PM, controlled with electrostatic precipitator in combustion of lignite with atmospheric fluidized bed combustion technology (circulating bed, SCC : 10100317) or bubbling bed (SCC : 10100318)
[4] for filterable PM, controlled with electrostatic precipitator in combustion of lignite with atmospheric fluidized bed combustion technology (circulating bed, SCC : 10100317) or bubbling bed (SCC : 10100318)

In the plant, electrostatic filter is used as dust abatement technology with more than 95% abatement efficiency. Therefore, country-specific EF, which is 0.26 g/GJ, is very low compared to EMEP [54] (10.2 g/GJ) and EPA [193] (minimum 17.3 g/GJ). Furthermore, the EF generated from in-situ measurements is quite lower than the lower limit of the EMEP CI. Since most of the points fall into the 50% CI range in probability

band of in-situ measurements given in Figure 3.20, Gamma distribution is appropriate for EFs derived from in-situ EFs.
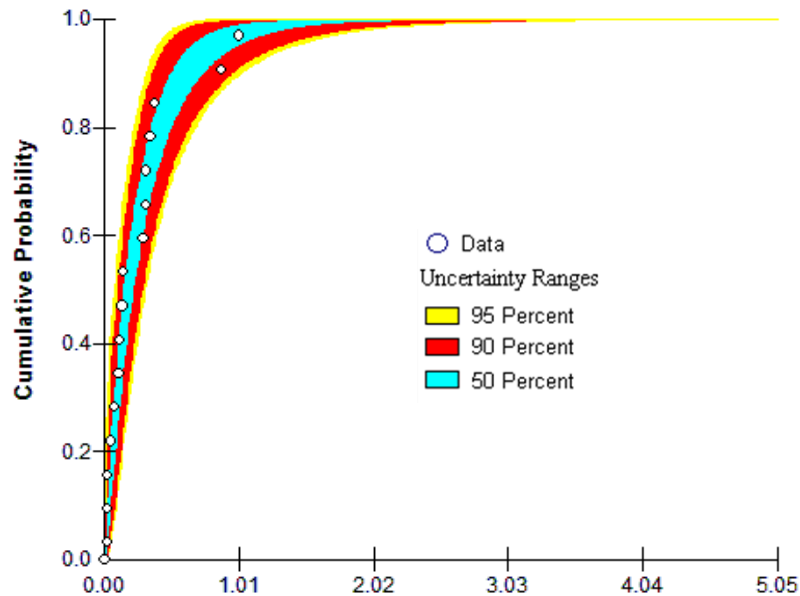

Figure 3.20 : Probability band of dust EFs for "1A1a-10101-3.16" as cumulative distribution of Gamma distribution fitted to dust EFs derived from in-situ measurements.

Consequently, country specific dust EF is 0.26 g/GJ for "1.A.1.a–10101-3.16" SNAP/NFR category, with 95% lower CI as 0.14 g/GJ and upper CI as 0.41 g/GJ.

CO

Summary statistics of CO EFs for "1.A.1.a–10101–3.16" SNAP/NFR category are given in Table 3.24 for EFs derived from both in-situ and EMR EFs. CO emissions were measured as zero in all 16 in-situ measurements. When min, max and median of the EFs derived from EMR are considered in Table 3.24, it is clear that variability is large. The large Cv, as 81%, also proves large variability.

In Figure 3.21, EFs are not distributed homogeneously in the CDF of EMR EFs, they show a clustered distribution. 35% of EFs are less than 5 g/GJ, where 30% of EFs are larger than 42 g/GJ. When the EFs from EMRs are examined, it is seen that each clustered data represents the measurements taken from different stacks of the plant, which also contributes to large variability in EMR EFs. There is positive but low skewness which indicates low asymmetry in the EFs derived from EMRs, where there is negative and relatively large kurtosis which indicates the peakedness of the distribution.

Table 3.24 : Summary statistics of CO EFs derived from both in-situ measurements and EMRs for "1.A.1.a–10101–3.16".

	In-situ Measurements	EMR
Number of data points	16	10
Minimum	0	0.14
Maximum	0	44.7
Median	0	24.5
Variance [1]	0	297.6
Standard Deviation [2]	0	17.25
Cv (%) [3]	0	81
Skewness [4]	0	0.08
Kurtosis [5]	0	-1.8

[1] According to equation 2.12
[2] According to equation 2.13
[3] According to equation 2.14
[4] According to equation 2.15
[5] According to equation 2.16

According to Figure 3.21, looking at the CDF and histogram of EFs derived from EMRs, lognormal and gamma distributions are close to CDF and histogram of the EFs derived from EMRs. However, they are not totally fit to the points (EFs) because there are diffuse clustered data points. In addition to CDF and histograms given in Figure 3.21, goodness-of-fit statistics and goodness-of-fit criteria for CO EFs derived EMRs were also calculated and given in Table 3.25.
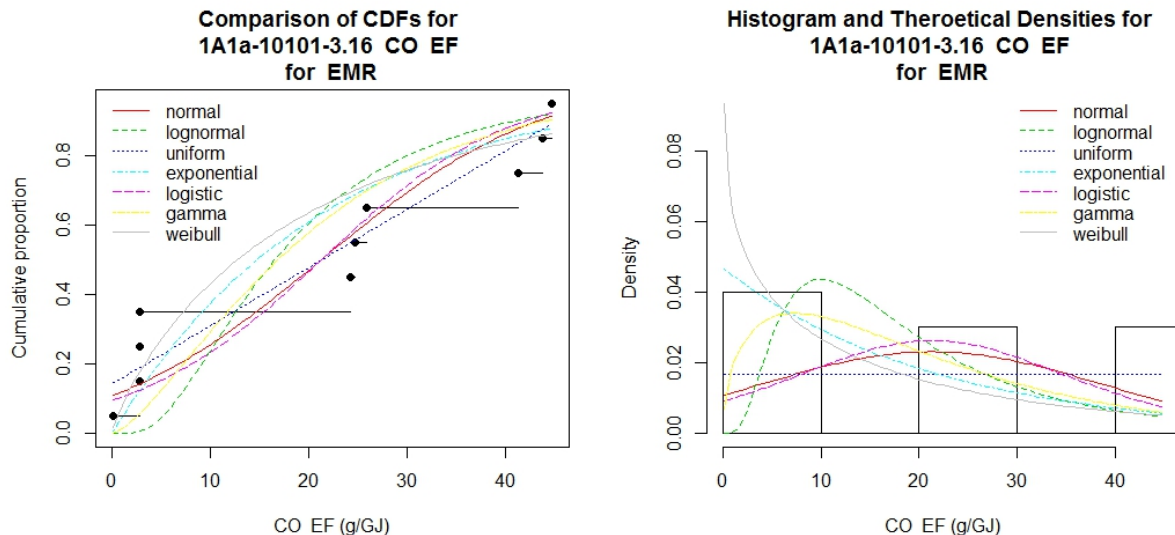
Figure 3.21 : Distribution fitting comparisons of CO EFs on CDF and Histogram for EFs derived from EMRs of "1.A.1.a – 10101 – 3.16".

Table 3.25 : Goodness-of-fit statistics/criteria for CO EF derived from EMRs of "1.A.1.a – 10101 – 3.16".

Type of distribution	Goodness-of-fit statistics			Goodness-of-fit criteria	
	Kolmogorov-Smirnov statistic	Cramer-von Mises	Anderson-Darling statistic	Akaike's Information Criterion	Bayesian Information Criterion
Normal	0.26	0.10	0.71	89.34	89.94
Lognormal	0.39	0.34	7.38	130.53	131.14
Uniform	**0.21**	**0.07**	**0.50**	85.81	86.41
Exponential	0.28	0.17	1.13	**83.20**	**83.50**
Logistic	0.28	0.12	0.85	90.76	91.37
Gamma	0.34	0.23	2.20	89.45	90.06
Weibull	0.29	0.15	0.85	84.75	85.35

* Bold values indicate lowest values.

Critical value of Kolmogorov-Smirnov statistic is 0.213, as it is given in Table 3.25. Kolmogorov-Smirnov statistic of entire of the distributions are more than critical value (0.213), except Uniform distribution. Other goodness-of-fit statistics are also lowest for Uniform distribution. Goodness-of-fit criteria are not lowest in Uniform distribution; however, they are close to minimum. Finally, most appropriate parametric probability distribution is selected as Uniform distribution. After assigning best fitting parametric distribution, Monte Carlo simulation is applied as in Section 2.2.4.4 and Bootstrap method is applied as in Section 2.2.4.5. Then, average EF and confidence intervals are calculated for EMR EFs and results are given in Table 3.26.

Table 3.26 : Uncertainty analysis results for CO EF of 1.A.1.a – 10101 – 3.16 and comparisons with other studies.

	In-situ measurements	EMR	EMEP [54]	EPA [193]
Fitted distribution type	Uniform	Uniform		
Mean	0	21.2 g/GJ	13 g/GJ	
95% CI (Lower, Upper) as g/GJ	0-0	10.5–32.8	0.1-26	8.12 [3]
% Uncertainty (Lower, Upper)	-	50-55	99-100	g/GJ
First parameter	-	-10.1 [1]		
Second parameter	-	52.8 [2]		

[1] minimum value (a) for Uniform parametric probability distribution function
[2] maximum value (b) for Uniform parametric probability distribution function
[3] for uncontrolled combustion of lignite with atmospheric fluidized bed combustion technology (SCC is 10100316)

It is seen that, the EF calculated from EMRs is significantly larger than EMEP and EPA EFs. However, the EF derived from EMR is within the EMEP confidence interval limits. In-situ EF is 0 g/GJ, which is not compatible with other studies.

One important indication that a distribution is properly fitted is that almost all points on the probability band are within 50% CI range [219]. It is seen that EFs derived from EMR are beyond the 50% CI limits. When the low reliability of emission measurements in EMRs (as discussed in Section 2.2.1) are also considered, it is recommended to use those EFs cautiously. Consequently, CO EF is 21.2 g/GJ for "1.A.1.a–10101-3.16" SNAP/NFR category, with 95% lower CI as 10.5 g/GJ and upper CI as 32.8 g/GJ.
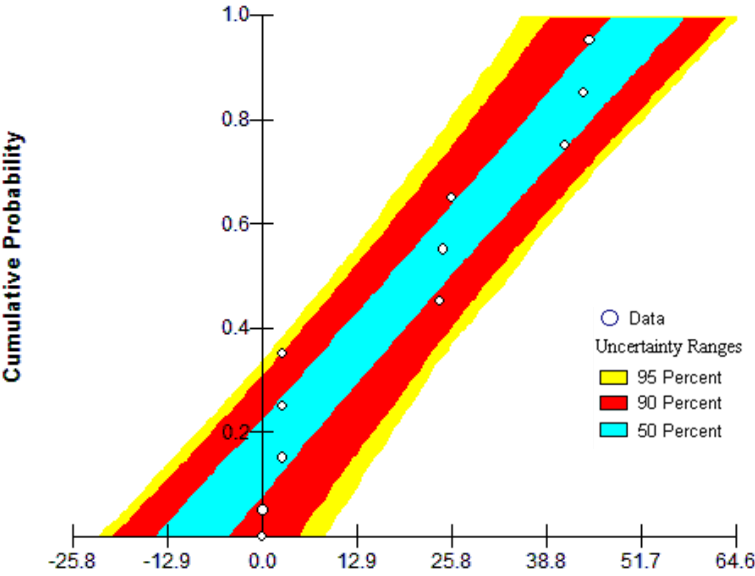
Figure 3.22 : Probability band of CO EFs for "1A1a-10101-3.16" as cumulative distribution of uniform distribution fitted to CO EFs derived EMRs.

SO$_2$

Summary statistics of SO$_2$ EFs for "1.A.1.a–10101–3.16" SNAP/NFR category are given in Table 3.27 for EFs derived from EMRs. For this SNAP/NFR category, SO$_2$ emissions were not detected in in-situ measurements, therefore they are zero. However, seven SO$_2$ emissions are available in EMRs.

When min, max and median of the EFs derived from EMR are considered in Table 3.27, it is clear that variability is large. The high coefficient of variation, as 1403%, also proves large variability. The low number of data points is also effective in high Cv.

Table 3.27 : Summary statistics of SO_2 EFs derived from both in-situ measurements and EMRs for "1.A.1.a–10101–3.16".

	In-situ Measurements	EMR
Number of data points	16	7
Minimum (g/GJ)	0	0.61
Maximum (g/GJ)	0	2.44
Median (g/GJ)	0	1.2
Variance [1]	0	330.6
Standard Deviation [2]	0	17.25
Coefficient of variation (%) [3]	0	1403
Skewness [4]	0	0.08
Kurtosis [5]	0	-1.8

[1] According to equation 2.12
[2] According to equation 2.13
[3] According to equation 2.14
[4] According to equation 2.15
[5] According to equation 2.16

In Figure 3.23, EFs are distributed heterogeneously in the CDF of EFs derived from EMRs. When the EMR data was examined, it is seen that each clustered data represents the measurements taken from different stacks of the plant.
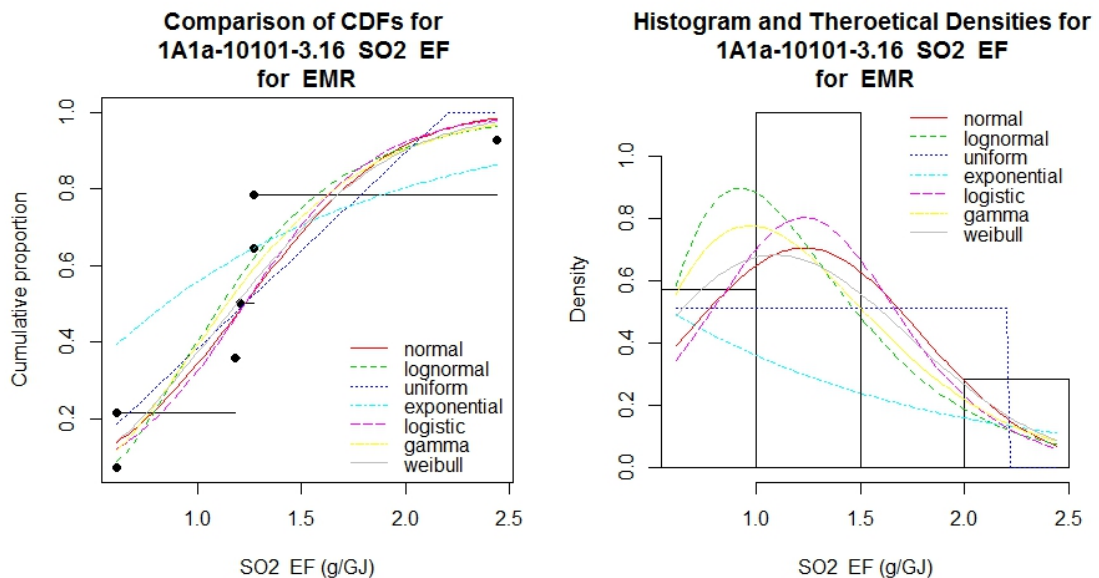
Figure 3.23 : Distribution fitting comparisons of SO_2 EF on CDF and Histogram for both in-situ measurements and EMRs of "1.A.1.a – 10101 – 3.16".

Generally none of the distributions provide a perfect fit on the CDF of EMR EFs. However, the histogram in Figure 3.23 shows that the lognormal distribution is most favourable compared to the others. Table 3.28 is created in order to quantitatively support this qualitative interpretation and includes goodness-of-fit criteria for SO_2 EFs derived from EMRs. Since number of data points is not sufficient, goodness-of-fit

statistics cannot be calculated. In Table 3.28, lognormal distribution is found to be the lowest value in terms of goodness-of-fit criteria.

Table 3.28 : Goodness-of-fit statistics/criteria for SO_2 EF derived from EMRs of "1.A.1.a – 10101 – 3.16".

Type of distribution	Goodness-of-fit criteria	
	Akaike's Information Criterion	Bayesian Information Criterion
Normal	15.85	15.74
Lognormal	**13.93**	**13.82**
Uniform	-	-
Exponential	18.89	18.83
Logistic	15.58	15.47
Gamma	14.24	14.13
Weibull	14.97	14.86

* Bold values indicate lowest values.

After assigning best fitting parametric distribution, Monte Carlo simulation is applied as in Section 2.2.4.4 and Bootstrap method is applied as in 2.2.4.5. Then average EF and confidence intervals are calculated for EMR EFs and given in Table 3.29.

Table 3.29 : Uncertainty analysis results for SO_2 EF of "1.A.1.a – 10101 – 3.10" and comparisons with other studies.

	EMR	EMEP [54]	EPA [193]
Fitted distribution type	Lognormal		
Mean (g/GJ)	1.21	1680	
95% CI (Lower, Upper) as g/GJ	0.85-1.63	330-5000	896 [3]
% Uncertainty (Lower, Upper)	30-35	80-198	g/GJ
First parameter	0.11 [1]		
Second parameter	0.43 [2]		

[1] mean of lnx for Lognormal parametric probability distribution function
[2] standard deviation of lnx for Lognormal parametric probability distribution function
[3] as SO_x, for uncontrolled external combustion of lignite for electricity generation (SCC is 10100301, 10100302, 10100303, 10100304, 10100306, 10100316 and 10100317)

It is seen that the EFs derived from EMRs are pretty lower than the EMEP and EPA EFs. Adding limestone (for combusting jointly with the coal) is used as the abatement technology for SO_2 and NO_x emissions. Therefore, SO_2 EF is expected to be low.

Lower and upper CI range of SO_2 EF is given on a probability band in Figure 3.24. It is seen that EFs derived from EMR are even beyond the 95% CI limits. When the low reliability of emission measurements in EMRs (as discussed in Section 2.2.1) and low number of data points used in the calculation of this EF are considered, it is

recommended to use those EFs cautiously. Consequently, SO_2 EF is 1.21 g/GJ for "1.A.1.a–10101-3.16" SNAP/NFR category, with 95% lower CI as 0.85 g/GJ and upper CI as 1.63 g/GJ.
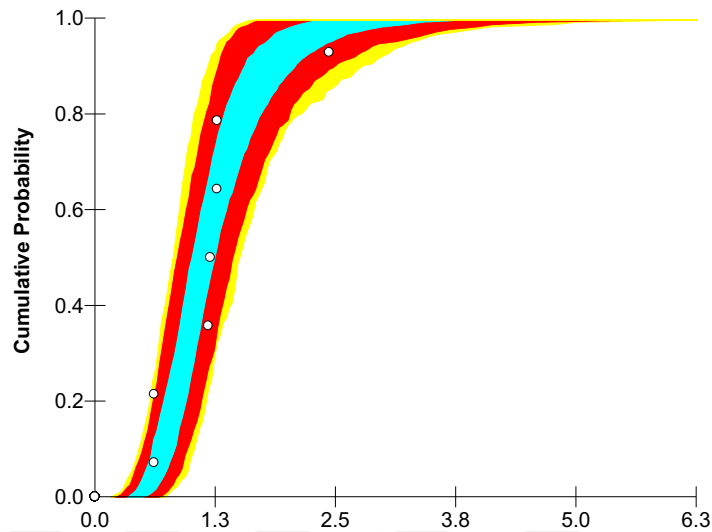

Figure 3.24 : Probability band of SO_2 EFs for "1A1a-10101-3.16" as cumulative distribution of lognormal distribution fitted to SO_2 EFs derived EMRs.

NO

Summary statistics of NO EFs for "1.A.1.a–10101–3.16" SNAP/NFR category are given in Table 3.30 for EFs derived from both in-situ measurements and EMRs.

Table 3.30 : Summary statistics for NO EFs derived from both in-situ measurements and EMRs for "1.A.1.a–10101–3.16".

	In-situ Measurements	EMR
Number of data points	16	10
Minimum	28.8	0.3
Maximum	35	28.3
Median	33	14.6
Variance [1]	2.6	109
Standard Deviation [2]	1.61	9.9
Cv (%) [3]	4.9	70.2
Skewness [4]	-0.88	0.21
Kurtosis [5]	0.72	-1.53

[1] According to equation 2.12
[2] According to equation 2.13
[3] According to equation 2.14
[4] According to equation 2.15
[5] According to equation 2.16

Variance and standard deviation calculated from EMR EFs are greater than those derived from in-situ measurements. Furthermore, Cv value, which represents the

variability in the EFs as a percentage, is pretty large (70.2%) in EMR EFs where it is pretty low (4.9%) in EFs derived from in-situ measurements.

Consequently, variability of EMR are larger than in-situ EFs. However, one outlier value in the EMR EFs, which is 0.3 g/GJ, increases variability in the EMR EFs, as it is clear on the CDF of EFs derived from EMRs which is given in Figure 3.25. Additionally, the fact that EFs from EMRs are generally clustered, as seen in CDF of EMR EFs in Figure 3.25, variability of EMRs is also large.
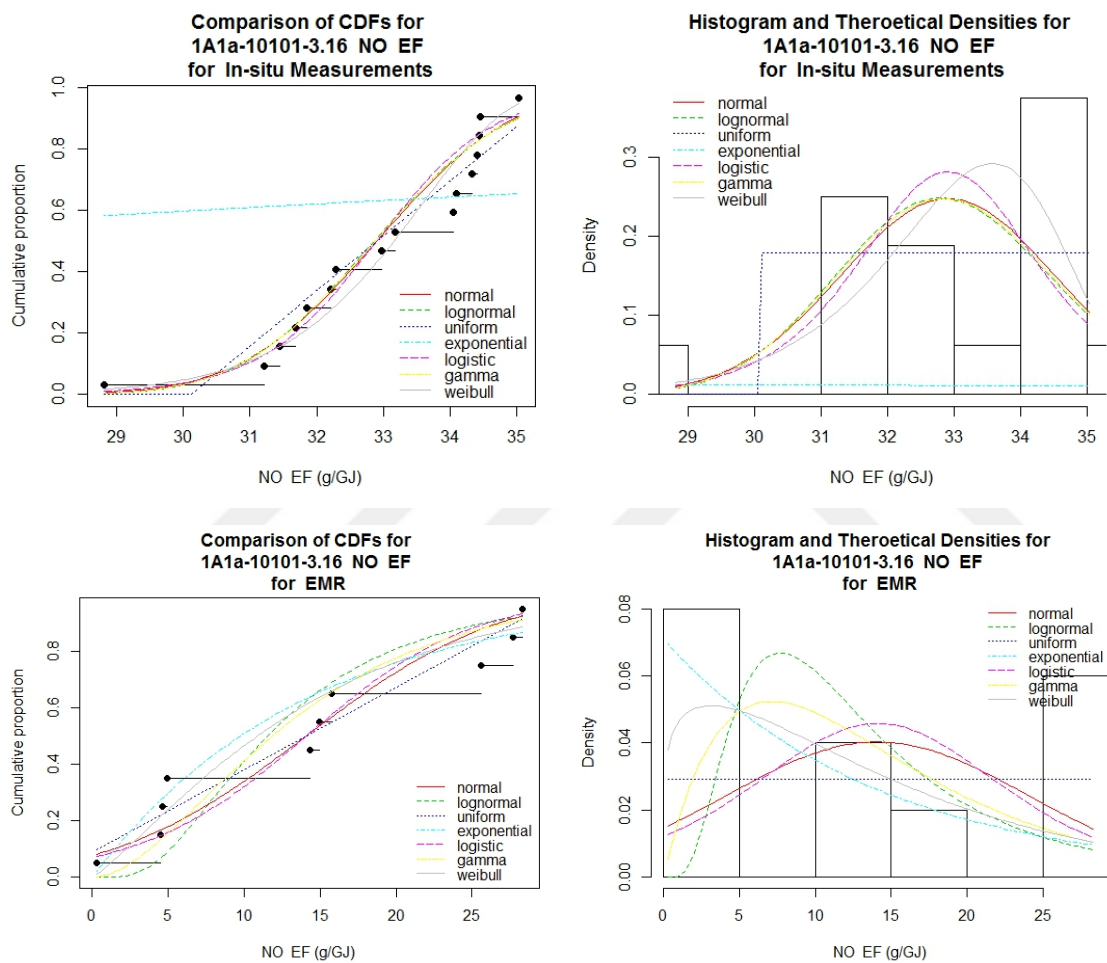
Figure 3.25 : Distribution fitting comparisons of NO EF on CDF and Histogram for both in-situ measurements and EMRs of "1.A.1.a–10101–3.16".

CDFs and histograms are given in the Figure 3.25 with possible fitting options. According to Figure 3.25, looking at the CDF and histogram of EFs derived from in-situ measurements, none of the distribution is best due to high variability. Weibull can be considered as the closest distribution to in-situ EFs.

In addition to CDF and histograms given in Figure 3.25, goodness-of-fit statistics and goodness-of-fit criteria for NO EFs derived from in-situ measurements were also

calculated and given in Table 3.31, in order to determine best fitting parametric probability distribution function for our data.

Table 3.31 : Goodness-of-fit statistics/criteria for NO EFs derived from in-situ measurements of "1.A.1.a–10101–3.16".

Type of distribution	Goodness-of-fit statistics			Goodness-of-fit criteria	
	Kolmogorov-Smirnov statistic	Cramer-von Mises	Anderson-Darling statistic	Akaike's Information Criterion	Bayesian Information Criterion
Normal	0.198	**0.078**	0.546	64.715	66.260
Lognormal	0.202	0.082	0.589	65.416	66.961
Uniform	**0.160**	0.078	-	-	-
Exponential	0.583	1.457	6.675	145.796	146.569
Logistic	0.221	0.098	0.618	65.157	66.703
Gamma	0.200	0.080	0.573	65.166	66.711
Weibull	0.190	0.089	**0.517**	**62.126**	**63.671**

* Bold values indicate lowest values.

In Table 3.31, Weibull distribution appears to be one of the good fitting distributions. Consequently, Weibull distribution is fitted to EFs derived from in-situ measurements since it has acceptable values for most of the goodness-of-fit statistics and criteria. Goodness-of-fit statistics and criteria of EFs derived from EMRs are given in Attachment F. Uniform distribution is selected as best fitting parametric distribution for EMR EFs. Average EF and confidence intervals are calculated for each of in-situ EFs and EMR EFs, and given in Table 3.32.

Table 3.32 : Uncertainty analysis results for NO EF of "1.A.1.a–10101–3.16" and comparisons with other studies.

	In-situ measurements	EMR	EMEP [54]	EPA [193]
Fitted distribution type	Weibull	Uniform		
Mean	32.8 g/GJ	14 g/GJ	60 [5] g/GJ	
95% CI (Lower, Upper) as g/GJ	31.9-33.7	7.5-20.6	35-85.2	195 [6]
Uncertainty (Lower, Upper)	2-3	46-47	42-42	g/GJ
First parameter	33.6 [1]	-3.9 [3]		
Second parameter	23.3 [2]	32.1 [4]		

[1] scale parameter (k) for Weibull parametric probability distribution function
[2] shape parameter (c) for Weibull parametric probability distribution function
[3] minimum value (a) for Uniform parametric probability distribution function
[4] maximum value (b) for Uniform parametric probability distribution function
[5] as NO_x
[6] as NO_x, for uncontrolled external combustion of lignite with atmospheric fluidized bed technology (SCC: 10100316 and 10100317)

It is seen that in-situ EF is more than two times of EF derived from EMRs. Country-specific NO EF is calculated as 32.8 g/GJ, where it is 14 g/GJ for EF derived from

EMR. NO EFs are not supplied by EMEP [54] and EPA [193] therefore, NO_x EFs are given for comparison.

Since almost all EFs of in-situ measurements fall into the 50% CI range in Figure 3.26, which is considered a criterion of goodness-of-fit [219], Weibull distribution is appropriate for EFs derived from in-situ EFs. Also, it is seen that, Uniform distribution not fitted good in EFs derived from EMR, since they are mostly beyond the 50% CI range. Furthermore, CI range is pretty large in EFs derived from EMR (lower bound is 46% and upper bound is 47%) when compared to in-situ EF CI range (lower bound is 2% and upper bound is 3%).
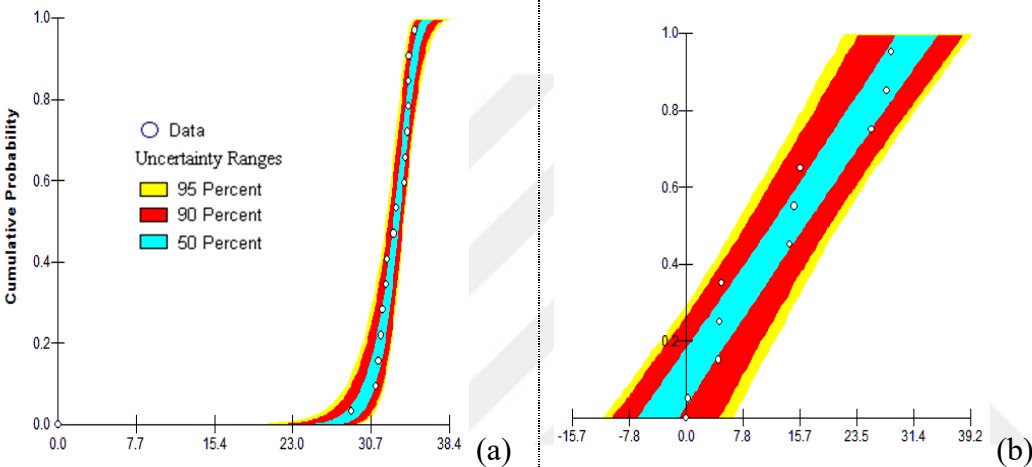
Figure 3.26 : Probability band of NO EFs for "1A1a-10101-3.16" as cumulative distribution of (a)Weibull distribution fitted to NO EFs derived from in-situ measurements (b)Uniform distribution fitted to NO EFs derived from EMRs.

NO$_2$

Summary statistics of NO_2 EFs for "1.A.1.a–10101–3.16" SNAP/NFR category are given in Table 3.33 for EFs derived from both in-situ measurements and EMRs. When min, max and median of the EFs derived from in-situ measurements and those derived from EMR are compared in Table 3.33, it is clear that NO_2 EFs obtained from in-situ measurements are more than two times than calculated from EMRs. Variance and standard deviation calculated from EFs derived from EMRs are greater than those derived from in-situ measurements. Furthermore, Cv value, which represents the variability in the EFs as a percentage, is pretty large (68%) in EMR EFs where it is pretty low (5%) in EFs derived from in-situ measurements.

Table 3.33 : Summary statistics for NO_2 EFs derived from both in-situ measurements and EMRs for "1.A.1.a–10101–3.16".

	In-situ Measurements	EMR
Number of data points	16	10
Minimum	46.3	0.11
Maximum	56.6	43.6
Median	53.1	23.3
Variance [1]	7.5	253
Standard Deviation [2]	2.65	15.1
Cv (%) [3]	5	68
Skewness [4]	-0.85	0.15
Kurtosis [5]	0.76	-1.5

[1] According to equation 2.12
[2] According to equation 2.13
[3] According to equation 2.14
[4] According to equation 2.15
[5] According to equation 2.16

Consequently, variability of EMR EFs are larger than in-situ EFs. However, one outlier value in the EMR EFs, which is 0.11 g/GJ, increases variability in the EMR EFs, as it is clear on the CDF of EFs derived from EMRs which is given in Figure 3.27. Additionally, the fact that EFs from EMRs are generally clustered, as visualized in CDF of EMR EFs in Figure 3.27, variability increases.

CDFs and histograms are given in the Figure 3.27 with possible fitting options. According to Figure 3.27, looking at the CDF and histogram of EFs derived from in-situ measurements, Weibull is the best fitting distribution to in-situ EFs. In addition to CDF and histograms given in Figure 3.27, goodness-of-fit statistics and goodness-of-fit criteria for NO_2 EFs derived from in-situ measurements were also calculated and given in Table 3.34, in order to determine best fitting parametric probability distribution function for our data. Even in this table, the Weibull distribution appears to be the best fitting distribution since it has the lowest values for most of goodness-of-fit statistics and criteria.

Goodness-of-fit statistics and criteria of EFs derived from EMRs are given in Attachment F. Uniform distribution is selected as best fitting parametric distribution for EMR EFs.
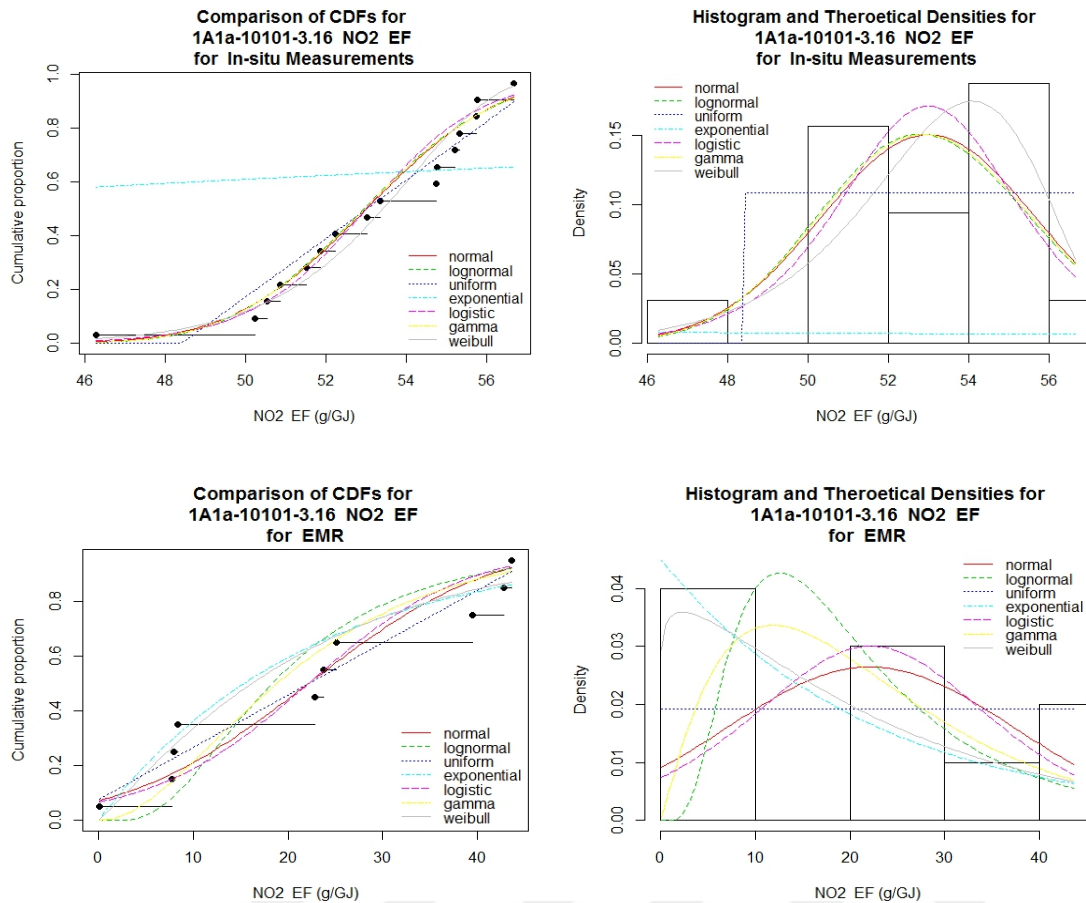
Figure 3.27 : Distribution fitting comparisons of NO$_2$ EF on CDF and Histogram for both in-situ measurements and EMRs of "1.A.1.a–10101–3.16".

After assigning best fitting parametric distribution, Monte Carlo simulation is applied as in Section 2.2.4.4 and Bootstrap method is applied as in 2.2.4.5. Then average EF and confidence intervals are calculated for each of in-situ EFs and EMR EFs and given in Table 3.35.

Table 3.34 : Goodness-of-fit statistics/criteria for NO$_2$ EF derived from in-situ measurements of "1.A.1.a–10101–3.16"

Type of distribution	Goodness-of-fit statistics			Goodness-of-fit criteria	
	Kolmogorov-Smirnov statistic	Cramer-von Mises	Anderson-Darling statistic	Akaike's Information Criterion	Bayesian Information Criterion
Normal	0.180	**0.055**	0.407	80.638	82.183
Lognormal	0.185	0.059	0.453	81.336	82.881
Uniform	**0.138**	0.060			
Exponential	0.582	1.452	6.656	161.051	161.824
Logistic	0.203	0.071	0.459	80.993	82.538
Gamma	0.183	0.057	0.437	81.086	82.631
Weibull	0.164	0.058	**0.339**	**78.307**	**79.852**

* Bold values indicate lowest values.

138

It is seen that the EF derived from in-situ measurements is more than two times of EF derived from EMRs. Country-specific NO_2 EF is calculated as 52.9 g/GJ, where it is 22 g/GJ for EF derived from EMR. NO_2 EFs are not supplied by EMEP [54] or EPA [193], therefore there is no room for comparison. In the plant that in-situ measurements are conducted, limestone is combusted jointly with the coal as an abatement procedure of SO_2 and NO_x emissions. Therefore, NO_2 EF is expected to be low.

Table 3.35 : Uncertainty analysis results for NO_2 EF of "1.A.1.a–10101–3.16" and comparisons with other studies.

	In-situ Measurements	EMR
Fitted distribution type	Weibull	Uniform
Mean (g/GJ)	52.9	22
95% CI (Lower, Upper) as g/GJ	51.4-54.3	12.7-32.3
% Uncertainty (Lower, Upper)	3-3	42-47
First parameter	54.2 [1]	-5.3 [3]
Second parameter	23 [2]	49.7 [4]

[1] scale parameter (k) for Weibull parametric probability distribution function
[2] shape parameter (c) for Weibull parametric probability distribution function
[3] minimum value (a) for Uniform parametric probability distribution function
[4] maximum value (b) for Uniform parametric probability distribution function

Since almost all in-situ EFs fall into the 50% CI range in probability band given in Figure 3.28, which is considered a criterion of goodness-of-fit [219], Weibull distribution is appropriate for EFs derived from in-situ EFs.
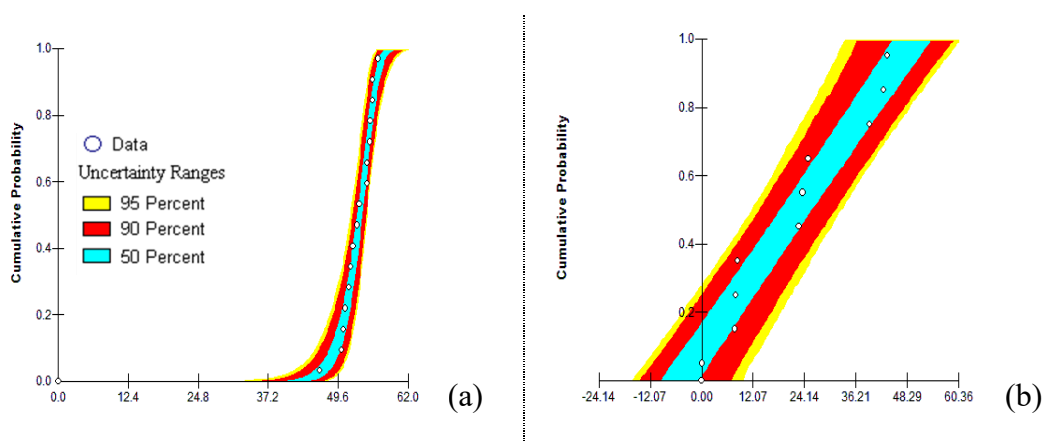
Figure 3.28 : Probability band of NO_2 EFs for "1A1a-10101-3.10" as cumulative distribution of (a)Weibull distribution fitted to NO_2 EFs derived from in-situ measurements. (b)Uniform distribution fitted to NO_2 EFs derived from EMRs.

Also, it is seen that, Uniform distribution is not fitted good in EMR EFs, since they are mostly beyond the 50% CI range. Furthermore, CI range is pretty large in EFs derived from EMR (lower bound is 42% and upper bound is 47%) when compared to in-situ EFs where both of lower and upper bounds are 3%. Consequently, country specific

NO$_2$ EF is accepted as 52.9 g/GJ for "1.A.1.a–1010-3.16" SNAP/NFR category, with 95% lower CI as 51.4 g/GJ and upper CI as 54.3 g/GJ.

NO$_x$

NOx EF is calculated as the sum of NO and NO$_2$ emissions. However, since the uncertainty levels of NO and NO$_2$ EFs are different, the formulas given in equation 2.1a-2.1d were applied in order to calculate the total uncertainty of NO$_x$ EF. NOx EF of "1.A.1.a–10101–3.16" SNAP/NFR category and comparisons with other studies are given in Table 3.36.

Table 3.36 : NO$_x$ EF of "1.A.1.a–10101–3.16" and comparisons with other studies.

	In-situ Measurements	EMR	EMEP [54]	EPA [193]
NOx EF (NO+NO$_2$) as g/GJ	85.7	36	60	
95% CI (Lower, Upper) as g/GJ	83.95-88.48	24.7-48.2	35-85.2	195 [1]
% Uncertainty (Lower, Upper)	2-3.2%	31.5-34%	42-131%	g/GJ
NO/NO$_2$ share	0.62	0.64		

[1] as NO$_x$, for uncontrolled external combustion of lignite with atmospheric fluidized bed technology (SCC is 10100316 and 10100317)

It is seen that the EFs derived from in-situ measurements (85.7 g/GJ) and from EMRs (36 g/GJ) are compatible with EMEP EF CI range, which is 24.7 g/GJ lower and 48.2 upper g/GJ range, however they are less than half the EPA EF (195 g/GJ). EPA EF is valid for uncontrolled conditions, however, limestone is added to the system for combusting jointly with the coal, as an abatement technology for SO$_2$ and NO$_x$ emissions in the plant that we conducted in-situ measurements. Therefore, NO$_x$ EF is expected to be low. Consequently, country specific NO$_x$ EF is calculated as 85.7 g/GJ which is almost two times of EF calculated from EMRs.

3.2.3 Coal combusting large wet and dry bottom boilers

Brown coal or lignite combustion plants with a capacity range between 50 and 300 MW (SNAP/NFR code is 1.A.1.a–10102–3.10), and with wet and dry bottom boilers as the combustion technology for production of public power is investigated in this part of study.

In Marmara region there is one plant falling under this SNAP/NFR category. Therefore in-situ measurements were conducted in only this plant within the context of KAMAG project [194]. Consequently, 16 in-situ measurements from one plant is used in the

calculation of country-specific EF for this SNAP/NFR code. There were no EMR available for this plant.

Dust

Summary statistics of dust EFs for "1.A.1.a–10102–3.10" SNAP/NFR category are given in Table 3.37 for EFs derived from only in-situ measurements, because EMR was not available for this plant. Standard deviation, variance and Cv are calculated large in in-situ measurements, which indicate large variability between EFs. Furthermore, Cv is 116% which is pretty large and indicates large variability between measurements. There is positive skewness and kurtosis in the in-situ EFs.

Table 3.37 : Summary statistics of dust EFs derived from in-situ measurements for "1.A.1.a–10102–3.10".

	In-situ Measurements
Number of data points	16
Minimum	0.13
Maximum	6
Median	0.6
Variance [1]	2.38
Standard Deviation [2]	1.54
Cv (%) [3]	116
Skewness [4]	2
Kurtosis [5]	4.3

[1] According to equation 2.12
[2] According to equation 2.13
[3] According to equation 2.14
[4] According to equation 2.15
[5] According to equation 2.16

Large variability is heavily affected from outliers. In Figure 3.29, comparison of CDFs and histograms with possible parametric distribution fitting options are given. According to Figure 3.29, looking at the CDF, it is seen that 90% of EFs are less than 3 g/GJ, however, there is one EF which is more than 6 g/GJ, which can be treated as outlier. Variability contribution of one outlier value in the CDF should be considered when evaluating large variability.

There is asymmetry in the histogram given in Figure 3.29, therefore, the skewness value for in-situ measurements in Table 3.37 is large. Due to a large peak in the histogram given in Figure 3.29, the kurtosis value is high in Table 3.37.

According to Figure 3.29, looking at the CDF and histogram of EFs derived from in-situ measurements, Gamma and lognormal distributions are close to CDF and

histogram of the in-situ EFs. In addition to CDF and histograms given in Figure 3.29, goodness-of-fit statistics and goodness-of-fit criteria for dust EFs derived from in-situ measurements were also calculated in Table 3.38, in order to determine best fitting parametric probability distribution function for our data.
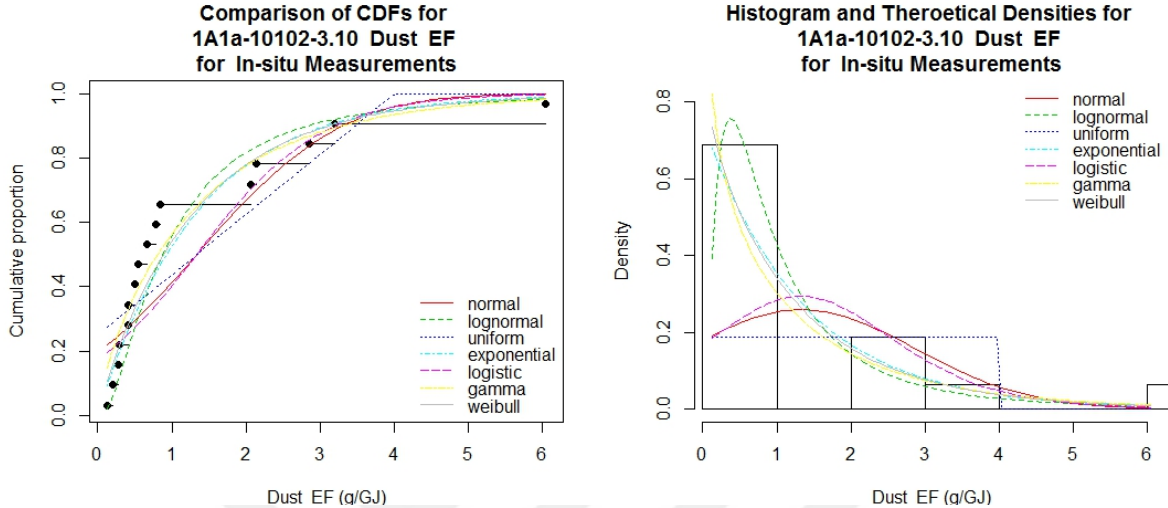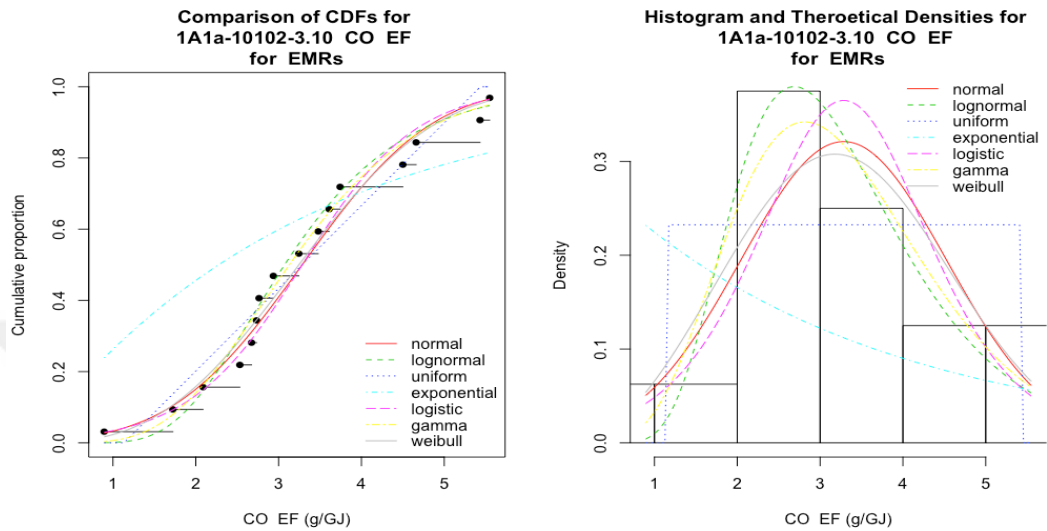

Figure 3.29 : Distribution fitting comparisons of dust EF on CDF and Histogram for in-situ measurements of "1.A.1.a–10102–3.10".

Critical value of Kolmogorov-Smirnov statistic is 0.213, as it is given in Table 2.9. The lowest Kolmogorov-Smirnov statistic is in Logistic distribution. However, logistic distribution is not a good fitting distribution in the histogram of Figure 3.29 although it has lowest Kolmogorov-Smirnov statistic. Uniform distribution has lowest goodness-of-fit criteria, but it doesn't give good results when the number of values within the 0 and 1 g/GJ is large, as in our dataset. However, as it is clear in CDF Figure 3.29, the number of EFs between 0 and 1 g/GJ is large and cannot be disregarded. Gamma distribution doesn't have best values in Table 3.38. Nevertheless, best fitting distribution is selected as Gamma distribution for dust EFs derived from in-situ measurements for "1.A.1.a–10102-3.10" SNAP/NFR category.

After assigning best fitting parametric distribution, Monte Carlo simulation is applied as in Section 2.2.4.4 and Bootstrap method is applied as in Section 2.2.4.5. Then, average EF and confidence intervals are calculated for in-situ EFs, and results are given in Table 3.39.

Table 3.38 : Goodness-of-fit statistics/criteria for dust EF derived from in-situ measurements of "1.A.1.a–10102–3.10".

Type of distribution	Goodness-of-fit statistics			Goodness-of-fit criteria	
	Kolmogorov-Smirnov statistic	Cramer-von Mises	Anderson-Darling statistic	Akaike's Information Criterion	Bayesian Information Criterion
Normal	0.202	0.178	0.936	43.319	44.864
Lognormal	0.279	0.308			
Uniform	0.219	0.130	0.669	**43.241**	**44.013**
Exponential	0.328	0.315	1.632	61.594	63.140
Logistic	**0.175**	**0.096**	0.595	46.079	47.624
Gamma	0.202	0.108	**0.587**	45.162	46.707
Weibull	0.202	0.178	0.936	43.319	44.864

* Bold values indicate lowest values.

The EF calculated from in-situ measurements (1.32 g/GJ) is significantly lower than the EMEP (11.7 g/GJ) and EPA EFs (minimum 17 g/GJ). Besides, it is pretty lower than EPA EFs even though EPA EFs are for controlled conditions. In the plant, electrostatic filter is used as the dust abatement technology with more than 95% abatement efficiency, however country-specific EF, which is 1.32 g/GJ, is very low compared to EMEP [54] (11.7 g/GJ) and EPA [193] (minimum 17 g/GJ).

Table 3.39 : Uncertainty analysis results for dust EF of "1.A.1.a–10102–3.10" and comparisons with other studies.

	In-situ measurements	EMEP [54]	EPA [193]
Fitted distribution type	Gamma		
Mean	1.32 g/GJ	11.7 g/GJ	between
95% CI (Lower, Upper) as g/GJ	0.68–2.27	1.2-117	17 [3] and
Uncertainty (Lower, Upper)	48-110	90-900	100 [4]
First parameter	0.7 [1]		g/GJ
Second parameter	1.9 [2]		

[1] scale parameter (α) for Gamma parametric probability distribution function
[2] shape parameter (β) for Gamma parametric probability distribution function
[3] for condensable PM, fluidized bed combustion technology controlled with electrostatic precipitator or dry limestone injection (SCC 10100316, 10100317 and 10100318)
[4] for filterable PM, fluidized bed combustion technology controlled with electrostatic precipitator or dry limestone injection (SCC 10100316, 10100317 and 10100318)

One important indication that a distribution is properly fitted is that almost all points on the probability band are within 50% CI range [219]. EFs derived from in-situ measurements often remain within the 50% CI limits in Figure 3.30. However, EF is lower than literature (EMEP and EPA).
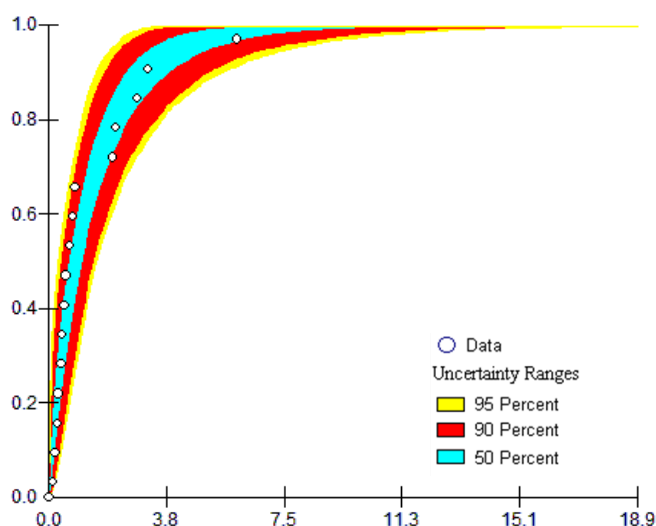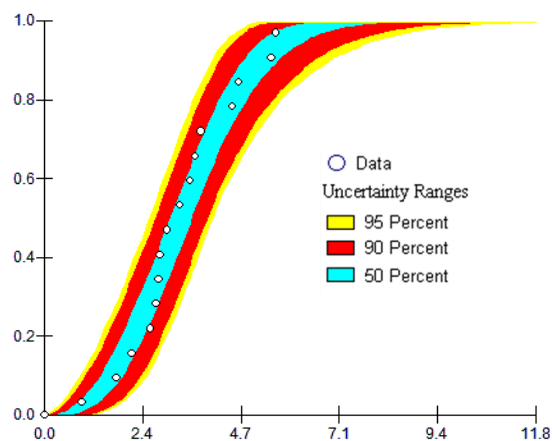
Figure 3.30 : Probability band of dust EFs for "1A1a-10102-3.10" as cumulative distribution of Gamma distribution fitted to dust EFs derived from in-situ measurements.

CO

Summary statistics of CO EFs for "1.A.1.a–10102–3.10" SNAP/NFR category are given in Table 3.40 for EFs derived from in-situ measurements. When min, max and median of the EFs derived from in-situ measurements are investigated in Table 3.40, it is clear that CO EFs are properly distributed between zero and five, with 38% Cv, low variance and standard deviation. Homogeneous distribution of the EFs is also clear on the CDF in Figure 3.31.

Table 3.40 : Summary statistics for CO EFs derived from in-situ measurements for "1.A.1.a–10102–3.10".

	In-situ Measurements
Number of data points	16
Minimum	0.89
Maximum	5.54
Median	3.09
Variance [1]	1.54
Standard Deviation [2]	1.24
Cv (%) [3]	38
Skewness [4]	0.21
Kurtosis [5]	-0.22

[1] According to equation 2.12
[2] According to equation 2.13
[3] According to equation 2.14
[4] According to equation 2.15
[5] According to equation 2.16

According to Figure 3.31, looking at the CDF and histogram of EFs derived from in-situ measurements, Normal, Weibull and Gamma distributions are close to CDF and histogram of the in-situ EFs. Table 3.41 is created in order to quantitatively support this qualitative interpretation and includes goodness-of-fit statistics and goodness-of-fit criteria for CO EFs derived from in-situ measurements.
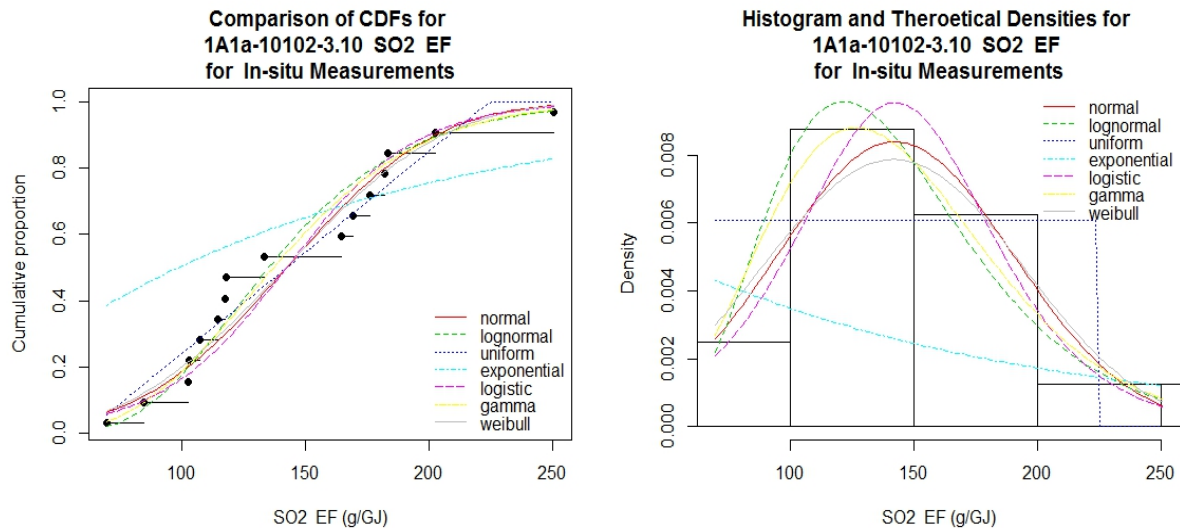

Figure 3.31 : Distribution fitting comparisons of CO EF on CDF and Histogram for in-situ measurements of "1.A.1.a–10102–3.10".

Critical value of Kolmogorov-Smirnov statistic is 0.213, as it is given in Table 2.9. Kolmogorov-Smirnov statistic of entire of the distributions are less than critical value (0.213), except exponential distribution. Minimum Kolmogorov-Smirnov statistic is in Weibull distribution.

Table 3.41 : Goodness-of-fit statistics/criteria for CO EF derived from in-situ measurements of "1.A.1.a–10102–3.10".

Type of distribution	Goodness-of-fit statistics			Goodness-of-fit criteria	
	Kolmogorov-Smirnov statistic	Cramer-von Mises	Anderson-Darling statistic	Akaike's Information Criterion	Bayesian Information Criterion
Normal	0.1104	0.038	0.25	56.34	57.89
Lognormal	0.1107	0.031	0.44	60.22	61.77
Uniform	0.1437	0.067	-	-	-
Exponential	0.3499	0.569	2.84	72.06	72.83
Logistic	0.1245	0.041	0.27	56.98	58.53
Gamma	0.1102	**0.026**	0.26	57.20	58.74
Weibull	**0.1018**	0.033	**0.23**	**56.00**	**57.55**

* Bold values indicate lowest values.

Other goodness-of-fit statistics and criteria are also lowest for Weibull distribution, except Cramer-von Mises statistic. Due to the close CDF and histogram of Weibull distribution to the in-situ EFs in Figure 3.31, and due to lowest goodness-of-fit statistics in Table 3.41, best fitting distribution is selected as the Weibull distribution for CO EFs derived from in-situ measurements.

Table 3.42 : Uncertainty analysis results for CO EF of "1.A.1.a–10102–3.10" and comparisons with other studies.

	In-situ measurements	EMEP [54]	EPA [193]
Fitted distribution type	Weibull		
Mean	3.3 g/GJ	8.7 g/GJ	
95% CI (Lower, Upper) as g/GJ	2.65-3.99	6.72 -60.5	8.12 [3]
Uncertainty (Lower, Upper)	20-21	23-595	g/GJ
First parameter	3.721 [1]		
Second parameter	2.657 [2]		

[1] scale parameter (k) for Weibull parametric probability distribution function
[2] shape parameter (c) for Weibull parametric probability distribution function
[3] for uncontrolled fluidized bed combustion technology (SCC 10100316 and 1010 0318)

After assigning best fitting parametric distribution, Monte Carlo simulation is applied as in Section 2.2.4.4 and Bootstrap method is applied as in 2.2.4.5. Then average EF and confidence intervals are calculated for in-situ EFs and given in Table 3.42. It is seen that the EFs derived from in-situ measurements are pretty lower than EMEP and EPA EFs. Furthermore, EMEP and EPA EFs are close to each other. There is no abatement technology for CO emissions in the plant.

Figure 3.32 : Probability band of CO EFs for "1A1a-10102-3.10" as cumulative distribution of Weibull distribution fitted to CO EFs derived from in-situ measurements.

Consequently, country-specific CO EF is calculated as 3.3 g/GJ. Lower and upper confidence interval range of country-specific CO EF is small when compared to EMEP

and EPA confidence interval ranges. In probability band in Figure 3.32, almost all points on the probability band are within 50% CI. Thus, this EF can be considered as country-specific EF.
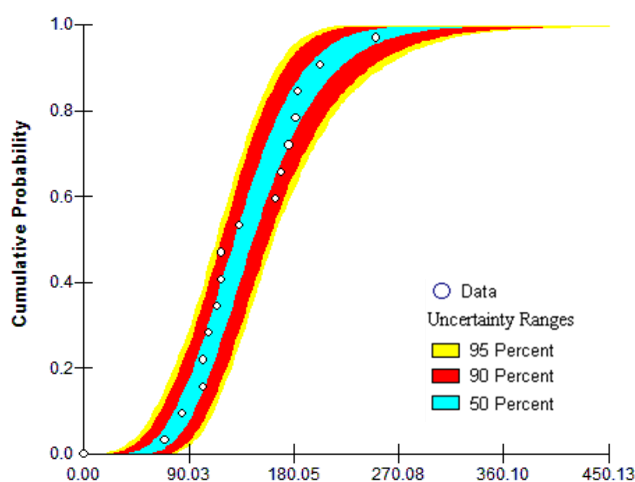
SO₂

Summary statistics of SO_2 EFs for "1.A.1.a–10102–3.10" SNAP/NFR category are given in Table 3.43 for EFs derived from in-situ measurements. When min, max and median of the EFs derived from in-situ measurements are investigated in Table 3.43, it is clear that SO_2 EFs are properly distributed between 70 g/GJ and 250 g/GJ, with 33% Cv, low variance and standard deviation. Homogeneously distribution of the EFs is also clear on the CDF in Figure 3.33.

Table 3.43 : Summary statistics for SO_2 EFs derived from both in-situ measurements and EMRs for "1.A.1.a–10102–3.10".

	In-situ Measurements
Number of data points	16
Minimum	69.5
Maximum	250.7
Median	125.7
Variance [1]	2407
Standard Deviation [2]	47.5
Cv (%) [3]	33
Skewness [4]	0.57
Kurtosis [5]	-0.17

[1] According to equation 2.12
[2] According to equation 2.13
[3] According to equation 2.14
[4] According to equation 2.15
[5] According to equation 2.16

Low skewness and kurtosis in EFs derived from in-situ measurements in Table 3.43 indicate strong asymmetry and a small peak in the distribution as it is also visualized in histogram of Figure 3.33.

According to Figure 3.33, looking at the CDF and histogram of EFs derived from in-situ measurements, Gamma distribution seems best fitting distribution to CDF and histogram of the in-situ EFs. Table 3.44 is created in order to quantitatively support this qualitative interpretation and includes goodness-of-fit statistics and goodness-of-fit criteria for SO_2 EFs derived from in-situ measurements.
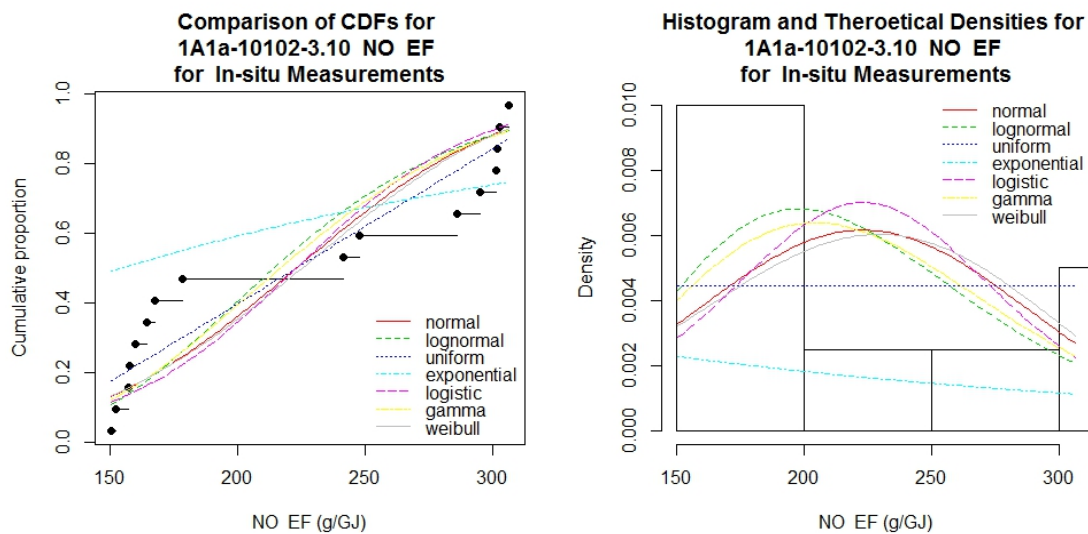
Figure 3.33 : Distribution fitting comparisons of SO₂ EF on CDF and Histogram for in-situ measurements of "1.A.1.a–10102–3.10".

Critical value of Kolmogorov-Smirnov statistic is 0.213, as it is given in Table 2.9. Kolmogorov-Smirnov statistic of entire of the distributions are less than critical value (0.213), except exponential and logistic distributions. Minimum Kolmogorov-Smirnov statistic is in lognormal distribution. However other goodness-of-fit statistics and criteria are lowest for Gamma distribution. Due to the close CDF and histogram of Gamma distribution to the in-situ EFs in Figure 3.33, and due to lowest goodness-of-fit statistics in Table 3.44, best fitting distribution is selected as the Gamma distribution for CO EFs derived from in-situ measurements.

Table 3.44 : Goodness-of-fit statistics/criteria for SO₂ EF derived from in-situ measurements of "1.A.1.a–10102–3.10".

Type of distribution	Goodness-of-fit statistics			Goodness-of-fit criteria	
	Kolmogorov-Smirnov statistic	Cramer-von Mises	Anderson-Darling statistic	Akaike's Information Criterion	Bayesian Information Criterion
Normal	0.197	0.080	0.43	172.96	174.50
Lognormal	**0.164**	0.070	0.37	**171.57**	173.12
Uniform	0.149	0.060	-	-	-
Exponential	0.387	0.684	3.38	192.68	193.45
Logistic	0.218	0.109	0.56	173.94	175.48
Gamma	0.168	**0.065**	**0.34**	**171.57**	**173.11**
Weibull	0.184	0.068	0.38	172.64	174.19

* Bold values indicate lowest values.

After assigning best fitting parametric distribution, Monte Carlo simulation is applied as in Section 2.2.4.4 and Bootstrap method is applied as in 2.2.4.5. Then average EF and confidence intervals are calculated for in-situ EFs and given in Table 3.45. It is

seen that the EFs derived from in-situ measurements are pretty lower than EMEP and EPA EFs. Furthermore, EMEP and EPA EFs are close to each other. EPA EF is given for uncontrolled conditions. Since EMEP EF is close to EPA EF, it may also be for uncontrolled conditions. However, there is SO_2 abatement technology, which is flue gas desulphurization in the plant that in-situ measurements were conducted. That is why SO_2 EF of in-situ measurements is pretty lower than EPA and EMEP EFs.

Table 3.45 : Uncertainty analysis results for SO_2 EF of "1.A.1.a–10102–3.10" and comparisons with other studies.

	In-situ measurements	EMEP [54]	EPA [193]
Fitted distribution type	Gamma		
Mean	142 g/GJ	1680 g/GJ	
95% CI (Lower, Upper) as g/GJ	120.1–167.4	330 -5000	1625 [3]
Uncertainty (Lower, Upper)	15-18	80-198	g/GJ
First parameter	8.43 [1]		
Second parameter	16.9 [2]		

[1] scale parameter (α) for Gamma parametric probability distribution function
[2] shape parameter (β) for Gamma parametric probability distribution function
[3] for uncontrolled fluidized bed combustion technology (SCC 10100316 and 10100318)

Consequently, country specific SO_2 EF is calculated as 142 g/GJ. Lower and upper confidence interval range of country-specific CO EF is small when compared to EMEP and EPA confidence interval ranges. In probability band in Figure 3.34, almost all points on the probability band are within 50% CI range.
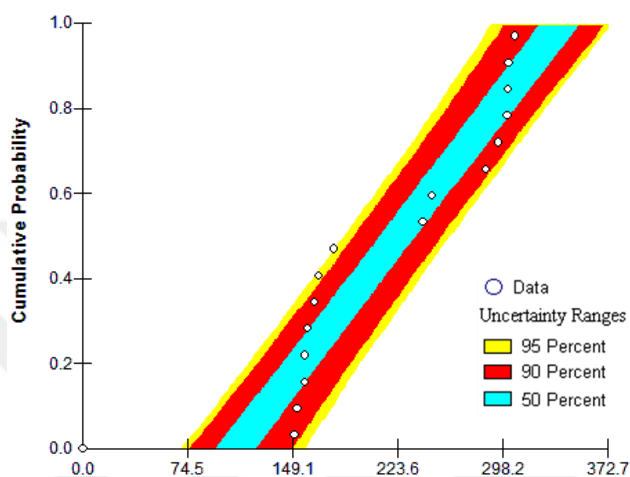

Figure 3.34 : Probability band of SO_2 EFs for "1A1a-10102-3.10" as cumulative distribution of Gamma distribution fitted to SO_2 EFs derived from in-situ measurements.

NO

Summary statistics of NO EFs for "1.A.1.a–10102–3.10" SNAP/NFR category are given in Table 3.46 for EFs derived from in-situ measurements. When min, max and median of the EFs derived from in-situ measurements are investigated in Table 3.46, it is clear that NO EFs are distributed between 150 g/GJ and 306 g/GJ, with 29% Cv, large variance and standard deviation.

Table 3.46 : Summary statistics for NO EFs derived from both in-situ measurements and EMRs for "1.A.1.a–10102–3.10".

	In-situ Measurements
Number of data points	16
Minimum	150.5
Maximum	306.5
Median	210
Variance [1]	4194
Standard Deviation [2]	64.7
Cv (%) [3]	29
Skewness [4]	0.17
Kurtosis [5]	-2

[1] According to equation 2.12
[2] According to equation 2.13
[3] According to equation 2.14
[4] According to equation 2.15
[5] According to equation 2.16

EFs are distributed heterogeneously on the CDF in Figure 3.35. Large negative kurtosis, which is -2, indicates a peak in lower EFs.

Figure 3.35 : Distribution fitting comparisons of NO EF on CDF and Histogram for in-situ measurements of "1.A.1.a–10102–3.10".

According to Figure 3.35, looking at the CDF and histogram of EFs derived from in-situ measurements, although lognormal distributions seems as one of the closest distributions none of the distributions perfectly fit to the data due to a large peak in low EFs. Table 3.47 includes goodness-of-fit statistics and goodness-of-fit criteria for NO EFs derived from in-situ measurements.
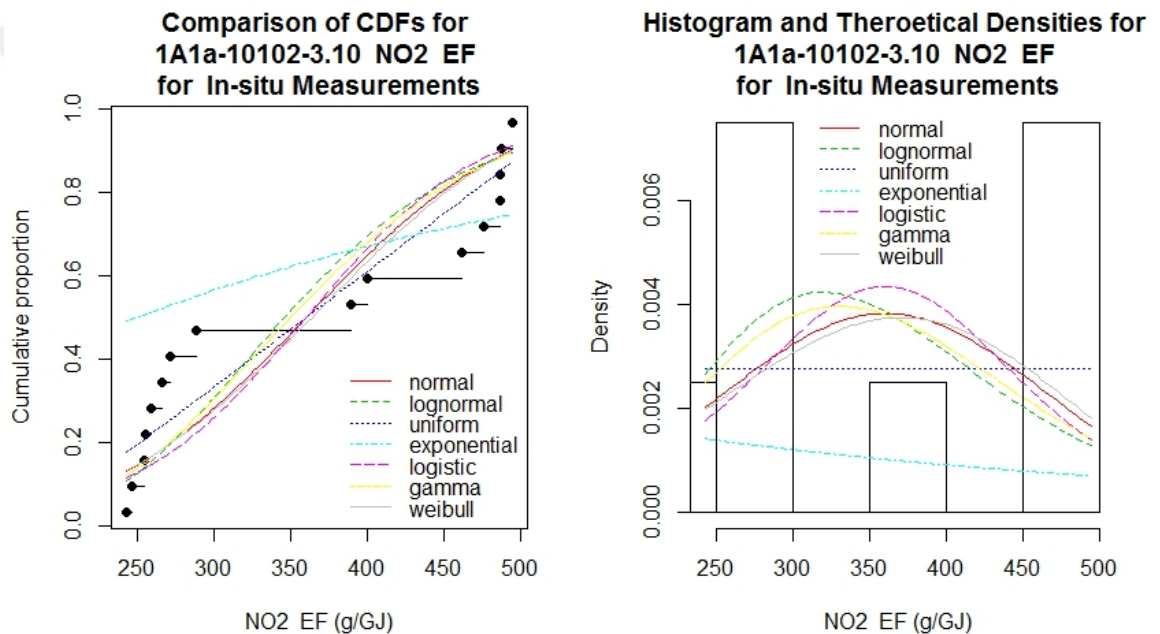
Table 3.47 : Goodness-of-fit statistics/criteria for NO EF derived from in-situ measurements of "1.A.1.a–10102–3.10"

Type of distribution	Goodness-of-fit statistics			Goodness-of-fit criteria	
	Kolmogorov-Smirnov statistic	Cramer-von Mises	Anderson-Darling statistic	Akaike's Information Criterion	Bayesian Information Criterion
Normal	0.255	0.236	1.474	182.9	184.4
Lognormal	0.244	0.256	1.572	181.9	183.5
Uniform	**0.199**	**0.149**	**0.983**	**177.2**	**178.8**
Exponential	0.490	0.804	3.927	207.1	207.8
Logistic	0.278	0.286	1.816	185.7	187.2
Gamma	0.240	0.238	1.465	182.0	183.6
Weibull	0.258	0.230	1.442	182.4	183.9

* Bold values indicate lowest values.

In Table 3.47, it is seen that all distribution types exceed the critical value of Kolmogorov-Smirnov statistic, which is 0.213 according to Table 2.9, except Uniform distribution. Uniform distribution is also minimum in all goodness-of-fit tests and criteria. Consequently, best fitting distribution is selected as the Uniform distribution for NO EFs derived from in-situ measurements.

After assigning best fitting parametric distribution, Monte Carlo simulation is applied as in Section 2.2.4.4 and Bootstrap method is applied as in 2.2.4.5. Then average EF and confidence intervals are calculated for in-situ EFs and given in Table 3.48.

Table 3.48 : Uncertainty analysis results for NO EF of "1.A.1.a–10102–3.10" and comparisons with other studies.

	In-situ measurements
Fitted distribution type	Uniform
Mean	223 g/GJ
95% CI (Lower, Upper) as g/GJ	190.8–256.2
% Uncertainty (Lower, Upper)	14.4-14.9
First parameter	107.3 [1]
Second parameter	339 [2]

[1] minimum value (a) for Uniform parametric probability distribution function
[2] maximum value (b) for Uniform parametric probability distribution function

Country-specific EF of NO is calculated as 223 g/GJ. There is no abatement technology in the plant. NO EFs are not supplied by EMEP [54] and EPA [193], therefore there is no room for comparison. In probability band in Figure 3.36, almost all points beyond the 50% probability CI range, which means that Uniform distribution is not a perfect matching distribution. However, it was the best distribution between all distributions discussed above. In such cases it is better to apply empirical distribution. However, in this thesis only parametric distributions are considered.

Figure 3.36 : Probability band of NO EFs for "1A1a-10102-3.10" as cumulative distribution of Uniform distribution fitted to NO EFs derived from in-situ measurements.

NO$_2$

Summary statistics of NO$_2$ EFs for "1.A.1.a–10102–3.10" SNAP/NFR category are given in Table 3.49 for EFs derived from in-situ measurements.

Table 3.49 : Summary statistics for NO$_2$ EFs derived from both in-situ measurements and EMRs for "1.A.1.a–10102–3.10".

	In-situ Measurements
Number of data points	16
Minimum	242.8
Maximum	494.6
Median	338.5
Variance [1]	10887
Standard Deviation [2]	104.3
Cv (%) [3]	28.9
Skewness [4]	0.17
Kurtosis [5]	-2

[1] According to equation 2.12
[2] According to equation 2.13
[3] According to equation 2.14
[4] According to equation 2.15
[5] According to equation 2.16

When min, max and median of the EFs derived from in-situ measurements are investigated in Table 3.49, it is clear that NO_2 EFs are distributed between 242 g/GJ and 495 g/GJ, with 29% Cv, large variance and large standard deviation. EFs are distributed heterogeneously on the CDF in Figure 3.37. Large negative kurtosis, which is -2, indicates a peak in lower EFs.

According to Figure 3.37, looking at the CDF and histogram of EFs derived from in-situ measurements, none of the distributions perfectly fit to the data due to large peaks although lognormal and Gamma distributions seems as one of the closest distributions. Table 3.50 includes goodness-of-fit statistics and goodness-of-fit criteria for NO_2 EFs derived from in-situ measurements.

Figure 3.37 : Distribution fitting comparisons of NO_2 EF on CDF and Histogram for in-situ measurements of "1.A.1.a–10102–3.10".

In Table 3.50, it is seen that all distribution types exceed the critical value of Kolmogorov-Smirnov statistic, which is 0.213 according to Table 2.9, except Uniform distribution. Uniform distribution is also minimum in all goodness-of-fit tests and criteria. Consequently, best fitting distribution is selected as the Uniform distribution for NO_2 EFs derived from in-situ measurements.

Table 3.50 : Goodness-of-fit statistics/criteria for NO_2 EF derived from in-situ measurements of "1.A.1.a–10102–3.10".

Type of distribution	Goodness-of-fit statistics			Goodness-of-fit criteria	
	Kolmogorov-Smirnov statistic	Cramer-von Mises	Anderson-Darling statistic	Akaike's Information Criterion	Bayesian Information Criterion
Normal	0.256	0.236	1.47	198.1	199.7
Lognormal	0.244	0.255	1.57	197.2	198.8
Uniform	**0.200**	**0.149**	**0.98**	**192.5**	**194.0**
Exponential	0.491	0.804	3.93	222.4	223.1
Logistic	0.278	0.286	1.81	200.9	202.5
Gamma	0.241	0.237	1.46	197.3	198.9
Weibull	0.258	0.230	1.44	197.7	199.2

* Bold values indicate lowest values.

After assigning best fitting parametric distribution, Monte Carlo simulation is applied as in Section 2.2.4.4 and Bootstrap method is applied as in 2.2.4.5. Then average EF and confidence intervals are calculated for in-situ EFs and given in Table 3.51.

Table 3.51 : Uncertainty analysis results for NO_2 EF of "1.A.1.a–10102–3.10" and comparisons with other studies.

	In-situ measurements
Fitted distribution type	Uniform
Mean	360 g/GJ
95% CI (Lower, Upper) as g/GJ	307.8–413.2
% Uncertainty (Lower, Upper)	14.5-14.8
First parameter	173.4 [1]
Second parameter	546.7 [2]

[1] minimum value (a) for Uniform parametric probability distribution function
[2] maximum value (b) for Uniform parametric probability distribution function

Country-specific EF of NO_2 is calculated as 360 g/GJ. There is no abatement technology in the plant. NO_2 EFs are not supplied by EMEP [54] and EPA [193], therefore there is no room for comparison. In probability band in Figure 3.38, almost all points beyond the 50% probability CI range, which means that Uniform distribution is not perfect matching distribution. However, it was the best distribution between all distributions discussed above. In such cases it is better to apply empirical distribution. However, in this thesis only parametric distributions are considered.
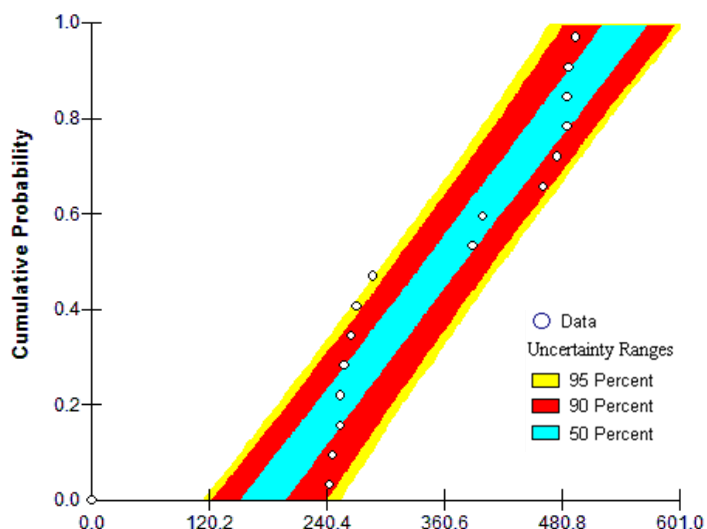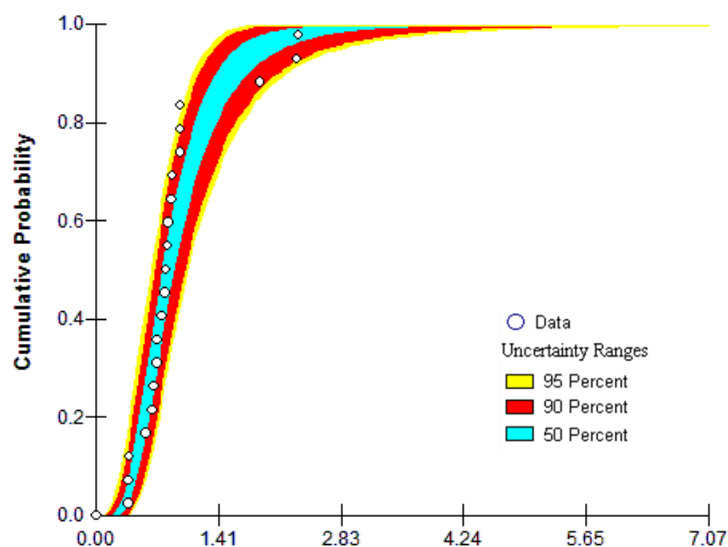
Figure 3.38 : Probability band of NO_2 EFs for "1A1a-10102-3.10" as cumulative distribution of Uniform distribution fitted to NO_2 EFs derived from in-situ measurements.

NO_x

NOx EF is calculated as the sum of NO and NO_2 emissions. However, since the uncertainty levels of NO and NO_2 EFs are different, the formulas given in equation 2.1a-2.1d were applied in order to calculate the total uncertainty of NO_x EF. NOx EF of "1.A.1.a–10102–3.10" SNAP/NFR category and comparisons with other studies are given in Table 3.20.

Table 3.52 : NO_x EF of "1.A.1.a–10102–3.10" and comparisons with other studies.

	In-situ Measurements	EMEP [54]	EPA [193]
NOx EF (NO+NO_2) as g/GJ	583	247	between
95% CI (Lower, Upper) as g/GJ	521.67-645.7	143-571	249.1 [1]
% Uncertainty (Lower, Upper)	10.5-10.8%	42-131%	and 704 [2]
NO/NO_2 share	0.62		g/GJ

[1] for external combustion of lignite with dry bottom / wall fired boilers for electricity generation with an abatement technology as overfire air and low NOx burners (SCC is 10100301)
[2] for uncontrolled external combustion of lignite with dry bottom / wall fired boilers for electricity generation (SCC is 10100301)

Country specific NOx EF is calculated as 583 g/GJ which is more than twice of EMEP EF [54], which is 247 g/GJ, however it is within 95% CI of EMEP. There is no NO_x abatement technology in the plant. The ratio of NO and NO_2 is 0.6 for EFs derived from in-situ measurements for "1.A.1.a–10102–3.10" SNAP/NFR category.

155

3.2.4 Natural gas combusting medium size dry bottom boilers

"1.A.1.a–10102–3.12" code represents natural gas combustion plants with a capacity between 50 and 300 MW, and with dry bottom boilers as the combustion technology for production of public power.

In Marmara region there are seven plants falling under this SNAP/NFR category. There were no in-situ measurements for this SNAP/NFR category in KAMAG project [194]. However, EMRs were available for two of the plants. Since the data in EMRs are questionable as discussed in Section 2.2.1 , EFs from "1.A.1.a–10102–3.12" SNAP/NFR category should be used cautiously. Country-specific EFs are generated for this SNAP/NFR category, but not used in the emission inventory part of this study.

Dust

Summary statistics of dust EFs for "1.A.1.a–10102–3.12" SNAP/NFR category are given in Table 3.53. Standard deviation, variance and Cv are calculated large in EFs derived from EMRs which indicate large variability between EFs.

Table 3.53 : Summary statistics of dust EFs derived from EMRs for "1.A.1.a–10102-3.12".

	EMR
Number of data points	21
Minimum	0.37
Maximum	2.34
Median	0.8
Variance [1]	0.3
Standard Deviation [2]	0.55
Cv (%) [3]	58
Skewness [4]	1.78
Kurtosis [5]	2.53

[1] According to equation 2.12
[2] According to equation 2.13
[3] According to equation 2.14
[4] According to equation 2.15
[5] According to equation 2.16

The large variability is heavily affected from outliers. In Figure 3.39, comparison of CDFs and histograms with possible parametric distribution fitting options are given. According to Figure 3.39, looking at the CDF of EFs derived from EMR, it is seen that 80% of EFs are between 0.5 g/GJ and 1 g/GJ. However, 15% of the EFs (three EFs)

are more than 2 g/GJ, which can be treated as outlier. Those outliers contribute to variability in the EFs.
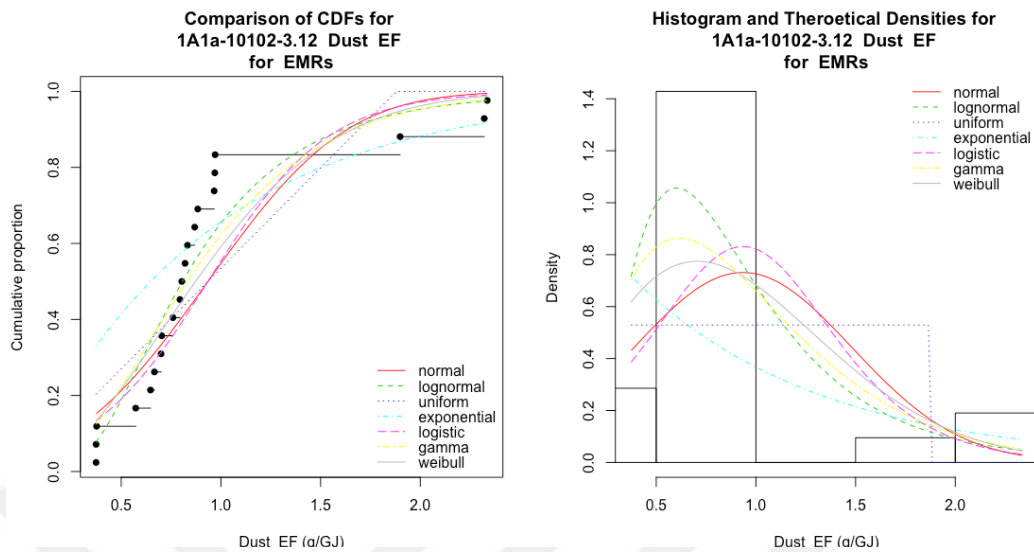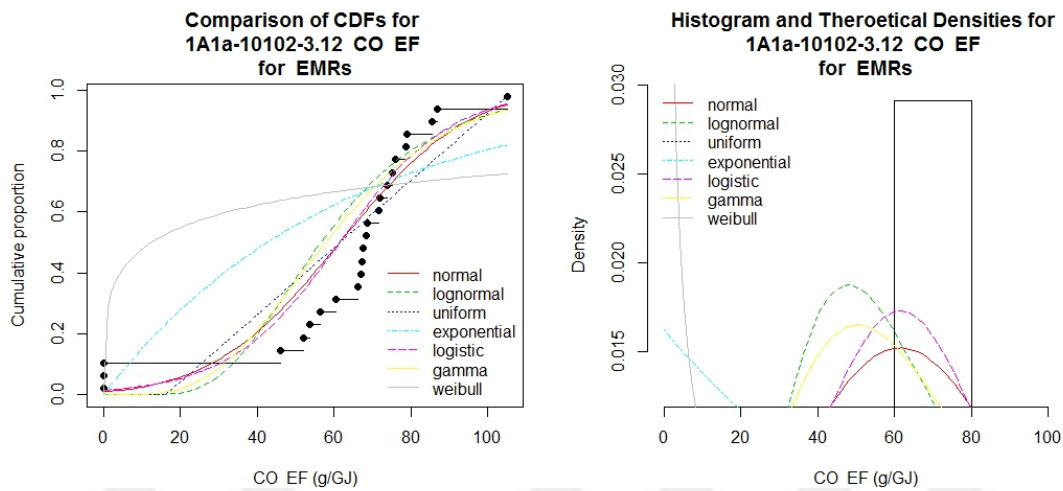

Figure 3.39 : Distribution fitting comparisons of dust EF on CDF and Histogram for EMRs of "1.A.1.a–10102–3.12".

There is positive skewness and kurtosis in the EFs derived from EMRs. Large skewness and kurtosis of in-situ measurements in Table 3.53 indicate strong asymmetry and large peak in the distribution, respectively, as it is also visualized in Figure 3.39.

According to Figure 3.39, looking at the CDF and histogram of EFs derived from EMRs, lognormal distribution is close to CDF and histogram of the in-situ EFs. In addition to CDF and histograms given in Figure 3.39, goodness-of-fit statistics and goodness-of-fit criteria for dust EFs derived from in-situ measurements are also calculated and given in Table 3.54.

Critical value of Kolmogorov-Smirnov statistic (0.188 as it is given in Table 2.9) is exceeded by entire of the distributions, however, lognormal distribution is the closest distribution to the critical value. Other goodness-of-fit statistics and criteria are also lowest for lognormal distribution. Therefore, best fitting distribution is selected as lognormal distribution for dust EFs derived from EMRs for "1.A.1.a–10102-3.12" SNAP/NFR category. After assigning best fitting parametric distribution, Monte Carlo simulation is applied as in Section 2.2.4.4 and Bootstrap method is applied as in

Section 2.2.4.5. Then, average EF and confidence intervals are calculated for EMR EFs, and results are given in Table 3.55.

Table 3.54 : Goodness-of-fit statistics/criteria for dust EF derived from EMRs of "1.A.1.a–10102 –3.12".

Type of distribution	Goodness-of-fit statistics			Goodness-of-fit criteria	
	Kolmogorov-Smirnov statistic	Cramer-von Mises	Anderson-Darling statistic	Akaike's Information Criterion	Bayesian Information Criterion
Normal	0.331	0.413	2.29	38.15	40.24
Lognormal	**0.224**	**0.168**	**0.94**	**25.86**	**27.95**
Uniform	0.338	0.471	-	-	-
Exponential	0.329	0.633	3.16	41.18	42.23
Logistic	0.327	0.409	2.14	35.88	37.97
Gamma	0.254	0.229	1.26	29.10	31.19
Weibull	0.286	0.287	1.58	31.73	33.82

* Bold values indicate lowest values.

It is seen that, the EF derived from EMRs (0.93 g/GJ) is higher than EMEP EF (0.281 g/GJ) [54]. However it is within the EPA EF range which is between 0.9 g/GJ and 3.59 g/GJ but close to lower CI of EPA [193]. Probability band of EFs derived from EMRs is given in Figure 3.40.

Table 3.55 : Uncertainty analysis results for dust EF of "1.A.1.a–10102–3.12" and comparisons with other studies.

	EMR	EMEP [54]	EPA [193]
Fitted distribution type	Lognormal		between 0.9 [3] and 3.59 [4] g/GJ
Mean	0.93 g/GJ	0.281 g/GJ	
95% CI (Lower, Upper) as g/GJ	0.73–1.2	0.169-0.393	
Uncertainty (Lower, Upper)	22-29	40-40	
First parameter	-0.21 [1]		
Second parameter	0.54 [2]		

[1] mean of ln(x) for lognormal parametric probability distribution function
[2] standard deviation of ln(x) for lognormal parametric probability distribution function
[3] for filterable PM, uncontrolled conditions, all size boilers except tangential (SCC:10100602)
[4] for filterable PM, uncontrolled conditions, all size and tangential boilers (SCC:10100601, 10100601 and 10100604)

One important indication that a distribution is properly fitted is that almost all points on the probability band are within 50% CI range [219]. However, half of the points are beyond 50% CI range. This situation is mainly caused by outliers. Anyway, dust EF

for "1.A.1.a–10102-3.12" SNAP/NFR category is 0.93 g/GJ with 95% lower CI as 0.73 g/GJ and upper CI as 1.2 g/GJ as it is given in Table 3.55.
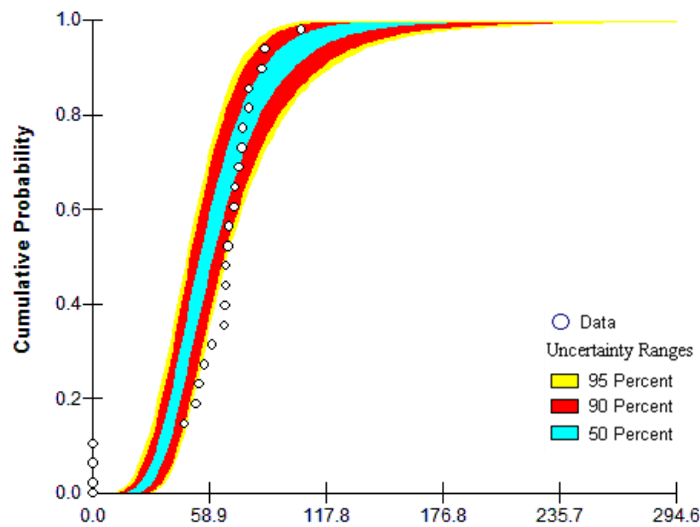

Figure 3.40 : Probability band of dust EFs for "1A1a-10102-3.12" as cumulative distribution of lognormal distribution fitted to dust EFs derived from EMRs.

CO

Summary statistics of CO EFs for "1.A.1.a–10102–3.12" SNAP/NFR category are given in Table 3.56. Standard deviation, variance and Cv are calculated large in EFs derived from EMRs which indicate large variability between EFs.

Table 3.56 : Summary statistics for CO EFs derived from EMRs for "1.A.1.a–10102–3.12".

	EMR
Number of data points	24
Minimum	0
Maximum	105.05
Median	67.9
Variance [1]	686
Standard Deviation [2]	26.2
Cv (%) [3]	43
Skewness [4]	-1.41
Kurtosis [5]	1.82

[1] According to equation 2.12
[2] According to equation 2.13
[3] According to equation 2.14
[4] According to equation 2.15
[5] According to equation 2.16

Large variability is heavily affected from outliers. In Figure 3.41, comparison of CDFs and histograms with possible parametric distribution fitting options are given. According to Figure 3.41, looking at the CDF of EFs derived from EMR, it is seen that

85% of EFs are more than 45 g/GJ. However, 10% of the EFs (three EFs) are 0 g/GJ, which can be treated as outlier. Those outliers contribute to variability in the EFs.

Figure 3.41 : Distribution fitting comparisons of CO EF on CDF and Histogram for EMRs of "1.A.1.a–10102–3.12".

There is negative skewness and positive kurtosis in the EFs derived from EMRs. Large skewness and kurtosis of EFs in Table 3.53 indicate strong asymmetry and large peak in the distribution, respectively, as it is also visualized in Figure 3.41.

According to Figure 3.41, looking at the CDF and histogram of EFs derived from EMRs, none of the distributions perfectly fit to data points. This situation is mainly caused by "zero value" outliers. However, lognormal distribution is not fitting good but closest to CDF and histogram of the EFs. In addition to CDF and histograms given in Figure 3.41, goodness-of-fit statistics and goodness-of-fit criteria for CO EFs derived from EMRs are also calculated and given in Table 3.57.

Critical value of Kolmogorov-Smirnov statistic (0.188 as it is given in Table 2.9) is exceeded by entire of the distributions, however, Uniform, Normal and Logistic distributions are close distributions to the critical value. Normal and logistic distributions have lowest values in Cramer Von Mises, Anderson-Darling statistics and Akaike's Information Criterion. Logistic and Weibull are lowest in Bayesian Information criteria. If logistic distribution was included in AuvTool, it would be selected since it has lowest values in most of the statistics and criteria in Table 3.57. As seen, decision on the good-fitting distribution is not possible with this table. Besides, most of the statistics are not available for lognormal distribution since it takes infinite value due to zero values in the dataset. Lognormal, Gamma and Normal distributions are close to the peak value in histogram given in Figure 3.41.

Consequently, Lognormal distribution is selected as the fitting distribution by obeying expert opinion, because it has the highest histogram on Figure 3.41, even if this peak is not as high as the peak in the data itself.

Table 3.57 : Goodness-of-fit statistics/criteria for CO EF derived from in-situ measurements of "1.A.1.a–10102–3.12".

Type of distribution	Goodness-of-fit statistics			Goodness-of-fit criteria	
	Kolmogorov-Smirnov statistic	Cramer-von Mises	Anderson-Darling statistic	Akaike's Information Criterion	Bayesian Information Criterion
Normal	0.24	**0.30**	**1.86**	**229**	231
Lognormal	0.32	0.58	-	-	-
Uniform	**0.23**	0.39	-	-	-
Exponential	0.40	1.04	13.52	248	249
Logistic	0.25	**0.29**	**1.64**	**227**	**229**
Gamma	0.29	0.48	55.61	920	922
Weibull	0.51	1.46	8.14	192	**195**

* Bold values indicate lowest values.

After assigning best fitting parametric distribution, Monte Carlo simulation is applied as in Section 2.2.4.4 and Bootstrap method is applied as in Section 2.2.4.5. Then, average EF and confidence intervals are calculated for EMR EFs, and results are given in Table 3.58.

Table 3.58 : Uncertainty analysis results for CO EF of "1.A.1.a–10102–3.12" and comparisons with other studies.

	EMR	EMEP [54]	EPA [193]
Fitted distribution type	Lognormal		
Mean (g/GJ)	61.5	39	between
95% CI (Lower, Upper) as g/GJ	51.38-73.02	20-60	13 [3] and
% Uncertainty (Lower, Upper)	16-19	49-54	32 [4]
First parameter	4.03 [1]		g/GJ
Second parameter	0.4 [2]		

[1] mean of ln(x) for lognormal parametric probability distribution function
[2] standard deviation of ln(x) for lognormal parametric probability distribution function
[3] for uncontrolled external combustion of natural gas with any size boilers (except tangential fired) for electricity generation (SCC is 10100601 and 10100602)
[4] for uncontrolled external combustion of natural gas with tangentially fired units for electricity generation (SCC is 10100604)

It is seen that, the EF derived from EMRs (61.5 g/GJ) is higher than EMEP EF (39 g/GJ) [54] and EPA EF [193]. At the same time, it is also larger than the upper bound of the CI in both EMEP and EPA EFs. Probability band of EFs derived from EMRs is given in Figure 3.42.
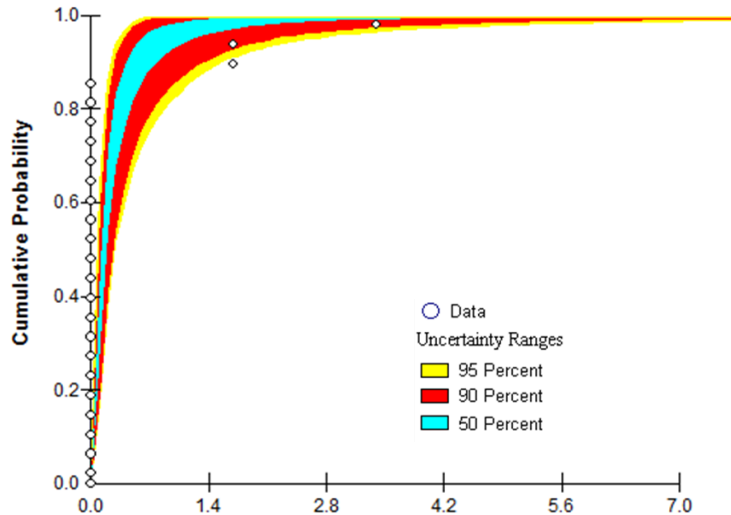
Figure 3.42 : Probability band of CO EFs for "1A1a-10102-3.12" as cumulative distribution of lognormal distribution fitted to dust EFs derived from EMRs.

Most of the EFs are beyond 50% CI range, which was a properly fitting criterion [219]. Anyway, CO EF for "1.A.1.a–10102-3.12" SNAP/NFR category is 61.5 g/GJ with 95% lower CI as 51.38 g/GJ and upper CI as 73.02 g/GJ as it is given in Table 3.58.

SO₂

Summary statistics of SO_2 EFs for "1.A.1.a–10102–3.12" SNAP/NFR category are given in Table 3.59. Standard deviation, variance and Cv are calculated large in EFs derived from EMRs which indicate large variability between EFs.

Large variability is heavily affected from outliers. In Figure 3.43, comparison of CDFs and histograms with possible parametric distribution fitting options are given. According to Figure 3.43, looking at the CDF of EFs derived from EMR, it is seen that 85% of EFs are 0 g/GJ. However, 15% of the EFs (three EFs) are more than 2 g/GJ, which can be treated as outlier. Those outliers contribute to large variability in the EFs. Large skewness and kurtosis are also related with the distribution of those outliers.

Table 3.59 : Summary statistics for SO_2 EFs derived from EMRs for "1.A.1.a–10102–3.12".

	EMR
Number of data points	24
Minimum	0
Maximum	3.39
Median	0
Variance [1]	0.67
Standard Deviation [2]	0.8
Cv (%) [3]	283
Skewness [4]	3.06
Kurtosis [5]	9.45

[1] According to equation 2.12
[2] According to equation 2.13
[3] According to equation 2.14
[4] According to equation 2.15
[5] According to equation 2.16

According to Figure 3.43, looking at the CDF and histogram of EFs derived from EMRs, Weibull distribution is close to CDF of the in-situ EFs.
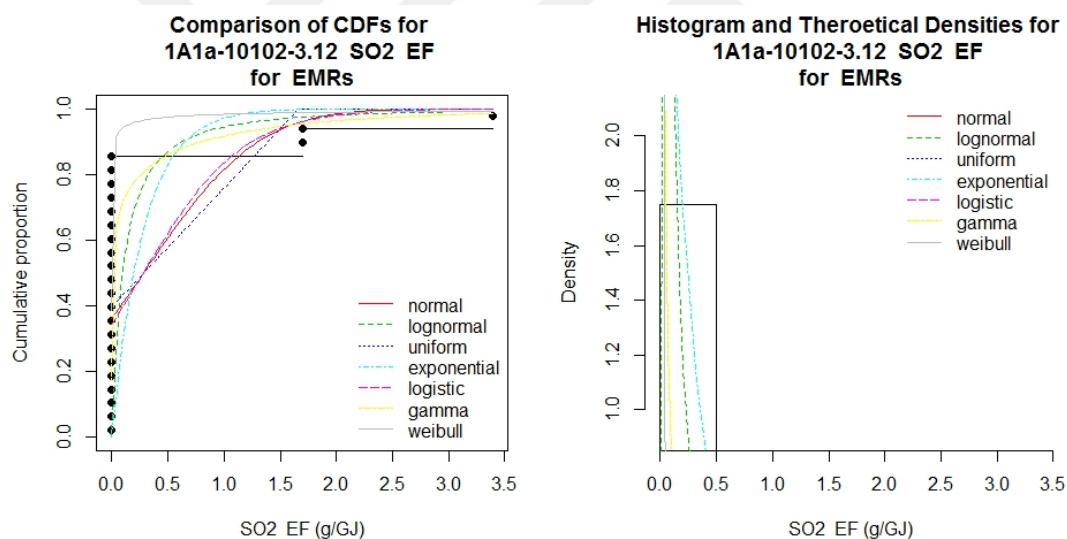
Figure 3.43 : Distribution fitting comparisons on CDF and Histogram for SO_2 EFs derived from EMRs for "1.A.1.a–10102–3.12".

In addition to CDF and histograms given in Figure 3.43, goodness-of-fit statistics and goodness-of-fit criteria for SO_2 EFs derived from in-situ measurements were also calculated and given in Table 3.60. Weibull distribution gets lowest values in goodness-of-fit criteria, and Logistic distribution gets lowest values in goodness-of-fit statistics except Kolmogorov-Smirnov statistic. Since logistic distribution is not included in Auvtool and Weibull distribution doesn't give good results in distribution fitting, Lognormal distribution is selected as best fitting distribution for SO_2 EFs of "1.A.1.a-10102-3.12" SNAP/NFR category. Most of the statistics are not available for

Lognormal distribution, since Lognormal distribution logarithm gives infinite values in goodness-of-fit statistics/criteria with zero values.

Table 3.60 : Goodness-of-fit statistics/criteria for SO$_2$ EF derived from EMRs of "1.A.1.a–10102–3.12".

Type of distribution	Goodness-of-fit statistics			Goodness-of-fit criteria	
	Kolmogorov-Smirnov statistic	Cramer-von Mises	Anderson-Darling statistic	Akaike's Information Criterion	Bayesian Information Criterion
Normal	0.24	0.30	1.86	229	231
Lognormal	0.32	0.58	-	-	-
Uniform	0.23	0.39	-	-	-
Exponential	0.40	1.04	13.52	248	249
Logistic	0.25	0.29	1.64	227	229
Gamma	0.29	0.48	55.61	920	922
Weibull	0.51	1.46	8.14	192	195

* Bold values indicate lowest values.

After assigning best fitting parametric distribution, Monte Carlo simulation is applied as in Section 2.2.4.4 and Bootstrap method is applied as in Section 2.2.4.5. Then, average EF and confidence intervals are calculated for EMR EFs, and results are given in Table 3.61.

Table 3.61 : Uncertainty analysis results for SO$_2$ EF of "1.A.1.a–10102–3.12" and comparisons with other studies.

	EMR	EMEP [54]	EPA [193]
Fitted distribution type	Lognormal		
Mean (g/GJ)	0.28	0.281	
95% CI (Lower, Upper) as g/GJ	0-0.66	0.169-0.393	0.26 [3] g/GJ
% Uncertainty (Lower, Upper)	100-136	40-40	
First parameter	-2.36 [1]		
Second parameter	1.48 [2]		

[1] mean of ln(x) for lognormal parametric probability distribution function
[2] standard deviation of ln(x) for lognormal parametric probability distribution function
[3] for uncontrolled external combustion of natural gas with any type of boilers for electricity generation (SCC is 10100601, 10100602 and 10100604)

It is seen that, the EF derived from EMRs (0.28 g/GJ) is compatible with EMEP EF (0.281 g/GJ) [54] and EPA EF (0.26 g/GJ) [193]. However, almost all points are beyond 50% CI range in Figure 3.44.

Figure 3.44 : Probability band of SO$_2$ EFs for "1A1a-10102-3.12" as cumulative distribution of lognormal distribution fitted to dust EFs derived from EMRs.

NO

Summary statistics of NO EFs for "1.A.1.a–10102–3.12" SNAP/NFR category are given in Table 3.62. Standard deviation, variance and Cv are calculated large in EFs derived from EMRs which indicate large variability between EFs.

Table 3.62 : Summary statistics of NO EFs derived from EMRs for "1.A.1.a–10102–3.12".

	EMR
Number of data points	24
Minimum	15.05
Maximum	172.6
Median	33.1
Variance [1]	1904
Standard Deviation [2]	43.6
Cv (%) [3]	95
Skewness [4]	2.14
Kurtosis [5]	3.5

[1] According to equation 2.12
[2] According to equation 2.13
[3] According to equation 2.14
[4] According to equation 2.15
[5] According to equation 2.16

Large variability is heavily affected from outliers. In Figure 3.45, comparison of CDFs and histograms with possible parametric distribution fitting options are given. According to Figure 3.45, looking at the CDF of EFs derived from EMR, it is seen that 85% of EFs are less than 55 g/GJ. However, 15% of the EFs (three EFs) are more than

150 g/GJ, which can be treated as outlier. Those outliers contribute to variability in the EFs.
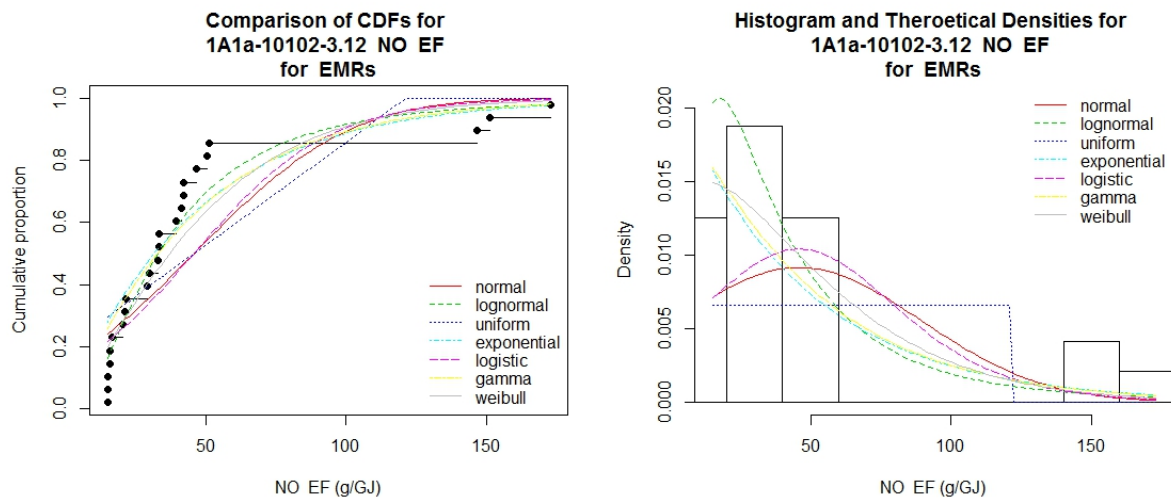
Figure 3.45 : Distribution fitting comparisons on CDF and Histogram for NO EFs derived from EMRs for "1.A.1.a–10102–3.12".

There is positive skewness and kurtosis in the EFs derived from EMRs. Large skewness and kurtosis of in-situ measurements in Table 3.62 indicate strong asymmetry and large peak in the distribution, respectively, as it is also visualized in Figure 3.45.

Table 3.63 : Goodness-of-fit statistics/criteria for NO EF derived from EMRs of "1.A.1.a–10102–3.12".

Type of distribution	Goodness-of-fit statistics			Goodness-of-fit criteria	
	Kolmogorov-Smirnov statistic	Cramer-von Mises	Anderson-Darling statistic	Akaike's Information Criterion	Bayesian Information Criterion
Normal	0.324	0.614	3.45	253.35	255.71
Lognormal	**0.168**	**0.123**	**0.91**	**225.43**	**227.78**
Uniform	0.338	0.686	-	-	-
Exponential	0.280	0.316	1.90	233.57	234.75
Logistic	0.318	0.607	3.24	249.60	251.95
Gamma	0.259	0.279	1.74	234.35	236.71
Weibull	0.229	0.268	1.71	233.45	235.80

* Bold values indicate lowest values.

According to Figure 3.45, looking at the CDF and histogram of EFs derived from EMRs, lognormal distribution is close to CDF and histogram of EFs. In addition to CDF and histograms given in Figure 3.45, goodness-of-fit statistics and goodness-of-fit criteria for NO EFs derived from EMRs were also calculated and given in Table

3.63. Lognormal distribution gets lowest values in each of goodness-of-fit statistic and criteria, therefore fitted as distribution of NO EFs for "1.A.1.a–10102–3.12".

Table 3.64 : Uncertainty analysis results for NO_x EF (as NO) of "1.A.1.a–10102–3.12" and comparisons with other studies.

	EMR	EMEP [54]	EPA [193]
Fitted distribution type	Lognormal		between 42.96 [4] and 120.2 [5] g/GJ
Mean (g/GJ)	45.68 g/GJ	89 [3]	
95% CI (Lower, Upper) as g/GJ	31.3-66.5	15-185	
% Uncertainty (Lower, Upper)	%	%	
First parameter	3.5 [1]		
Second parameter	0.8 [2]		

[1] mean of lnx for Lognormal parametric probability distribution function
[2] standard deviation of lnx for Lognormal parametric probability distribution function
[3] NO_x EF
[4] NO_x for uncontrolled external combustion of natural gas with boilers (except tangential) with a capacity less than 100 Million Btu for electricity generation (SCC is 10100602)
[5] NO_x for uncontrolled external combustion of natural gas with boilers (except tangential) with a capacity more than 100 Million Btu for electricity generation (SCC is 10100601)

After assigning best fitting parametric distribution, Monte Carlo simulation is applied as in Section 2.2.4.4 and Bootstrap method is applied as in Section 2.2.4.5. Then, average EF and confidence intervals are calculated for EMR EFs, and results are given in Table 3.64.
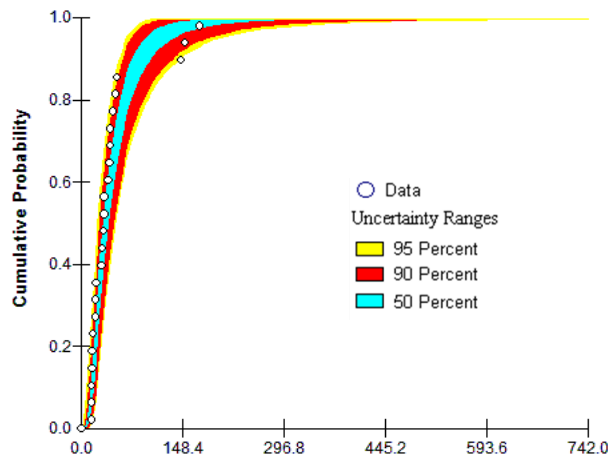
Figure 3.46 : Probability band of NO EFs for "1A1a-10102-3.12" as cumulative distribution of lognormal distribution fitted to dust EFs derived from EMRs.

It is seen that, the EF derived from EMRs (45.68 g/GJ) [54] is close to lower bound of EPA EF (42.96 g/GJ) [193] range. Furthermore, it is less than EMEP EF (89 g/GJ), meanwhile it is in the range of EMEP EF. However, it should be considered that EMEP and EPA EFs are NOx EF where it is NO EF in this study. Probability band of EFs derived from EMRs is given in Figure 3.46.

One important indication that a distribution is properly fitted is that almost all points on the probability band are within 50% CI range [219]. However, half of the points are beyond 50% CI range. This situation is mainly caused by outliers. Anyway, NO EF for "1.A.1.a–10102-3.12" SNAP/NFR category is 45.68 g/GJ with 95% lower CI as 31.3 g/GJ and upper CI as 66.5 g/GJ as it is given in Table 3.64.

NO$_2$

Summary statistics of NO$_2$ EFs for "1.A.1.a–10102–3.12" SNAP/NFR category are given in Table 3.65. Standard deviation, variance and Cv are calculated large in EFs derived from EMRs due to one outlier value in 24 EFs. The large variability is heavily affected from outliers. In Figure 3.47, comparison of CDFs and histograms with possible parametric distribution fitting options are given. According to Figure 3.47, looking at the CDF of EFs derived from EMR, it is seen that all EFs are 0 g/GJ, except one EF which is 8.78 g/GJ. This outlier causes large variability in the EFs.

Table 3.65 : Summary statistics of NO$_2$ EFs derived from both in-situ measurements and EMRs for "1.A.1.a–10102–3.12".

	EMR
Number of data points	24
Minimum	0
Maximum	8.78
Median	0
Variance [1]	3.09
Standard Deviation [2]	1.76
Cv (%) [3]	480
Skewness [4]	4.9
Kurtosis [5]	24

[1] According to equation 2.12
[2] According to equation 2.13
[3] According to equation 2.14
[4] According to equation 2.15
[5] According to equation 2.16

According to Figure 3.47, looking at the CDF and histogram of EFs derived from EMRs, none of the distributions fit well. By considering outlier value as a measurement error, NO$_2$ EF is accepted 0 g/GJ.
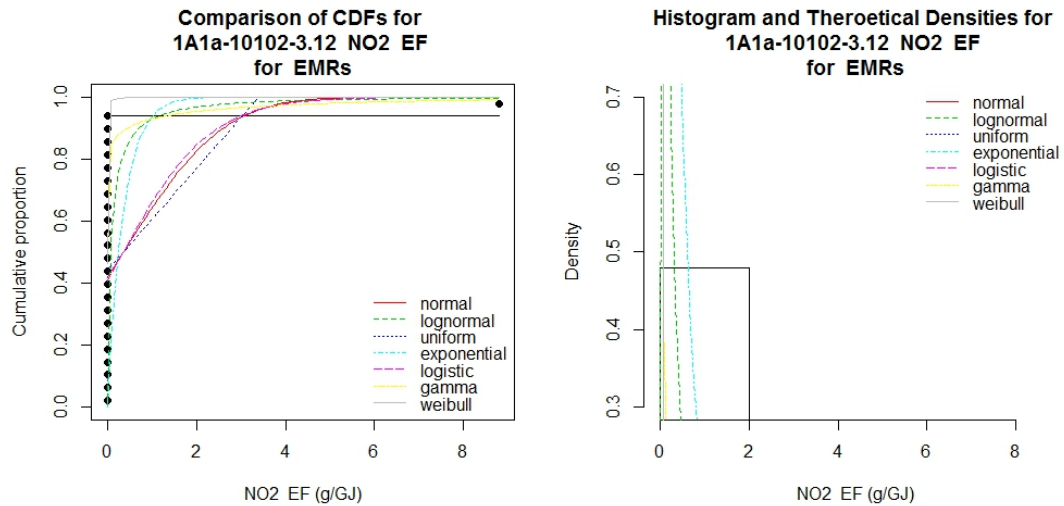
Figure 3.47 : Distribution fitting comparisons on CDF and Histogram for "1.A.1.a–10102–3.12" code NO_2 EFs derived from EMRs.

NO_x

As explained in Section 0, NO_2 EF is 0 g/GJ. Hence, there is no need for summing NO and NO_2 EFs in order to obtain NO_x EF. In this case, for this SNAP/NFR category all NO emissions are accepted as NO_x emissions. Consequently, NO_x EF for "1.A.1.a–10102-3.12" SNAP/NFR category is 45.68 g/GJ with 95% lower CI as 31.3 g/GJ and upper CI as 66.5 g/GJ as it is given in Table 3.64. Comparisons with other studies are also available in Table 3.64.

3.2.5 Gaseous fuels combusting gas turbines

"1.A.1.a–10104–3.17" code represents gaseous fuel combustion plants with gas turbines as the combustion technology for production of public power.

In Marmara region there are 44 plants under this SNAP/NFR category. In-situ measurements were conducted in five plants in Marmara region within the context of KAMAG project [194]. Furthermore, EMRs were available for 18 plants. Consequently, 72 in-situ measurements from five plants are used in the calculation of country-specific EF for this SNAP/NFR code. 26 to 79 emission measurements (according to the type of the air pollutant) from EMRs were also used for comparison.

Dust

Summary statistics of dust EFs for "1.A.1.a–10104–3.17" SNAP/NFR category are given in Table 3.66 for EFs derived from both in-situ measurements and EMRs. Standard deviation, variance and Cv are calculated large in both EMR and in-situ

measurements. Cv of in-situ measurements is more than three times of EMR's. This situation indicates large variability between in-situ EFs.

Table 3.66 : Summary statistics of dust EFs derived from both in-situ measurements and EMRs for "1.A.1.a–10104–3.17".

	In-situ Measurements	EMR
Number of data points	72	26
Minimum	0.01	0.14
Maximum	4.81	4.23
Median	0.039	1.44
Variance [1]	0.56	1.42
Standard Deviation [2]	0.75	1.19
Cv (%) [3]	255	76
Skewness [4]	4.04	0.54
Kurtosis [5]	19.2	-0.8

[1] According to equation 2.12
[2] According to equation 2.13
[3] According to equation 2.14
[4] According to equation 2.15
[5] According to equation 2.16

Outliers cause large variability in datasets. In Figure 3.48, comparison of CDFs and histograms with possible parametric distribution fitting options are given. According to Figure 3.48, looking at the CDF of EFs derived from in-situ measurements, it is seen that 85% of EFs are less than 0.5 g/GJ. However, there are two values more than 3 g/GJ, which contribute to large variability (Cv is 255%) in-situ EFs. In the CDF of EFs derived from EMRs, EFs are distributed between 0.14 and 4.23 g/GJ, homogenously. This is almost same range with EFs derived from in-situ measurements. However, Cv of EMRs (76%) is almost one third of in-situ measurements (255%) because EFs are distributed within this range homogenously, and there are no outliers.

When the histograms given in Figure 3.48 are compared, it is seen that the asymmetry in the histogram of EFs derived from in-situ measurements is higher than those derived from EMR. Therefore, the skewness value for in-situ measurements in Table 3.66 is higher than EMR's. Due to a large peak in the in-situ measurements' histogram, the kurtosis value is large when compared to EFs derived from EMRs.
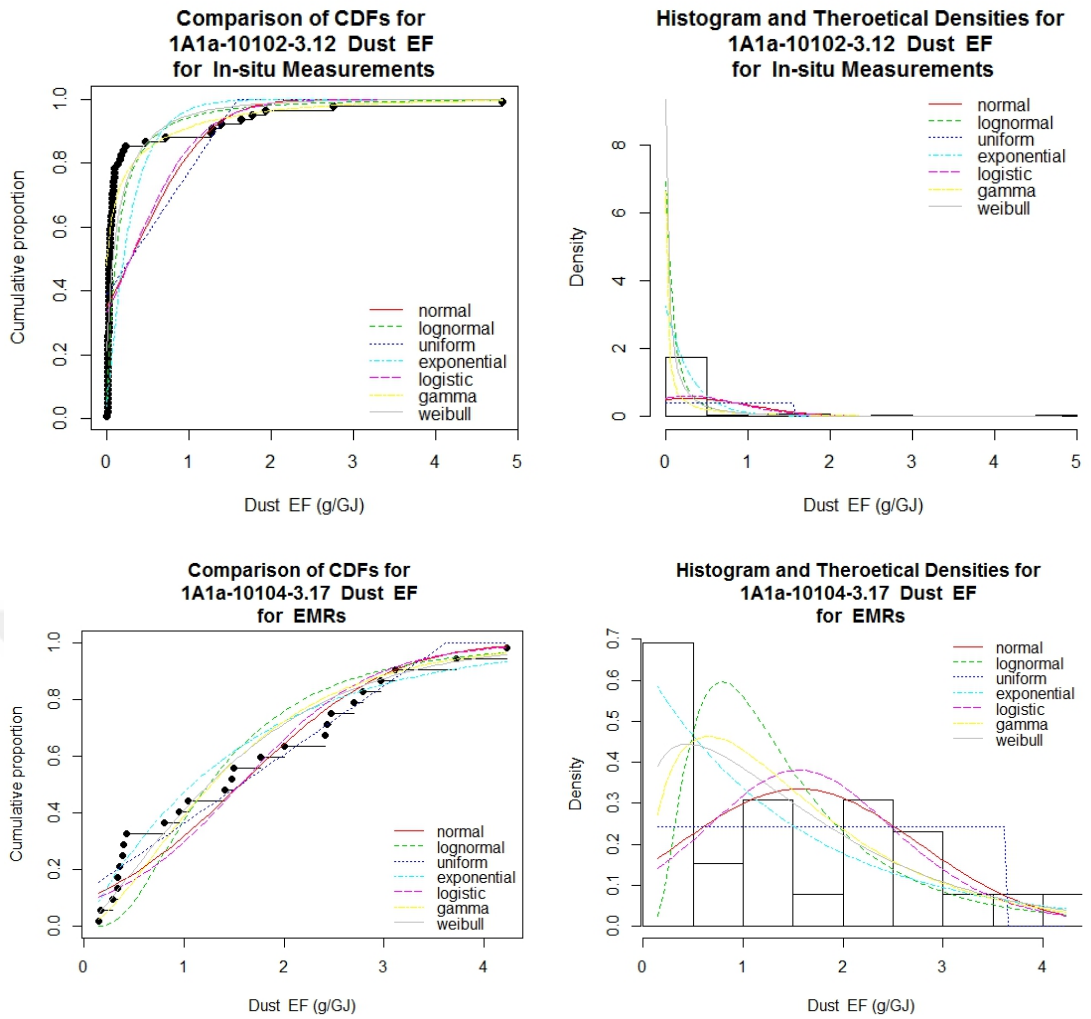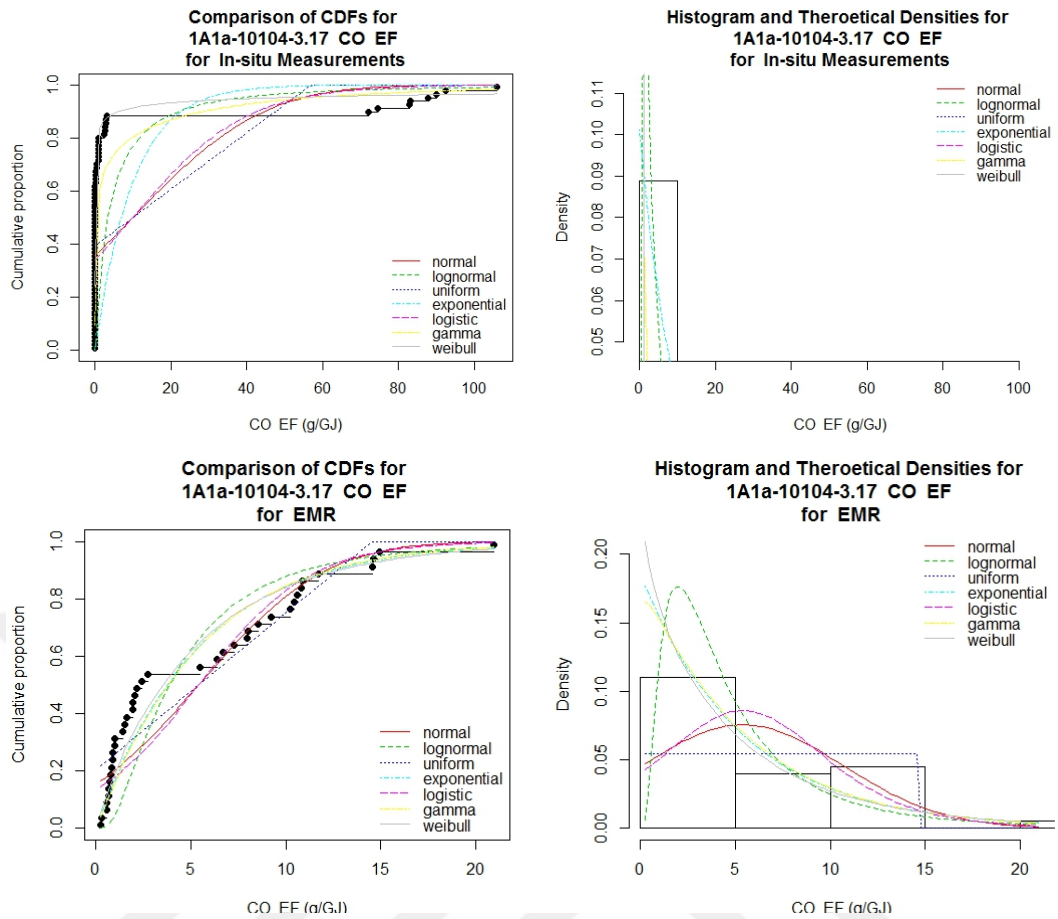
Figure 3.48 : Distribution fitting comparisons of dust EF on CDF and Histogram for both in-situ measurements (above) and EMRs (below) of "1.A.1.a–10104-3.17".

According to Figure 3.48, looking at the CDF and histogram of EFs derived from in-situ measurements, Weibull, Gamma and Lognormal distributions are close to CDF and histogram of the in-situ EFs. In addition to CDF and histograms given in Figure 3.48, goodness-of-fit statistics and goodness-of-fit criteria for dust EFs derived from in-situ measurements were also calculated and given in Table 3.67, in order to determine best fitting parametric probability distribution function for our in-situ EFs.

Table 3.67 : Goodness-of-fit statistics/criteria for dust EF derived from in-situ measurements of "1.A.1.a–10104-3.17".

Type of distribution	Goodness-of-fit statistics			Goodness-of-fit criteria	
	Kolmogorov-Smirnov statistic	Cramer-von Mises	Anderson-Darling statistic	Akaike's Information Criterion	Bayesian Information Criterion
Normal	0.40	3.58	16.9	167	171
Lognormal	0.32	2.61	12.2	-123	-118
Uniform	0.39	3.58	-	-	-
Exponential	0.51	6.44	35.7	-29	-27
Logistic	0.41	3.64	16.9	137	142
Gamma	0.48	3.59	16.4	-36	-31
Weibull	**0.24**	**1.20**	**6.5**	-99	-95

* Bold values indicate lowest values.

Critical value of Kolmogorov-Smirnov statistic is 0.222, as it is given in Table 2.9. It is exceeded by entire of the distributions, however Kolmogorov-Smirnov statistic of the Weibull distribution is closest one to the critical value. Other goodness-of-fit statistics and criteria are also lowest for Weibull distribution. Therefore, best fitting distribution is selected as Weibull distribution for dust EFs derived from in-situ measurements for "1.A.1.a–10104-3.17" SNAP/NFR category. The table of EFs derived from EMRs is given in Attachment F since the use of EFs derived from in-situ measurements is given priority in the thesis, and in order to save space in the thesis text. Weibull distribution is also selected as the fitted distribution for EFs derived from EMRs.

After assigning best fitting parametric distribution, Monte Carlo simulation is applied as in Section 2.2.4.4 and Bootstrap method is applied as in Section 2.2.4.5. Then, average EF and confidence intervals are calculated for each of in-situ EFs and EMR EFs and results are given in Table 3.68.

Table 3.68 : Uncertainty analysis results for dust EF of "1.A.1.a–10104–3.17" and comparisons with other studies.

	In-situ measurements	EMR	EMEP [54]	EPA [193]
Fitted distribution type	Weibull	Weibull		
Mean	0.179	1.59	0.2 g/GJ	between
95% CI (Lower, Upper) as g/GJ	0.128-0.24	1.1-2.18	0.05 -0.8	0.81 [3]
Uncertainty (Lower, Upper) as %	28-34	31-37	75-300	and 2.44 [4]
First parameter	0.144 [1]	1.68 [1]		g/GJ
Second parameter	0.7 [2]	1.17 [2]		

[1] scale parameter (k) for Weibull parametric probability distribution function
[2] shape parameter (c) for Weibull parametric probability distribution function
[3] for uncontrolled filterable PM, for production of electricity with natural gas (SCC is 10100601, 10100602 or 10100604)
[4] for uncontrolled condensable PM, for production of electricity with natural gas (SCC is 10100601, 10100602 or 10100604)

It is seen that, average EF of EMRs is higher than average EF of in-situ measurements. The EF generated from in-situ measurements (0.179 g/GJ) is so low that it is almost one fourth of the lower limit of the EPA EF [193] (0.81 g/GJ), however it is within 95% confidence interval range of EMEP EF [54]. Average EF derived from EMRs (1.59 g/GJ) is larger than upper 95% CI of EMEP [54] (0.8 g/GJ), however compatible with EPA [193]. Probability band of dust EFs for each of average in-situ EF and EMR EF is given in Figure 3.49.
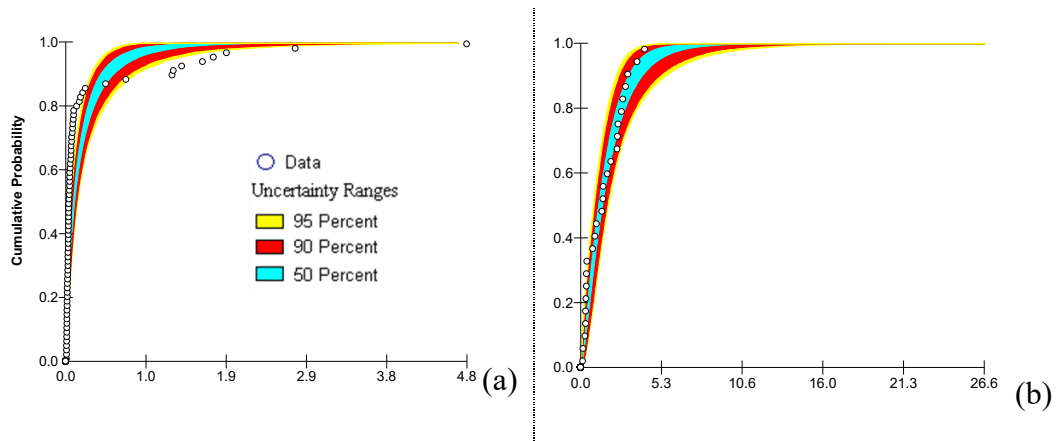
Figure 3.49 : Probability band of dust EFs for "1A1a-10104-3.17" as cumulative distribution of Weibull distribution fitted to dust EFs derived from (a)in-situ measurements (b)EMRs.

One important indication that a distribution is properly fitted is that almost all points on the probability band are within 50% CI range [219]. Although EFs derived from EMR's often remain within the 95% CI limits, it is seen that EFs derived from in-situ measurements are even beyond the 95% CI limits.

CO

Summary statistics of CO EFs for "1.A.1.a–10104–3.17" SNAP/NFR category are given in Table 3.69 for EFs derived from both in-situ measurements and EMRs. Standard deviation, variance and Cv are calculated large in both EMR and in-situ measurements, however Cv of in-situ measurements is almost three times of EMR's. This situation indicates large variability between EFs derived from in-situ measurements. Skewness and Kurtosis is positive in both in-situ EFs and EMR EFs.

Table 3.69 : Summary statistics of CO EFs derived from both in-situ measurements and EMRs for "1.A.1.a–10104–3.17".

	In-situ Measurements	EMR
Number of data points	72	40
Minimum	0	0.24
Maximum	105.87	21
Median	0	2.27
Variance [1]	737	28
Standard Deviation [2]	27.15	5.3
Cv (%) [3]	274	98
Skewness [4]	2.59	0.97
Kurtosis [5]	5.07	0.21

[1] According to equation 2.12
[2] According to equation 2.13
[3] According to equation 2.14
[4] According to equation 2.15
[5] According to equation 2.16

In Figure 3.50, EFs are distributed homogeneously in the CDF of EFs derived from EMRs, while EFs derived from in-situ measurements show a clustered distribution. One of the two clustered EFs are around zero, and the other one is clustered above 80 g/GJ. Clustered data represents the measurements taken from different stacks or the plants. Consequently, this clustered distribution of in-situ EFs causes large variability.

According to Figure 3.50, looking at the CDF and histogram of EFs derived from in-situ measurements, Weibull distribution is close to CDF and histogram of the in-situ EFs. Table 3.70 is created in order to quantitatively support this qualitative interpretation and includes goodness-of-fit statistics and goodness-of-fit criteria for CO EFs derived from in-situ measurements.

Figure 3.50 : Distribution fitting comparisons of CO EF on CDF and Histogram for both in-situ measurements (above) and EMRs (below) of 1"1.A.1.a–10104-3.17".

Critical value of Kolmogorov-Smirnov statistic is 0.222, as it is given in Table 2.9. Kolmogorov-Smirnov statistic of entire of the distributions are more than critical value (0.222). However, Weibull distribution is lowest and closest to critical value. Other goodness-of-fit statistics are also lowest for Weibull distribution. Due to the close CDF and histogram of Weibull distribution to the in-situ EFs in Figure 3.50, and due to lowest goodness-of-fit statistics in Table 3.70, best fitting distribution is selected as the Weibull distribution for CO EFs derived from in-situ measurements. Goodness-of-fit statistics/criteria for CO EF derived from EMRs are given Attachment F. Weibull distribution is also fitted to CO EFs derived from EMRs.

Table 3.70 : Goodness-of-fit statistics/criteria for CO EF derived from in-situ measurements of "1.A.1.a–10104-3.17".

Type of distribution	Goodness-of-fit statistics			Goodness-of-fit criteria	
	Kolmogorov-Smirnov statistic	Cramer-von Mises	Anderson-Darling statistic	Akaike's Information Criterion	Bayesian Information Criterion
Normal	0.49	4.4	21	684	688
Lognormal	0.65	11.6	1563	3824	3828
Uniform	0.46	4.2	-	-	-
Exponential	0.71	13.7	460	476	478
Logistic	0.50	4.6	22	666	670
Gamma	0.53	4.1	27	-636	-632
Weibull	**0.38**	**1.81**	**9.6**	-668	-664

* Bold values indicate lowest values.

After assigning best fitting parametric distribution, Monte Carlo simulation is applied as in Section 2.2.4.4 and Bootstrap method is applied as in 2.2.4.5. Then average EF and confidence intervals are calculated for each of in-situ EFs and EMR EFs and given in Table 3.71. It is seen that, the EF derived from EMRs is lower than the EF derived from in-situ measurements. There is no abatement technology for CO emissions in the plant, however both of them are compatible with EMEP, where they are low when compared to EPA.

Table 3.71 : Uncertainty analysis results for CO EF of "1.A.1.a–10104-3.17" and comparisons with other studies.

	In-situ measurements	EMR	EMEP [54]	EPA [193]
Fitted distribution type	Weibull	Weibull		
Mean	6.26	5.27	4.8	between
95% CI (Lower, Upper) as g/GJ	2.79-12.5	3.69-7.12	1-70	11 [3] and
Uncertainty (Lower, Upper) as %	55-100	30-35	79-1358	39 [4]
First parameter	1.61 [1]	5.177 [1]		g/GJ
Second parameter	0.37 [2]	0.94 [2]		

[1] scale parameter (k) for Weibull parametric probability distribution function
[2] shape parameter (c) for Weibull parametric probability distribution function
[3] for uncontrolled combustion of natural gas with tangentially fired units for production of electricity (SCC is 10100604)
[4] for uncontrolled combustion of natural gas with any size of boilers for production of electricity (SCC is 10100601 and 10100602)

Since the variability is large in EFs derived from in-situ measurements, assigned Weibull distribution cannot be able to include all points. Furthermore, almost all points are beyond 50% CI range in probability band of EFs derived from in-situ measurements in Figure 3.51. However, most of the points are within 50% CI limit in the probability band of EFs derived from EMRs.
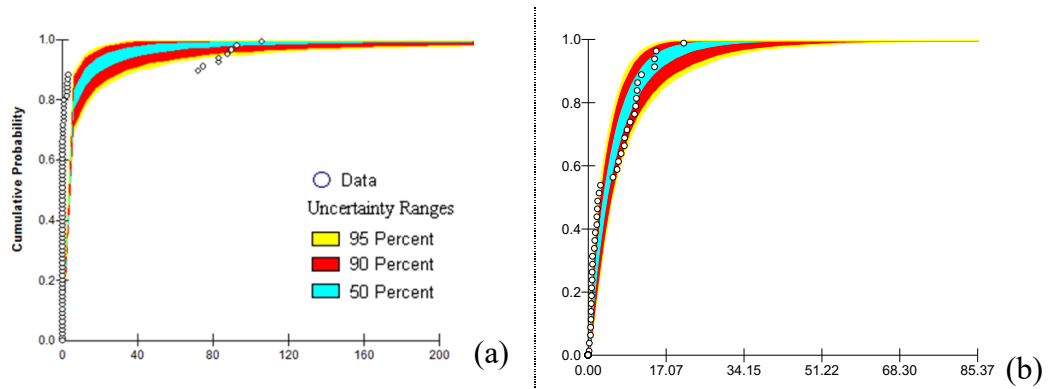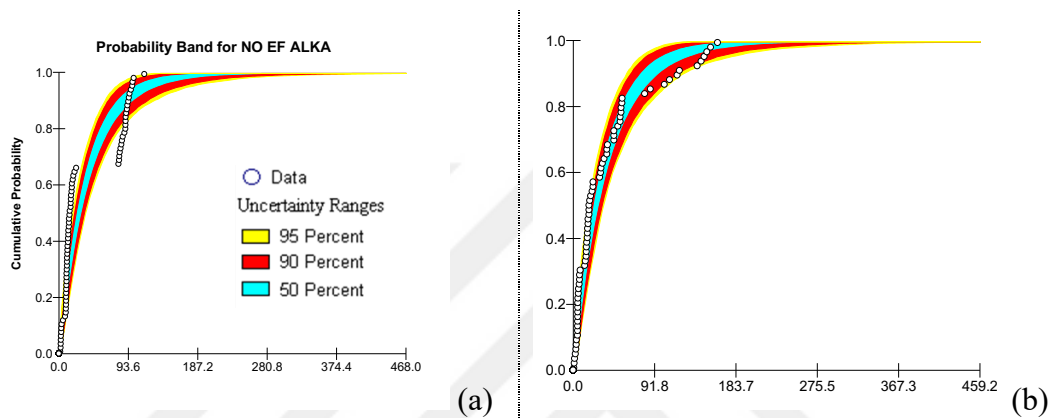
Figure 3.51 : Probability band of CO EFs for "1A1a-10104-3.17" as cumulative distribution of Weibull distribution fitted to CO EFs derived from (a)in-situ measurements (b) EMRs.

SO₂

Summary statistics of SO_2 EFs for "1.A.1.a–10104–3.17" SNAP/NFR category are given in Table 3.72 for EFs derived from both in-situ measurements and EMRs. Standard deviation, variance and Cv are calculated pretty large in EFs derived from in-situ measurements, which indicate large variability between EFs. They are also high in EFs derived from EMRs but not as high as in-situ EFs.

Table 3.72 : Summary statistics of SO_2 EFs derived from both in-situ measurements and EMRs for "1.A.1.a–10104–3.17".

	In-situ Measurements	EMR
Number of data points	72	27
Minimum	0	0
Maximum	2.13	28.2 [6]
Median	0	0.98
Variance [1]	0.13	71
Standard Deviation [2]	0.36	8.3
Cv (%) [3]	407	215
Skewness [4]	5.23	2.61
Kurtosis [5]	27.8	5.33

[1] According to equation 2.12
[2] According to equation 2.13
[3] According to equation 2.14
[4] According to equation 2.15
[5] According to equation 2.16
[6] In one plant which uses refinery gas as fuel

Since the power plants considered in calculations are generally use natural gas as fuel and sulphur content of natural gas is low, SO_2 EFs are generally around 0. This is clearly seen in the CDFs given in Figure 3.52. Since the majority of the EFs is around zero, small number of EFs greater than zero contribute significantly to the variability.

Hence, Cv is so large in in-situ EFs and EMR EFs. EFs derived from both in-situ measurements and EMRs have close Kurtosis and Skewness values.

According to Figure 3.52, Lognormal and Weibull parametric distributions seem best fitting distributions for in-situ EFs, where Weibull and Gamma distributions are appropriate for EMR EFs. In addition to CDF and histograms given in Figure 3.52, goodness-of-fit criteria are also calculated in order to determine best fitting parametric probability distribution function for our data, and given in Table 3.73 for EFs derived from in-situ measurements.
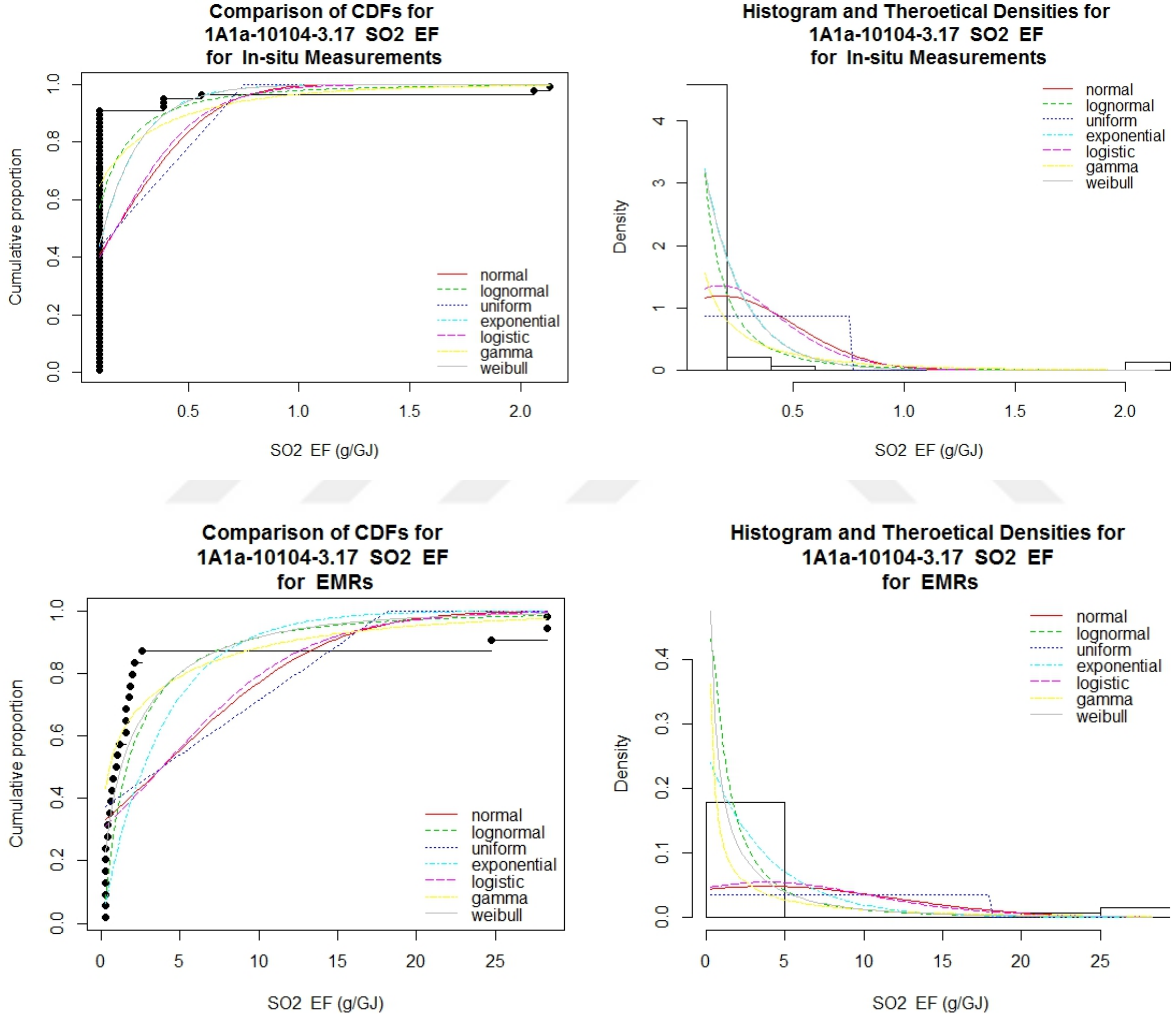
Figure 3.52 : Distribution fitting comparisons of SO$_2$ EF on CDF and Histogram for both in-situ measurements (above) and EMRs (below) of "1.A.1.a–10104-3.17".

Critical value of Kolmogorov-Smirnov statistic is 0.222 for EFs of in-situ measurements, as it is given in Table 2.9. All of the distribution's passed critical value of Kolmogorov-Smirnov statistic (0.222). However, Weibull distribution is minimum in almost all goodness-of-fit statistics and criteria for in-situ EFs. Finally, best fitting

distribution is selected as the Weibull distribution for SO_2 EFs derived from in-situ measurements. Weibull distribution is also considered as best fitting distribution for EFs derived from EMRs. Goodness-of-fit statistics of EMR EFs are given in Attachment F.

Table 3.73 : Goodness-of-fit statistics/criteria for SO_2 EF derived from in-situ measurements of "1.A.1.a–10104-3.17".

Type of distribution	Goodness-of-fit statistics			Goodness-of-fit criteria	
	Kolmogorov-Smirnov statistic	Cramer-von Mises	Anderson-Darling statistic	Akaike's Information Criterion	Bayesian Information Criterion
Normal	0.50	4.84	22.9	59.11	63.66
Lognormal	0.91	18.48	1074	557	562
Uniform	0.48	4.77	-	-	-
Exponential	0.91	18.49	616.39	-213.7	-211.4
Logistic	0.52	4.91	22.7	15.9	20.45
Gamma	0.47	4.65	**21.15**	-1297	-1292
Weibull	**0.49**	**4.72**	22.22	**-1371**	**-1366**

* Bold values indicate lowest values.

After assigning best fitting parametric distribution, Monte Carlo simulation is applied as in Section 2.2.4.4 and Bootstrap method is applied as in 2.2.4.5. Then average EF and confidence intervals are calculated for each of in-situ EFs and EMR EFs and given in Table 3.74. It is seen that in-situ EF is one seventeenth of in EMR-EF, however it is compatible with EMEP and EPA EFs.

Table 3.74 : Uncertainty analysis results for SO_2 EF of "1.A.1.a–10104-3.17" and comparisons with other studies.

	In-situ measurements	EMR	EMEP [54]	EPA [193]
Fitted distribution type	Weibull	Weibull		
Mean	0.176	3.11	0.281	
95% CI (Lower, Upper) as g/GJ	0.118-0.257	1.75-5.02	0.169-0.393	0.25 [3]
% Uncertainty (Lower, Upper)	33-46	44-61	40-40	g/GJ
First parameter	-2.5 [1]	2.69 [1]		
Second parameter	1.24 [2]	0.77 [2]		

[1] scale parameter (k) for Weibull parametric probability distribution function
[2] shape parameter (c) for Weibull parametric probability distribution function
[5] for uncontrolled combustion of natural gas by reciprocating engines for production of electricity (SCC is 20100202)

Although EF derived from in-situ measurements (0.176 g/GJ) appears to be well calculated and appropriate when compared to literature, almost all points are beyond 50% CI limits. This is due to the large number of zero values. Consequently, country

specific SO$_2$ EF is accepted as 0.176 g/GJ for "1.A.1.a–10104-3.17" SNAP/NFR category.
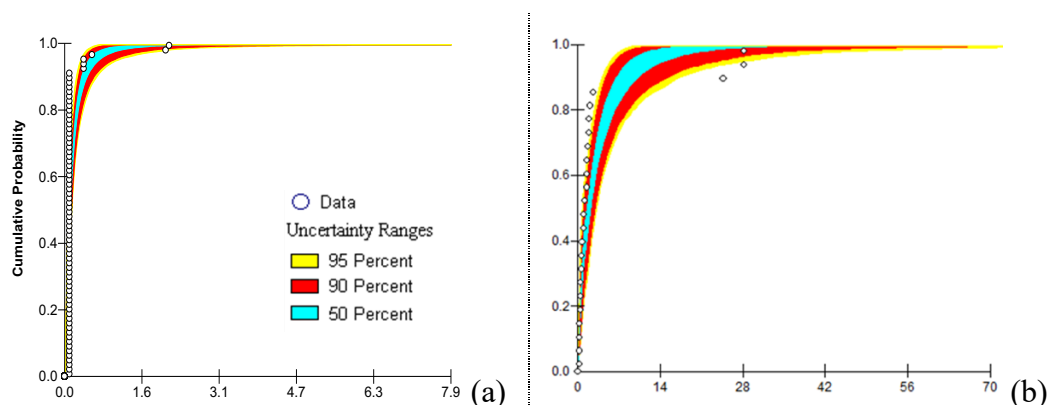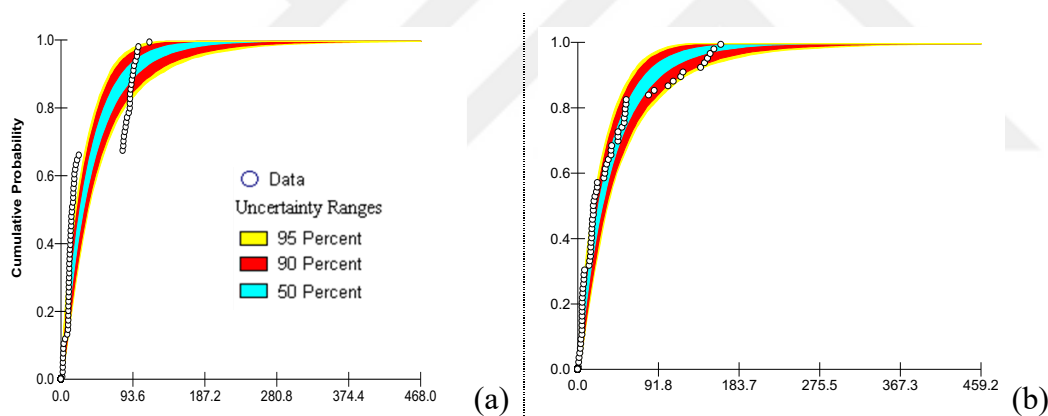

Figure 3.53 : Probability band of SO$_2$ EFs for "1A1a-10104-3.17" as cumulative distribution of Weibull distribution fitted to SO$_2$ EFs derived from (a) in-situ measurements (b) EMRs.

NO

Summary statistics of NO EFs for "1.A.1.a–10104–3.17" SNAP/NFR category are given in Table 3.75 for EFs derived from both in-situ measurements and EMRs. Standard deviation, variance and Cv are calculated large in both EMR and in-situ measurements, which indicate large variability between EFs. As it is clear on the Cv, maximum, minimum and median in Table 3.75, variability between emission factors are large. There is positive skewness in the EFs derived from both in-situ measurements and EMRs, where both sources have negative Kurtosis.

Table 3.75 : Summary statistics of NO EFs derived from both in-situ measurements and EMRs for "1.A.1.a–10104–3.17".

	In-situ Measurements	EMR
Number of data points	72	71
Minimum	1.99	0.99
Maximum	115.35	163
Median	14.61	17.98
Variance [1]	1445	1935
Standard Deviation [2]	38	44
Cv (%) [3]	100	114
Skewness [4]	0.73	1.56
Kurtosis [5]	-1.3	1.41

[1] According to equation 2.12
[2] According to equation 2.13
[3] According to equation 2.14
[4] According to equation 2.15
[5] According to equation 2.16

CDFs and histograms are given in the Figure 3.54 with possible fitting options. According to Figure 3.54, looking at the CDF and histogram of EFs derived from in-situ measurements, EFs are distributed around two peak values. One of it is between 0 and 20, and the other one is more than 85 g/GJ. In the CDF and histogram of EFs derived from EMRs, EFs are homogenously distributed between 0.99 and 163, however variability is high since they are distributed in a wide range of values.
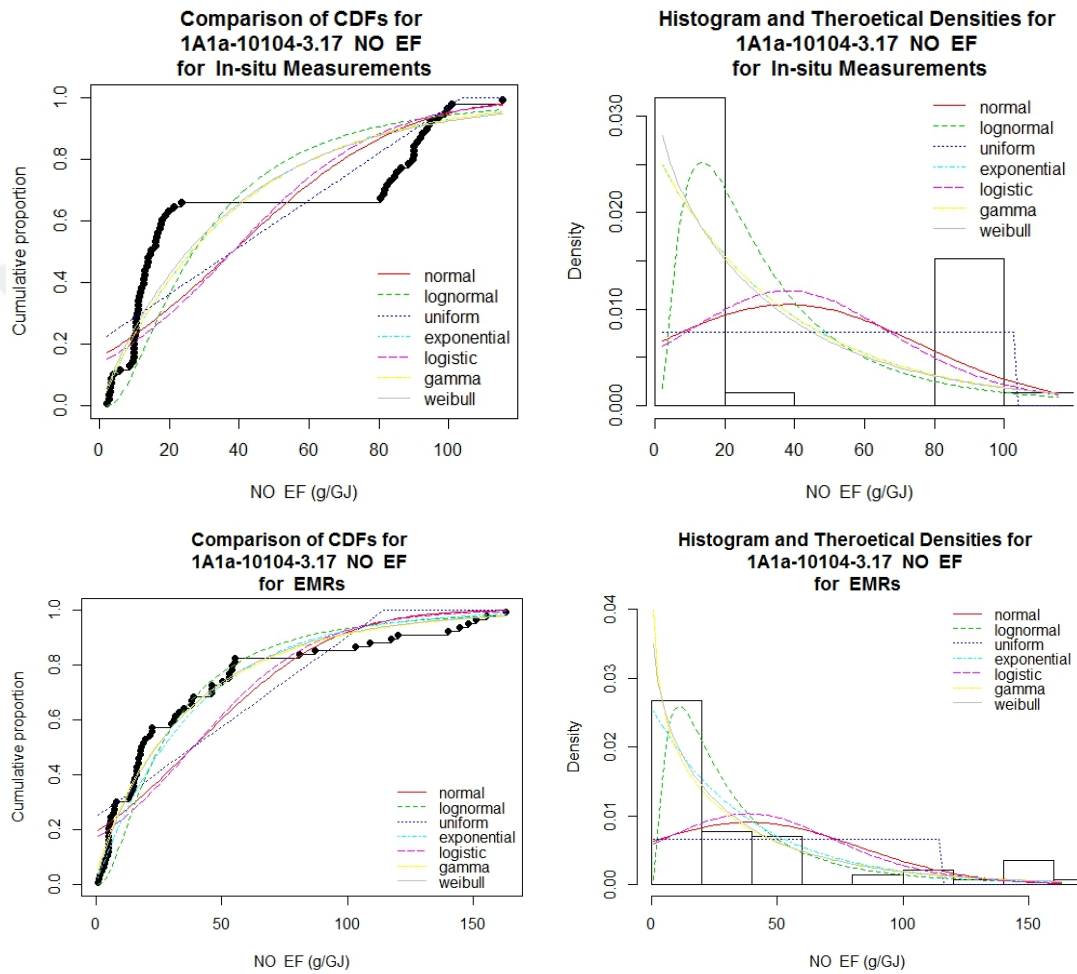
Figure 3.54 : Distribution fitting comparisons of NO EF on CDF and Histogram for both in-situ measurements (above) and EMRs (below) of "1.A.1.a–10101–3.10".

According to Figure 3.54, looking at the CDF and histogram of EFs derived from in-situ measurements, none of the distribution is best for in-situ EFs due to high variability. In this case, Uniform distribution may be considered. In addition to CDF and histograms given in Figure 3.54, goodness-of-fit statistics and goodness-of-fit criteria for NO EFs derived from in-situ measurements were also calculated and given

in Table 3.76, in order to determine best fitting parametric probability distribution function for our data.

Table 3.76 : Goodness-of-fit statistics/criteria for NO EF derived from in-situ measurements of "1.A.1.a–10104–3.17".

Type of distribution	Goodness-of-fit statistics			Goodness-of-fit criteria	
	Kolmogorov-Smirnov statistic	Cramer-von Mises	Anderson-Darling statistic	Akaike's Information Criterion	Bayesian Information Criterion
Normal	0.32	1.77	9.49	732.22	736.77
Lognormal	0.30	2.15	13.70	692.76	697.31
Uniform	0.28	1.37	-	-	-
Exponential	0.24	1.06	5.77	669.80	672.07
Logistic	0.34	2.03	11.03	741.62	746.17
Gamma	0.24	1.06	5.76	671.79	676.34
Weibull	**0.22**	**0.92**	**5.11**	**671.46**	**676.01**

Critical value of Kolmogorov-Smirnov statistic is 0.222 for EFs of in-situ measurements, as it is given in Table 2.9. All of the distribution's passed critical value of Kolmogorov-Smirnov statistic (0.222), except Weibull. Besides, Weibull distribution appears to be the best fitting distribution since it has the lowest values for entire of goodness-of-fit statistics and criteria. Weibull distribution is also considered as best fitting distribution for EFs derived from EMRs. Goodness-of-fit statistics of EMR EFs are given in Attachment F.

Table 3.77 : Uncertainty analysis results for NO EF of "1.A.1.a–10104–3.17" and comparisons with other studies.

	In-situ measurements	EMR	EMEP [54]	EPA [193]
Fitted distribution type	Weibull	Weibull		
Mean	36.7	35.8	48 [3]	between
95% CI (Lower, Upper) as g/GJ	29.1-45.8	27.8-44.8	28-68	42.5 [4]
Uncertainty (Lower, Upper) as %	21-25	22-25	42-42	and 137
First parameter	36.8 [1]	35.77 [1]		[5] g/GJ
Second parameter	0.99 [2]	0.97 [2]		

[1] scale parameter (k) for Weibull parametric probability distribution function
[2] shape parameter (c) for Weibull parametric probability distribution function
[3] as NOx
[4] as NOx for controlled (pre-combustion chamber) combustion of natural gas with turbines (SCC is 20100201)
[5] as NOx for uncontrolled combustion of natural gas with turbines (SCC is 20100201)

After assigning best fitting parametric distribution, Monte Carlo simulation is applied as in Section 2.2.4.4 and Bootstrap method is applied as in 2.2.4.5. Then average EF and confidence intervals are calculated for each of in-situ EFs and EMR EFs and given

in Table 3.77. It is seen that the EFs derived from both in-situ measurements and EMRs are close to each other. Probability bands are created and given in Figure 3.55. Due to the high variability between in-situ EFs and because the data is clustered around two ends of in-situ EFs, almost all EFs of in-situ measurements fall above the 50% CI range, which is an indicator of a bad fit [219]. It is not possible to determine a better representing distribution from the available distribution types for in-situ EFs. Nevertheless, it can be used as country specific EF since it is compatible with other studies as indicated in Table 3.77.

Figure 3.55 : Probability band of NO EFs for "1A1a-10104-3.17" as cumulative distribution of Weibull distribution fitted to NO EFs derived from (a) in-situ measurements (b) EMRs.

Consequently, country-specific EF of NO is calculated as 36.7 g/GJ, where it is 35.8 g/GJ for EF derived from EMR.

NO$_2$

Summary statistics of NO$_2$ EFs for "1.A.1.a–10104–3.17" SNAP/NFR category are given in Table 3.78 for EFs derived from both in-situ measurements and EMRs. Standard deviation, variance and Cv are calculated large in both EMR and in-situ measurements, which indicate large variability between EFs. As it is clear on the maximum, minimum and median, variability between emission factors are large. There is positive skewness in the EFs derived from both in-situ measurements and EMRs, where both of them have negative Kurtosis.

Table 3.78 : Summary statistics of NO$_2$ EFs derived from both in-situ measurements and EMRs for "1.A.1.a–10104–3.17".

	In-situ Measurements	EMR
Number of data points	72	61
Minimum	3.06	0.28
Maximum	186.03	264.3
Median	23.72	25.6
Variance [1]	3770	5820
Standard Deviation [2]	61.4	76.3
Cv (%) [3]	100	138
Skewness [4]	0.73	1.7
Kurtosis [5]	-1.36	1.48

[1] According to equation 2.12
[2] According to equation 2.13
[3] According to equation 2.14
[4] According to equation 2.15
[5] According to equation 2.16

CDFs and histograms are given in the Figure 3.56 with possible fitting options.
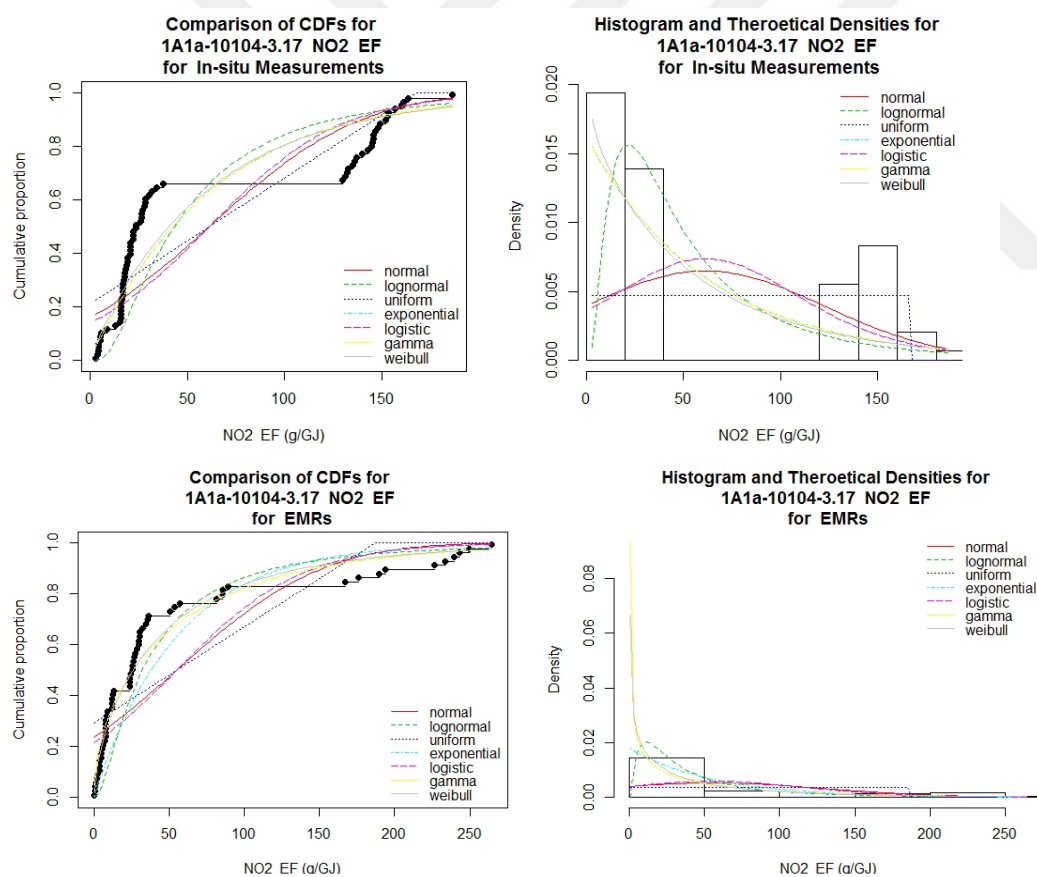
Figure 3.56 : Distribution fitting comparisons of NO$_2$ EF on CDF and Histogram for both in-situ measurements (above) and EMRs (below) of "1.A.1.a–10104–3.17".

According to Figure 3.56, looking at the CDF and histogram of EFs derived from in-situ measurements, EFs are distributed around two peak values. One of it is between 0 and 35, and the other one is more than 140 g/GJ. In the CDF and histogram of EFs

derived from EMRs, EFs are distributed more homogenous than in-situ EFs (between 0.28 and 263.4), however variability is high since they are distributed within a wide range of values.

According to Figure 3.56, looking at the CDF and histogram of EFs derived from in-situ measurements, none of the distribution is best due to high variability. In this case Uniform distribution may be considered. In addition to CDF and histograms given in Figure 3.56, goodness-of-fit statistics and goodness-of-fit criteria for NO_2 EFs derived from in-situ measurements are also calculated and given in Table 3.79, in order to determine best fitting parametric probability distribution function for our data.

Table 3.79 : Goodness-of-fit statistics/criteria for NO_2 EF derived from in-situ measurements of "1.A.1.a–10104–3.17".

Type of distribution	Goodness-of-fit statistics			Goodness-of-fit criteria	
	Kolmogorov-Smirnov statistic	Cramer-von Mises	Anderson-Darling statistic	Akaike's Information Criterion	Bayesian Information Criterion
Normal	0.32	1.76	9.45	801.25	805.80
Lognormal	0.30	2.13	13.75	763.71	768.27
Uniform	0.28	1.37			
Exponential	0.24	1.05	5.72	**738.78**	**741.06**
Logistic	0.35	2.02	10.98	810.64	815.19
Gamma	0.24	1.05	5.70	740.77	745.33
Weibull	**0.22**	**0.90**	**5.01**	**740.40**	**744.96**

Critical value of Kolmogorov-Smirnov statistic is 0.222 for EFs of in-situ measurements, as it is given in Table 2.9. All of the distribution's passed critical value of Kolmogorov-Smirnov statistic (0.222), except Weibull. Besides, Weibull distribution appears to be the best fitting distribution since it has low values for most of goodness-of-fit statistics and criteria. Weibull distribution is also considered as best fitting distribution for EFs derived from EMRs. Goodness-of-fit statistics of EMR EFs are given in Attachment F.

After assigning best fitting parametric distribution, Monte Carlo simulation is applied as in Section 2.2.4.4 and Bootstrap method is applied as in 2.2.4.5. Then average EF and confidence intervals are calculated for each of in-situ EFs and EMR EFs and given in Table 3.80. It is seen that the EFs derived from both in-situ measurements and EMRs are close to each other.

Table 3.80 : Uncertainty analysis results for NO_2 EF of "1.A.1.a–10104–3.17" and comparisons with other studies.

	In-situ measurements	EMR	EMEP [54]	EPA [193]
Fitted distribution type	Weibull	Weibull		
Mean	59.4	48.7	48 [3]	betwee
95% CI (Lower, Upper) as g/GJ	45.9-74	34.4-65.6	28-68	n 42.5 [4]
Uncertainty (Lower, Upper) as %	23-25	29-35	42-42	and 137
First parameter	59.3 [1]	0.761 [1]		[5] g/GJ
Second parameter	0.99 [2]	50.75 [2]		

[1] scale parameter (k) for Weibull parametric probability distribution function
[2] shape parameter (c) for Weibull parametric probability distribution function
[3] as NOx
[4] as NOx for controlled (pre-combustion chamber) combustion of natural gas with turbines (SCC is 20100201)
[5] as NOx for uncontrolled combustion of natural gas with turbines (SCC is 20100201)

Probability bands are created and given in Figure 3.57. Due to the high variability between in-situ EFs and because the data is clustered around two ends of in-situ EFs, almost all EFs of in-situ measurements fall above the 50% CI range, which indicates bad fitting of the distribution [219].

Figure 3.57 : Probability band of NO_2 EFs for "1A1a-10104-3.17" as cumulative distribution of Weibull distribution fitted to NO_2 EFs derived from (a) in-situ measurements (b) EMRs.

It is not possible to determine a better representing distribution from the available distribution types for in-situ EFs. Nevertheless, it can be used for country specific EF since it is compatible with other studies as indicated in 0. Consequently, country-specific EF of NO_2 is calculated as 59.4 g/GJ, where it is 48.7 g/GJ for EF derived from EMR.

NO$_x$

NOx EF is calculated as the sum of NO and NO$_2$ emissions. However, since the uncertainty levels of NO and NO$_2$ EFs are different, the formulas given in equation 2.1a-2.1d were applied in order to calculate total uncertainty of NO$_x$ EF. NO$_x$ EF of "1.A.1.a–10104–3.17" SNAP/NFR category and comparisons with other studies are given in Table 3.81.

Table 3.81 : NO$_x$ EF of "1.A.1.a–10104–3.17" and comparisons with other studies.

	In-situ Measurements	EMR	EMEP [54]	EPA [193]
NOx EF (NO+NO$_2$) as g/GJ	96.1	95.2	48	between
95% CI (Lower, Upper) as g/GJ	80.61-113.3	68.9-106.1	28-68	42.5 [1]
% Uncertainty (Lower, Upper)	16-18%	28-11.5%	42-42%	and 137 [2]
NO/NO$_2$ share	0.62	0.60		g/GJ

[1] as NOx for controlled (pre-combustion chamber) combustion of natural gas with turbines (SCC is 20100201)

[2] as NOx for uncontrolled combustion of natural gas with turbines (SCC is 20100201)

Country specific NO$_x$ EF is calculated as 96.1 g/GJ which is compatible with EMRs. NO$_x$ EF is almost three times of EMEP EF [54], which is 48 g/GJ. NO$_x$ EF is within EF range of EPA EFs [193]. There is no NO$_x$ abatement technology in the plants considered in this study.

The ratio of NO and NO$_2$ is 0.6 for both of in-situ EFs and EMR EFs for "1.A.1.a–10104–3.17" SNAP/NFR category.

3.2.6 Comparison of EFs

Comparison of dust EFs according to SNAP/NFR codes are given in Figure 3.58. In general, in-situ dust EFs are quite low compared to EMEP [54] and EPA [193] EFs. In addition, the EFs obtained from EMRs are significantly lower than the literature although they are more than in-situ measurements, as it is clear on Figure 3.58.
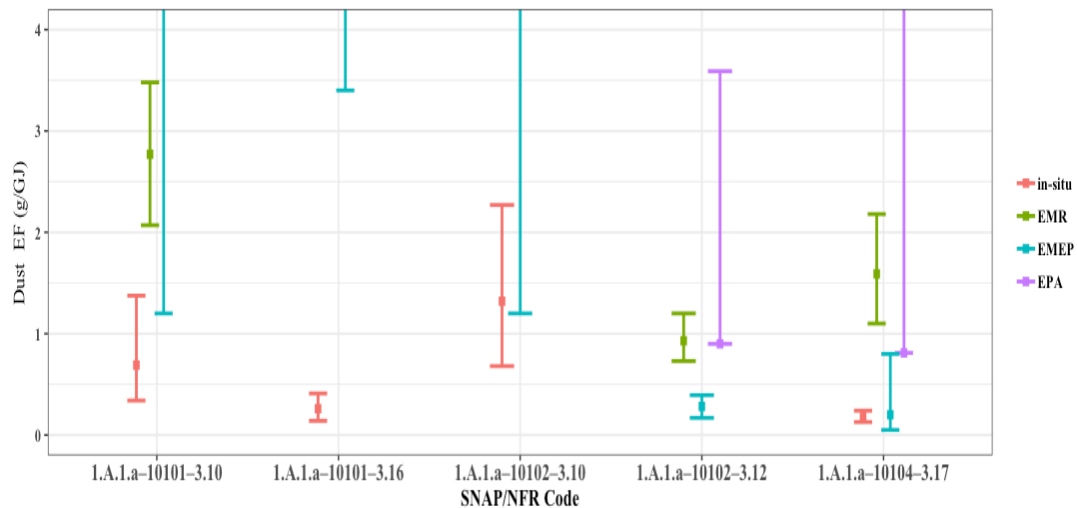
Figure 3.58 : Comparison of dust EFs according to SNAP/NFR codes.

The reason of these large differences between in-situ measurements and literature EFs may be due to wide usage of abatement technologies in Turkish energy production plants. The highest in-situ dust EF (1.32 g/GJ) is calculated for the plants with a capacity range between 50 and 300 MW and producing energy by combusting brown coal and lignite (SNAP/NFR codes are 1A1a-10102-3.10). This EF is also compatible with EMEP EF [54]. The lowest in-situ dust EF (0.179 g/GJ) is calculated for the plants combusting gaseous fuels with gas turbines (SNAP/NFR codes are 1A1a-10104-3.17). However, this EF is so low when compared to EMR and EPA EFs, but compatible with EMEP EF [54].

Comparison of CO EFs according to SNAP/NFR codes are given in Figure 3.59. Largest in-situ CO EFs is in power plants with a capacity larger than 300 MW (SNAP/NFR code is 1A1a-10101-3.10). Furthermore in-situ CO EF is also larger than EMR, EMEP [54] and EPA [193] EFs in 1A1a-10101-3.10 and 1A1a-10104-3.17 (plants combusting gaseous fuels with gas turbines).
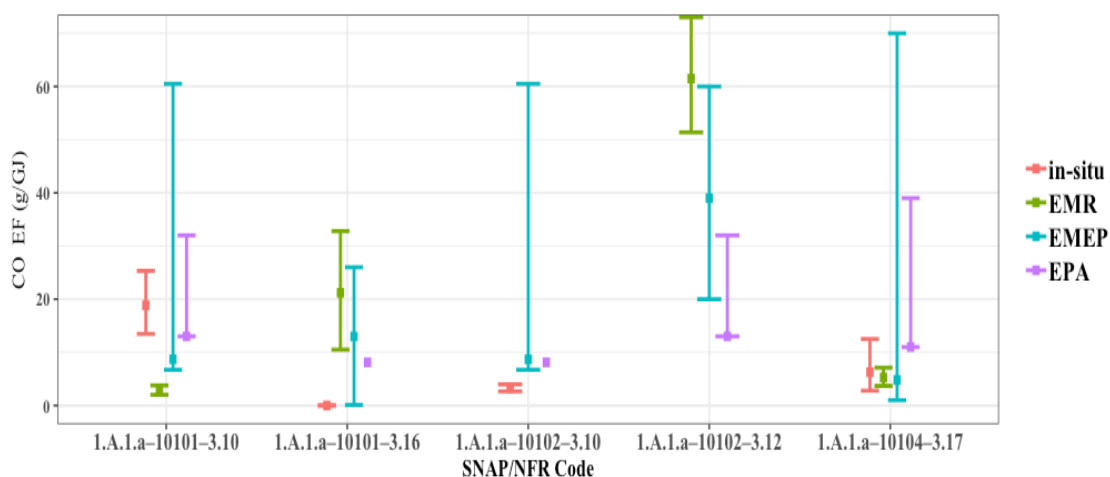
Figure 3.59 : Comparison of CO EFs according to SNAP/NFR codes.

In Figure 3.59, EMR EFs are larger than in-situ EFs in 1A1a-10101-3.16. Furthermore, EMR EFs are also larger than EMEP [54] and EPA [193] EFs in 1A1a-10101-3.16 and 1A1a-10102-3.12.

Comparison of SO_2 EFs according to SNAP/NFR codes are given in Figure 3.60. Upper bound of EMEP EFs stretches up to 5000 g/GJ in 1A1a-10101-3.10, 1A1a-10101-3.16 and 1A1a-10102-3.10. Largest in-situ SO_2 EF (229.2 g/GJ) is in power plants with a capacity larger than 300 MW (SNAP/NFR code is 1A1a-10101-3.10). It is also less than EMEP EF range, however compatible with EPA EF. In-situ EF of 1A1a-10102-3.10 is also less than EMEP EF. Lowest SO_2 EF is in 1A1a-10104-3.17. In-situ SO_2 EF is lowest in 1A1a-10104-3.17, but compatible with EMEP EF range.
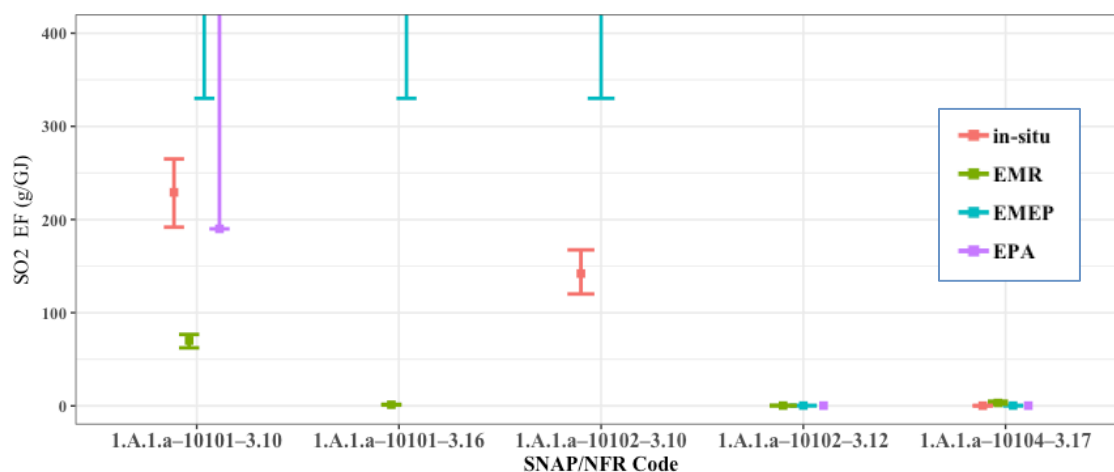
Figure 3.60 : Comparison of SO_2 EFs according to SNAP/NFR codes.

Comparison of NO, NO_2 and NO_x EFs according to SNAP/NFR codes are given in Figure 3.61. Average of in-situ NO (Figure 3.61a) and NO_2 (Figure 3.61b) EFs (shown as square dots on the figure) are larger than all other EFs. As a result of that, in-situ

NO$_x$-EFs are larger than all other EFs. As explained in Section 3.2, NOx EFs are calculated as sum of NO and NO$_2$ EFs, however uncertainty levels are calculated in a different way as explained in section 2.2.4.6.

Although country specific (in-situ) NOx EF is larger than all other studies, range of confidence interval is narrow when compared to them. This situation indicates low uncertainty in in-situ EFs. The largest NOx EF (583 g/GJ) is in 1A1a-10102-3.10 which is compatible with both EMEP and EPA EF ranges.
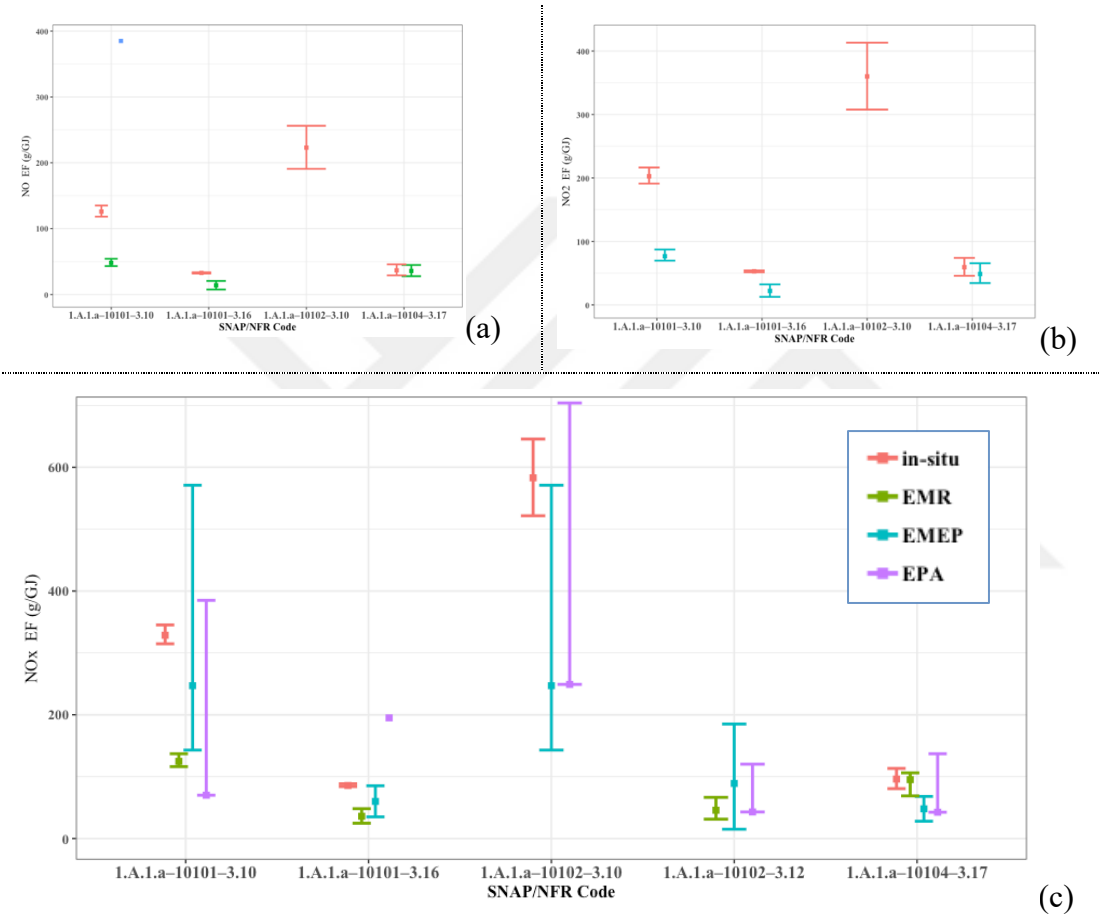
Figure 3.61 : Comparison of (a)NO (b)NO$_2$ (c)NO$_x$ EFs according to SNAP/NFR codes.

As it is clear in above figures, uncertainty range of in-situ EFs is rather narrow compared to EMR, EPA and EMEP [54] EFs. This is a desired condition in emission inventory calculations.

3.3 Probabilistic Emission Inventory

As discussed in section 3.1.3 , different AQMs (as summarized in Figure 2.1) give poor results in Eastern European countries when compared to Western countries of

Europe, regardless of usage of different AQMs, meteorology models and emission inventories. In this case, the inputs of AQMs came into consideration. As explained in Section 1, most commonly used emission inventories, as an input to the AQMs, by air quality modellers are TNO-MACC [66] and EDGAR-HTAP [60] emission inventories. Detailed information is available in Chapter 1 for those emission inventories.

In this part of study, a sample emission inventory is prepared for public energy production sector of Marmara Region in order to compare with TNO-MACC [66] and EDGAR-HTAP [60] emission inventories. The inventory in this study was prepared for the energy production plants in Marmara Region of Turkey for SO_2, NO_x, CO and dust emissions. Total number of plants considered in this study is 57 where it is 19 in TNO-MACC [66] emission inventory and 34 in EDGAR-HTAP [60] emission inventory.

The comparison charts in this section will show 5 titles: "This study", "EMEP", "EPA", "TNO" and "EDGAR-HTAP". The contents of these titles are as follows.

The emission inventory given under the title of "This study" in the following figures is compiled by using country specific EFs calculated in this study for our country (Chapter 3.2). In the absence of country specific EFs, EMEP [54] EFs were used. Consequently, country specific EFs calculated within the context of this study were used for 47 plants of 57. The emission inventory given under the title of "EMEP" in the following figures is compiled for the same plants using the same activity data but with only EMEP [54] EFs. "EPA" titled emission inventory is compiled for the same plants using the same activity data but with only EPA [193] EFs. Here, attention should be paid to the confidence interval of "EPA" inventory on the figure. When determining the upper and lower limits of the EPA, no statistics were made for EFs. This was not possible since the catalogue system is applied in the calculation of uncertainty in EFs of EPA. In order to decide correct EPA EF, more detailed information is needed than in EMEP and other EF sources. Generally, abatement technology should be considered in EF selection. In plants without abatement technology, controlled emissions were accepted as uncontrolled emissions, because the controlled emission left blank would be counted as zero in the inventory total. Hence, the lower bound of the EPA was calculated by using the same activity data with controlled EPA EFs as much as possible, and the upper bound is calculated by using the same activity data with

uncontrolled EPA EFs. Consequently, it is best practice to compare the results of "This study" with the lower bound of "EPA". Middle point is average of these two emission inventories. There are two reasons for adopting this approach in calculation of same emission inventory with EPA EFs. First, it is difficult to achieve the data about emission abatement technologies that are used by the plants in Turkey. Second, the usage practices of the existing abatement technologies are questionable.

In order to facilitate the comparison of the TNO-MACC [66] and EDGAR-HTAP [66] inventories with emission inventory of "This study", the same plants were identified from TNO-MACC [66] and EDGAR-HTAP [66] inventories by using the coordinate information. With the help of a Python code, the coordinate information in these inventories was converted to address information, energy production plants in the Marmara region were extracted and matched with the plants in the emission inventory prepared in the scope of "This study". Then, the sum of the emissions from the facilities in the TNO-MACC [66] inventory was added to the following figures under the title "TNO". Likewise, "EDGAR-HTAP" title in the following figures represents the sum of emissions in EDGAR-HTAP [66] emission inventory for the same power plants as in "This study". Uncertainty calculations include uncertainties arises from EFs only. Uncertainties arising from activity data were excluded and left for future study.

One of the most challenging parts when preparing an emission inventory is the industrial emission inventory part. This is because detailed sectoral information is kept confidential unless it is requested by official means, thus it is difficult to obtain information from Turkish industries. This situation makes a major contribution to the overall uncertainty of the emissions inventory. In the worst case, the facility is not included in the inventory due to data inadequacy. As a matter of fact, this situation is easily seen when TNO-MACC [66] and EDGAR-HTAP [60] emission inventories are examined. Those emission inventories have missing plants especially in industrial part. The number of plants considered in each emission inventory according to regions of Turkey are given in Table 3.82.

In TNO emission inventory which was prepared for 2011 base year, the number of sources under energy production category with SNAP 1 (in SNAP/NFR coding system it matches with 1.A.1 public electricity and heat production) was 19 for Marmara

region of Turkey, where it was 34 in EDGAR-HTAP (version 4.2 prepared for year 2008 [60]) emission inventory (in SNAP/NFR coding system it matches with 1.A.1.a). In this study a deep research was conducted in order to include almost all power plants located in Marmara region of Turkey, and finally it was counted as 57. As it is clear, the EDGAR-HTAP [60] emission inventory contains much more plants than TNO-MACC [66] but is still far from the actual number of plants (57 plants) for Marmara region of Turkey.

Table 3.82 : Number of public electricity and heat production plants considered by TNO-MACC [66] and EDGAR-HTAP [60] emission inventories.

	TNO-MACC	EDGAR-HTAP
base year:	2011	2008
Marmara Region	19	34
Aegean Region	9	20
Black Sea Region	4	9
Eastern Anatolia Region	0	7
South Eastern Anatolia Region	1	4
Central Anatolia Region	10	17
Mediterranean Region	7	9
Total	50	100

When Turkey's other regions are examined, it is seen that TNO-MACC [66] emission inventory has almost no facilities in Eastern and South-Eastern Anatolia regions while EDGAR-HTAP [60] emission inventory has more plants. Furthermore EDGAR-HTAP [60] emission inventory has more plants than TNO-MACC [66] in all regions of Turkey. From this point of view, it is clear that EDGAR-HTAP [60] emission inventory is more inclusive than TNO-MACC [66] emission inventory in Turkey in terms of number of plants, and it is more inclusive in Eastern Anatolian regions of Turkey where TNO-MACC [66] emission inventory has almost no plants for public electricity and heat production sector.

In Figure 3.62, SO_2 emission inventory calculated in the scope of "This study" and their comparisons with other inventories are given. 57 plants were taken into account in the calculation of SO_2 emission. Lignite is used as an energy source in 6 of these 57 power plants, where gaseous fuels are used by 50 plants and motorin is used by 2 plants. Some of the power plants use more than one fuel as the energy source.

3 of the 6 power plants are coal combusting plants with fluid bed boilers (SNAP/NFR code is 1A1a-10101-3.16 for large plants and 1A1a-10102-3.16 for medium size

plants). In this study, in-situ measurements were conducted in one of those three plants. However, as shown in Table 3.27, SO_2 EF was found to be zero in all measurements. This plant is a new plant that was commissioned in 2012, however other plants are old plants. In EMEP, SO_2 EF is given as 1680 g/GJ for uncontrolled conditions. When an average of 95% abatement efficiency of the fluid bed boilers are considered, SO_2 EF as zero is impossible. In such large energy production plants which are burning lignite, since SO_2 EF could not be zero, EMEP EF (1680 g/GJ) was used for these 3 plants.
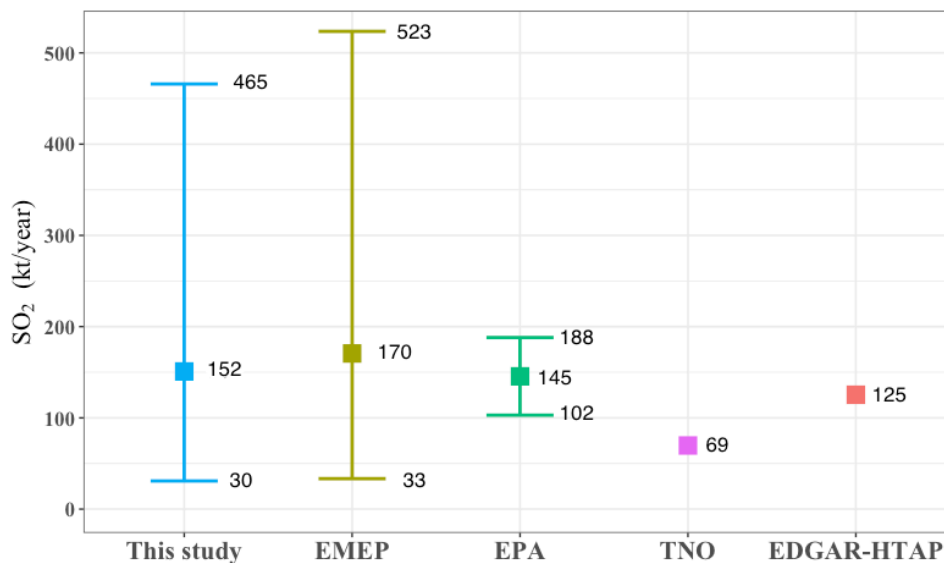
Figure 3.62 : SO_2 emission inventory with uncertainties and comparison with other studies.

2 of the 6 power plants use pulverized coal combustion technology (SNAP/NFR code is 1A1a-10102-3.10). In-situ measurements were conducted within the context of KAMAG project for this category (Table 3.45), and SO_2 EF was calculated as 142 g/GJ which is quite lower than EMEP EF (1680 g/GJ). Since this EF, which is smaller than the EMEP EF, is used for two plants, the final emissions of "This study" appear to be lower than the "EMEP" in Figure 3.62.

It is apparent from Figure 3.62 that, SO_2 emissions are calculated as 152,379 tonne/year in this study. Same activity data is used in calculation of EMEP emission inventory and resulted 170,596 tonne/year. Approximately 19,000 tonne/year difference is mainly due to one plant. Uncontrolled conditions are considered for this one plant in TNO-MACC and EDGAR-HTAP emission inventories.

Of the 57 power plants, 48 generate energy by burning gaseous fuels (mostly natural gas). 47 of these power plants use gas turbines as combustion technology (SNAP/NFR

code is "1A1a-10104-3.17"). Here it is worth explaining that, it is generally assumed that power plant owns a gas turbine when there is no consistent information about the combustion technology of a natural gas burning plant since gas turbines are highly preferred in the combustion of gas fuels. The deepening of the information in this section is left to the future part of this study. In 5 of these 47 facilities, in-situ measurements were carried out within the scope of KAMAG project. As shown in Table 3.74, the EF calculated from these measurements is 0.176 g/GJ and it is consistent with EMEP EF (0.281 g/GJ). This country specific EF was used in all 47 power plants.

As a result, country specific SO_2 EF derived from this study were used in the emission calculation of 48 of the 57 plants. 47 of these 48 facilities are gas-fuelled. The formation of SO_2 emissions from gas fuels is quite low compared to solid and liquid fuels. This means that SO_2 emissions in these 47 plants are expected to be low.

In Figure 3.60, SO_2 emissions are shown on the Marmara region map. The large bubbles show intensive SO_2 emitting power plants which are mainly lignite combusting power plants. Other plants emit very little SO_2 in quantity (because they use gaseous fuels), therefore the size of the representative bubbles was not large enough to be observed visually on the map.

The main reason that the "EDGAR-HTAP" emission inventory is 27,000 tons/year lower than "This study" is due to absence of two lignite-fired incineration plants in the EDGAR-HTAP inventory.

Of the 57 facilities considered in this study, only 17 are in the TNO inventory. As a matter of fact, there are many big and small plants which are not taken into consideration in TNO emission inventory. 4 large lignite combustion plants, which are not included in the TNO inventory, have resulted in 73,500 tons less SO_2 emissions in TNO emission inventory when compared to this study. 1000 tonnes of SO_2 emissions is also not included in the TNO inventory due to about 40 missing natural gas incineration plants.

Figure 3.63 : Map of SO$_2$ emissions calculated according to this study.

The contribution of these missing natural gas plants to SO$_2$ emissions in TNO inventory is not as much as that of lignite, but their absence will be effective in the calculation of NOx emissions. In Figure 3.64, NO$_x$ emission inventory which is calculated in the scope of this study and its comparison with other inventories are given.
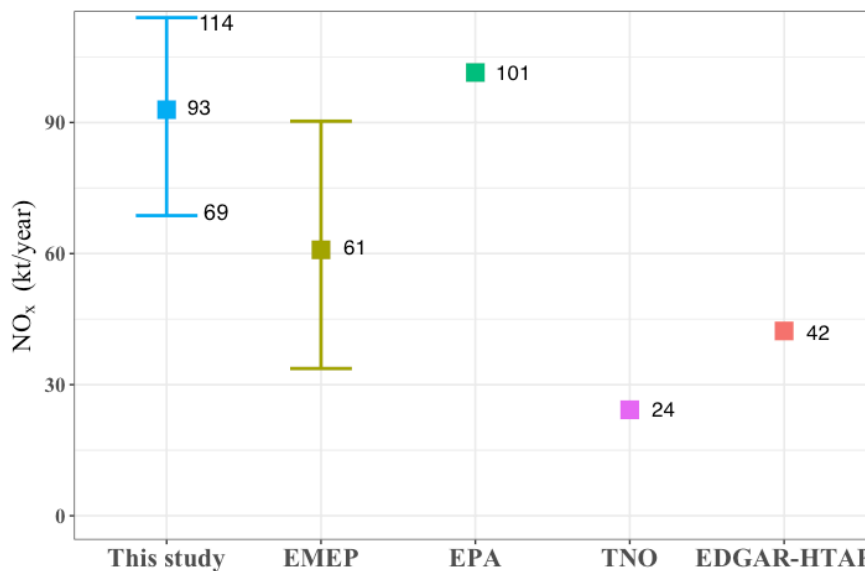
Figure 3.64 : NO$_x$ emission inventory with uncertainties and comparison with other studies.

It should be noted that, "EMEP" emissions are calculated for the same plants and same activity data of "This study" but with EMEP EFs [54]. In this case, NO$_x$ emissions

(93,000 ton/year) calculated within the scope of "This study" is even higher than the upper bound (90,000 ton/year) of the "EMEP" emissions. The reason for this is that NOx EFs calculated in "This study" are generally larger than EMEP EFs, as it is clear on Figure 3.61c.

Although the NO_x emissions calculated in this study (93,000 ton/year) appear to be lower than those calculated with EPA EFs (101,000 ton/year), the difference is acceptable. As it is clear on Figure 3.62, NO_x emissions calculated in this study is considerably higher than TNO (24,000 ton/year) and EDGAR-HTAP (42,000 ton/year). When compared to "This study", TNO inventory has 39 missing plants (yields 45,000 ton/year NO_x emissions less) and EDGAR-HTAP emission inventory has 35 missing plants which yields 33,000 ton/year missing NO_x emissions. NOx emissions are also calculated lower for plants already exist in TNO and EDGAR-HTAP inventories when compared to "This study". This may be due to usage of EMEP EFs in TNO and EDGAR-HTAP inventories.

In Figure 3.65, NO_x emissions are shown on the Marmara region map. Unlike the SO_2 map (Figure 3.63), we see more plants on the NO_x map as there are more plants using natural gas when compared to lignite (natural gas combustion is an effective source of NO_x emissions). It is also known that plants with high NO_x emissions use natural gas as well as fuel oil and diesel when required. These fuels also cause intensive NO_x emissions.

In Figure 3.66, CO emissions are compared. The country-specific CO EFs calculated in this study were generally higher than the EMEP EFs and lower than the EPA EFs, as it is given in Figure 3.59. The effect of these difference is clearly seen on Figure 3.66. The CO inventory (9000 tons/year) calculated using EFs derived from this study was close to, but more than, the inventory calculated using EMEP EFs (6000 tons/year). It is quite low compared to CO emissions calculated with EPA EFs (22,000 ton/year).
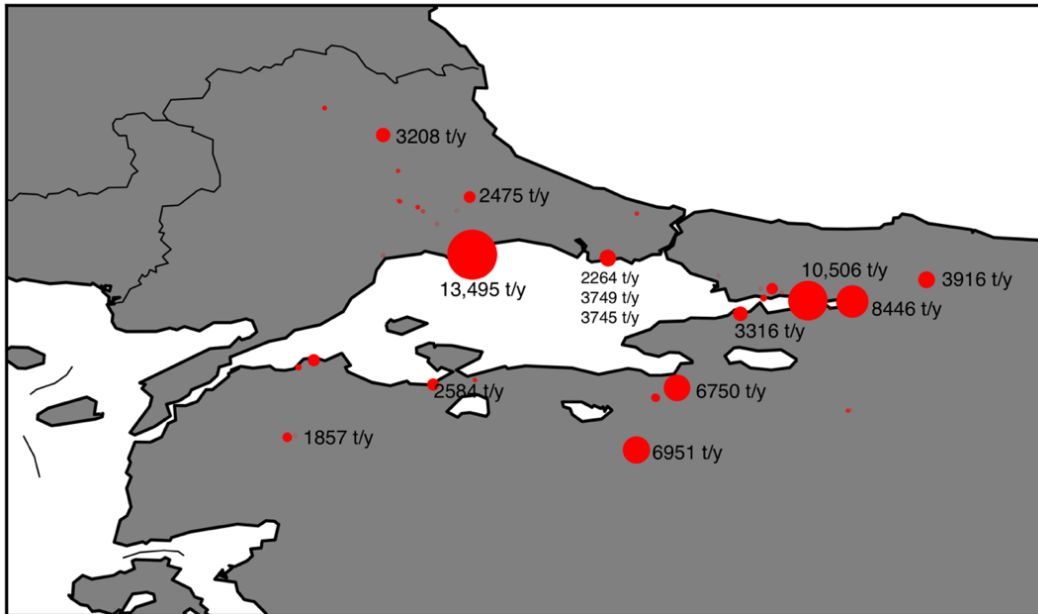
Figure 3.65 : Map of NO_x emissions calculated according to this study.

Unlike on the SO_2 map (Figure 3.63), we see more plants on the NO_x map as there are more plants using natural gas when compared to lignite (natural gas combustion is an effective source of NO_x emissions). It is also known that plants with high NO_x emissions use natural gas as well as fuel oil and diesel when required. These fuels also cause intensive NO_x emissions.

It is seen that the uncertainty range of the inventory prepared with country specific EFs, given under the title of "This study", is quite low compared to EMEP. The same situation is observed in SO_2 (Figure 3.62) and NO_x (Figure 3.64) inventories. Based on these results, it can be said that country-specific calculations reduce uncertainty.
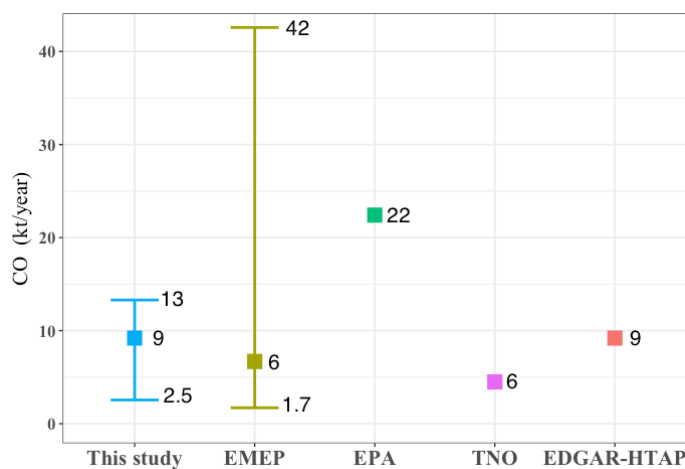
Figure 3.66 : CO emission inventory with uncertainties and comparison with other studies.

198

A total of 4800 tons/year of CO emissions was ignored with 36 missing plants in the EDGAR-HTAP inventory. Despite this incomplete number of CO emission sources in the EDGAR-HTAP inventory, the total amount of CO emissions calculated in EDGAR-HTAP inventory is almost same with "This study". This is due to calculation of approximately 1000 tons/year emissions in the EDGAR-HTAP inventory for only one fuel oil burning plant located in Istanbul. In inventories calculated with neither EPA nor EMEP EFs, such high CO emissions have not been calculated for this plant. Just as in this example, in EDGAR-HTAP inventory, CO emissions from the same plants are generally calculated more than twice of "This study". In other words, although EDGAR_HTAP inventory seems to have the same results with "This study" in terms of total CO emissions, the EDGAR-HTAP inventory is less than that calculated by "This study" in the background.

In Figure 3.67, CO emissions are shown on the Marmara region map. On the map, the CO emissions are mostly emitted by coal firing plants or by the plants using dual fuel. The largest source of CO emissions (1572 g/GJ) is a production facility in Kocaeli using both fuel oil and refinery gas for production of power.

Figure 3.67 : Map of CO emissions calculated according to this study.

In Figure 3.68, dust emissions are compared. Dust emissions calculated in this study are lower than all other studies. Although there is no big difference between EMEP and "This study", EPA's emissions are high, because dust EFs are also high. The difference in the EPA emission inventory, which is significantly higher than this study

and EMEP caused by these 5 lignite burning power plants, because EPA considers that dust emissions of lignite-fired plants are quite high even in controlled conditions. For example, for a plant with the SNAP/NFR code "1A1a-10102-3.16", the EF included in this study was 0.26 g/GJ (generated by in-situ measurements), while it was 10.2 g/GJ in EMEP and 143 g/GJ in EPA for controlled conditions. The reason for this is that the official standards applied for these plants are kept low because of the high amount of dust emission emitted from the coal fired power plants. This means that these plants are equipped with flue gas technologies with high dust reduction efficiency in order to meet regulation and obtain official emission permits. Therefore, dust emission from the stacks is low, so the dust EF is also low in this study.

Moreover, EPA emissions are given as PM_{10}, not dust. TNO and EDGAR-HTAP emissions are also given as PM_{10}. The emissions calculated by TNO and EDGAR for these five plants are close to those calculated with EPA EF. Therefore, TNO and EDGAR emissions are close to each other and close to EPA. Validation of in-situ measurements which were conducted in this study is considered as future study.
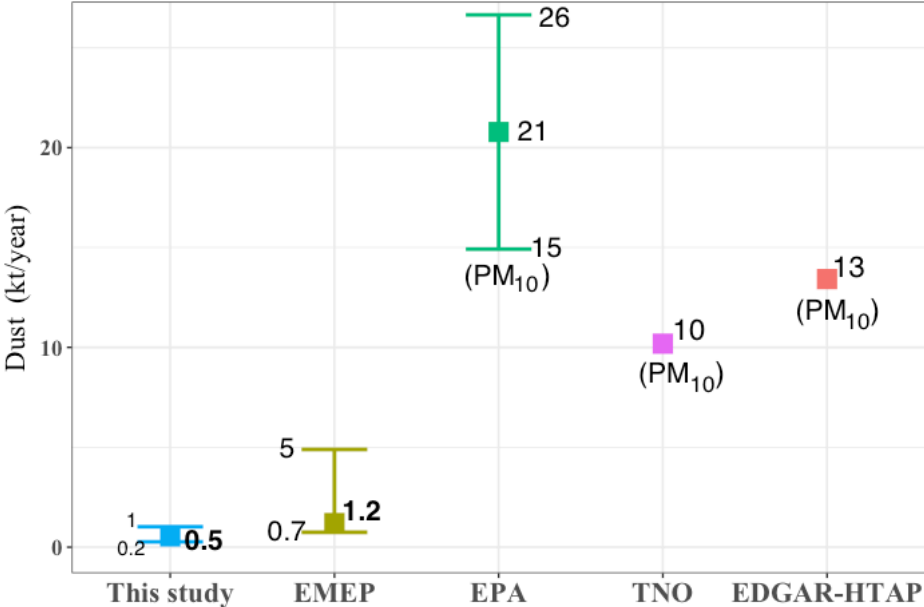
Figure 3.68 : Dust emission inventory with uncertainties and comparison with other studies.

In Figure 3.69, dust emissions are shown on the Marmara region map. As can be seen, dust emissions of all plants are below 300 ton/year. The largest dust emission (292 ton/year) is emitted from a facility in Kocaeli that generates energy by burning fuel oil.

The SO$_2$ emission inventory calculated in this study is more than twice that calculated by TNO. When number of plants considered in TNO (19) and our study (57), it is inferred that, 19 plants were not adequate for representing emission inventory of Marmara Region. Although SO$_2$ emission inventory calculated in this study is 20% higher than the inventory calculated by EDGAR-HTAP, there are unidentified sources of excessive emissions in the EDGAR inventory. Therefore, it is not logical to compare the final values in the EDGAR inventory with the results of this study. Country specific SO$_2$ EFs calculated for coal combustion plants in this study are less than EMEP and more than EPA EFs. Since the impact of coal burning plants is dominant in the SO$_2$ emission calculation, high emissions may be calculated in the inventory if the emissions of these plants are calculated with EMEP EFs.

Figure 3.69 : Map of dust emissions calculated according to this study.

The NO$_x$ emission inventory calculated in this study is approximately four times that calculated by TNO and more than twice that of EDGAR-HTAP. If the same inventory was calculated by using EMEP EFs rather than the EFs calculated within the scope of this study, it would be 35% less. The inventory calculated with EPA EFs is close to the inventory calculated in this study. When calculating the NO$_x$ inventory, the results differ more than the SO$_2$ inventory, because the number of natural gas combustion plants in this region is numerous.

The CO emission inventory calculated in this study is more than twice that calculated by TNO; however, it is same with EDGAR-HTAP inventory. Although CO emission

inventory calculated in this study is almost equal to the inventory calculated by EDGAR-HTAP, there are unidentified sources of excessive emissions in the EDGAR inventory. Therefore, it is not logical to compare the final values in the EDGAR inventory with the results of this study. If the same inventory was calculated by using EMEP EFs rather than the EFs calculated within the scope of this study, it would be 30% less. The country-specific CO EFs calculated in this study were generally higher than the EMEP EFs and lower than the EPA EFs. Therefore, large emissions are calculated in the inventory when the same emission inventory is calculated with EPA EFs.

4. CONCLUSIONS

Correlations between models and PM_{10} observations are 8% less in Eastern European countries when compared to Western European countries where BIAS is 2.5-fold of Western European countries. Furthermore, In Eastern European countries, RMSE is 90%, MAE is 99% and MNE is 25% more than Western European countries. From these results it is clear that, average of model predictions is significantly beyond the observations in East when compared to West Europe.

Turkey, which is located in the Eastern Europe, has one of the worst results calculated by all models. All models predict PM_{10} concentrations with an average of -40 $\mu g/m^3$ BIAS in stations of Turkey, where it is the worst value within 34 countries of Europe considered in this study. Models predict close to each other but quite far from the observations in 80% of the stations in Turkey. Remaining 20% of the stations encounters 18 over 101 stations, and those stations are mostly in Istanbul and in some other big cities. Generally, models predict better in big cities, however they are not good as big cities in small towns.

In Istanbul, MNE is between 29 to 118% where it is between 35 to 64% in Berlin, 9 to 40% in Paris, and 4 to 18% in London. Although models predict well in Istanbul stations when compared to other cities of Turkey, it is clear that those predictions are not good as other metropoles in Europe.

In seasonal evaluation of model predictions in Turkey on station basis, it is seen that emissions cannot be predicted well in Winter, but in Summer it is predicted relatively better. This difference can be caused by inadequate representation of increased emissions (in the model inputs) in Winter months from residential heating and traffic emissions when compared to other months. In this case, it would not be unreasonable to suspect that the inputs to the models do not cover this difference.

Model inputs to the model are considered as a reason for poor model predictions in this study. However, problems caused by the model itself or erroneous measurements, or combination of all, can also cause this. In this study, problems due to the model

itself are out of consideration since 6 different AQMs were used by 13 modelling groups. In stations where model estimates are poor, the CDFs of these 6 AQMs are close to each other, but quite different from the measurements. All models give close CDFs in Western Europe despite they have different modelling configurations, where they are not close to observations in Eastern Europe countries even in same models. In this situation, it would not be wrong to ignore "the problems caused by models" among the primary causes of this poor prediction problem. Problems due to observations are not subject of this study, since number of stations more. Systematic errors are not thought to occur at all stations at the same time.

Emission inventories, which are important inputs of AQMs, do not represent the ultimate result, but the approximate result, unless in-situ measurements and full activity data are available for all sources. Quality of an emission inventory is directly proportional to how close it is to the real value and how low its uncertainty is. Using most representative EFs, or measurements when possible, increases the quality of an emission inventory. In this study, in-situ measurements were conducted within the scope of the KAMAG project in order to generate country-specific EFs and an emission inventory was prepared in the light of the most consistent information possible.

Dust EFs obtained from in-situ measurements are significantly lower than the literature for coal combusting plants. The reason of this large difference between in-situ measurements and literature EFs may be due to wide usage of dust abatement technologies in Turkish energy production plants. CO and SO_2 EFs are significantly larger than EMR, EMEP [54] and EPA [193] EFs in large coal combusting plants and in plants combusting gaseous fuels with gas turbines. But in all EFs, uncertainty is low when compared to EMEP EFs. Country specific NOx EFs are generally larger than all other studies and range of confidence interval is narrow when compared to them. This situation indicates low uncertainty in in-situ EFs.

In emission inventory part of the study, a deep research was conducted in order to include almost all power plants located in Marmara region of Turkey, and finally it was counted as 57. Lignite is used as an energy source in 6 of these 57 power plants, where gaseous fuels are used by 50 plants and motorin is used by 2 plants. Some of the power plants use more than one fuel as the energy source.

EDGAR-HTAP [60] emission inventory contains much more plants (34 plants) than TNO-MACC [66] (19 plants) but is still far from the actual number of plants (57 plants) for Marmara region of Turkey. Furthermore EDGAR-HTAP [60] emission inventory has more plants than TNO-MACC [66] in all regions of Turkey. From this point of view, it is clear that EDGAR-HTAP [60] emission inventory is more inclusive than TNO-MACC [66] emission inventory in Turkey in terms of number of plants, and it is more inclusive in Eastern Anatolian regions of Turkey where TNO-MACC [66] emission inventory has almost no plants for public electricity and heat production sector. There are missing plants in both EDGAR-HTAP and TNO emission inventories. Furthermore, there some unidentified plants in those emission inventories.

NO_x emissions calculated in this study is 93,000 ton/year with lower CI is 69,000 ton/year and upper CI as 114,000 ton/year. When same emission inventory is calculated with EMEP EFs 60,000 ton/year with lower CI as 33,000 and upper CI as 90,000 ton/year. The inventory compiled by this study beyond the upper CI of EMEP and it is considerably larger than TNO (24,000 ton/year) and EDGAR-HTAP (42,000 ton/year). When compared to "This study", TNO inventory has 39 missing plants (yields 45,000 ton/year NO_x emissions less) and EDGAR-HTAP emission inventory has 35 missing plants which yields 33,000 ton/year missing NO_x emissions.

SO_2 emissions are calculated as 152,379 tonne/year in this study. Same activity data is used in calculation of EMEP emission inventory and resulted 170,596 tonne/year. This is mainly due to lower country specific SO_2 EF calculated by this study for lignite firing power plants when compared to EMEP. It is 69,000 ton/year in TNO and 125,00 ton/year in EDGAR-HTAP emission inventory. 4 large lignite combustion plants, which are not included in the TNO inventory, have resulted in 73,500 tons less SO_2 emissions in TNO emission inventory when compared to this study. 1000 tonnes of SO_2 emissions is also not included in the TNO inventory due to about 40 missing natural gas incineration plants. SO_2 uncertainty of this study is between 80 and 209%.

Although SO_2 and CO emission inventories of TNO is within the uncertainty range of this study, they are close to lower bound of confidence intervals. Furthermore SO_2 and CO emission inventories are approximately half of this study. In EDGAR-HTAP emission inventory CO emissions are close to each other however emissions are not equal on plant basis. This means that, emissions are not representative for the plants in

EDGAR-HTAP emission inventory although overall emissions are same with this study. This situation causes large uncertainty other than counted by this study.

Uncertainty range of NO_x emission inventory of this study is between 26 (lower) to 23% (upper). When same emission inventory is compiled with EMEP EFs, overall uncertainty range is 45 (lower) to 48% (upper). As it is clear, country specific EFs decrease uncertainty when compared to usage of EFs from literature. This situation is dominant in NO_x emission inventory than SO_2 and CO emission inventories, because number of natural gas combusting power plants are large (48 over 57 plants in Marmara region). TNO and EDGAR HTAP emission inventories are out of the uncertainty range of this study.

In this study a deep uncertainty analysis technique is applied which is including Monte Carlo and Bootstrap simulations. The uncertainty analysis described in this study can be used as a basis for developing probabilistic emission inventories, which in turn can be used to determine the likelihood that an emission budget will be met and an as input to air quality models. At the end, probabilistic emission inventories may be used to etermine the likelihood that air quality management goals will be achieved.

No matter how many and high-quality measurements are conducted, no matter how good models are used, it is not possible for air quality models to predict accurate results without a good emission inventory. Therefore, consistent, low uncertainty and comprehensive emission inventories should be compiled for the Eastern European countries, including Turkey. Development country specific EFs is the preliminary step of emission inventory development. Access to activity data used in these studies should be facilitated in order to make room for calculation of the representative EFs easily.

REFERENCES

[1] **Environmental Protection Agency** (2018). NAAQS Table. Retrieved June 18, 2019, from: https://www.epa.gov/criteria-air-pollutants/naaqs-table.

[2] **Brunekreef, B., Dockery, D.W., Krzyzanowski, M.** (1995). Epidemiologic Studies on Short-Term Effects of Low Levels of Major Ambient Air Pollution Components. *Environmental Health Perspectives*. Mar 1995; *103* (Suppl 2), 3–13.

[3] **Schwartz, J., Dockery, D.W., Neas, L.M.** (1996). Is daily mortality associated specifically with fine particles? *Journal of Air Waste Management Association*, *46*, 2–14.

[4] **Samet, J.M., Dominici, F., Currieror, F.C., Coursac, I., Zeger, S.L.** (2000). Fine particulate air pollution and mortality in 20 US cities, 1987–1994. *N Engl J Med*, *343*:1742–9.

[5] **European Environment Agency** (2013). Air Quality in Europe – 2013 Report. Retrieved May 14, 2018, from http://www.eea.europa.eu/publications/air-quality-in-europe-2013

[6] **Kim, K.-H., Kabir, E., Kabir, S.,** (2015). A review on the human health impact of airborne particulate matter. *Environ. Int*., *74*, 136-143.

[7] **Juda-Rezler, K., Reizer, M., Oudinet, J.P.** (2011). Determination and analysis of PM_{10} source apportionment during episodes of air pollution in Central Eastern European urban areas. The case of wintertime. *Atmospheric Environment*, *45*, 6557–66.

[8] **Sacks J., D., Stanek, L.W., Luben, T., J., Johns, D.O., Buckley, B.J., Brown, J.S., Ross** (2011). *M. Environ Health Perspect*, *119*(4), 446-54. doi: 10.1289/ehp.1002255. Epub. Review.

[9] **Karagulian F., Belis, C.A., Dora, C.F.C., Prüss-Ustün, A.M., Bonjour, S., Adair-Rohani, H., Amann, M.** (2015). Contributions to cities' ambient particulate matter (PM): A systematic review of local source contributions at global level. *Atmospheric Environment*, *120*, 475-483. https://doi.org/10.1016/j.atmosenv.2015.08.087

[10] **Common Information to European Air Project (CITEAIR)** (2014). *Air Quality in Europe*. Retrieved April 28, 2014, from http://www.airqualitynow.eu

[11] **Berger, M.** (2013). 50 Cities with Terrible Air Pollution. Retrieved May 15, 2019, from http://www.weather.com/news/science/cities-terrible-air-pollution-20131030

[12] **Ministry of Environment and Forestry of Turkey.** *Air quality database*. Retrieved June 20, 2019, from https://havaizleme.gov.tr/Services/AirQuality.

[13] **World Health Organization** (2019). *Ambient Air Quality Database Application*. Retrieved June 18, 2019, from : https://whoairquality.shinyapps.io/AmbientAirQualityDatabase/.

[14] **Environmental Protection Agency.** Air Quality Management Process Cycle.. Retrieved June 18, 2019, from https://www.epa.gov/air-quality-management-process/air-quality-management-process-cycle

[15] **Yatkin, S., Bayram, A.** (2007). Source apportionment of PM(10) and PM(2.5) using positive matrix factorization and chemical mass balance in Izmir, Turkey. *Sci Total Environ*, *390*(1), 109-23.

[16] **Contini, D., Cesari, D., Conte, M., Donateo, A.** (2016). Application of PMF and CMB receptor models for the evaluation of the contribution of a large coal-fired power plant to PM_{10} concentrations. *Sci Total Environ*, *560-561*, 131-40. doi: 10.1016/j.scitotenv.2016.04.031

[17] **NASA** (2013). Introduction to Remote Sensing and Air Quality Applications Summer School Webinar presentation, Week1. Date attended; July 2013.

[18] **European Environment Agency** (1998). Guidance Report on preliminary assessment under EC air quality directives. Chapter 5. Retrieved June 20, 2019, from https://www.eea.europa.eu/publications/TEC11a.

[19] **Seinfeld, J. H., Pandis, S., N.,** (2006). *Atmospheric Chemistry and Physics: From Air Pollution To Climate Change*. 2nd. Ed. Wiley International Library, N.Y.

[20] **Builtjes, P.** (2003). *The Problem – Air Pollution. Chapter 1 of Air Quality Modeling – Theories, Methodologies, Computational Techniques, and Available Databases and Software. Vol I – Fundamentals* (P. Zannetti, Editor). EnviroComp Institute (http://www.envirocomp.org/) and Air & Waste Management Association (http://www.awma.org/)

[21] **Juda-Rezler, K.** (1991). *Classification and Characteristics of Air Pollution Models*. In: Pawlowski L., Lacy W.J., Dlugosz J.J. (eds) Chemistry for the Protection of the Environment. Environmental Science Research, vol 42. Springer, Boston, MA

[22] **Schmidt, W**. (1925). *Der Massenaustauch in freier Lıft und Verwandte Erscheinungen. Probleme der Kosmichen Physic*, Hamburg, Verlag Von Henri Grand. 176 pp.

[23] **Collett, R., S., Oduyemi, K.** (1997). Air quality modelling: a technical review of mathematical approaches. *Meteorol. Appl, 4*, 235–246.

[24] **Vallero, D.** (2019). *Air Pollution Calculations: Quantifying Pollutant Formation, Transport, Transformation, Fate and Risks*. Elsevier Books. 568 pages. eBook ISBN: 9780128149355

[25] **Foley, K. M., Roselle, S. J., Appel, K. W., Bhave, P. V., Pleim, J. E., Otte, T. L., … Bash, J. O.** (2010) Incremental testing of the Community Multiscale Air Quality (CMAQ) modelling system version 4.7, *Geosci. Model Dev.*, *3*, 205–226. doi:10.5194/gmd-3-205-2010.

[26] **WRF-Chem Official web page.** Retrieved May 19, 2019, from https://ruc.noaa.gov/wrf/wrf-chem/,

[27] **CAMx web page.** Retrieved May 19, 2019, from http://www.camx.com/home.aspx

[28] **Menut, L., Bessagnet, B., Khvorostyanov, D., Beekmann, M., Blond, N., Colette, … Vivanco, M. G.** (2013). CHIMERE 2013: a model for regional atmospheric composition modelling, *Geosci. Model Dev.*, *6*, 981–1028. doi:10.5194/gmd- 6-981-2013

[29] **TNO Report** (2016). *LOTOS-EUROS v2.0 Reference Guide*. Retrieved May 13 2019, from https://lotos-euros.tno.nl/media/10360/reference_guide_v2-0_r10898.pdf

[30] **Christensen, J.H.**, (1997). The Danish Eulerian Hemispheric Model e a three-dimensional air pollution model used for the Arctic. *Atmos. Environ. 1997* (31), 4169. http://dx.doi.org/10.1016/S1352-2310(97)00264-1

[31] **Hanna, S. R.** (1993). Uncertainties in air quality model predictions. *Boundary-Layer Meteorology 62* (1-4), 3-20.

[32] **Fox, D.G.** (1984). Uncertainty in air quality modelling. *Bull. Am. Meteorol. Soc.*, *65*, 27-36.

[33] **Smith, M.E**. (1984). Review of the attributes and performance of lO rural diffusion models. *Bull. Am Meteorol. Soc.*, *65*, 554-558.

[34] **Irwin, J.S., Rao, S.T., Petersen, W.B., Turner, D.B.** (1987). Relating error bounds for maximum concentration estimates to diffusion meteorology uncertainty. *Atmos. Environ.*, *21*, 1927-1937.

[35] **U.S. Environmental Protection Agency** (2011). *Exposure Factors Handbook*. 2011 Edition. Technical Report Number EPA/600/R-090/052F. Retrieved May 14, 2019, from https://hero.epa.gov/hero/index.cfm/reference/details/reference_id/786546

[36] **Hanna, S. R., A. G. Russell, J. Wilkinson, and J. Vukovich, Hansen D. A**.. (2005). Monte Carlo estimation of uncertainties in BEIS3 emission outputs and their effects on uncertainties in chemical transport model predictions. *J. of Gephys. Research*, *110* (D1). https://doi.org/10.1029/2004JD004986

[37] **Rao, K., S.** (2005). Uncertainty analysis in atmospheric dispersion modelling. *Pure and Applied Geophys*, *162*, 1893-1967.

[38] **Guenther, A., Geron, C., Pierce, T., Lamb, B., Harley, P., and Falle, R**. (2000). Natural emissions of non-methane volatile organic compounds, carbon monoxide, and oxides of nitrogen from North America. *Atmospheric Environment*, *34*, 2205- 2230.

[39] **NRC** (1991). Committee on Tropospheric Ozone Formation and Measurement. Rethinking the ozone problem in urban and regional air pollution, *National Academy Press*.

[40] **Placet, M., Mann, C. O., Gilbert, R. O., and Niefer, M. J.** (2000). Emissions of ozone precursors from stationary sources: a critical review. *Atmospheric Environment*, *34*, 2183-2204.

[41] **Russell, A. G., and Dennis, R**. (2000). NARSTO critical review of photochemical models and modelling. *Atmospheric Environment, 34*, 2283-2324.

[42] **Sawyer, R. F., Harley, R. A., Cadle, S. H., Norbeck, J. M., Slott, R., and Bravo, A**. (2000). Mobile sources critical review: 1998 NARSTO assessment. *Atmospheric Environment*, *34*, 2161-2181.

[43] **P. Thunis, A. Pederzoli, D. Pernigotti** (2012). Performance criteria to evaluate air quality modelling applications *Atmospheric Environment*, *59*, 476–482.

[44] **D. Pernigotti, M. Gerboles, C.A. Belis, P. Thunis** (2013). Model quality objectives based on measurement uncertainty. Part II: NO_2 and PM_{10}, *Atmospheric Environment*, *79*, 869-878. doi:10.10162013.07.045.

[45] **P. Thunis, D. Pernigotti, M. Gerboles** (2013). Model quality objectives based on measurement uncertainty. Part I: Ozone, *Atmospheric Environment*, *79*, 861-868. doi: 10.10162013.05.018.

[46] **Napelenok S. L., Foley K. M., Kang D., Mathur R., Pierce T., Trivikrama S. R** (2011). Dynamic evaluation of regional air quality model's response to emission reductions in the presence of uncertain emission inventories, *Atmospheric Environment*, *45* (24), 4091-4098. doi: 10.10162011.03.030.

[47] **Sax T., Isakov V**. (2003). A case study for assessing uncertainty in local-scale regulatory air quality modelling applications, *Atmospheric Environment*, *37* (25), 3481-3489. http://dx.doi.org10.1016/S1352-2310(03)00411-4.

[48] **Hanna, S. R., Lu, Z. G., Frey, H. C., Wheeler, N., Vukovich, J., Arunachalam, S**., **Hansen, D. A.** (2001). Uncertainties in predicted ozone concentrations due to input uncertainties for the UAM-V photochemical grid model applied to the July 1995 OTAG domain. *Atmospheric Environment*, *35*(5), 891-903. doi: 10.1016/s1352-2310(00)00367-8

[49] **Bergin, M. S., Noblet, G. S., Petrini, K., Dhieux, J. R., Milford, J. B., & Harley, R. A.** (1999). Formal uncertainty analysis of a Lagrangian photochemical air pollution model. *Environmental Science & Technology*, *33*(7), 1116-1126. doi: 10.1021/es980749y

[50] **Hanna, S. R., Chang, J. C., & Fernau, M. E.** (1998). Monte Carlo estimates of uncertainties in predictions by a photochemical grid model (UAM-IV) due to uncertainties in input variables. *Atmospheric Environment*, *32*(21), 3619-3628. doi: 10.1016/s1352-2310(97)00419-6

[51] **Url-1** <http://www.unece.org/env/treaties/> Retrieved May 1, 2019.

[52] **Url-2** <http://www.ceip.at/ms/ceip_home1/ceip_home/emep_countries/,> Retrieved May 1, 2019.

[53] **Url-3** <http://www.ceip.at/ms/ceip_home1/ceip_home/status_reporting/> Retrieved May 1, 2019.

[54] **European Environment Agency** (2013). *EMEP/EEA air pollutant emission inventory guidebook*, 2013.

[55] **Intergovernmental Panel on Climate Change (IPCC)** (2006) *Revised 1996 IPCC Guidelines for National Greenhouse Gas Inventories: reference Manual*, p1.37. Retrieved August 23, 2019, from www.ipcc-nggip.iges.or.jp/public/gl/invs6a.html

[56] **Url-4** <https://edgar.jrc.ec.europa.eu/overview.php?v=431. Retrieved May 1, 2019.

[57] **Janssens-Maenhout, G., Dentener, F., Aardenne, J.v., Monni, S., Pagliari, V., Orlandini, L., Klimont, Z., Kurokawa, J., Akimoto, H., Ohara, T., Wankmüller, R., Battye, B., Grano, D., Zuber, A., Keating, T.** (2012). EDGAR-HTAP: a harmonized gridded air pollution emission dataset based on national inventories. *JRC Scientific and Technical Reports*. ISSN 1831-9424 (online) doi:10.2788/14069.

[58] **Url-5** <http://edgar.jrc.ec.europa.eu , Retrieved July 1, 2019.

[59] **Vukovich, J.** (2009). Conversion of the 2002 and 2005 *National Emission Inventories (NEI) to Gridded Inventories for the Emission Database for Global Atmospheric Research (EDGAR), US EPA (OAR/OPAR)– EC/R Inc*., Contract No. EP-D-07-001

[60] **Janssens-Maenhout, G., Crippa, M., Guizzardi, D., Dentener, F., Muntean, M., Pouliot, G., Keating, T., … Li, M.** (2015). HTAP_v2.2: a mosaic of regional and global emission grid maps for 2008 and 2010 to study hemispheric transport of air pollution, *Atmos. Chem. Phys*., *15*, 11411–11432, doi:10.5194/acp- 15-11411-2015

[61] **EDGAR Archived datasets :** http://edgar.jrc.ec.europa.eu/archived_datasets.php#ap, Retrieved May 1, 2019.

[62] **EOLO Edgar On Line Open Access**. http://edgar.jrc.ec.europa.eu/eolo_new/

[63] **ECCAD: Emissions of atmospheric Compounds and Compilation of Ancillary Data.** http://eccad.aeris-data.fr/#WelcomePlace:

[64] **GEIA: Global Emissions InitiAtive.** http://www.geiacenter.org/access/interoperability/ciera,.. Retrieved May 1, 2019.

[65] **Kuenen, J. J. P., Visschedijk, A. J. H., Jozwicka, M., and Denier van der Gon, H. A. C.** (2014). TNO-MACC_II emission inventory; a multi-year (2003–2009) consistent high-resolution European emission inventory for air quality modelling, *Atmos. Chem. Phys*., *14*, 10963–10976, doi:10.5194/acp-14-10963-2014

[66] **TNO Database** , https://eccad3.sedoo.fr Retrieved May 1, 2019.

[67] **International Institute for Applied Systems Analysis** (2009*). GAINS detailed emissions by source and activity*, http://gains.iiasa.ac.at/gains/EUN/index.login?logout, PRIMES baseline scenario 2009

[68] **Schöpp, W., Amann, M., Cofala, J., Heyes, C., and Klimont, Z**. (1999). Integrated assessment of European air pollution emission control strategies, *Environ. Modell. Softw*., *14*, 1–9, doi:10.1016/S1364-8152(98)00034-6

[69] **De Ceuster, G., Franckx, L., van Herbruggen, B., Logghe, S., van Zeebroeck, B., Tastenhoye, S., … Firello, D.** (2005). TREMOVE 2.30 Model and Baseline description, Final Report, *Transport and Mobility Leuven*, http://www.tremove.org

[70] **EDGAR-HTAP Hemispheric Transport of Air Pollution web page**. Available from : http://edgar.jrc.ec.europa.eu/history.php

[71] **Solazzo, E., Bianconi, R., Hogrefe, C., Curci, G., Tuccella, P., Alyuz, U., … Galmarini, S**. (2017). Evaluation and error apportionment of an ensemble of atmospheric chemistry transport modelling systems: multivariable temporal and spatial breakdown, *Atmospheric Chemistry and Physics*, *17*, 3001-3054, https://doi.org/10.5194/acp-17-3001-2017

[72] **Turkish Statistical Institute** (2018). *National Greenhouse gas Emission Inventory Report of Turkey for 2015.*

[73] **Ministry of Environment and Urbanization** (2018). *Informative Inventory report of Turkey for 2016.*

[74] **Frey, C.H., Bharvirkar, R.R., Zheng, J.** (1999). Quantitative Analysis of Variability and Uncertainty in Emissions Estimation. Prepared for Office of Research and Development *U.S. Environmental Protection Agency*, Research Triangle Park, NC.

[75] **European Commission Joint Research Centre**. AQMEII web page. Available from http://aqmeii.jrc.ec.europa.eu/aqmeii_docs/Phase3/. Retrieved May 14, 2019.

[76] **European Joint Research Center.** ENSEMBLE, *JRC Evaluation Platform for Dispersion Models.* Retrieved May 17, 2019, from http://ensemble.jrc.ec.europa.eu (not for public use),.

[77] **Geyer, B.** (2014). High-resolution atmospheric reconstruction for Europe 1948–2012: coastDat2, *Earth Syst. Sci. Data*, *6,* 147–164, doi:10.5194/essd-6-147-2014

[78] **Sofiev, M., Vira, J., Kouznetsov, R., Prank, M., Soares, J., and Genikhovich, E.** (2015) Construction of the SILAM Eulerian atmospheric dispersion model based on the advection algorithm of Michael Galperin, *Geosci. Model Dev., 8,* 3497–3522, doi:10.5194/gmd-8-3497-2015

[79] **Sauter, F., Swaluw, E. van der, Manders-Groot, A., Wichink Kruit, R., Segers, A., and Eskes, H**. (2012). LOTOS-EUROS v1.8 Reference Guide, *TNO Report* TNO-060-UT-2012-01451, Utrecht, the Netherlands

[80] **Environ** International Corporation (2014). CAMx (Comprehensive Air Quality Model with Extensions) User's Guide Version 6.1 *ENVIRON International Corporation*, Novato, CA.

[81] **Brandt, J., Silver, J. D., Frohn, L. M., Geels, C., Gross, A., Hansen, A. B., Hansen, K. M., Hedegaard, G. B., Skjøth, C. A., Villadsen, H., Zare, A., and Christensen, J. H**. (2012). An integrated model study for Europe and North America using the Danish Eulerian Hemispheric Model with focus on intercontinental transport, *Atmos. Environ*., *53*, 156–176

[82] **Byun, D. W. and Schere, K**. (2006). Review of the governing equations, computational algorithms, and other components of the Models- 3 community Multiscale Air Quality (CMAQ) modelling system*, Appl. Mech. Rev*., *59*, 51–77

[83] **Berrisford, P., Dee, D.P., Poli, P., Brugge, R., Fielding, M., Fuentes, M, Kållberg, P.W., Kobayashi, S., Uppala, S., Simmons, A.** (2011). *The ERA-Interim archive Version 2.0*. ERA Report Series of ECMWF. Document No 1, p 23. Shinfield Park, Reading.

[84] **ECMWF.** ERA Interim daily dataset. Retrieved May 1, 2019, from https://apps.ecmwf.int/datasets/data/interim-full-daily/levtype=sfc/

[85] **NCAR UCAR Research Data Archive.** NCEP FNL Operational Model Global Tropospheric Analyses, continuing from July 1999. DOI: 10.5065/D6M043C6. Retrieved June 27, 2019, from https://rda.ucar.edu/datasets/ds083.2/

[86] **NCAR UCAR Research Data Archive.** NCEP GFS Operational Model Global Tropospheric Analyses, continuing from July 1999. DOI: 10.5065/D65D8PWK. Retrieved June 27, 2019, from https://rda.ucar.edu/datasets/ds084.1/

[87] **Flemming, J., Huijnen, V., Arteta, J., Bechtold, P., Beljaars, A. Blechschmidt, A.-M., … Tsikerdekis, A**. (2015). Tropospheric chemistry in the Integrated Forecasting System of ECMWF, *Geosci. Model Dev*., *8,* 975-1003, doi:10.5194/gmd-8-975-2015

[88] **Flemming, J., Huijnen, V., Arteta, J., Bechtold, P., Beljaars, A., Blechschmidt, A.-M., … Tsikerdekis, A**. (2015). Tropospheric chemistry in the Integrated Forecasting System of ECMWF, *Geosci. Model Dev*., *8*, 975-1003, https://doi.org/10.5194/gmd-8-975-2015

[89] **Guenther, A. B., Jiang, X., Heald, C. L., Sakulyanontvittaya, T., Duhl, T., Emmons, L. K., andWang, X**. (2012). The Model of Emissions of Gases and Aerosols from Nature version 2.1 (MEGAN2.1): an extended and updated framework for modelling biogenic emis- sions, *Geosci. Model Dev*., *5*, 1471–1492, doi:10.5194/gmd-5- 1471-2012

[90] **Vukovich, J. M. and T. E. Pierce** (2002). The Implementation of BEIS3 within the SMOKE Modelling Framework." Presented at 11th *International Emission Inventory Conference* "Emission Inventories - Partnering for the Future, Atlanta, GA, April 15-18. www.epa.gov/ttn/chief/conference/ei11/modeling/vukovich.pdf

[91] **Poupkou, A., Giannaros, T., Markakis, K., Kioutsioukis, I., Curci, G., Melas, D., and Zerefos, C**. (2010). A model for European Biogenic Volatile Organic Compound emissions: Software development and first validation, *Environ. Model. Softw*., *25*, 1845– 1856, doi:10.1016/j.envsoft.2010.05.004

[92] **Beltman, J. B., Hendriks, C., Tum, M., and Schaap, M.** (2013). The impact of large scale biomass production on ozone air pollution in Europe, *Atmos. Environ*., *71*, 352–363, doi:10.1016/j.atmosenv.2013.02.019

[93]   **Makar, P. A., Nissen, R., Teakles, A., Zhang, J., Zheng, Q., Moran, M. D., Yau, H., and diCenzo, C**. (2014). Turbulent transport, emissions and the role of compensating errors in chemical transport models, *Geosci. Model Dev.*, *7*, 1001–1024, doi:10.5194/gmd-7-1001- 2014

[94]   **Pouliot, G., Denier van der Gon, H. A. C., Kuenen, J., Zhang, J., Moran, M. D., and Makar, P. A**. (2015). Analysis of the emission inven- tories and model-ready emission datasets of Europe and North America for phase 2 of the AQMEII project, *Atmos. Environ.*, *115*, 340–360

[95]   **Mason, R., Zubrow, A., and Eyth, A.** (2012). Technical Support Document (TSD) Preparation of Emissions Inventories for the Version 5.0, 2007 Emissions Modelling Platform. Retrieved May 17, 2019 from https://www.epa.gov/sites/production/files/2015-10/documents/2007v5_2020base_emismod_tsd_13dec2012.pdf.

[96]   **EURODELTA Factors**. Retrieved May 20, 2019, from: https://wiki.met.no/emep/emep-experts/tfmmtrendeurodelta

[97]   **Pouliot, G., Pierce, T., van der Gon, H. D., Schaap, M., Moran, M., and Nopmongcol, U**.(2012). Comparing emission inventories and model-ready emission datasets between Europe and North America for the AQMEII project, *Atmos. Environ., 53*, 4–14, 2012

[98]   **European Monitoring and Evaluation Programme.** Surface air quality monitoring network of Europe. Available from: http://www.emep.int/

[99]   **European Air Quality Database (Airbase).** Retrieved May 17, 2019, from https://www.eea.europa.eu/data-and-maps/data#c0=5&c11=&c5=all&b_start=0.

[100]   **United Nations Statistics Division web site.** Retrieved May 1, 2019, from https://unstats.un.org/unsd/statcom/.

[101]   **United States Department of Energy - CDIAC Carbon Dioxide Analysis Center web site.** Retrieved May 1, 2019, from https://cdiac.ess-dive.lbl.gov/trends/emis/weulist.html.

[102]   **WorldBank indicators.** Retrieved May 1, 2019, from https://databank.worldbank.org/data/indicator/

[103]   **San José, R., Baklanov, A., Sokhi, R.S., Karatzas, K., Pérez, J.L.** (2008). Chapter Fourteen Computational Air Quality Modelling, *Developments in Integrated Environmental Assessment*, *3*, 247-267, https://doi.org/10.1016/S1574-101X(08)00614-5

[104]   **Rockel, B., Geyer, B.** (2008). The performance of the regional climate model CLM in different climate regions, based on the example of precipitation. *Meteorologische Zeitschrift*, *17* (4), 487-498.

[105]   **The Weather Research & Forecasting Model** web page. Available from : http://www.wrf-model.org/index.php

[106]   **Nakanishi, M. and Niino, H.** (2006). An improved Mellor-Yamada Level-3 Model: its numerical stability and application to a regional prediction of advection fog, *Bound.-Lay. Meteorol.*, *119*, 397–407, doi:10.1007/s10546-005-9030-8

[107] **Janji´c Z. I.** (1994). The Step-Mountain Eta Coordinate Model: Further Developments of the Convection, Viscous Sublayer, and Turbulence Closure Schemes, *Mon. Weather Rev.*, *122*, 927–945

[108] **Hong, S.-Y., Noh, Y., and Dudhia, J.** (2006). A new vertical diffusion package with explicit treatment of entrainment processes, *Mon. Weather Rev.*, *134*, 2318–2341

[109] **Pleim, J. E.** (2007). A Combined Local and Nonlocal Closure Model for the Atmospheric Boundary Layer, Part II: application and evaluation in a mesoscale meteorological model, *J. Appl. Meteorol. Clim.*, *46*, 1396– 1409

[110] **Cohen, A. E., Cavallo, S. M., Coniglio, M. C., and Brooks, H. E.** (2015). A Review of Planetary Boundary Layer Parameterization Schemes and Their Sensitivity in Simulating Southeastern US Cold Sea- son Severe Weather Environments, *Weather Forecast.*, *30*, 591– 612

[111] **Banks, R.F., Baldasano, J.M.** (2016). Impact of WRF model PBL schemes on air quality simulations over Catalonia, Spain. *Science of the Total Environment*, *572*, 98-113. DOI: 10.1016/j.scitotenv.2016.07.167

[112] **Stull, R. B.** (1988). An Introduction to Boundary Layer Meteorology. *Kluwer Academic Publishers*, 666 pp.

[113] **Saide, P.E., Carmichael, G.R., Spak, N.S., Gallardo, L., Osses, A.E., Mena-Carrasco, M.A. and Pagowski, M.** (2011). Forecasting Urban PM10 and PM2.5 Pollution Episodes in Very Stable Nocturnal Conditions and Complex Terrain Using WRF-Chem CO Tracer Model. *Atmospheric Environment*, *45*, 2769-2780. http://dx.doi.org/10.1016/j.atmosenv.2011.02.001

[114] **Shin, H., H., Hong, S. Dudhia, J.** (2012). Impacts of the Lowest Model Level Height on the Performance of Planetary Boundary Layer Parameterizations. *AMS Journals, Monthly Weather Review*, *40*, 664. doi: 10.1175/MWR-D-11-00027.1

[115] **Tewari, M., Chen, F., Wang, W., Dudhia, J., LeMone, M. A., Mitchell, K., Ek, M., Gayno, G., Wegiel, J., and Cuenca, R. H.** (2004). Implementation and verification of the unified NOAH land surface model in the WRF model, 20th conference on weather analysis and forecasting/*16th conference on numerical weather prediction*, 11–15.

[116] **Smirnova, T. G., Brown, J. M., Benjamin, S. G., and Kim, D**. (2000). Parameterization of cold-season processes in the MAPS land- surface scheme, *J. Geophys. Res.*, *105*, 4077–4086

[117] **Chen, F. and Dudhia, J.** (2001). Coupling an Advanced Land Surface– Hydrology Model with the Penn State NCAR MM5 Modeling System. Part I: Model Implementation and Sensitivity, *Mon. Weather Rev.*, *129*, 569–585

[118] **Skamarock, W. C., J. B. Klemp, J. Dudhia, D. O. Gill, D. M. Barker, M. G. Duda, X.-Y. Huang, W. Wang, and J. G. Powers** (2008). A description of the Advanced Research WRF version 3, NCAR Tech. Note NCAR/TN-4751STR, *Natl. Cent. for Atmos. Res.*, Boulder, Colo.

[119] **Mooney, P. A., Mulligan, F. J., and Fealy, R**. (2013). Evaluation of the sensitivity of the weather research and forecasting model to parameterization schemes for regional climates of europe over the period 1990–95, *J. Climate, 26*, 1002–1017

[120] **Zhang, D.L., Anthes, R.A.** (1982). A high-resolution model of the planetary boundary layer—sensitivity tests and comparisons with SESAME-79 data. *J. Appl. Meteorol. 21*, 1594–1609.

[121] **Xiu, A., Pleim, J. E.** (2001): Development of a land surface model. Part I: Application in a mesoscale meteorological model. *J. Appl. Meteor., 40,* 192–209

[122] **Benjamin, S.G., D. Dévényi, S.S. Weygandt, K.J. Brundage, J.M. Brown, G.A. Grell, D. Kim, B.E. … G.S. Manikin** (2004). An Hourly Assimilation–Forecast Cycle: The RUC. *Mon. Wea. Rev., 132*, 495–518, https://doi.org/10.1175/1520-0493(2004)132<0495:AHACTR>2.0.CO;2

[123] **Min, K., S. Choo, D. Lee, and G. Lee** (2015): Evaluation of WRF Cloud Microphysics Schemes Using Radar Observations. *Wea. Forecasting*, *30*, 1571–1589, https://doi.org/10.1175/WAF-D-14-00095.1

[124] **Hong, S.-Y., Dudhia, J., and Chen, S.-H.** (2004) A revised approach to ice microphysical processes for the bulk parameterization of clouds and precipitation, *Mon. Weather Rev., 132*, 103–120

[125] **Lim, K.-S. S. and Hong, S.-Y.** (2010) Development of an effective double moment cloud microphysics scheme with prognostic cloud condensation nuclei (CCN) for weather and climate models, *Mon. Weather Rev., 138,* 1587–1612

[126] **Lin, Y. L., Farley, R. D., and Orville, H. D.** (1993) Bulk parameterization of the snow field in a cloud model, *J. Clim. Appl. Meteorol., 22*, 1065–1092

[127] **Morrison, H., Thompson, G., and Tatarskii, V.** (2009) Impact of Cloud Microphysics on the Development of Trailing Stratiform Pre- cipitation in a Simulated Squall Line: Comparison of One- and Two-Moment Schemes, *Mon. Weather Rev., 137,* 991–1007, doi:10.1175/2008MWR2556.1

[128] **Betts, A.K.** (1970). *Cumulus Convection*. Ph.D. Thesis, Dept. of Meteorology, Imperial College, Univ. of London. 151pp. Retrieved from http://alanbetts.com/researchpaper/cumulus- convection/#abstract

[129] **Flaounas, E., Bastin, S., Janicot, S.** (2011). Regional climate modelling of the 2006 West African monsoon: sensitivity to convection and planetary boundary layer parameterization using WRF. *Clim Dyn 36*, 1083–1105. https://doi.org/10.1007/s00382-010-0785-3

[130] **Grell, G. A. and Freitas, S. R.** (2014). A scale and aerosol aware stochastic convective parameterization for weather and air quality modelling, *Atmos. Chem. Phys., 14*, 5233–5250. doi:10.5194/acp-14- 5233-2014

[131] **Kain, J. S.** (2004). The Kain-Fritsch convective parameterization: An up- date, *J. Appl. Meteorol., 43*, 170–181.

[132]   **Janjic, ZI.** (1996). The surface layer in the NCEP Eta Model. *Eleventh Conference on Numerical Weather Prediction*, 19–23 August, Norfolk, VA, American Meteorological Society, Boston, MA, 354–355.

[133]   **Janjic, Z.I**. (2002). Nonsingular Implementation of the Mellor–Yamada Level 2.5 Scheme in the NCEP Meso model, *National Centres for Environmental Prediction (NCEP) Office Note*, No. 437, Camp Springs, MD; 61 pp.

[134]   **Dudhia, J.** (1996). A multi-layer soil temperature model for MM5, Preprints, Sixth PSU/NCAR *Mesoscale Models User's Workshop*, Boulder, CO, NCAR, 49–50.

[135]   **Iacono, M. J., Delamere, J. S., Mlawer, E. J., Shephard, M. W., Clough, S. A., and Collins, W. D.** (2008) Radiative forcing by long-lived greenhouse gases: calculations with the AER radiative transfer models, *J. Geophys. Res*., *113,* D13103, doi:10.1029/2008JD009944

[136]   **Collins, W. D., Rasch, P. J., Boville, B. A., Hack, J. J., MaCaa, J. R., Williamson, D. L., … Dai, Y.** (2004). Description of the NCAR community atmosphere model (cam 3.0), Technical report, *National Center for Atmospheric Research*, NCAR/TN–464+STR, Retrieved April 19, 2019, from http://www.cesm.ucar.edu/models/atm-cam/docs/description/description.pdf

[137]   **Dudhia, J.** (1989). Numerical study of convection observed during theWin- ter Monsoon Experiment using a mesoscale two–dimensional model, *J. Atmos. Sci.*, *46*, 3077–3107

[138]   **Mlawer, E. J., Taubman, S. J., Brown, P. D., Iacono, M. J., and Clough, S. A.** (1997). Radiative transfer for inhomogeneous atmo- spheres: RRTM, a validated correlated-k model for the longwave, *J. Geophys. Res.*, *102,* 16663–16682

[139]   **Stauffer, D. R., and N. L. Seaman,** (1990). Use of four-dimensional data assimilation in a limited-area model. Part I: Experiments with synoptic-scale data. *Mon. Wea. Rev.*, *118*, 1250–1277.

[140]   **Mai, X., Ma, Y., Yang, Y., Li, D., Qiu, X.,** (2017). Impact of Grid Nudging Parameters on Dynamical Downscaling during Summer over Mainland China. *Atmosphere*, *8*(10), 184.

[141]   **Finnish Meteorological Institute** (2013). *Summer School presentations*. Retrieved May 13, 2019, from http://silam.fmi.fi/open_source/SILAM_school/index.htm

[142]   **Hodzic, A., Vautard, R., Bessagnet, B., Lattuati, M., Moreto, F.** (2005). Long-term urban aerosol simulation versus routine particulate matter observations. *Atmospheric Environment*, *39*, 5851-5864.

[143]   **École Polytechnique Institute, Le Laboratoire de Météorologie Dynamique web page.** Retrieved May 19, 2019, from http://www.lmd.polytechnique.fr/chimere/

[144]   **CMAQv4.7.1 Operational Guidance Document.** Retrieved from https://www.cmascenter.org/cmaq/documentation/4.7.1/Operational_Guidance_Document.pdf

[145] **Byun, D., Young, J., Gipson, J., Godowitch, J., Binkowski, F., Roselle, S., … Jang, C**. (1998). Description of the Models-3 Community Multiscale Air Quality (CMAQ) model. In: *Proceedings of the American Meteorological Society 78th Annual Meeting*, January 11–16, Phoenix, AZ.

[146] **Environmental Protection Agency** (1999). Science Algorithms of the EPA Models-3 Community Multiscale Air Quality (CMAQ) Modelling System. EPA/600/R-99/030

[147] **Otte, T. L. and Pleim, J. E**. (2010). The Meteorology-Chemistry Inter- face Processor (MCIP) for the CMAQ modelling system: up- dates through MCIPv3.4.1, *Geosci. Model Dev.*, *3*, 243–256, doi:10.5194/gmd-3-243-2010.

[148] **Guenther, A. B., Jiang, X., Heald, C. L., Sakulyanontvittaya, T., Duhl, T., Emmons, L. K., Wang, X**. (2012). The Model of Emissions of Gases and Aerosols from Nature version 2.1 (MEGAN2.1): an extended and updated framework for modelling biogenic emis- sions, *Geosci. Model Dev.*, *5,* 1471–1492, doi:10.5194/gmd-5- 1471-2012

[149] **Sofiev, M., Soares, J., Prank, M., de Leeuw, G., and Kukkonen, J**. (2011). A regional-to-global model of emission and transport of sea salt particles in the atmosphere, *J. Geophys. Res.*, *116,* D21302, doi:10.1029/2010JD014713

[150] **Monahan, E. C., Spiel, D. E., and Davidson, K. L.** (1986). A model of marine aerosol generation via whitecaps and wave disruption, in: Oceanic Whitecaps and their role in air/sea exchange, edited by: Monahan, E. C. and Mac Niocaill, G., Reidel, Norwell, Mass., USA, 167–174

[151] **de Leeuw, G., Neele, F. P., Hill, M., Smith, M. H., and Vignati, E.** (2000). Production of sea spray aerosol in the surf zone, *J. Geophys. Res., 105*, e29409, doi:10.1029/2000JD900549

[152] **Gong, S. L.** (2003). A parameterization of sea-salt aerosol source function for sub- and super-micron particles, Global Biogeochem. Cy., 1*7,* 1097–1104

[153] **Gantt, B., Kelly, J. T., and Bash, J. O.** (2015). Updating sea spray aerosol emissions in the Community Multiscale Air Quality (CMAQ) model version 5.0.2, *Geosci. Model Dev.*, *8,* 3733– 3746. doi:10.5194/gmd-8-3733-2015

[154] **Soares, J., Sofiev, M., and Hakkarainen, J**. (2015). Uncertainties of willand fires emission in AQMEII phase 2 case study, *Atmos. Environ.*, *115*, 361–370, doi:10.1016/j.atmosenv.2015.01.068

[155] **D.J. Luecken, S. Phillips, G. Sarwar, C. Jang.** (2008). Effects of using the CB05 vs. SAPRC99 vs. CB4 chemical mechanism on model predictions: Ozone and gas-phase photochemical precursor concentrations. *Atmospheric Environment*, *42*(23), 5805-5820. https://doi.org/10.1016/j.atmosenv.2007.08.056.

[156] **Kouznetsov, R. and Sofiev, M.** (2012). A methodology for evaluation of vertical dispersion and dry deposition of atmospheric aerosols, J. *Geophys. Res.*, *117*, D01202, doi:10.1029/2011JD016366

[157] **Kouznetsov, R. M. and Sofiev, M**. (2014). Wet deposition scheme for SILAM chemical transport model, *Proc. 16th Int. Conf. on Harmonisation within Atmospheric Dispersion Modelling for Regulatory Purposes*, 8–11 September 2014, Varna, Bulgaria, 336 pp

[158] **Zhang, L., Gong, S., Padro, J., and Barrie, L.** (2001). A size-segregated particle dry deposition scheme for an atmospheric aerosol module, *Atmos. Environ.*, *35*, 549–560.

[159] **Van Zanten, M. C., Sauter, F. J., Wichink Kruit, R. J., Van Jaarsveld, J. A., and Van Pul, W. A. J**. (2010). Description of the DEPAC module: Dry deposition modelling with DEPAC GCN2010, RIVM report 680180001/2010, Bilthoven, the Netherlands, 74 pp.

[160] **Emberson, L. D., Ashmore, M. R., Simpson, D., Tuovinen, J.-P., and Cambridge, H. M**. (2000a). Towards a model of ozone deposition and stomatal uptake over Europe. EMEP/MSC-W 6/2000, *Norwegian Meteorological Institute,* Oslo, Norway, 57 pp.

[161] **Emberson, L. D., Ashmore, M. R., Simpson, D., Tuovinen, J.-P**., **Cambridge, H. M**. (2000b). Modelling stomatal ozone flux across Europe, *Water Air Soil Pollut.*, *109,* 403–413

[162] **Menut, L., Bessagnet, B., Khvorostyanov, D., Beekmann, M., Blond, N., Colette, A., Coll, I., Curci, G., Foret, G., Hodzic, A., Mailler, S., Meleux, F., Monge, J.-L., Pison, I., Siour, G., Turquety, S., Valari, M., Vautard, R., and Vivanco, M. G.** (2013). CHIMERE 2013: a model for regional atmospheric composition modelling, *Geosci. Model Dev.*, *6*, 981–1028. doi:10.5194/gmd- 6-981-2013

[163] **Wesely, M. L.** (1989). Parameterization of surface resistances to gaseous dry deposition in regional-scale numerical models, *Atmos. Environ.*, *23*, 1293–1304

[164] **Easter, R. C., Ghan, S. J., Zhang, Y., Saylor, R. D., Chapman, E. G., Laulainen, N. S., Abdul-Razzak, H., Leung, L. R., Bian, X., and Zaveri, R. A.** (2004). MIRAGE: Model Description and Evaluation of Aerosols and Trace Gases, *J. Geophys. Res.*, *109*, D20210, doi:10.1029/2004JD004571

[165] **Zhang, L., Brook, J. R., and Vet, R.** (2003) A revised parameterization for gaseous dry deposition in air-quality models, *Atmos. Chem. Phys.*, *3*, 2067–2082, doi:10.5194/acp-3-2067-2003

[166] **Simpson, D., Fagerli, H., Jonson, J. E., Tsyro, S., Wind, P., and Tuovinen, J.-P.** (2003). Transboundary Acidification, Eutrophica- tion and Ground Level Ozone in Europe, PART I, Unified EMEP Model Description, 104 pp

[167] **Chang, J. S., Brost, R. A., Isaksen, I. S. A., Madronich, S., Middle- ton, P., Stockwell, W. R., and Walcek, C. J.** (1987). A three-dimensional Eulerian acid deposition model: physical concepts and formulation, *J. Geophys. Res.*, *92*, 14681–14700

[168] **Pleim, J. and Ran, L**. (2011). Surface Flux Modelling for Air Quality Applications, *Atmosphere*, *2*, 271–302

[169] **Yarwood, G., Rao, S., Yocke, M., and Whitten, G**. (2005). Updates to the Carbon Bond Chemical Mechanism: CB05, Final Report to the US EPA, RT-0400675. Retrieved May 20, 2019 from http://www.camx.com/files/cb05_final_report_120805.aspx

[170] **Whitten, G.Z., Heo, G., Kimura, Y., McDonald-Buller, E., Allen, D.T., Carter, W.P.L., Yarwood, G.** (2010). A new condensed toluene mechanism for carbon bond: *Atmos. Environ.*, *44*, 5346-5355.

[171] **M.W. Gery, G.Z. Whitten, J.P. Killus, M.C. Dodge** (1989). A photochemical kinetics mechanism for urban and regional scale computer modelling. *Journal of Geophysical Research*, *94* (D10), 12925-12956.

[172] **Lattuati M.** (1997). *Impact des emissions européennes sur le bilan d'ozone troposphérique à l'interface de l'Europe et de l'Atlantique Nord: apport de la modélisation lagrangienne et des mesures en altitude*, PhD Thesis, Université Pierre et Marie Curie, Paris, France

[173] **Kim, S. W., Heckel, A., Frost, G. J., Richter, A., Gleason, J., Burrows, J. P., McKeen, S., … Trainer, M**. (2009). NO_2 columns in the western United States observed from space and simulated by a regional chemistry model and their implications for NO_x emissions, *J. Geophys. Res.-Atmos.*, *114*(D11301). doi:10.1029/2008jd011343

[174] **Stockwell, W. R., Middleton, P., Chang, J. S., and Tang, X**. (1990). The second generation regional acid deposition model chemical mechanism for regional air quality modelling, *J. Geophys. Res. 95*, 16343-16367, doi:10.1029/JD095iD10p16343

[175] **IUPAC,** Task group on Atmospheric Chemical Kinetic Data Evaluation. Retrieved May 20, 2019, from http://iupac.pole-ether.fr

[176] **NASA Jet propuşsion Laboratory**. Chemical Kinetics and Photochemical Data for Use in Atmospheric Studies. *JPL Publication* No. 15-10. Retrieved May 20, 2019, from https://jpldataeval.jpl.nasa.gov

[177] **Environ** (2014). CAMx (Comprehensive Air Quality Model with Exten- sions) User's Guide Version 6.1 *ENVIRON International Corporation*, Novato, CA

[178] **Stockwell, W. R., Kirchner, F. K., Kuhn, M., and Seefeld, S**. (1997). A new mechanism for regional atmospheric chemistry modelling, *J. Geophys. Res.*, *102*, 25847–25879, doi:10.1029/97JD00849

[179] **Damski, J., Thölix, L., Backman, L., Taalas, P., and Kulmala, M**. (2007). FinROSE: middle atmospheric chemistry transport model, Boreal *Environ. Res.* 12, 535–550

[180] **Poppe, D., Andersson-Sköld, Y., Baart, A., Builtjes, P. J. H., Das, M., Fiedler, F., … W. R**. (1996). Gas-Phase reactions in atmospheric chemistry and transport models, Tech Rep. Garmisch-Partenkirchen, Germany: Eurotrac report

[181] **Fast, J. D., Gustafson Jr., W. I., Easter, R. C., Zaveri, R. A., Barnard, J. C., Chapman, E. G., Grell, G. A., and Peckham, S. E**. (2006). Evolution of ozone, particulates, and aerosol direct radia- tive forcing in the vicinity of Houston using a fully coupled meteorology-chemistry-aerosol model, *J. Geophys. Res., 111*, D21305, doi:10.1029/2005JD006721

[182] **Ahmadov, R., McKeen, S., Trainer, M., Banta, R., Brewer, A., Brown, S., … Zamora, R**. (2015). Understanding high wintertime ozone pollution events in an oil- and natural gas- producing region of the western US, *Atmos. Chem. Phys., 15*, 411–429, doi:10.5194/acp-15-411-2015

[183] **Vestreng, V. and Støren, E.** (2000). Analysis of the UNECE/EMEP Emission Data, MSC-W Status Report 2000, *Norwegian Meteorological Institute*, Blindern, Oslo

[184] **Briggs, G. A.** (1971). Some Recent Analyses of Plume Rise Observation in: *Proceedings of the Second International Clean Air Congress*, edited by: Englun, H. M. and Beery, W. T., Academic Press, New York, 1029–1032

[185] **Briggs, G. A.** (1972). Discussion on Chimney Plumes in Neutral and Stable Surroundings, *Atmos. Environ., 6*, 507–510

[186] **Bieser, J., Aulinger, A., Matthias, V., Quante, M., and Denier van der Gon, H. A. C.** (2011). Vertical emission profiles for Europe based on plume rise calculations, *Environ. Pollut., 159,* 2935–2946, doi:10.1016/j.envpol.2011.04.030

[187] **Sofiev, M.** (2000). A model for the evaluation of long-term airborne pollu- tion transport at regional and continental scales, *Atmos. Environ., 34,* 2481–2493, doi:10.1016/S1352-2310(99)00415-X

[188] **Ahmadov, R., McKeen, S. A., Robinson, A., Bahreini, R., Mid- dlebrook, A., de Gouw, J., Meagher, J., Hsie, E., Edgerton, E., Shaw, S., and Trainer, M**. (2012). A volatility basis set model for summertime secondary organic aerosols over the eastern United States in 2006, J. *Geophys. Res., 117*, D06301, doi:10.1029/2011JD016831

[189] **Fountoukis, C. and Nenes, A**. (2007). ISORROPIA II: a computationally efficient thermodynamic equilibrium model for K^+– Ca^{2+}–Mg^{2+}–NH^{+4} –Na^+–$SO2^{-4}$ –NO^{-3} –Cl^-–H_2O aerosols, *Atmos. Chem. Phys., 7,* 4639–4659, doi:10.5194/acp-7-4639-2007, 2007

[190] **Tuccella, P., Curci, G., Grell, G. A., Visconti, G., Crumeyrolle, S., Schwarzenboeck, A., and Mensah, A. A.** (2015). A new chem- istry option in WRF-Chem v. 3.4 for the simulation of direct and indirect aerosol effects using VBS: evaluation against IMPACT-EUCAARI data, *Geosci. Model Dev., 8,* 2749–2776, doi:10.5194/gmd-8-2749-2015

[191]   **Zare, A., Christensen, J. H., Gross, A., Irannejad, P., Glasius, M., and Brandt, J**. (2014). Quantifying the contributions of natural emissions to ozone and total fine PM concentrations in the Northern Hemi- sphere, *Atmos. Chem. Phys*., *14*, 2735–2756, doi:10.5194/acp- 14-2735-2014

[192]   **Taylor, K. E.** (2001) Summarizing multiple aspects of model performance in a single diagram, *J. Geophys. Res*., *106*(D7), 7183– 7192, doi:10.1029/2000JD900719

[193]   **Environmental Protection Agency (EPA)** (1995). *AP 42, Fifth Edition Compilation of Air Pollutant Emissions Factors, Volume 1: Stationary Point and Area Sources.* Retrieved from https://www.epa.gov/air-emissions-factors-and-quantification/ap-42-compilation-air-emissions-factors

[194]   **The Scientific and Technological Research Council of Turkey, Public Research Support Group** (2011). Development of National Air Pollution Emission Management System. Project number: 111G037

[195]   **Junyu, Z. , Frey, H.C.** (2002). Development of a Software Module for Statistical Analysis of Variability and Uncertainty. *Annual Meeting of the Air and Waste Management Association.*

[196]   **Frey, C.H., Zheng, J., Zhao, Y., Li, S., Zhu, Y.** (2002). Technical Documentation of the AuvTool Software Tool for the Analysis of Variability and Uncertainty. Prepared for Office of Research and Development U.S. Environmental Protection Agency, Research Triangle Park, NC.

[197]   **Cullen, A.C., Frey, H.C.** (1999). *Use of Probabilistic Techniques in Exposure Assessment: A Handbook for Dealing with Variability and Uncertainty in Models and Inputs*. Plenum Press, New York. H.

[198]   **NIST/SEMATECH.** *e-Handbook of Statistical Methods*. Retrieved August 9, 2019, from itl.nist.gov/div898/handbook/eda/section3/eda35b.htm

[199]   **Zheng, J** (2002). *Quantification of Variability and Uncertainty in Emission Estimation: General Methodology and Software Implementation.* PhD Dissertation from North Carolina State University by the supervison of Dr. H. Christopher Frey

[200]   **Efron, B.** (1979). Bootstrap Method: Another Look at the Jackknife. *The Analysis of Statistics*, *7*(1): 1-26.

[201]   **U.S. Environmental Protection Agency** (1999). Report of the Workshop on Selecting Input Distributions for Probabilistic Assessment, EPA/630/R-98/004, Washington, DC.

[202]   **Morgan, M.G., and M. Henrion** (1990). *Uncertainty: A Guide to Dealing with Uncertainty in Quantitative Risk and Policy Analysis*, Cambridge University Press, New York.

[203]   **Delignette-Muller, M., & Dutang, C.** (2015). fitdistrplus: An R Package for Fitting Distributions. *Journal of Statistical Software*, *64*(4), 1 - 34. doi:http://dx.doi.org/10.18637/jss.v064.i04

[204] **Frey, C.H., Zheng, J., Zhao, Y., Zhu, Y.** (2002). *Technical Documentation of the AuvTool Software Tool for Analysis of Variability and Uncertainty*. Prepared for U.S. Environmental Protection Agency.

[205] **D'Agostino, R.B., M.A. Stephens** (1986). *Goodness-of-Fit Techniques*, M. Dekker: New York

[206] **Massey, F.J.,** (1951). The Kolmogorov-Smirnov Test for Goodness-of-fit. *Journal of the American Statistical Association*, *46*, 68-78

[207] **Lilliefors, H.W.,** (1967). On the Kolmogorov-Smirnov Test for Normality with Mean and Variance Unknown. *Journal of the American Statistical Association*, 62, 399-402

[208] **Akaike, H.** (1974). A new look at the statistical model identification. *IEEE Transactions on Automatic Control*, *19*(6), 716-723. doi: 10.1109/TAC.1974.1100705.

[209] **Schwarz, Gideon E.** (1978). Estimating the dimension of a model. *Annals of Statistics*, *6* (2): 461–464, doi:10.1214/aos/1176344136

[210] **Holland, D.M., T. Fitz-Simmons (**1982). Fitting Statistical Distributions to Air Quality Data by Maximum Likelihood Method. *Atmospheric Environment*, *16*(5): 1071-1076

[211] **Hahn, G.J., Shapiro, S.S.** (1967). *Statistical Models in Engineering*. John Wiley and Sons, New York.

[212] **Casella, G., Berger, R. L.** (1990). *Statistical Inference*, Duxbury Press, Belmont, CA

[213] **Hazen, A**., (1914). Storage to be Provided in Impounding Reservoirs for Municipal Water Transactions of the American Society of Civil Engineers, *77*: 1539-1640.

[214] **Rubinstein, R. Y.** (1981). *Simulation and the Monte Carlo Method*, John Wiley & Sons: New York.

[215] **L'Ecuyer, P.** (1996). Multiple Recursive Random Number Generators. *Operations Research*, *44*, 816-822.

[216] **Marsaglia, G., T.A. Bray** (1964). A Convenient Method for Generating Normal SIAM Review, *6*, 260-264.

[217] **Law, A.M., W.D. Kelton** (1991). *Simulation Modeling and Analysis* 2nd Edition, McGraw-Hill: New York

[218] **U.S. EPA** (1997). *Guiding Principles for Monte Carlo Analysis*, EPA/630/R-97/001, U.S. Environmental Protection Agency, Washington, DC.

[219] **Frey, C., Rhodes, D. S.** (1998). Characterization and Simulation of Uncertain Frequency Distributions: Effects of Distribution Choice, Variability, Uncertainty, and Parameter Dependence, *Human and Ecological Risk Assessment*: *4*(2), 423-468, doi:10.1080/10807039891284406

[220]   **McMurray, A., Pearson, T., Casarim, F.** (2017). *Guidance on Applying the Monte Carlo Approach to Uncertainty Analyses in Forestry and Greenhouse Gas Accounting*. Winrock International. Retrieved August 27, 2019, from https://www.winrock.org/document/guidance-on-applying-the-monte-carlo-approach-to-uncertainty-analyses-in-forestry-and-greenhouse-gas-accounting/

[221]   **Harward University web page on Statistics**. Retrieved August 21, 2019, from http://ipl.physics.harvard.edu/wp-uploads/2013/03/PS3_Error_Propagation_sp13.pdf

[222]   **TOBB** (2018). *Industrial database*. Retrieved May 20, 2019, from http://sanayi.tobb.org.tr/Eng/

[223]   **Tuccella, P., Curci, G., Visconti, G., Bessagnet, B., Menut, L., and Park, R. J.** (2012). Modelling of gas and aerosol with WRF/Chem over Europe: Evaluation and sensitivity study, *J. Geophys. Res.*, *117*, D03303, doi:10.1029/2011JD016302

[224]   **Mass, C. F. and Ovens, D.** (2011). Fixing WRF's high speed wind bias: a new subgrid scale drag parameterization and the role of detailed verification, 91st AMS Annual Meeting, Seattle, WA. Retrieved May 20, 2019, from https://ams.confex.com/ams/91Annual/webprogram/Paper180011.html

[225]   **Turkish Ministry of Environment and Urbanization** (2008). Directive on Air Quality Evaluation and Management. *No: 26898*. Official Journal Date: 06.06.2008.

[226]   **European Parliament and of the Council** (2008). Directive on ambient air quality and cleaner air for Europe, Directive *2008/50/EC*. Entered into force on 11 June

APPENDICES

APPENDIX A: Questionnaire Form Answered by Plant Operators During In-Situ Measurements

APPENDIX B: Maps of Performance Metrics (BIAS, IoA, MAE, MFE, MNE, NBIAS, NMSE, PCC, r^2, RMSE, UPA) according to Models

APPENDIX C: MAE CDFs of stations (PM_{10}) for the countries with more than 10 stations.

APPENDIX D: Country Averages of Performance Metrics for All Models

APPENDIX E: Taylor Diagrams for all stations in Marmara Region

APPENDIX F: Goodness-of-fit Statistics/Criteria for EFs Derived from EMRs

APPENDIX A : Questionnaire Form Answered by Plant Operators During In-Situ Measurements

Table A.1 : Questionnaire form answered by plant operators during in-situ measurements.

Date	
Name, Surname and duty of the person completing this form	
Contact information	
Facility name	
Facility activity area	
Product type	
Annual production amount with unit	
Does the production quantity change during the day? (Yes/No) If yes, write down the hours of the production.	
Does the production quantity change intra-week and weekend? (Yes/No) If yes, briefly explain.	
Does the facility run 365 days? (Yes/No) If no, briefly explain.	
Are there seasonal changes in production quantities? (Yes/No) If yes, briefly explain.	
Fuel type	
Annual fuel amount (tonne/year)	
Heat power of the plant	
Facility combustion technology (i.e. Gas turbine, internal combustion engine)	
Briefly describe the process that the measured stack connected.	
Height of the stack that measured by our team	
Inner diameter of the stack that measured by our team	
Are there any flue gas control device in the stack that measured by our team, write their names.	
What is the frequency of the use of the flue gas control devices?	
Yield of the power plant (%)	

Figure B.1 : BIAS maps.

Figure B.1 (continued) : BIAS maps.
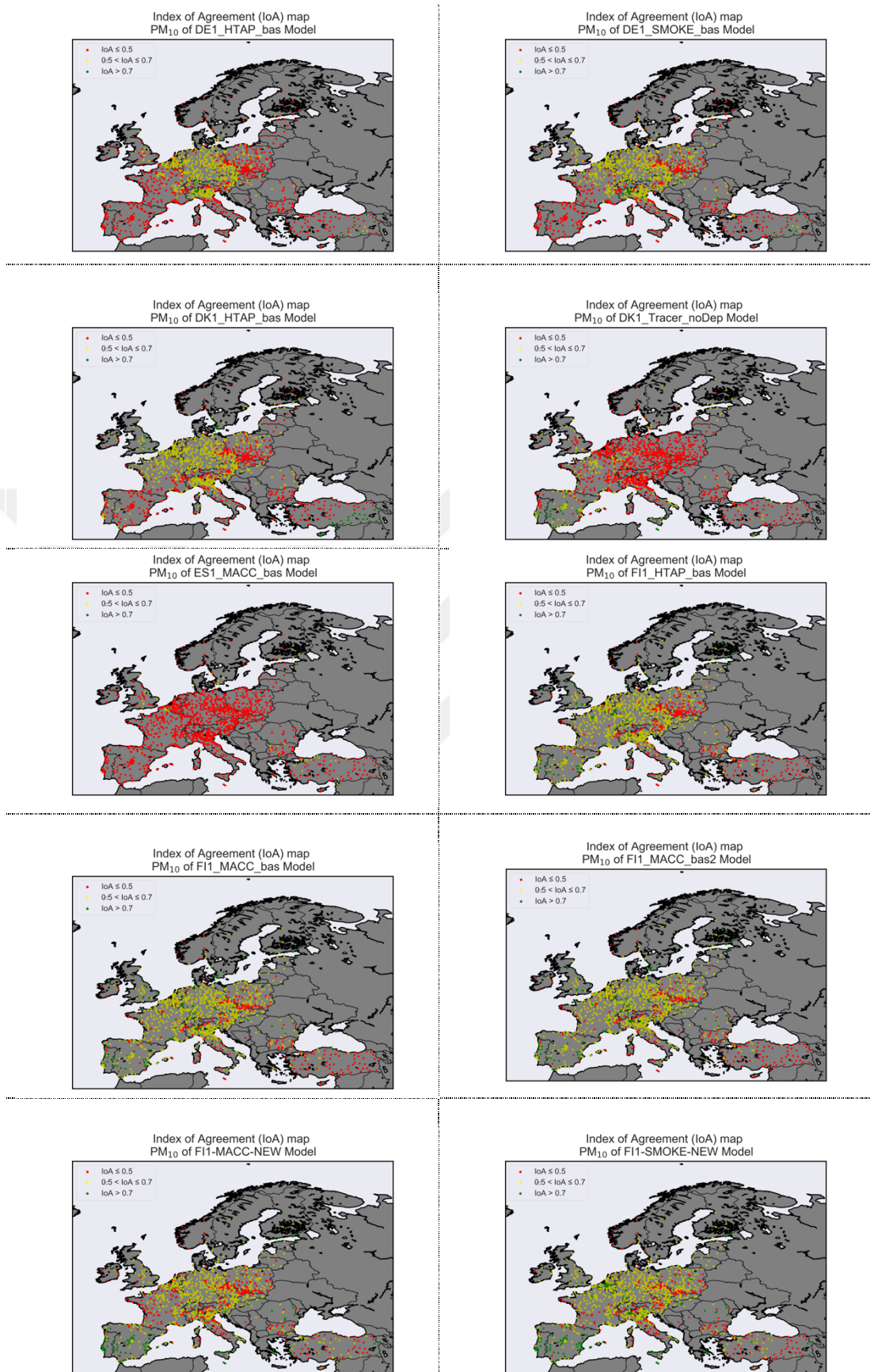
**Figure B.2 :** IoA maps.
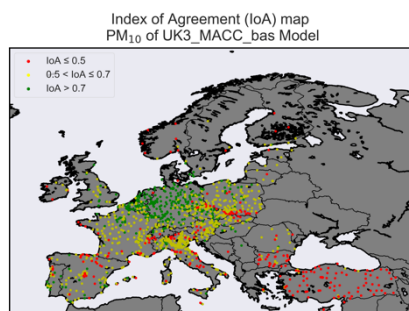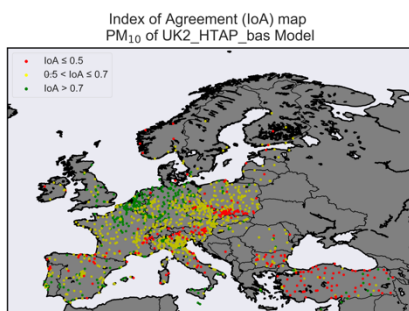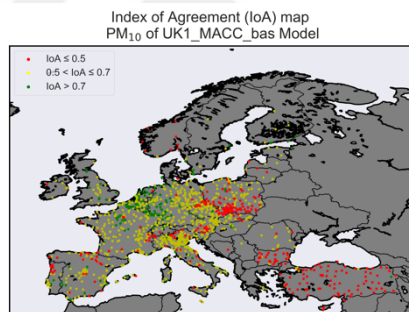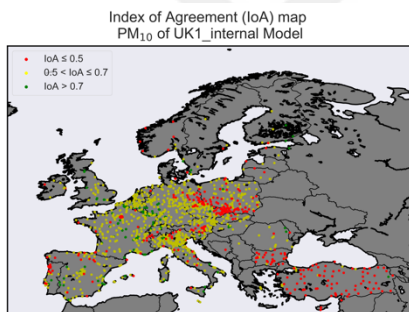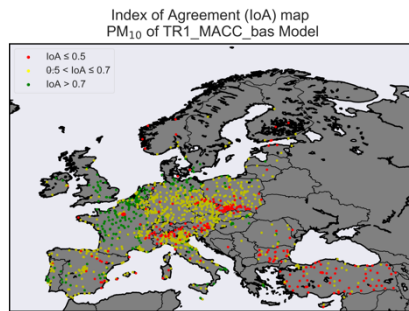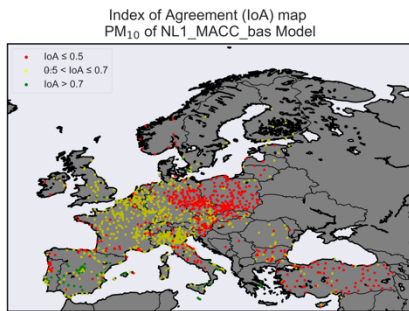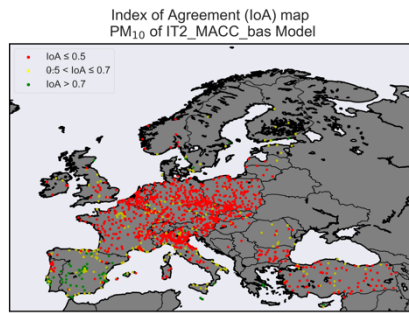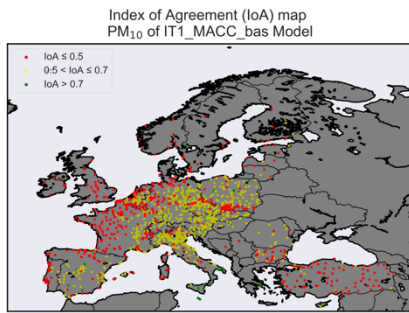
Figure B.2 (continued) : IoA maps.
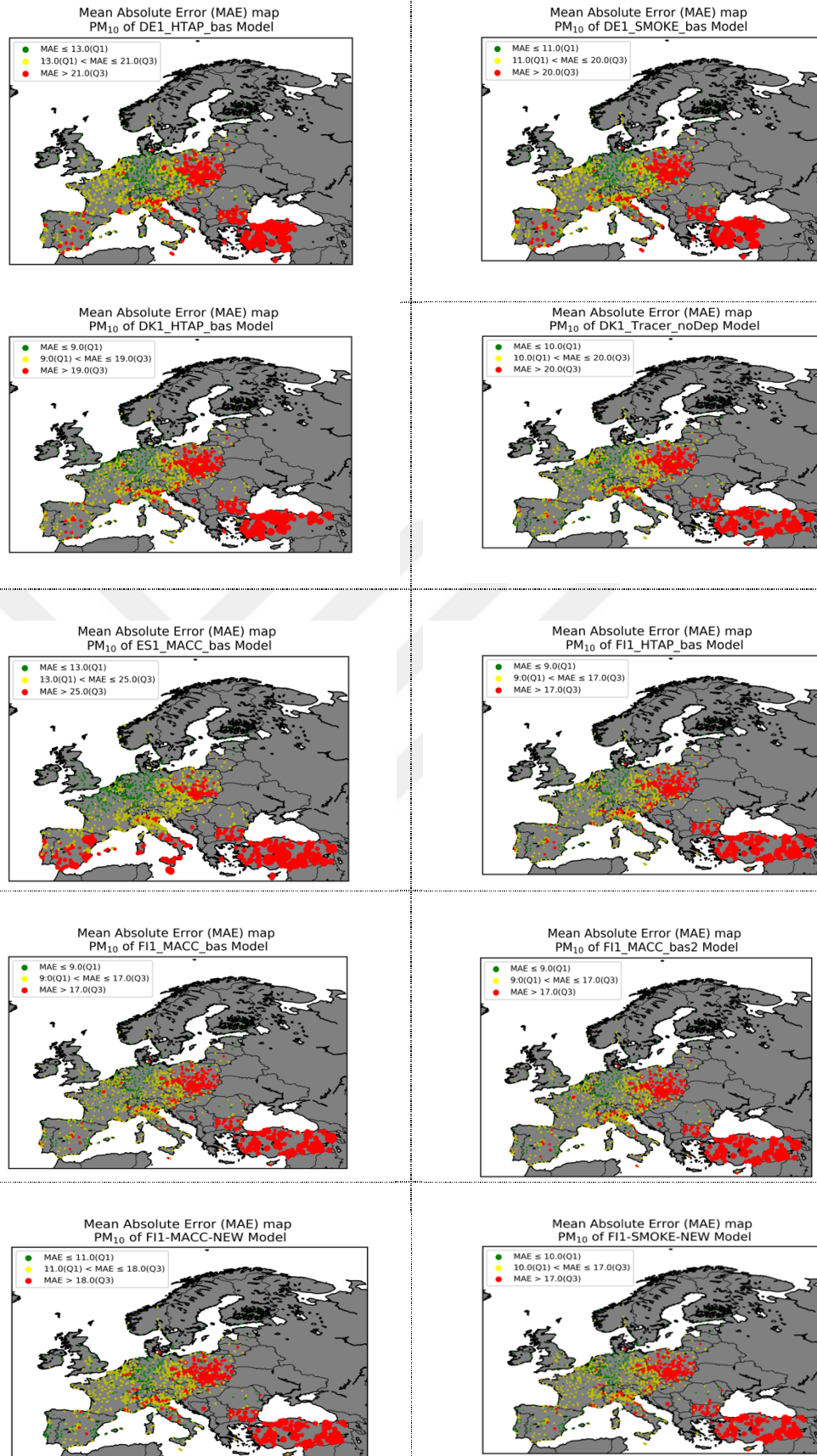
Figure B.3 : MAE maps.
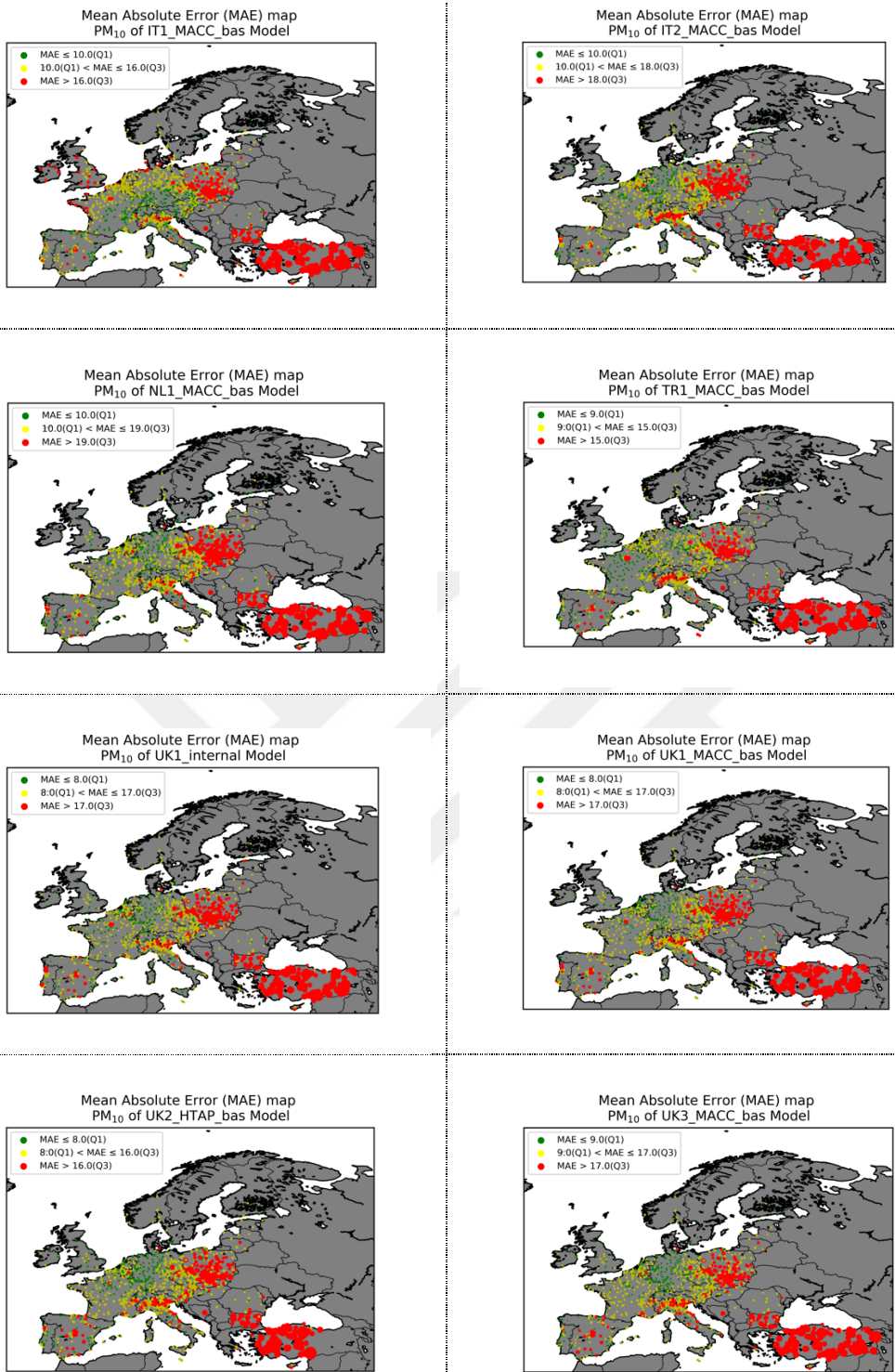
Figure B.3 (continued) : MAE maps.
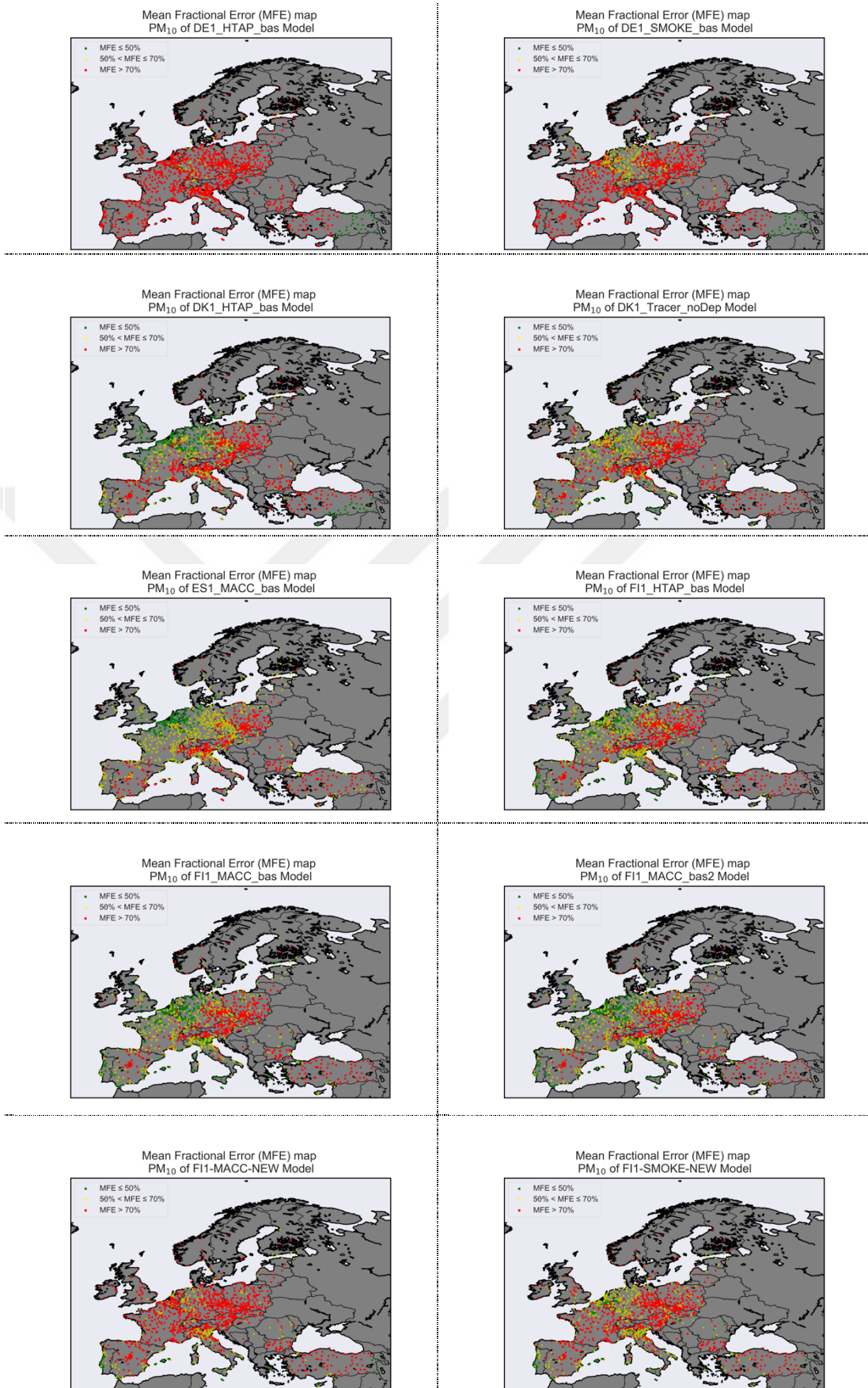
Figure B.4 : MFE maps.
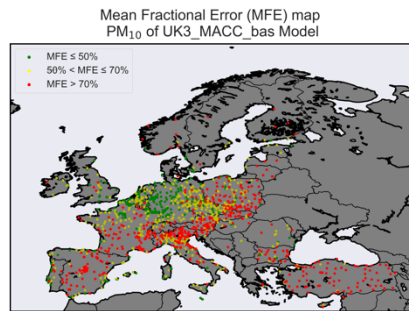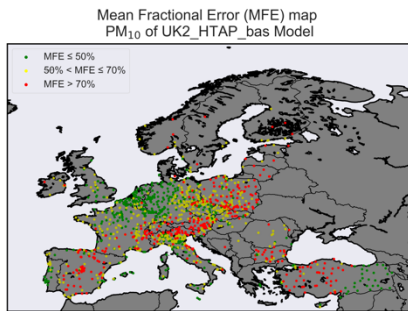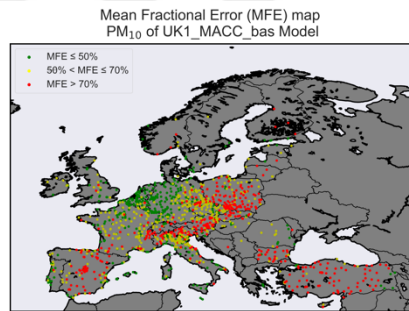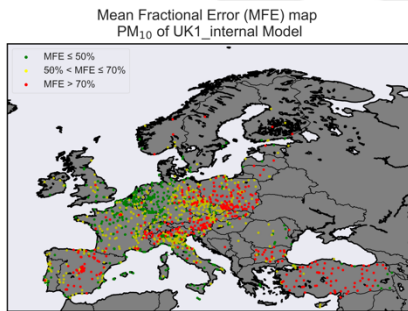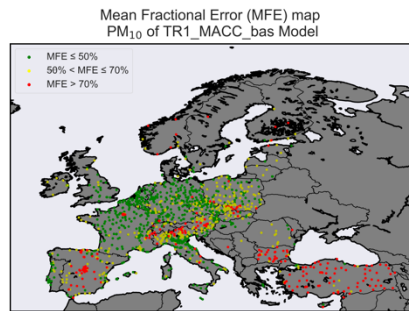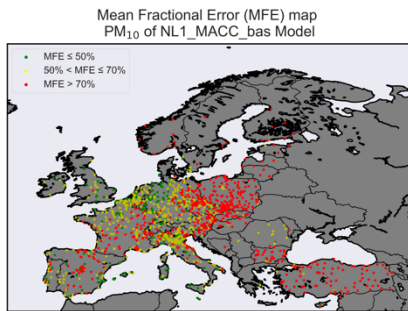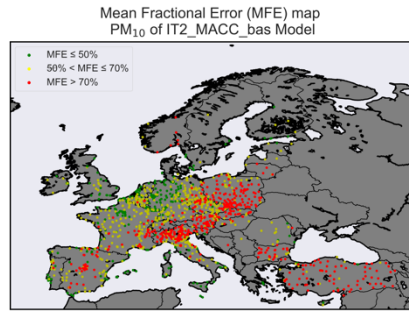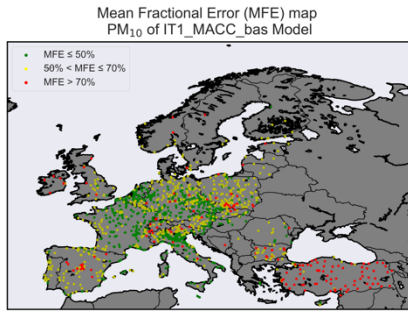
Figure B.4 (continued) : MFE maps.

236
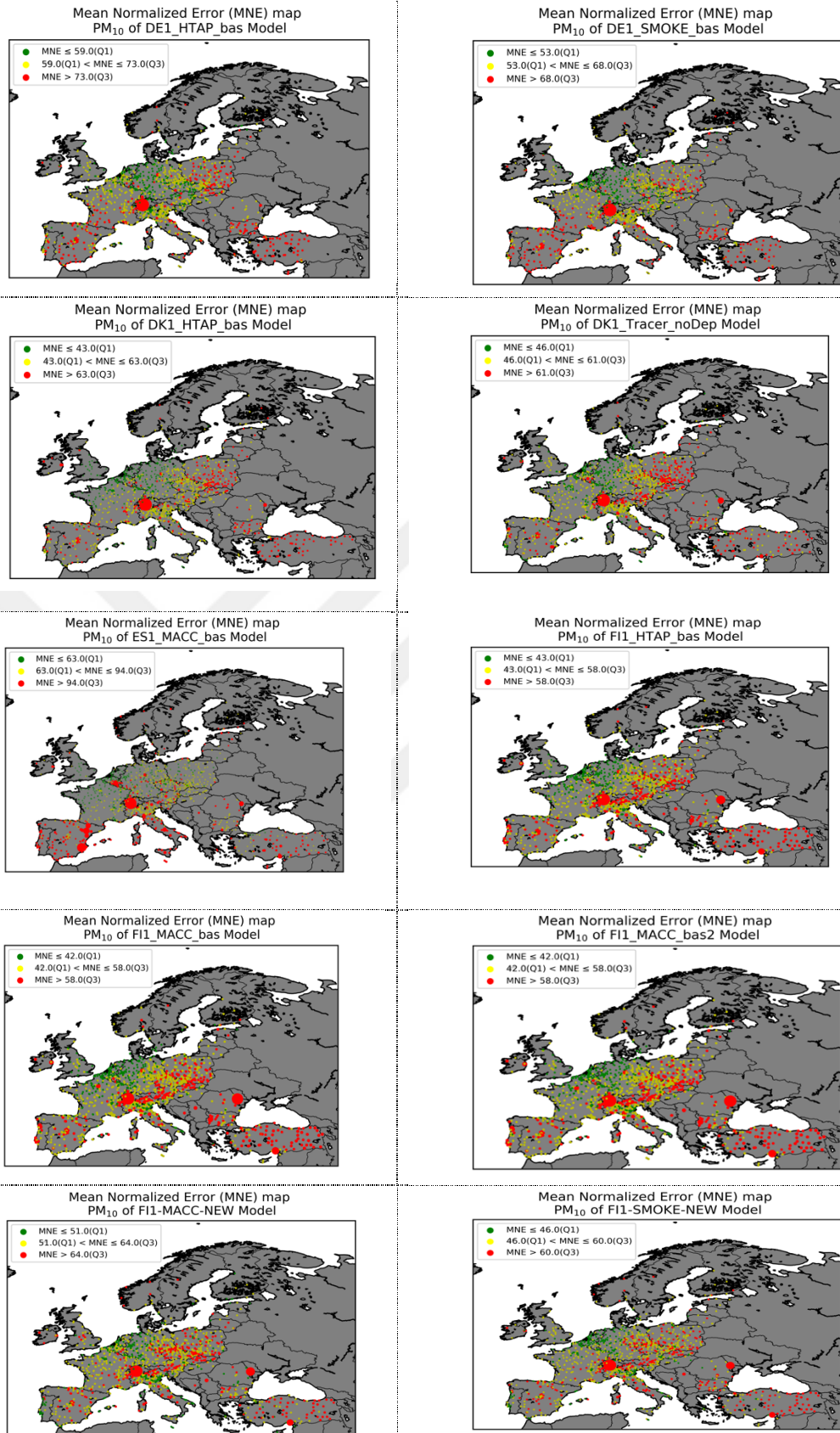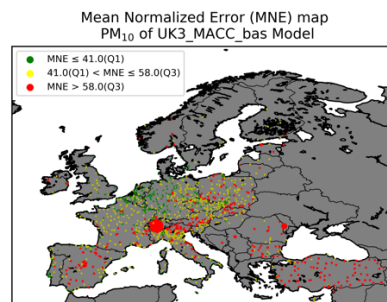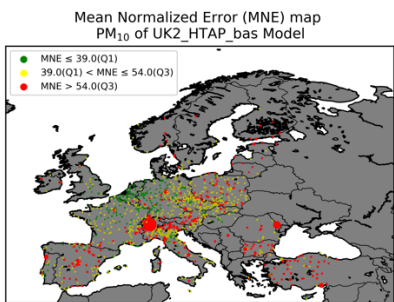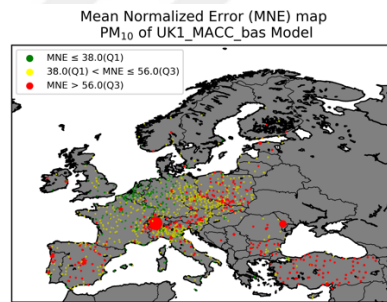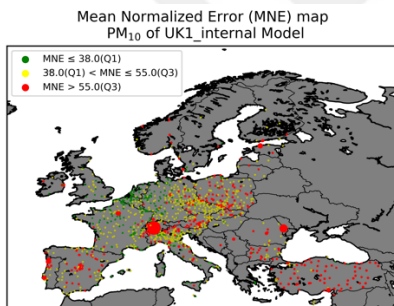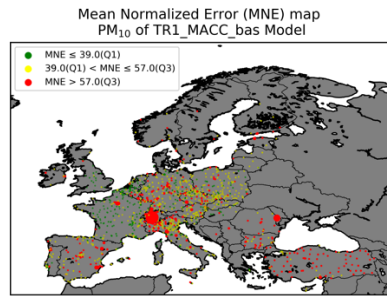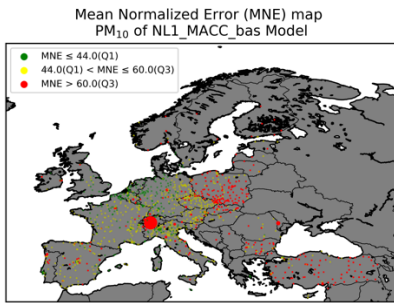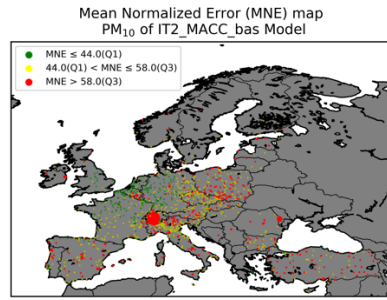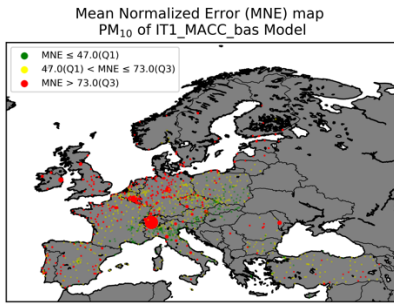
Figure B.5 : MNE maps.

Figure B.5 (continued) : MNE maps.
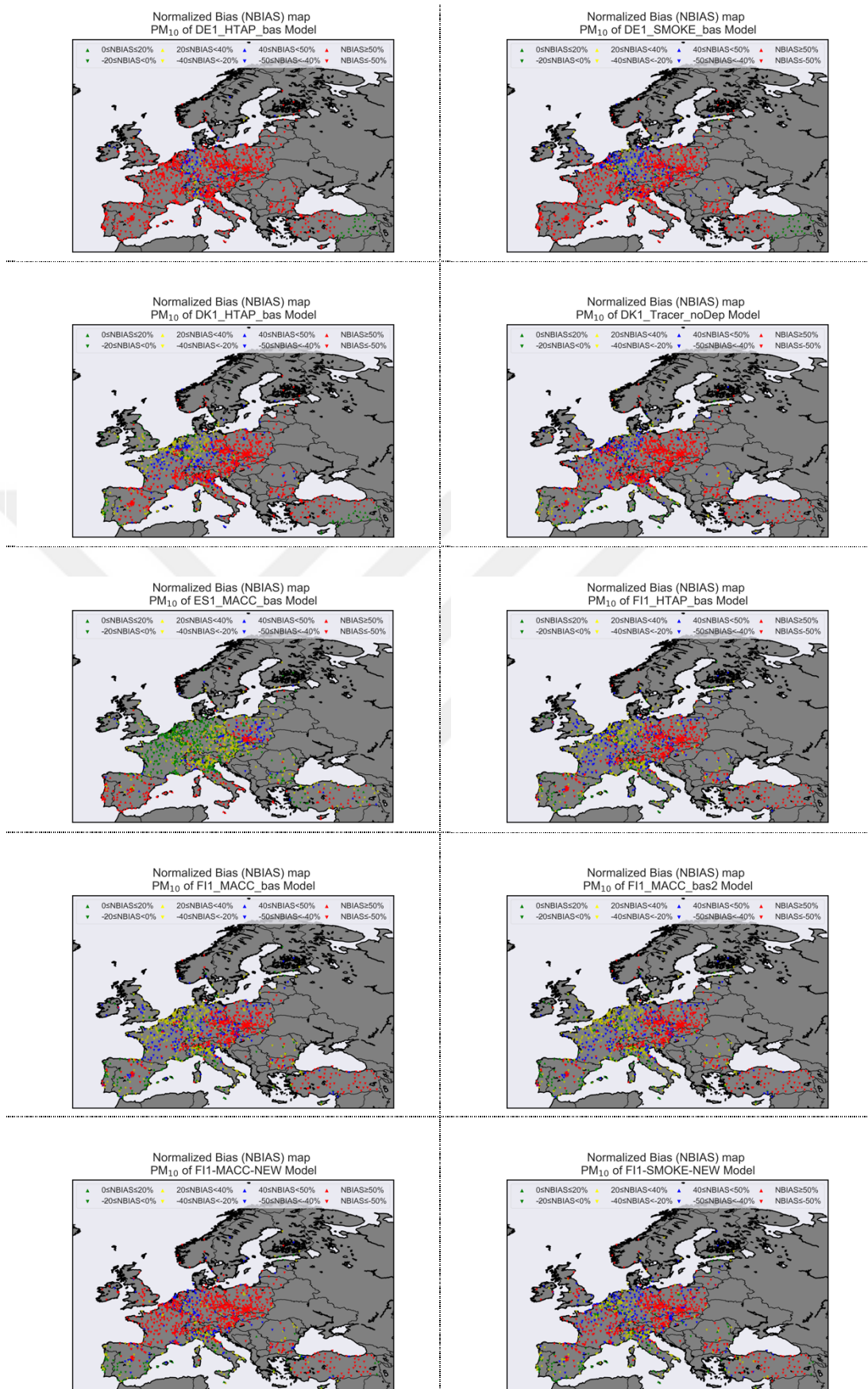
Figure B.6 : NBIAS maps.
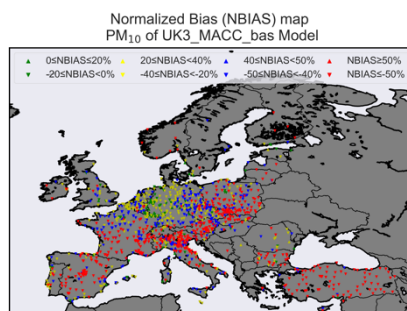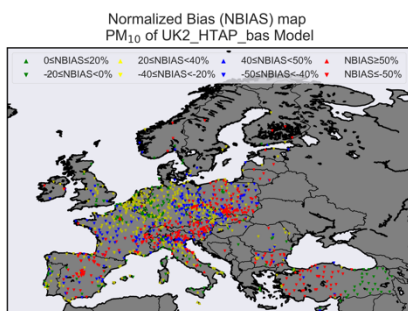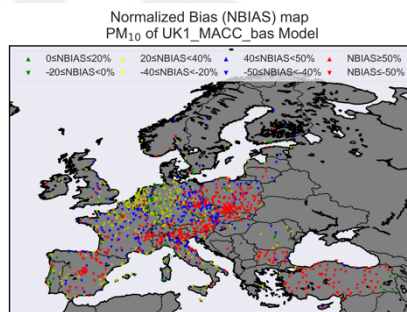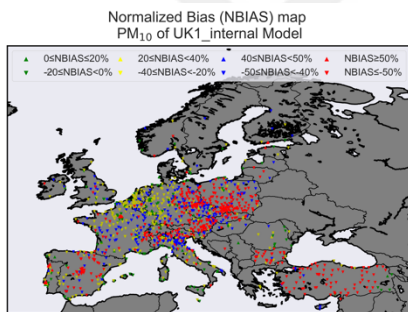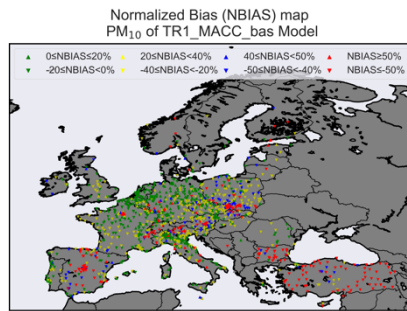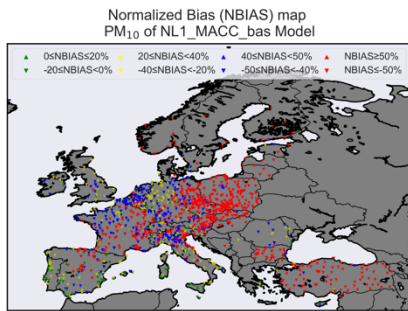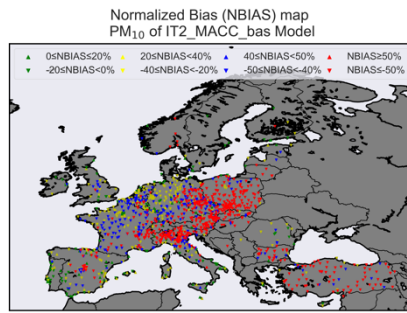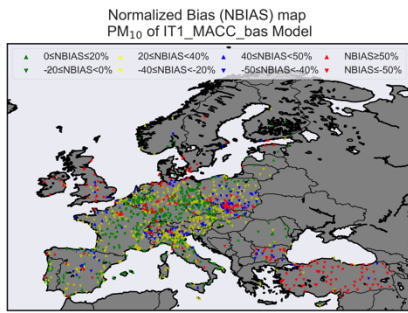
Figure B.6 (continued) : NBIAS maps.
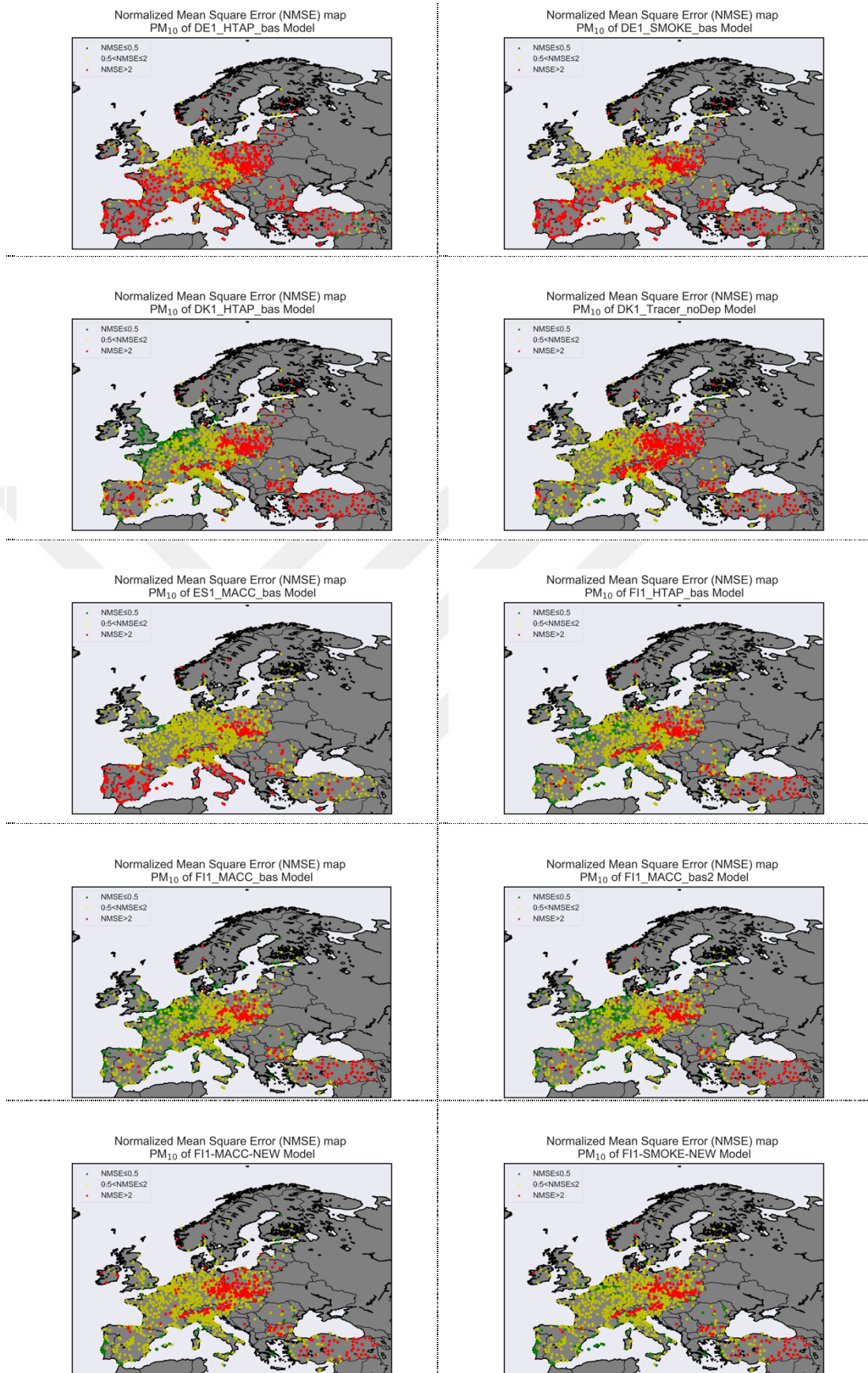
Figure B.7 : NMSE maps.
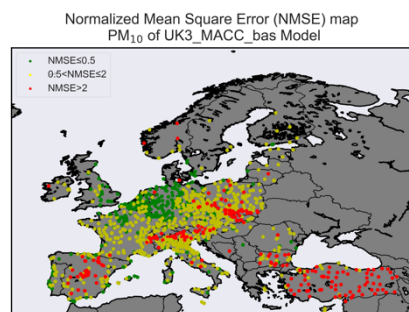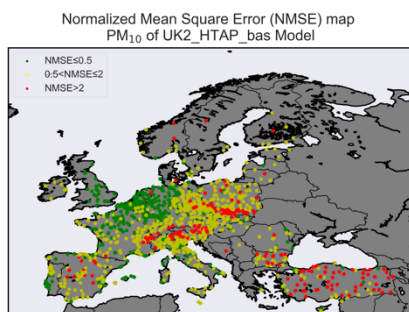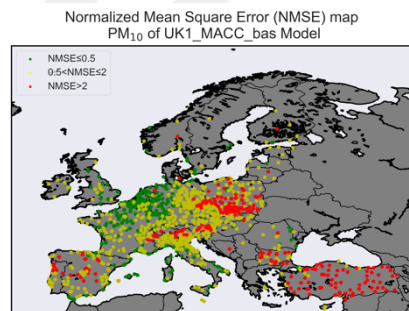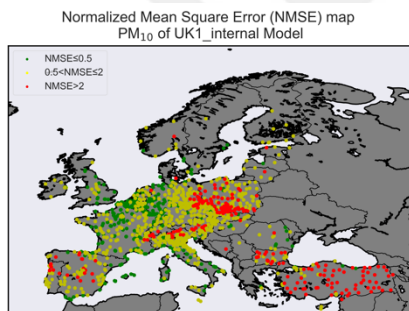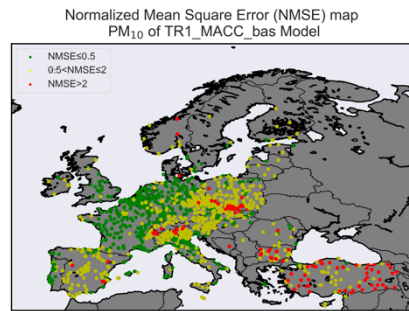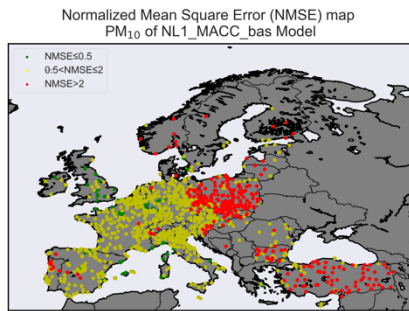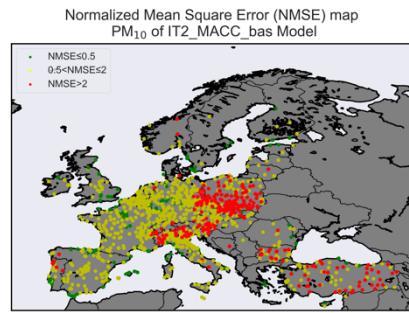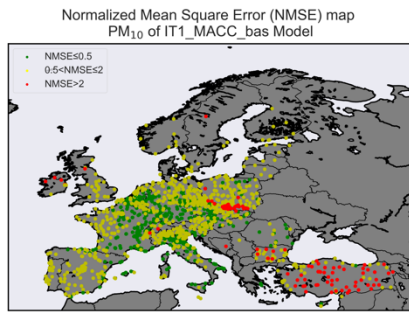
Figure B.7 (continued) : NMSE maps.
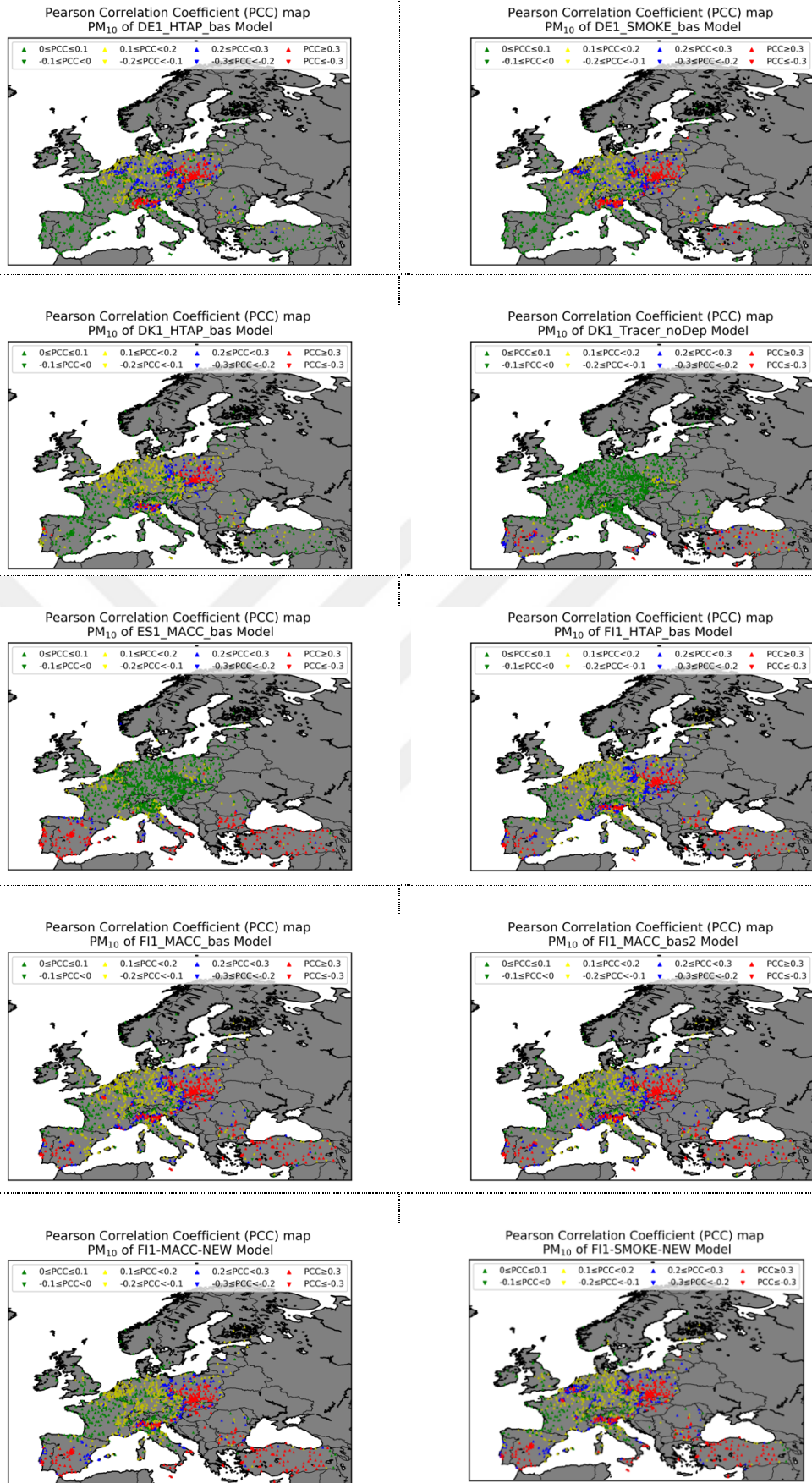
Figure B.8 : PCC maps.
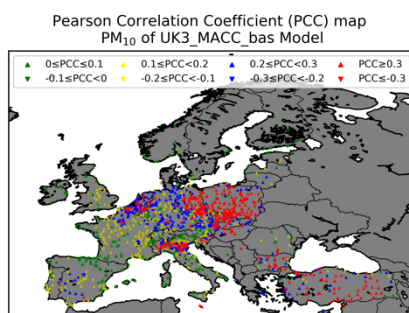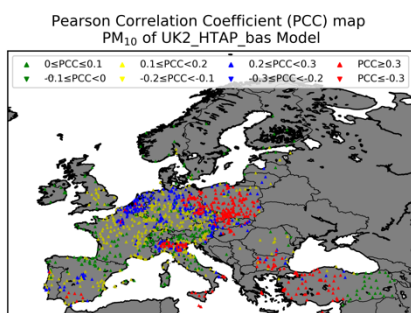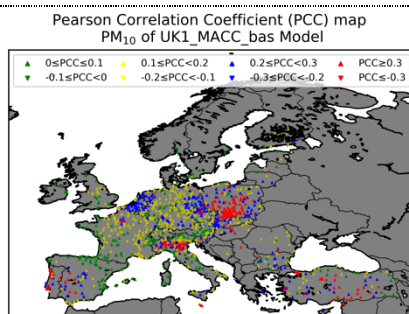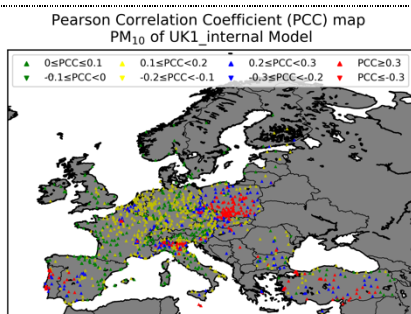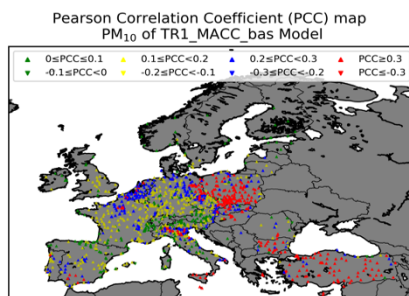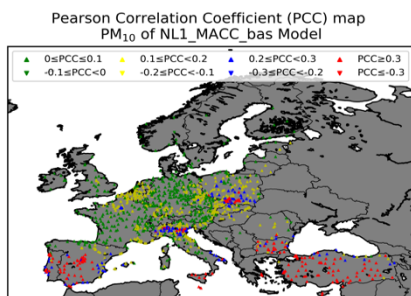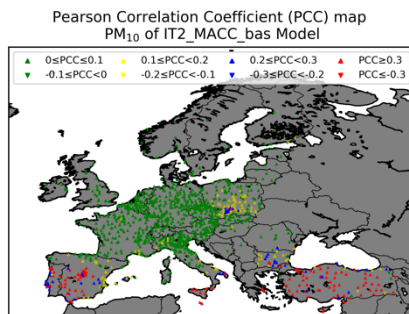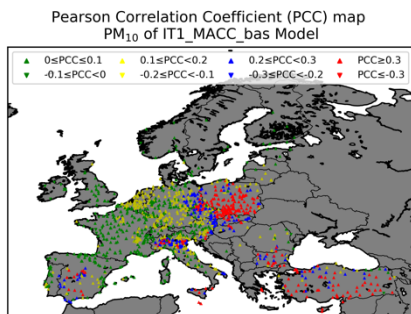
Figure B.8 (continued) : PCC maps
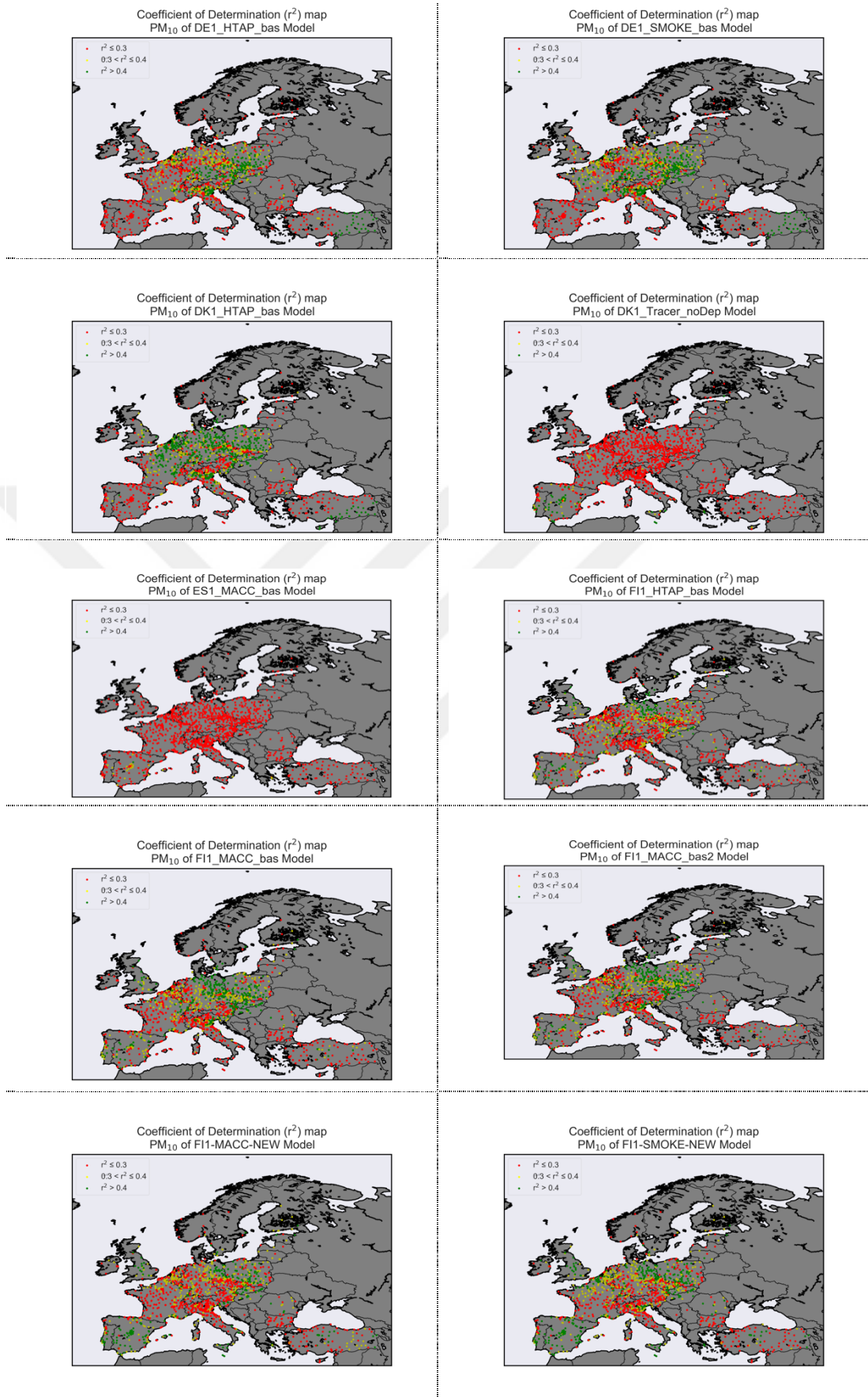
Figure B.9 : r^2 (coefficient of determination) maps.
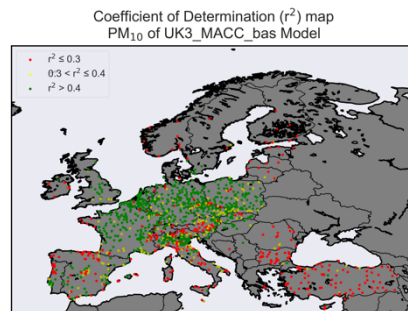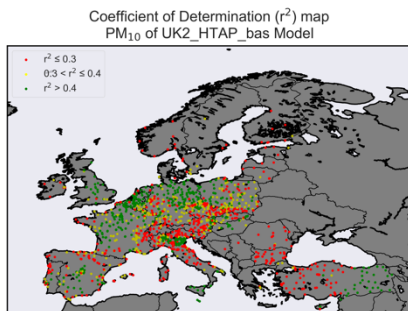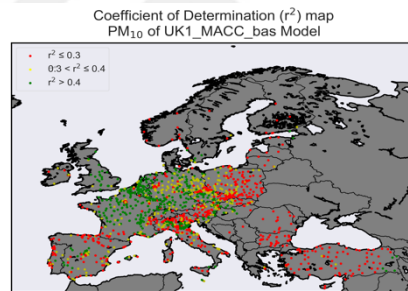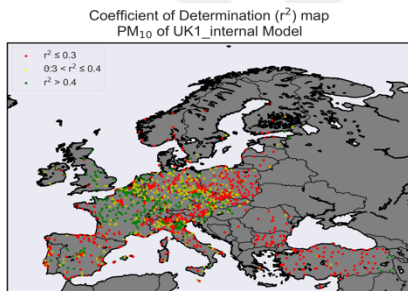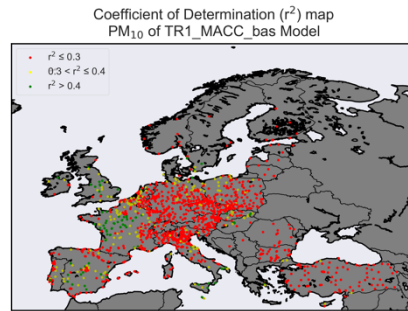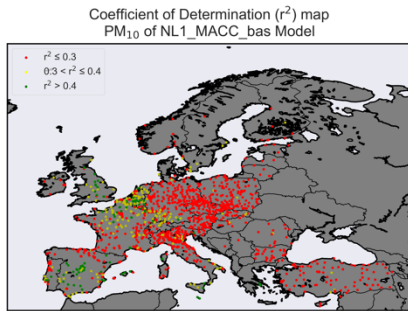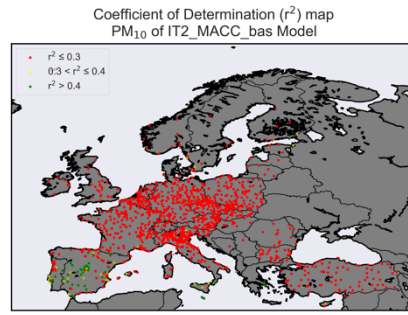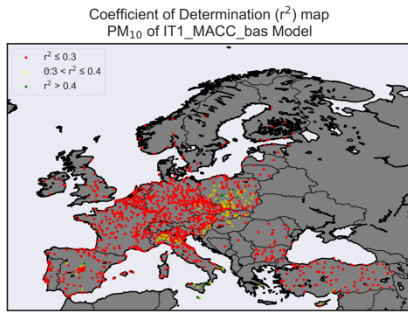
Figure B.9 (continued) : r^2 (coefficient of determination) maps.
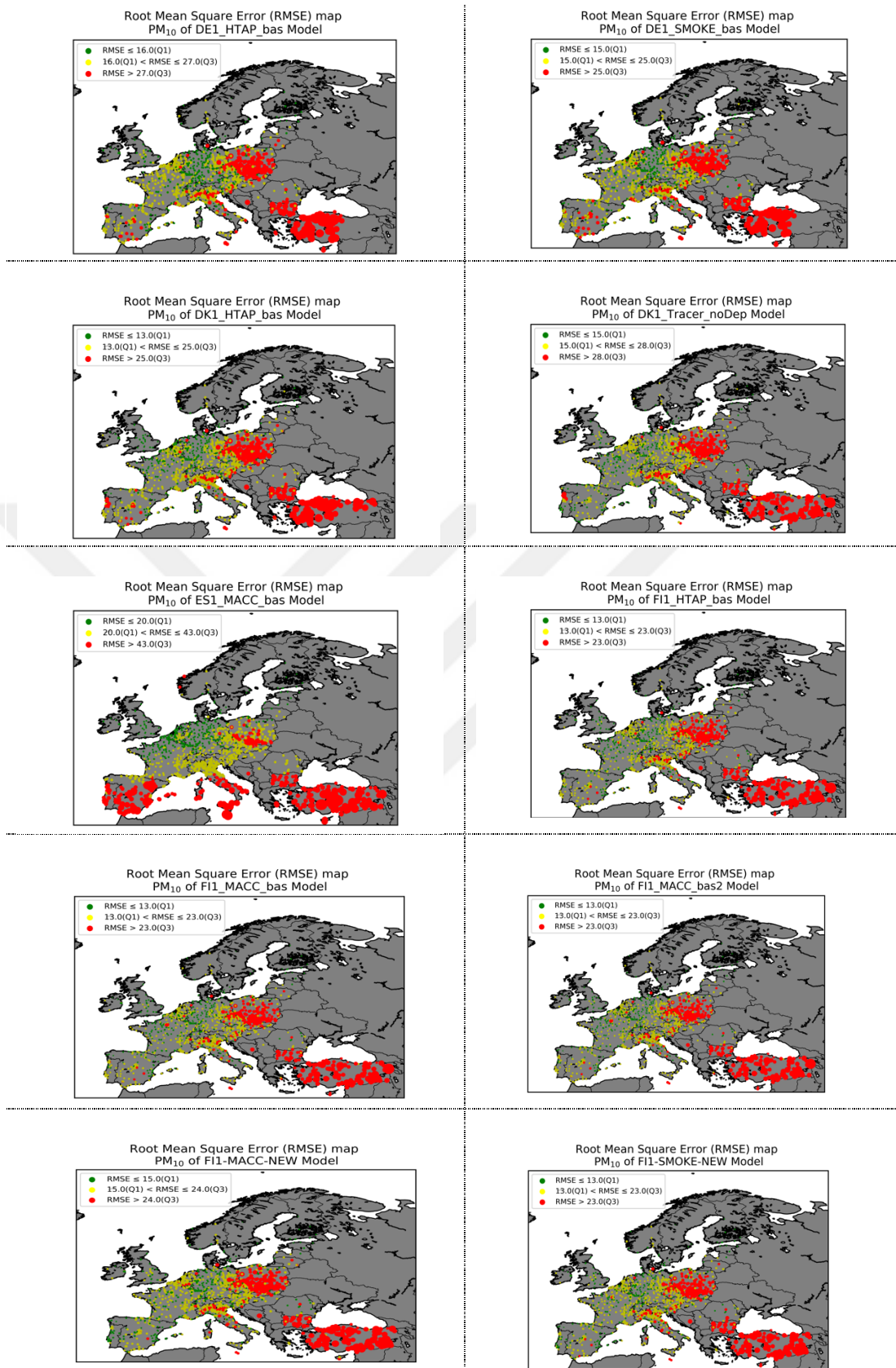
Figure B.10: RMSE maps.
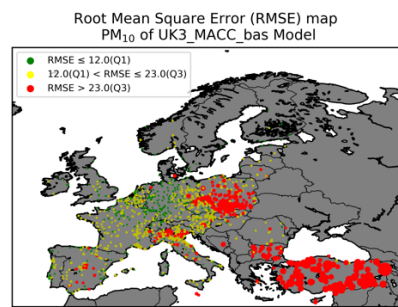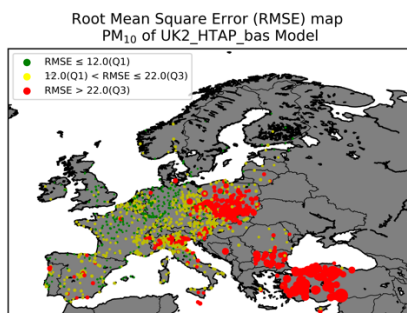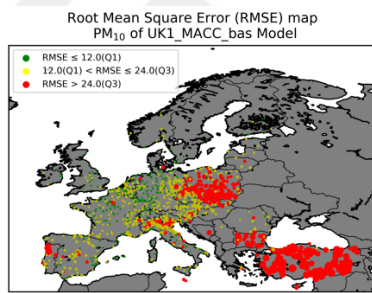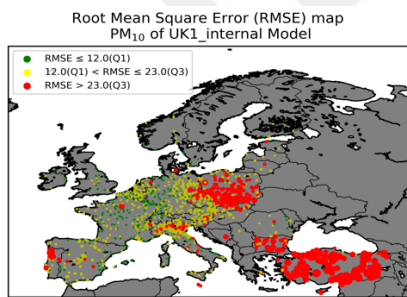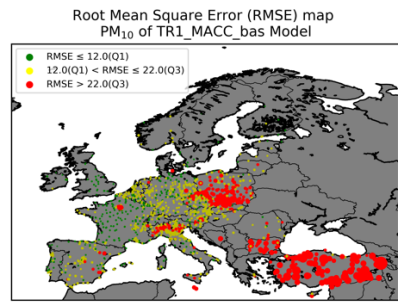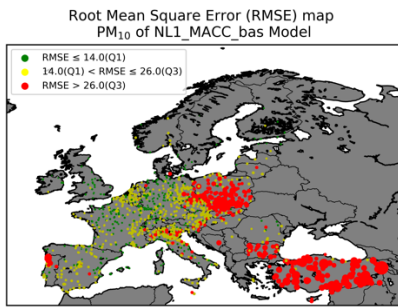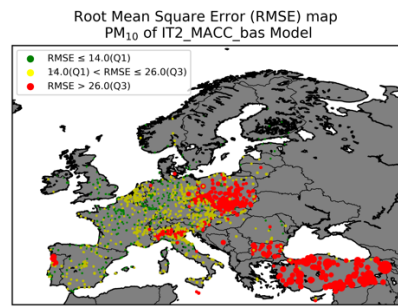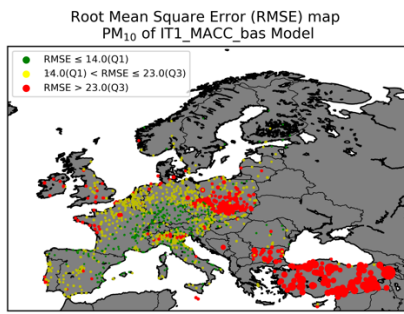
Figure B.10 (continued) : RMSE maps.
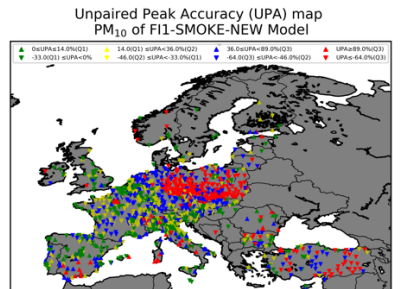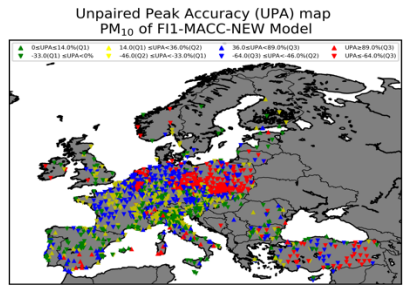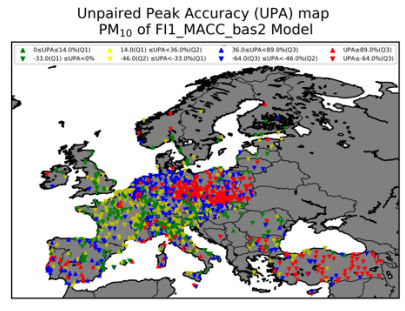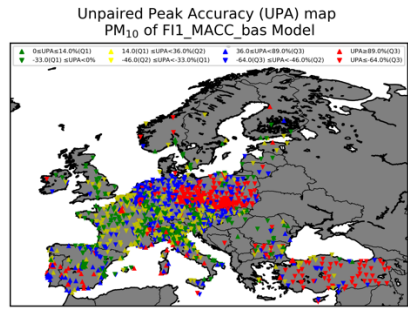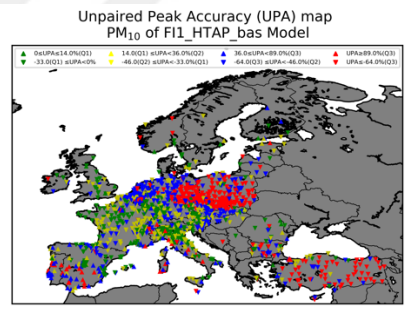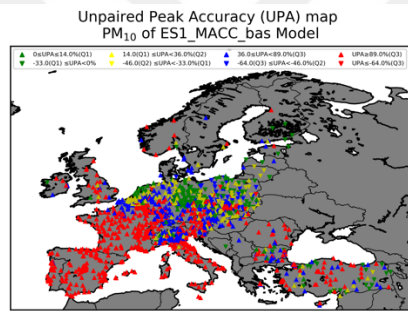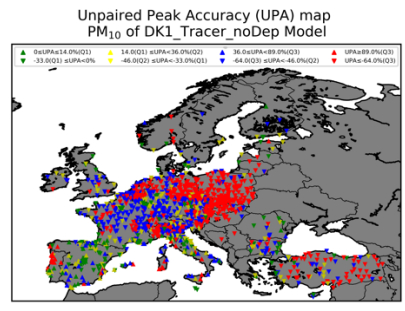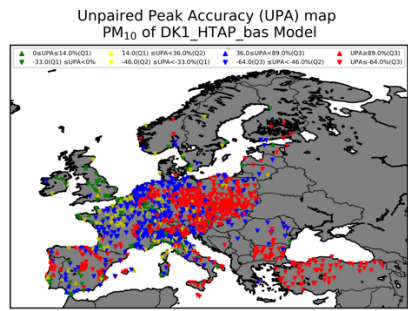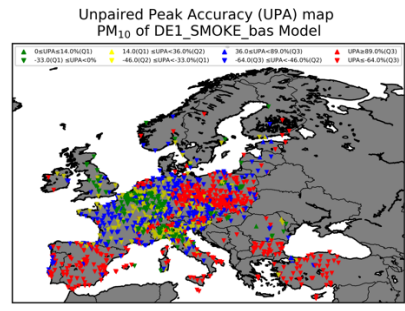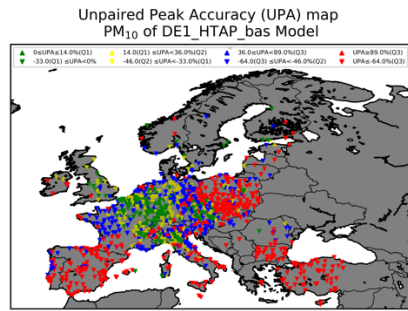
Figure B.11 : UPA maps.
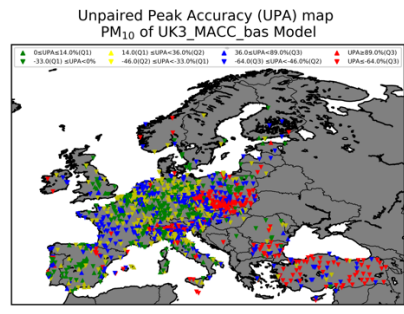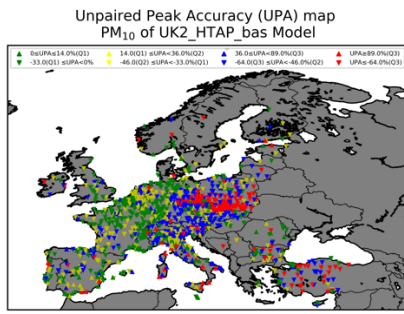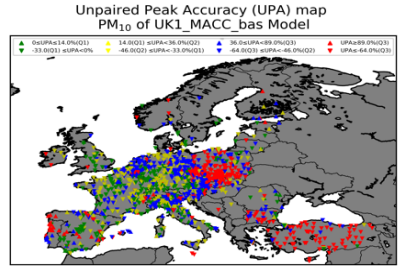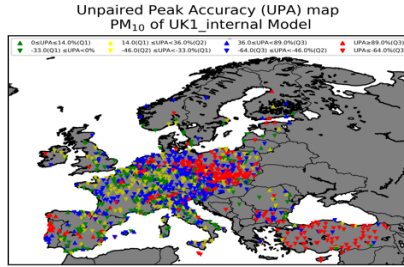
Figure B.11 (continued) : UPA maps.

APPENDIX C : MAE CDFs of stations (PM10) for the countries with more than 10 stations.

Figure C.1 : MAE CDFs of stations for PM$_{10}$, for the countries with more than 10 stations

Figure C.1 (continued) : MAE CDFs of stations for PM$_{10}$, for the countries with more than 10 stations.

APPENDIX D : Country Averages of Performance Metrics for All Models

Table D.1 : Country averages of performance metrics for all models.

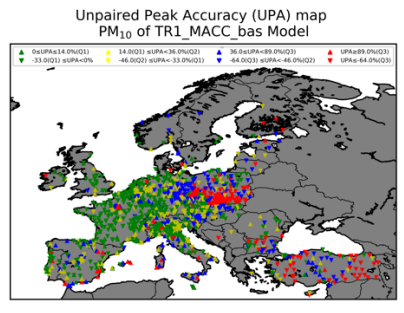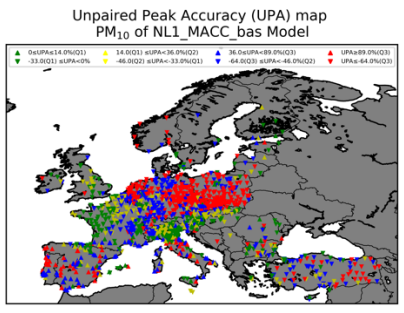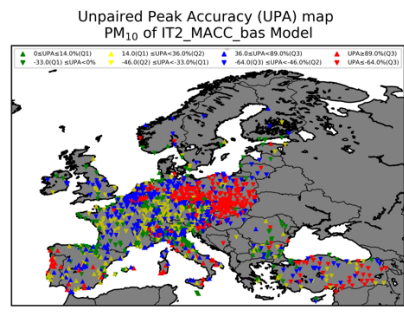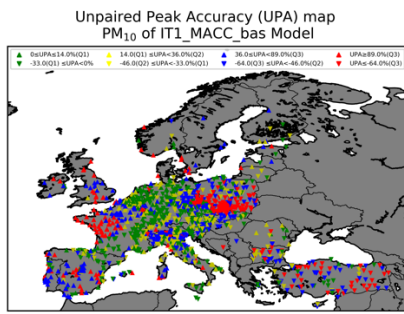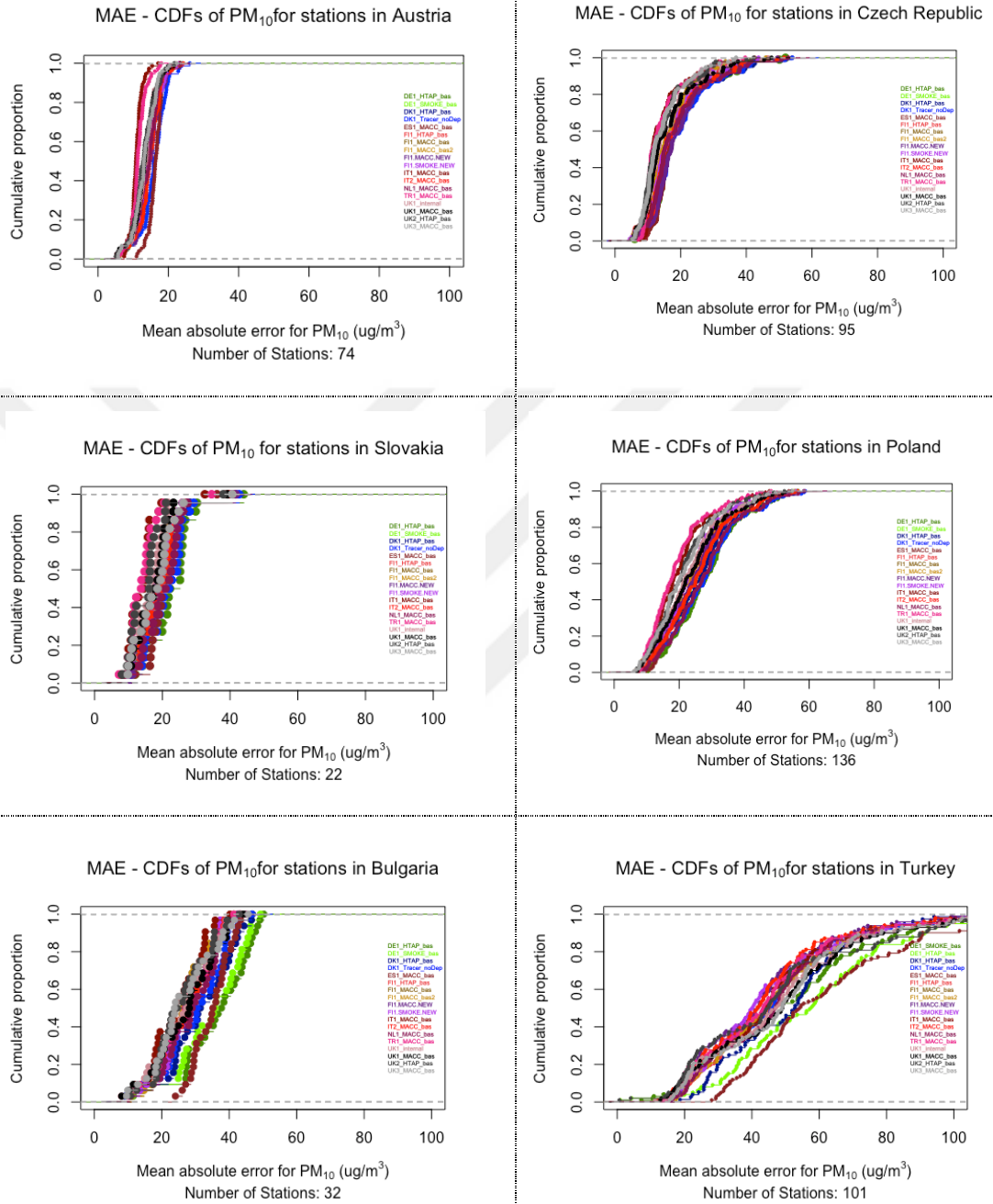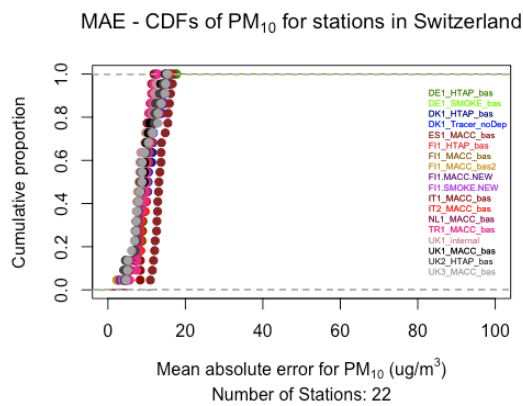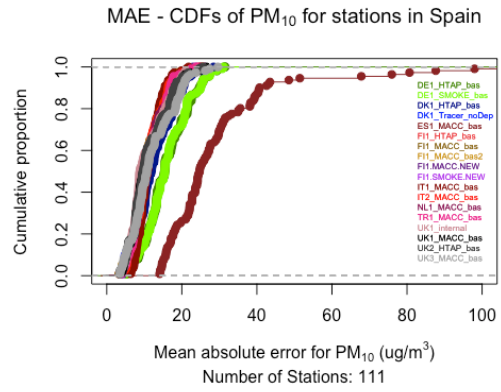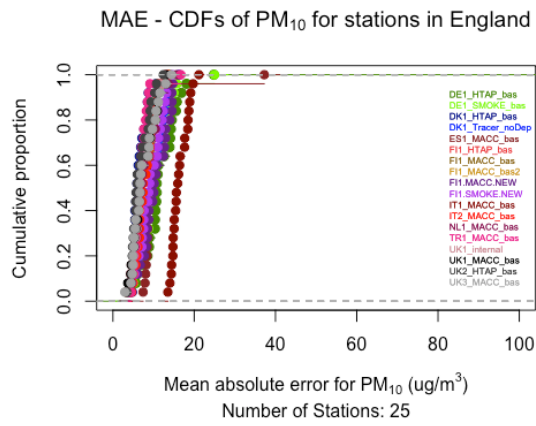| Country	Station Number	Mean	Median	stDev	Var	Cv	Skewness	RMSE	BIAS	MAE	NBIAS	NME	MFB	MFE	NMSE	PCC	r^2	UPA	IOA
Austria	74	12	10	8	74	70	0.82	19	-12	14	-49	59	-66	79	1.5	0.4	0.2	-37	0.5
Belgium	38	17	15	9	95	56	0.87	16	-9	12	-33	47	-40	56	0.7	0.5	0.3	-34	0.6
Bosnia.	1	11	9	9	135	77	0.82	55	-38	39	-78	81	-121	125	6.6	0.1	0.0	-80	0.4.
Bulgaria	32	18	14	15	324	75	0.80	41	-25	29	-53	67	-77	89	2.7	0.3	0.1	-47	0.5
Czech R.	95	14	12	9	88	64	0.85	27	-15	17	-48	58	-60	72	2.0	0.5	0.3	-60	0.5
Denmark	2	15	14	8	83	56	0.88	24	-5	13	-8	63	-12	61	2.3	0.3	0.1	-20	0.4
England	25	13	11	8	81	58	0.85	12	-5	9	-25	49	-39	57	0.7	0.5	0.3	-10	0.6
Estonia	4	11	9	8	78	77	0.80	11	-2	8	-12	61	-26	65	1.0	0.4	0.2	36	0.6
Finland	8	10	8	8	71	86	0.77	11	-3	7	-24	57	-39	67	1.2	0.4	0.2	1	0.6
France	231	15	13	9	109	61	0.85	16	-9	12	-36	51	-52	65	0.9	0.5	0.3	-11	0.6
Germany	199	13	11	8	70	61	0.86	15	-7	10	-32	50	-41	58	0.9	0.5	0.3	-42	0.6
Greece	4	28	22	20	691	65	0.84	26	-7	17	-19	50	-34	54	1.1	0.5	0.3	-30	0.6
Hungary	14	15	13	10	114	66	0.84	21	-13	15	-46	53	-62	69	1.2	0.6	0.4	-38	0.6
Iceland	2	13	9	12	547	77	0.77	28	2	12	16	92	0	60	6.8	0.0	0.0	-75	0.2
Ireland	9	11	9	7	58	62	0.83	12	-4	9	-25	58	-33	64	1.1	0.4	0.2	-33	0.5
Italy	188	17	14	12	213	69	0.83	20	-9	15	-31	57	-46	67	1.2	0.4	0.2	-6	0.6
Latvia	4	12	9	8	79	72	0.82	15	-7	11	-38	58	-49	71	1.3	0.3	0.1	-24	0.5
Lithuania	5	11	9	8	78	75	0.79	22	-15	16	-56	62	-79	86	1.8	0.4	0.2	-51	0.5
Luxemb.	3	15	13	9	79	57	0.87	10	-2	7	-12	41	-22	45	0.4	0.5	0.2	16	0.6
Malta	2	33	24	30	1484	79	0.77	36	1	19	2	58	-13	49	1.7	0.5	0.3	-42	0.6
Moldova	1	14	11	9	96	67	0.82	24	-8	19	-37	86	-2	111	2.1	0.0	0.0	-2	0.4
Netherl.	28	17	15	9	90	54	0.88	16	-8	11	-31	45	-39	52	0.7	0.5	0.3	-46	0.6
Norway	9	9	7	7	89	73	0.80	16	-8	11	-46	65	-69	83	2.0	0.2	0.1	-24	0.4

Table D.1 (continued) : Country averages of performance metrics for all models.

Country	Station Number	Mean	Median	stDev	Var	Cv	Skewness	RMSE	BIAS	MAE	NBIAS	NME	MFB	MFE	NMSE	PCC	r^2	UPA	IOA
Poland	136	15	13	10	104	65	0.84	35	-23	24	-57	62	-76	83	2.6	0.5	0.3	-65	0.5
Portugal	26	22	17	20	605	90	0.77	22	0	13	0	61	-20	58	1.4	0.5	0.2	78	0.6
Romania	13	17	14	12	208	71	0.81	18	-6	12	-25	54	-33	61	1.1	0.4	0.2	-1	0.6
Serbia	1	21	18	13	200	62	0.86	21	-2	14	-11	62	0	64	1.1	0.3	0.2	-28	0.5
Slovakia	22	14	11	9	94	67	0.84	24	-18	19	-54	60	-79	84	1.6	0.5	0.3	-46	0.5
Slovenia	11	14	12	9	103	67	0.85	21	-13	15	-48	56	-65	73	1.3	0.5	0.3	-38	0.6
Cyprus	2	28	23	21	800	66	0.84	36	-11	24	-24	57	-43	63	1.9	0.3	0.1	-52	0.5
Spain	111	14	10	13	341	89	0.77	18	-7	13	-29	62	-56	75	1.6	0.5	0.3	27	0.6
Sweden	9	10	8	6	50	70	0.83	8	-2	6	-20	51	-34	59	0.7	0.5	0.3	-15	0.6
Switzerl.	22	12	9	8	76	71	0.81	14	-6	10	12	96	-37	68	1.8	0.5	0.2	161	0.6
Turkey	101	27	22	20	727	70	0.83	62	-40	48	-50	65	-80	91	3.6	0.3	0.1	-45	0.5

Figure E.1 : Taylor Diagrams for stations in Marmara region.

Figure E.1 (continued) : Taylor Diagrams for stations in Marmara region.

Figure E.1 (continued) : Taylor Diagrams for stations in Marmara region.

Figure E.1 (continued) : Taylor Diagrams for stations in Marmara region.

Figure E.1 (continued) : Taylor Diagrams for stations in Marmara region.

Figure E.1 (continued) : Taylor Diagrams for stations in Marmara region.

Figure E.1 (continued) : Taylor Diagrams for stations in Marmara region.
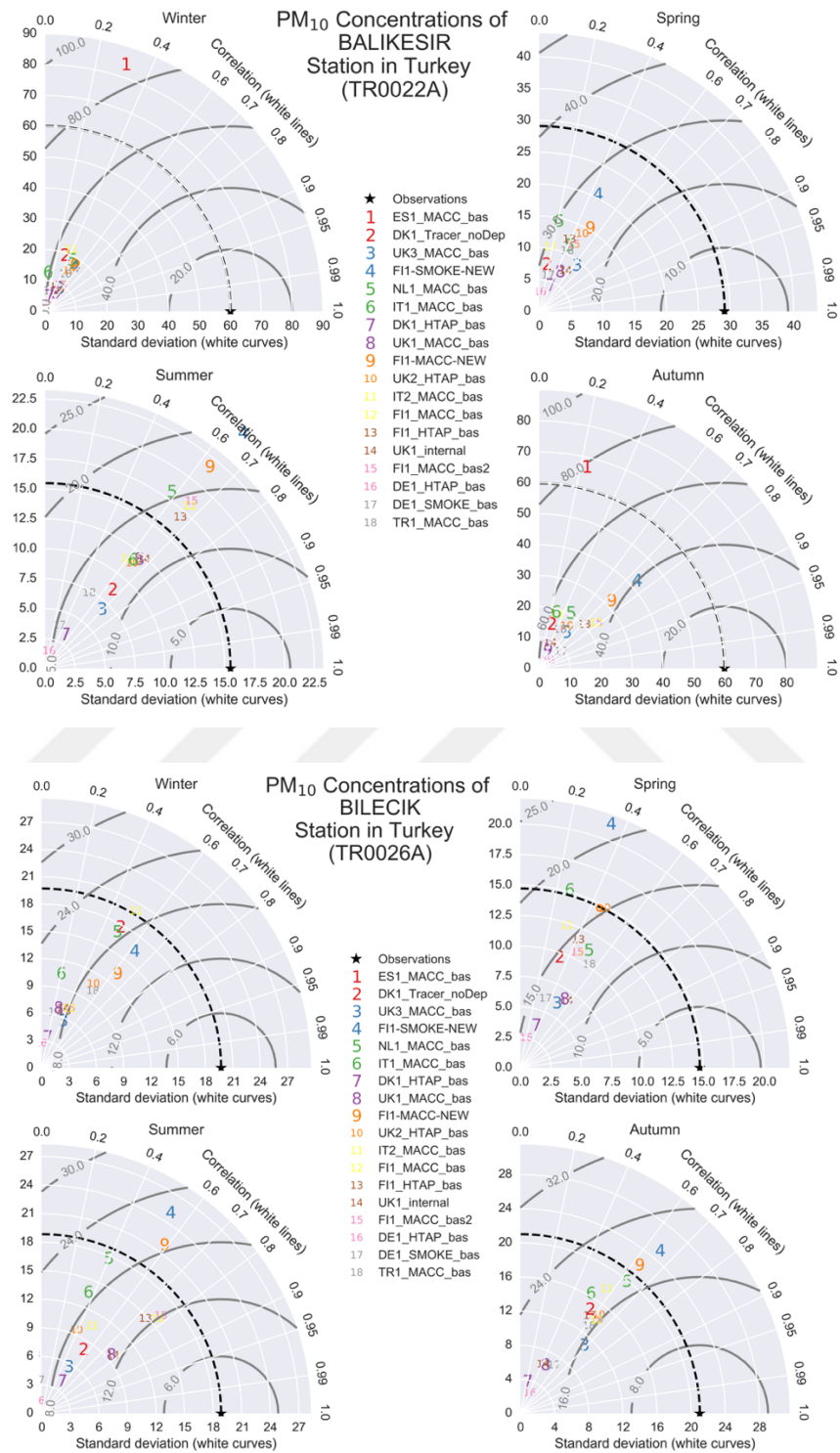
Figure E.1 (continued) : Taylor Diagrams for stations in Marmara region.

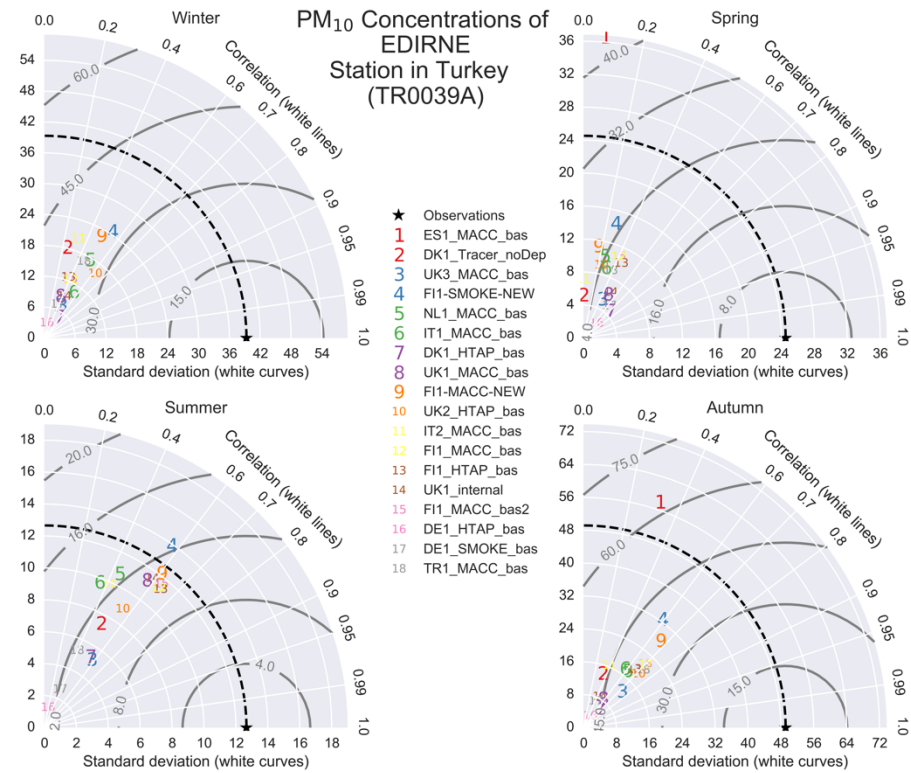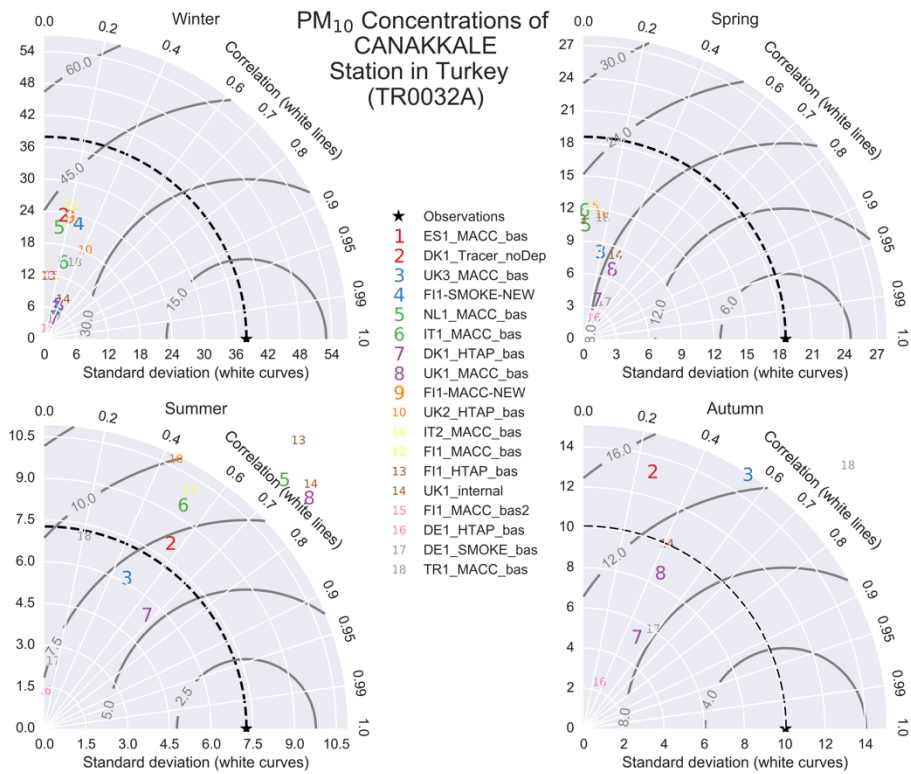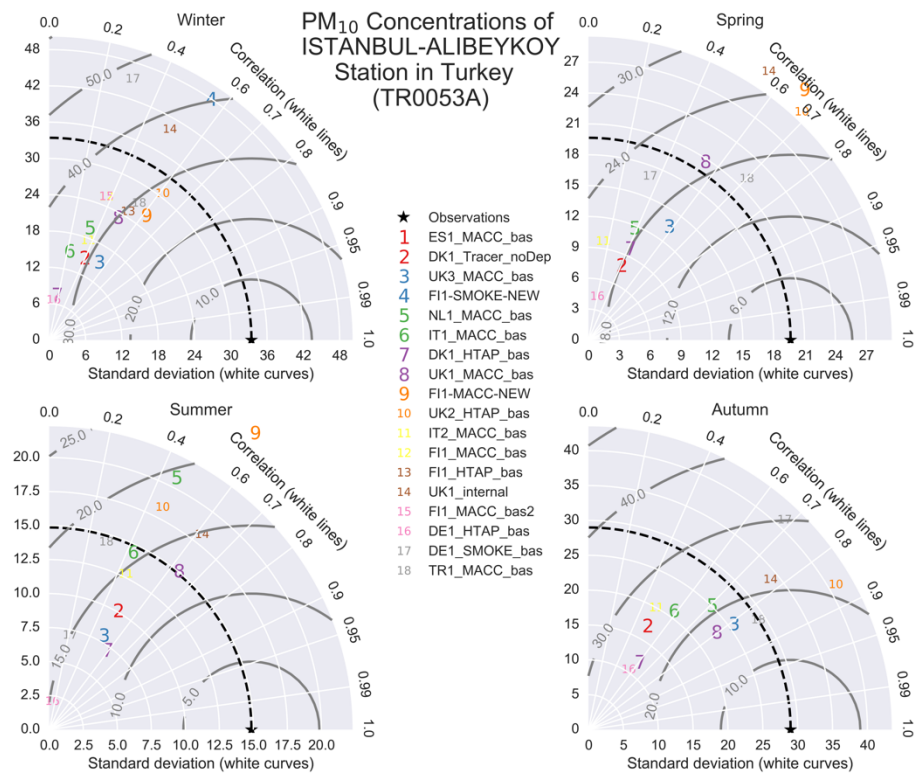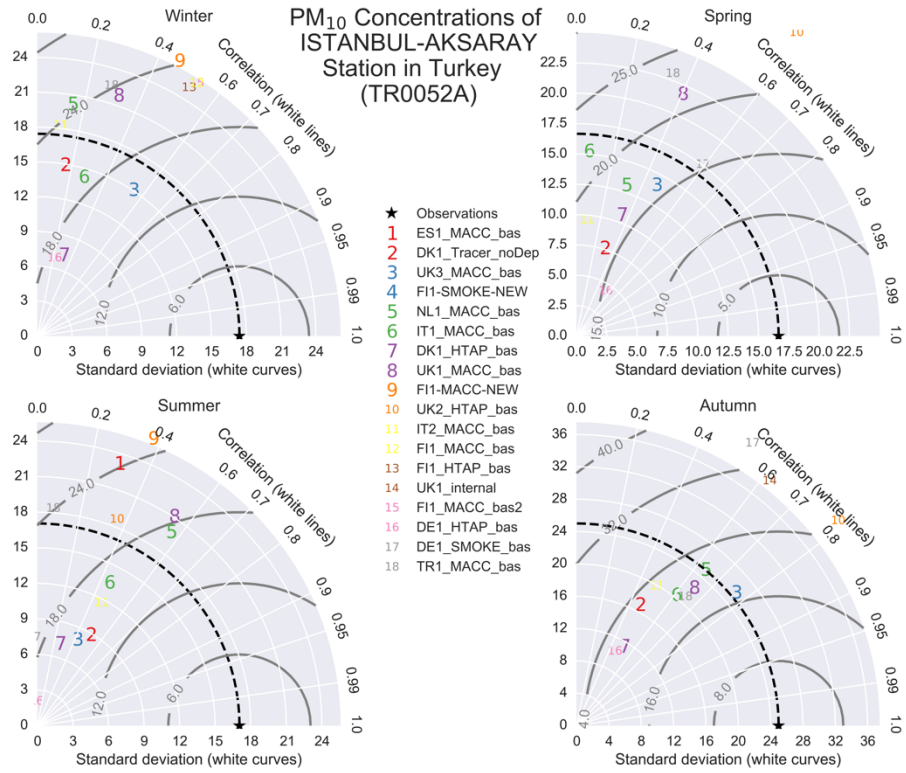**Figure E.1 (continued) :** Taylor Diagrams for stations in Marmara region.
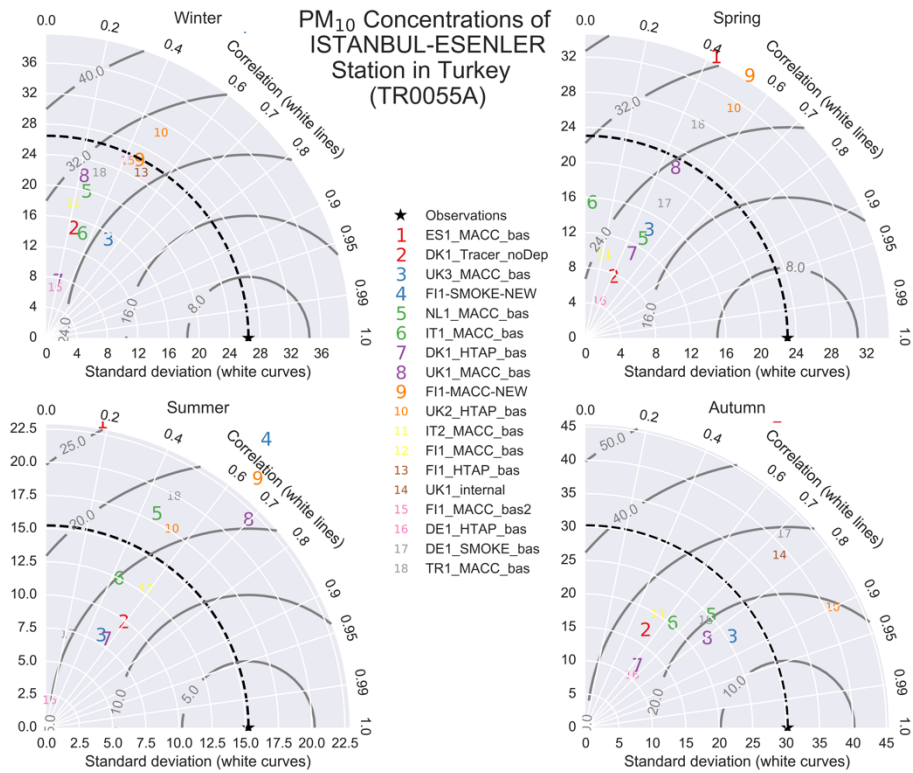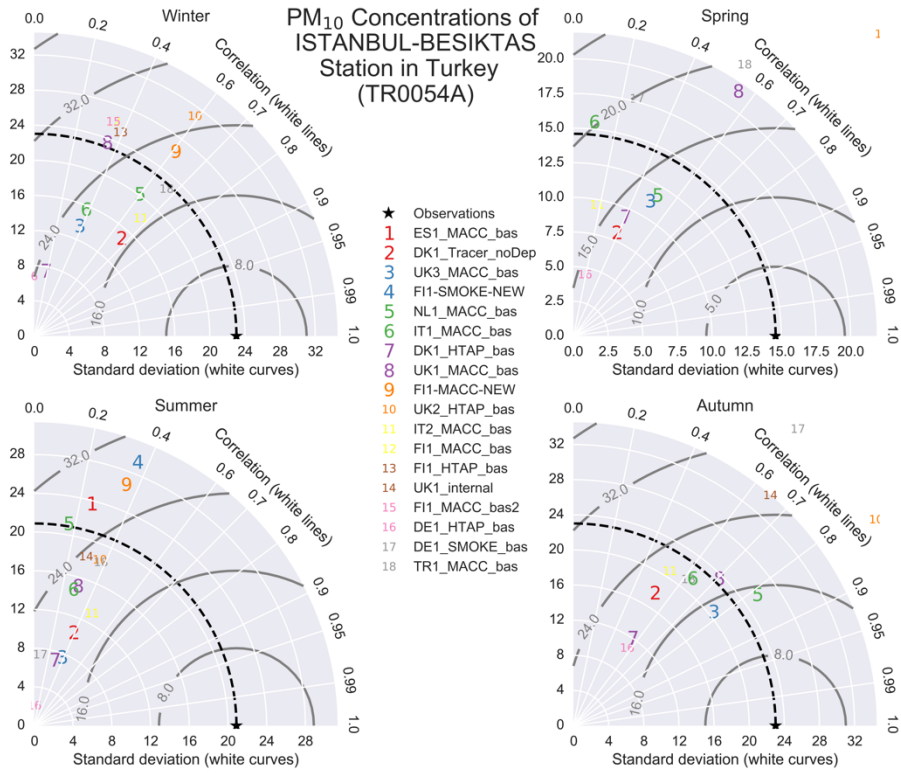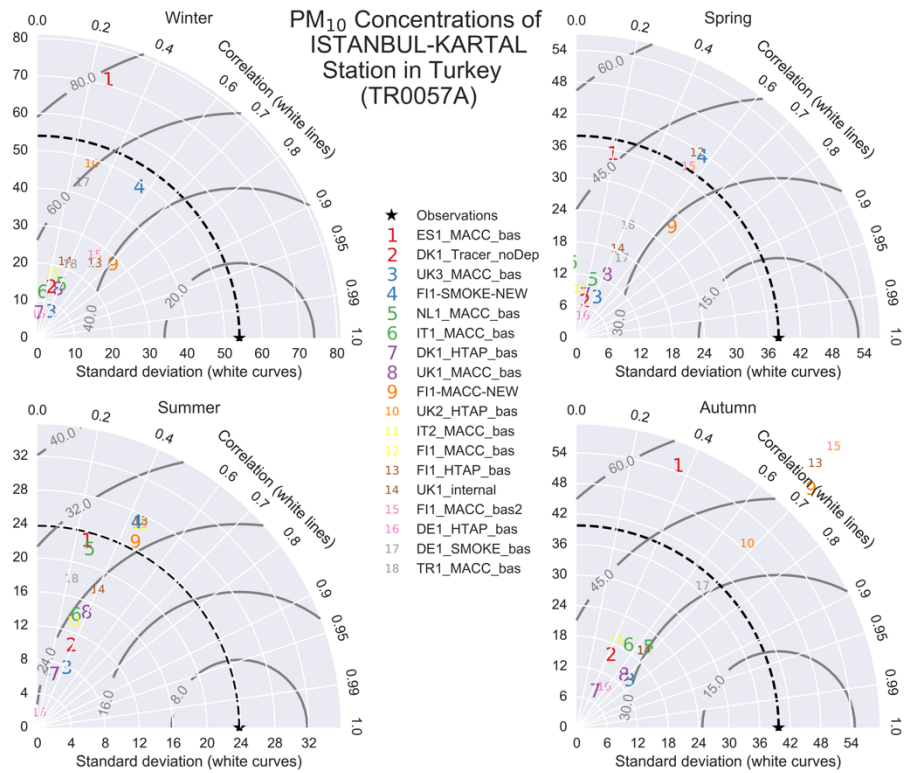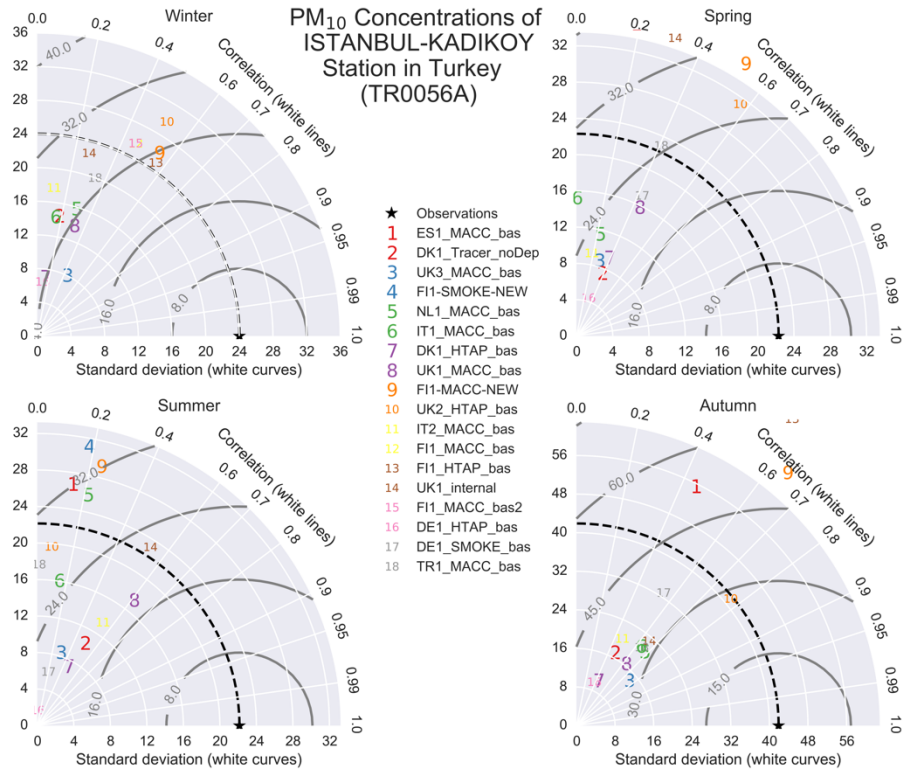
APPENDIX F : Goodness-of-fit Statistics/Criteria for EFs Derived from EMRs

Table F.1 : Goodness-of-fit statistics/criteria for dust EF derived from EMRs of 1.A.1.a – 10101– 3.10.

Type of distribution	Goodness-of-fit statistics			Goodness-of-fit criteria	
	Kolmogorov-Smirnov statistic	Cramer-von Mises	Anderson-Darling statistic	Akaike's Information Criterion	Bayesian Information Criterion
Normal	**0.24**	**0.12**	**0.67**	**43.61**	**44.58**
Lognormal	0.32	0.22	2.88	63.95	64.92
Uniform	0.27	0.16	-	-	-
Exponential	0.42	0.40	1.85	50.55	51.04
Logistic	**0.23**	**0.10**	**0.62**	**43.47**	**44.44**
Gamma	0.30	0.18	1.62	50.36	51.33
Weibull	0.29	0.16	1.01	44.95	45.92

Table F.2 : Goodness-of-fit statistics/criteria for CO EF derived from EMRs of 1.A.1.a – 10101 – 3.10.

Type of distribution	Goodness-of-fit statistics			Goodness-of-fit criteria	
	Kolmogorov-Smirnov statistic	Cramer-von Mises	Anderson-Darling statistic	Akaike's Information Criterion	Bayesian Information Criterion
Normal	0.28	0.15	**0.98**	49	50
Lognormal	0.32	0.30	4.97	77	78
Uniform	**0.22**	**0.14**	1.16	**45**	**46**
Exponential	0.34	0.29	1.43	52	52
Logistic	0.30	0.17	1.10	50	51
Gamma	0.30	0.25	2.49	57	58
Weibull	0.28	0.22	1.44	51	52

Table F.3 : Goodness-of-fit statistics/criteria for SO_2 EF derived from EMRs of 1.A.1.a – 10101 – 3.10.

Type of distribution	Goodness-of-fit statistics			Goodness-of-fit criteria	
	Kolmogorov-Smirnov statistic	Cramer-von Mises	Anderson-Darling statistic	Akaike's Information Criterion	Bayesian Information Criterion
Normal	0.13	0.03	0.23	97.89	98.86
Lognormal	0.14	0.04	0.38	99.69	100.66
Uniform	0.18	0.07	-	-	-
Exponential	0.49	0.82	3.84	127.86	128.35
Logistic	**0.10**	**0.02**	**0.17**	97.63	98.60
Gamma	0.14	0.03	0.31	98.86	99.83
Weibull	0.14	0.03	0.23	**97.62**	**98.59**

Table F.4 : Goodness-of-fit statistics/criteria for NO EF derived from EMRs of
1.A.1.a – 10101 – 3.10.

Type of distribution	Goodness-of-fit statistics			Goodness-of-fit criteria	
	Kolmogorov-Smirnov statistic	Cramer-von Mises	Anderson-Darling statistic	Akaike's Information Criterion	Bayesian Information Criterion
Normal	0.16	0.06	0.33	**91.15**	**92.12**
Lognormal	0.15	**0.05**	0.35	91.48	92.45
Uniform	0.20	0.06	-	-	-
Exponential	0.49	0.78	3.66	118.76	119.24
Logistic	0.18	0.07	0.41	91.94	92.91
Gamma	**0.15**	**0.05**	**0.33**	**91.22**	**92.19**
Weibull	0.17	0.06	0.35	91.39	92.36

Table F.5 : Goodness-of-fit statistics/criteria for NO_2 EF derived from EMRs of
1.A.1.a – 10101 – 3.10.

Type of distribution	Goodness-of-fit statistics			Goodness-of-fit criteria	
	Kolmogorov-Smirnov statistic	Cramer-von Mises	Anderson-Darling statistic	Akaike's Information Criterion	Bayesian Information Criterion
Normal	0.15	0.05	0.35	152.55	154.10
Lognormal	0.15	0.05	0.35	152.46	154.01
Uniform	**0.13**	**0.04**	**0.23**	**146.91**	**148.45**
Exponential	0.55	1.22	5.66	203.93	204.71
Logistic	0.18	0.07	0.48	154.11	155.66
Gamma	0.15	0.05	0.34	152.44	153.98
Weibull	0.15	0.06	0.39	153.24	154.78

Table F.6 : Goodness-of-fit statistics/criteria for dust EF derived from EMRs of
1.A.1.a – 10101 – 3.16.

Type of distribution	Goodness-of-fit statistics			Goodness-of-fit criteria	
	Kolmogorov-Smirnov statistic	Cramer-von Mises	Anderson-Darling statistic	Akaike's Information Criterion	Bayesian Information Criterion
Normal	0.27	**0.07**	**0.47**	**23.60**	**23.59**
Lognormal	0.33	0.12	1.83	36.37	36.26
Uniform	**0.22**	**0.07**	-	-	-
Exponential	0.33	0.21	1.04	27.15	27.10
Logistic	0.30	0.09	0.53	**24.20**	**24.09**
Gamma	0.31	0.10	1.04	28.15	28.04
Weibull	0.29	0.09	0.66	24.59	**24.48**

Table F.7 : Goodness-of-fit statistics/criteria for CO EF derived from EMRs of 1.A.1.a – 10101 – 3.16.

Type of distribution	Goodness-of-fit statistics			Goodness-of-fit criteria	
	Kolmogorov-Smirnov statistic	Cramer-von Mises	Anderson-Darling statistic	Akaike's Information Criterion	Bayesian Information Criterion
Normal	0.26	0.10	0.71	89.34	89.94
Lognormal	0.39	0.34	7.38	130.53	131.14
Uniform	**0.21**	**0.07**	**0.50**	85.81	86.41
Exponential	0.28	0.17	1.13	**83.20**	**83.50**
Logistic	0.28	0.12	0.85	90.76	91.37
Gamma	0.34	0.23	2.20	89.45	90.06
Weibull	0.29	0.15	0.85	84.75	85.35

Table F.8 : Goodness-of-fit statistics/criteria for NO EF derived from EMRs of 1.A.1.a – 10101 – 3.16.

Type of distribution	Goodness-of-fit statistics			Goodness-of-fit criteria	
	Kolmogorov-Smirnov statistic	Cramer-von Mises	Anderson-Darling statistic	Akaike's Information Criterion	Bayesian Information Criterion
Normal	0.20	**0.08**	0.55	64.71	66.26
Lognormal	0.20	0.08	0.59	65.42	66.96
Uniform	**0.16**	0.08	-	-	-
Exponential	0.58	1.46	6.67	145.80	146.57
Logistic	0.22	0.10	0.62	65.16	66.70
Gamma	0.20	0.08	0.57	65.17	66.71
Weibull	0.19	0.09	**0.52**	**62.13**	**63.67**

Table F.9 : Goodness-of-fit statistics/criteria for NO_2 EF derived from EMRs of 1.A.1.a – 10101 – 3.16.

Type of distribution	Goodness-of-fit statistics			Goodness-of-fit criteria	
	Kolmogorov-Smirnov statistic	Cramer-von Mises	Anderson-Darling statistic	Akaike's Information Criterion	Bayesian Information Criterion
Normal	0.22	0.07	0.50	86.66	87.27
Lognormal	0.30	0.18	4.51	141.28	141.89
Uniform	**0.16**	**0.05**	**0.33**	**83.13**	**83.74**
Exponential	0.24	0.10	0.69	83.98	84.28
Logistic	0.24	0.09	0.61	87.89	88.50
Gamma	0.24	0.11	1.31	91.74	92.34
Weibull	0.23	0.09	0.67	85.88	86.48

Table F.10 : Goodness-of-fit statistics/criteria for dust EF derived from EMRs of 1.A.1.a – 10104 – 3.17.

Type of distribution	Goodness-of-fit statistics			Goodness-of-fit criteria	
	Kolmogorov-Smirnov statistic	Cramer-von Mises	Anderson-Darling statistic	Akaike's Information Criterion	Bayesian Information Criterion
Normal	**0.177**	0.129	**0.846**	86.854	89.371
Lognormal	0.291	0.379	4.302	92.984	95.501
Uniform	**0.156**	**0.092**	-	-	-
Exponential	**0.133**	**0.105**	**0.680**	**77.226**	**78.484**
Logistic	0.196	0.172	1.097	89.219	91.735
Gamma	0.218	0.177	1.232	**78.801**	81.317
Weibull	0.180	**0.114**	**0.720**	**77.565**	**80.081**

Table F.11 : Goodness-of-fit statistics/criteria for CO EF derived from EMRs of 1.A.1.a – 10104 – 3.17.

Type of distribution	Goodness-of-fit statistics			Goodness-of-fit criteria	
	Kolmogorov-Smirnov statistic	Cramer-von Mises	Anderson-Darling statistic	Akaike's Information Criterion	Bayesian Information Criterion
Normal	0.24	0.41	2.39	250.75	254.13
Lognormal	0.28	1.00	8.92	244.10	247.48
Uniform	0.22	0.36	-	-	-
Exponential	0.18	0.32	1.72	**216.97**	**218.66**
Logistic	0.26	0.50	2.79	252.69	256.07
Gamma	0.18	0.36	1.92	219.27	222.65
Weibull	**0.15**	**0.25**	**1.34**	218.62	222.00

Table F.12 : Goodness-of-fit statistics/criteria for SO$_2$ EF derived from EMRs of 1.A.1.a – 10104 – 3.17.

Type of distribution	Goodness-of-fit statistics			Goodness-of-fit criteria	
	Kolmogorov-Smirnov statistic	Cramer-von Mises	Anderson-Darling statistic	Akaike's Information Criterion	Bayesian Information Criterion
Normal	0.451	1.40	7.06	195	197
Lognormal	0.278	0.66	3.52	**105**	**107**
Uniform	0.434	1.37	-	-	-
Exponential	0.433	1.73	9.46	129	131
Logistic	0.459	1.44	6.96	188	191
Gamma	0.430	0.92	4.59	130	133
Weibull	**0.240**	**0.37**	**2.34**	114	116

Table F.13 : Goodness-of-fit statistics/criteria for NO EF derived from EMRs of 1.A.1.a – 10104 – 3.17.

Type of distribution	Goodness-of-fit statistics			Goodness-of-fit criteria	
	Kolmogorov-Smirnov statistic	Cramer-von Mises	Anderson-Darling statistic	Akaike's Information Criterion	Bayesian Information Criterion
Normal	0.22	1.09	6.30	742.80	747.33
Lognormal	0.21	0.66	6.39	684.28	688.81
Uniform	0.25	1.24	-	-	-
Exponential	0.14	0.30	1.80	**663.02**	**665.28**
Logistic	0.24	1.12	6.16	738.46	742.99
Gamma	**0.09**	**0.12**	0.94	664.64	669.17
Weibull	0.10	0.13	**0.92**	**663.26**	**667.78**

Table F.14 : Goodness-of-fit statistics/criteria for NO_2 EF derived from EMRs of 1.A.1.a – 10104 – 3.17.

Type of distribution	Goodness-of-fit statistics			Goodness-of-fit criteria	
	Kolmogorov-Smirnov statistic	Cramer-von Mises	Anderson-Darling statistic	Akaike's Information Criterion	Bayesian Information Criterion
Normal	0.32	1.55	8.32	705.93	710.15
Lognormal	0.23	0.98	8.92	640.84	645.06
Uniform	0.29	1.61	-	-	-
Exponential	0.24	1.03	6.05	613.63	615.74
Logistic	0.33	1.61	8.34	701.48	705.71
Gamma	0.15	0.21	1.40	605.45	609.67
Weibull	**0.14**	**0.17**	**1.08**	**601.81**	**606.03**

CURRICULUM VITAE

Name Surname	: Ümmügülsüm ALYÜZ
Place and Date of Birth	: Malatya, 1984
E-Mail	: ummugulsumalyuz@gmail.com

EDUCATION

- **B.Sc.**   : 2008, Trakya University,
                        Environmental Engineering
- **MBA**   : 2010, Istanbul University,
                        Management & Business Institute
- **M.Sc.**   : 2012, Istanbul Technical University,
                        Environmental Science and Technology

EXPERIENCE

- 2012-cont. Research Assistant at Bahcesehir University Civil Engineering Department
- 2008-2012 Cevka Construction Co. Ltd. Technical Office Engineer

PROJECTS

- AQMEII 3 Project (2014 – 2019) for evaluating and comparing global and regional modeling systems driven by consistent emissions over North America and Europe against a common set of measurements and to perform model evaluation analyses on global models coordinated with the analyses of regional models. As Istanbul Technical University team member.

- TUBITAK Public Institutions Research Funding Program KAMAG Project (2013-2016). Development of a National Air Pollution Emission Management System. PhD Fellow

PROFESSIONAL TRAINING

- Atmospheric Chemistry and Dynamics Summer School, ACUD–2014. University of Cologne - University of Wuppertal - Jülich, Germany. 29.09.2014-03.10.2014

- ISO 14064-1 Training on greenhouse gas inventory and emissions calculation. Chamber of Environmental Engineers – Istanbul. 08.05.2014-09.05.2014

- Introduction to Remote Sensing and Air Quality Applications. NASA ARTES (National Aeronautics and Space Adm., Earth Science Division) Webinar. 24.06.2013-21.07.2013

- Sustainability and Economics. KTH (Sweden Royal Institute of Technology) Stockholm, Sweden. 27.06.2011-09.07.2011

COMPUTER SKILLS

- Programming: R, Python

- Applications: CMAQ (Community Multiscale Air Quality) Model, WRF (Weather Research and Forecasting) Model

- Platforms: User of MS Windows, OS X (Mac OS), Linux

PUBLICATIONS AND PRESENTATIONS

- Efisio Solazzo, Roberto Bianconi, Christian Hogrefe, Gabriele Curci, Paolo Tuccella, **Ummugulsum Alyuz**, (…), Stefano Galmarini (2017). Evaluation and error apportionment of an ensemble of atmospheric chemistry transport modelling systems: multivariable temporal and spatial breakdown, *Atmospheric Chemistry and Physics*, 17, 3001-3054, https://doi.org/10.5194/acp-17-3001-2017

- **Ummugulsum Alyuz** (2019). Marmara Municipalities Union, Marmara Urban Forum, 3 Minutes Thesis presentation. October 2, 2019. Istanbul Congress Center.

- **Ummugulsum Alyuz**, Goksel Demir, Alper Unal. *Development National Emission Factors of Turkish Public Energy Production Industry and Quantification of Variability and Uncertainty*. 12th International Conference on Air Quality – Sicence and Application. Thessaloniki, 9-13 March 2020. (Accepted for oral presentation).

- **Ummugulsum Alyuz**, Kadir Alp (2014). "*Emission Inventory of Primary Air Pollutants in 2010 from Industrial Processes in Turkey*". Science of the Total Environment. Volumes 488–489, Pages 369-381, ISSN 0048-9697, http://dx.doi.org/10.1016/j.scitotenv.2014.01.123.

- Gabriele Curci, **Ummugulsum Alyuz**, Rocio Barò, Roberto Bianconi, Johannes Bieser, (…), Stefano Galmarini (2019). *Modelling black carbon absorption of solar radiation: combining external and internal mixing assumptions.* Atmos. Chem. Phys., 19, 181–204, https://doi.org/10.5194/acp-19-181-2019

- Ulas Im, Jesper Heile Christensen, Camilla Geels, Kaj Mantzius Hansen, Jørgen Brandt, Efisio Solazzo, **Ummugulsum Alyuz**, (…), Stefano Galmarini (2018). *Influence of anthropogenic emissions and boundary conditions on multi-model simulations of major air pollutants over Europe and North America in the framework of AQMEII3.* Atmos. Chem. Phys., 18, 8929–8952, https://doi.org/10.5194/acp-18-8929-2018

- Stefano Galmarini, Ioannis Kioutsioukis, Efisio Solazzo, **Ummugulsum Alyuz**, Alessandra Balzarini, Roberto Bellasio, (…), Alper Unal (2018). *Two-scale multi-model ensemble: is a hybrid ensemble of opportunity telling us more?* Atmos. Chem. Phys., 18, 8727–8744, https://doi.org/10.5194/acp-18-8727-2018

- Marta G. Vivanco, Mark R. Theobald, Héctor García-Gómez, Juan Luis Garrido, Marje Prank, Wenche Aas, Mario Adani, **Ummugulsum Alyuz**, (…), Stefano Galmarini (2018). *Modeled deposition of nitrogen and sulfur in Europe estimated by 14 air quality model systems: evaluation, effects of changes in emissions and implications for habitat protection.* Atmos. Chem. Phys., 18, 10199–10218, https://doi.org/10.5194/acp-18-10199-2018

- Ulas Im, Jørgen Brandt, Camilla Geels, Kaj Mantzius Hansen, Jesper Heile Christensen, Mikael Skou Andersen, Efisio Solazzo, Ioannis Kioutsioukis, **Ummugulsum Alyuz**, (…), Stefano Galmarini (2018). *Assessment and economic valuation of air pollution impacts on human health over Europe and the United States as calculated by a multi-model ensemble in the framework of AQMEII3.* Atmos. Chem. Phys., 18, 5967–5989, https://doi.org/10.5194/acp-18-5967-2018

- Goksel Demir, **Ummugulsum Alyuz**, Mehmet Firat (2014). "*Evaluation of Exhaust Pollutants in Iskenderpasa Underground Parking Garage*". Journal of Environmental Science, 2014. Vol 3, p 116-120.

- Seda Erbas, H. Handan Demir, **Ummugulsum Alyuz**, Goksel Demir (2014). "*The Importance of new technologies in sustainable public transportation: a review of cost-benefit analysis in hybrid electric vehicle use and evaluation of a potential application in Turkey*". Journal of Environmental Science, 2014. Vol 3, p 111-116.

- Goksel Demir, Umut E. Kolay, H. Eser Okten, **Ummugulsum Alyuz**, Cuma Bayat (2016). *Selection of Alternative Landfill Location by Using a Geographical Information System. European Side of Istanbul. Case Study.* Env. Protection Eng. Vol. 42/1 DOI: 10.5277/epe160110

- Ulas Im, Jørgen Brandt, Camilla Geels, Kaj Mantzius Hansen, Jesper Heile Christensen, Mikael Skou Andersen, Efisio Solazzo, Ioannis Kioutsioukis, **Ummugulsum Alyuz**, (…), Stefano Galmarini (2020). *Multi-model Assessment of Air Pollution-Related Premature Mortality in Europe and U.S.: Domestic Versus Foreign Contributions.* In Mensink C., Gong W., Hakami A. (eds) Air Pollution Modeling and its Application XXVI. ITM 2018. Springer Proceedings in Complexity. Springer, Cham. doi: https://doi.org/10.1007/978-3-030-22055-6_73